Estimating the Trauma-Death Interval:
A Histological Investigation of Fracture Healing.

Anna Williams MA(Oxon) MSc

Submitted in part fulfilment of the requirements of the degree of PhD

Department of Forensic Pathology

December 2004

"How poor are they who have not patience!
What wound did ever heal but by degrees?"
Othello
William Shakespeare (1564 – 1616)

"Healing is a matter of time, but it is sometimes also a matter of opportunity".
Precepts
Hippocrates (460BC – 377BC)

I : Dedication

Mr C R Constant

for opening my eyes to the intricacies of fracture healing

I would like to thank the following people for their support and encouragement:

Dr Martin Evison	for supervision, encouragement and having confidence in me
Professor James Underwood	for co-supervision and providing excellent guidance
Professor Chris Milroy	for overseeing my progress
H M Coroner Mr Chris Dorries	for giving me his kind permission to use the case data for scientific research purposes
Dr Kenneth Shorrock	for some excellent ideas
Dr Phil Lumb	for finding time to help me
Dr Jason Stone	for brainstorming with me
Joanne Mason	for infinite patience, and for guiding me through in baby steps
Ian Newsome	for getting me equipment, yesterday
Linda Flemming	for teaching me how to cut sections
Roy Stewart	for help with *Scion Image*
Dr John Goepel	for telling the truth
Dr Jeremy Oakley	for explaining complicated statistics
Nicola Hewson-Stoate	for understanding everything I went through
Steph Borg	for answering all my stupid questions
Jan Bikker	for tolerating my 'thinking aloud' sessions
Lucy Morecroft	for statistics help and laughter therapy
Steph Davy	for helpful suggestions
My family	for crisis management and constant, unwavering love

I would also like to thank the Department of Forensic Pathology and the University of Sheffield for helping me to complete my thesis by providing a much-needed fee waiver, as well as a friendly, thought-provoking environment in which to work. Of course, the contribution of the twenty-nine individuals whose fractures form the basis of this research must not be forgotten. Without them, this research would not have been possible.

The accurate, reliable estimation of the 'age' of a fracture, or the time elapsed since trauma was sustained, has important implications in a variety of forensic contexts. Such information could greatly aid the forensic diagnosis of child abuse, the reconstruction of events during a violent incident such as homicide or a road traffic accident, and assist in the identification of unknown remains. Forensic fracture dating has largely relied on radiographical and histological evidence, but has lacked precision and consistency. The research presented here aims to test the hypothesis that correlations exist between the histologically- and immunohistochemically-observable phenomena at a fracture site and the known trauma-death interval of an individual. This was achieved by comparing the known trauma-death interval (TDI) to the extent of healing visible on histological slides prepared from formalin-fixed, paraffin-embedded, decalcified blocks of bone excised from the fracture site of 52 rib, skull and femur fractures from 29 individual forensic cases submitted to the Medico-Legal Centre Sheffield between 1992 and 2002. The slides were stained with haematoxylin and eosin to stain nuclei and cytoplasm, Perls' Prussian Blue stain for haemosiderin granules, mono-clonal anti-CD68 antibody for osteoclasts, and anti-bone sialoprotein antibody as an osteoblast and osteocyte marker. Quantifiable parameters such as the percentage cover of red blood cells, of living and necrotic compact bone, and the size, abundance and dispersal of immuno-positive and inflammatory cells were examined and compared to the TDI using human observers and *Scion Image* histomorphometry software. Statistically significant correlations were found between TDI and the presence of haemosiderin granules later than three days post-trauma; and the dispersal and location of CD68 positive cells; as well as the estimated percentage cover of fibroblasts and red blood cells at the fracture site. Other trends and correlations were found, which contribute to the understanding of bone's immediate responses to trauma. It is hoped that this research may aid the prediction of the time elapsed since trauma in a forensic context and broaden the scope of trauma analysis in forensic anthropology.

Keywords

forensic anthropology; fracture; fracture healing; trauma-death interval; histology; immunohistochemistry; CD68; bone sialoprotein

01 : INTRODUCTION

01 : 01 Bone histology

01 : 03 How do we detect fractures?

02 : PILOT STUDY

03 : MATERIALS AND METHODOLOGY

04 : RESULTS OF QUALITATIVE AND SEMI-QUANTITATIVE OBSERVATIONS

05 : RESULTS OF QUANTITATIVE OBSERVATIONS

06 : DISCUSSION

01 : INTRODUCTION

01 : 04 How do fractures heal?

01 : 05 Factors that influence healing

03 : MATERIALS AND METHODOLOGY

04 : RESULTS OF QUALITATIVE AND SEMI-QUANTITATIVE OBSERVATIONS

05 : RESULTS OF QUANTITATIVE OBSERVATIONS

06 : DISCUSSION

01 : INTRODUCTION

"The important thing in science is not so much to obtain new facts as to discover new ways of thinking about them."

Sir William Bragg (1862 - 1942)

Fractures are like gold dust to forensic anthropologists. They represent a source of information about the activity and lifestyle, general health and access to medical assistance of the individual reduced to the pile of remains on the mortuary gurney. Fractures are also instrumental in the identification process, as they are unique to the individual, and provide an easy point of comparison between ante-mortem and post-mortem radiographs. However, fractures have yet more information to yield. Clinical and forensic pathologists have already recognised the potential of the histological analysis of fractures to provide temporal information about the trauma present, and subsequently about the individual. This research is about introducing forensic anthropology to a valuable resource that has already been tapped to a certain extent by different scientific disciplines. It is about broadening the scope of trauma analysis in forensic anthropology, and maximising the value of forensic evidence, by initiating research into the dating of fractures using novel histological and immunohistochemical techniques. This research is based on the premise that it should be possible to accurately quantify the extent of healing at a fracture site by looking at the microscopic changes that occur as the body responds to trauma, and comparing this to the known time elapsed since trauma, which should subsequently allow estimation of the trauma-death interval. The term 'trauma-death interval' has been coined to describe the time elapsed, whether registered in seconds, hours, days or weeks, between the infliction of trauma and the death of the individual.

Existing scientific research on the radiological or histological dating of fractures has primarily been restricted to the field of forensic pathology and the problem of diagnosing the physical abuse of children. Physical child abuse or non-accidental injury is characterised by multiple fractures, occurring at regular, frequent intervals, and the correct diagnosis of child abuse is reliant on unequivocal evidence of fractures that do not tally with the reported history of injury. A lack of correlation between the given story and the skeletal evidence is usually the trigger of suspicion (O'Connor and Cohen, 1998). In order to substantiate claims of inconsistency between the given history and the medical evidence, an accurate method of estimating the age of an injury such as a bone fracture is vital. Estimation of the 'age' of the fractures can be used to weigh against the testimonies of alleged abusers and can aid the distinction between genuine accidental injury and repeated abuse. Conventionally, the forensic pathologist's estimation of the time elapsed since fracture has been reliant on an approximation of the extent of healing visible

radiographically, compared to the age of the child. It has focussed primarily on the degree of radio-opaque callus formation visible, and has thus been limited in its precision due to the lack of callus formation before about one week after fracture. The earliest feature visible radiographically is periosteal bone formation, which can be imaged at the earliest four days after injury, but generally appears between ten and 14 days post-fracture (Klotzbach *et al.* 2003; O'Connor and Cohen, 1998). Loss of fracture line demarcation, and the apposition of internal and external callus are also indications of healing that become visible between ten and 14 days after fracture. However, this timeline is only a generalised model, and individual factors such as the age and nutritional status of the child, the severity and location of the trauma, and the extent of displacement and immobility of the fracture, can all compound the precise estimation of the time since fracture from radiographs. A more accurate way of estimating the extent of healing is contact radiography, where thin sections of the dissected bone are placed directly on the x-ray film before exposure, which provides a high resolution image which can be used to examine periosteal reaction, fracture gap and evidence of resorption (Klotzbach *et al.* 2003). However, despite improved methods, evidence of healing in very recent fractures is still difficult to diagnose using radiography.

To date, histological analysis of the fracture site has been used simply as a tool to confirm conclusions drawn based on radiographical evidence. It is only recently that diversification has occurred within the discipline to investigate the possibilities of quantifying fracture healing using histological and - perhaps more excitingly - immunohistochemical techniques. The potential potency of this method of identifying cases of child abuse is gradually being recognised by more and more researchers in the field, and increasing emphasis is being placed on the specific dating of fractures (Islam *et al.* 2000; O'Connor and Cohen, 1998; Yeo and Reed, 1994).

Estimation of the time since fracture relies on the fact that bone healing follows a predictable pattern of stages. The stages of fracture healing have been demonstrated to last a certain length of time, although there are considerable overlaps between the different phases. However, it is this consistency between individuals, from fracture site to fracture site that allows the backwards projection of the time period elapsed since the onset of the trauma. The stages of healing can be investigated on a macroscopic or microscopic level, but obviously the smaller the increments of time between observable events, the greater the precision of the prediction.

Traditionally, fracture repair has been investigated using experimental animal analogues, through the creation of a standardised fracture in the diaphysis of a long bone, and subsequent investigations of healing visible after distinct time intervals (Oni, 1995). Likewise, protein and enzyme expression have been

examined immunohistochemically to date wound healing in soft tissue injuries in rat models (Raekallio and Mäkinen, 1967). Oni's study (1995) represents a preliminary foray into the use of immunohistochemical techniques to distinguish between different stages of healing in bone. Oni also suggested the use of bone sialoprotein as a marker of mature osteoblast function. He found its expression localised to the osteoid seams and newly-formed bone trabeculae (Oni, 1995).

The current research finds its niche within the context of previous work by supplementing the work of Oni (1995), Raekallio (1980) and Klotzbach (2003) by using novel immunohistochemical markers in order to attempt to date fractures, as well as introducing the concept of using microscopic analysis of fracture healing to mainstream forensic anthropology. Forensic anthropology methods traditionally have concentrated on the gross morphological changes associated with fracture healing as a means of estimating their age, focussing on the periosteal and callus formation visible with the unaided eye. There has been some recognition of histological methods of interpreting fractures, and the role it can play in the diagnosis of child abuse in forensic anthropology literature (Walker *et al.* 1997), but there has been little investigation of the way in which a reliable method of fracture age estimation could contribute to other forensic analyses of skeletal remains. It is hoped that this research can open the eyes of practitioners to the potential applications of trauma-death interval estimation, and that its use may become more widely recognised.

There are several important potential forensic applications of an accurate system of determining the trauma-death interval from a fractured bone. The ability to accurately determine the length of time between trauma and death would aid forensic anthropologists attempting to piece together the circumstances of an individual's death. Wherever there is bone trauma in a forensic context, there is likely to be a role for the estimation of the age of the fracture. The distinction between ante-, peri- and post-mortem trauma is one of the fundamental problems faced by forensic anthropologists. A study of the microscopic processes that occur immediately after fracture, and the typical timeframe of their expression histologically, could aid the distinction. In a violent attack, sequencing of the blows is often of forensic importance, and ageing fractures relative to each other would allow a physiological reconstruction of events. Such reconstruction, if detailed and thorough enough, may even be used to support or refute alibis. It has been said that 'even the cause of death is sometimes less important than the reconstruction of events' (Raekallio, 1980). Forensic scenarios are not always as straightforward as they first appear, and a detailed analysis of the timing of the trauma could lead to a greater understanding of what happened. For example, a dead body may be subject to trauma such as being hit by a motor vehicle or being caught in the propeller of a boat. In these situations, justice relies on accuracy of observation and robust interpretation of the wounds found

(Raekallio, 1980). The survival time of the victim represents a fundamental element to the investigation, and also may be possible to deduce from an estimation of the trauma-death interval. It can change the perspective of the events and provide crucial clues as to manner and cause of death.

For identification purposes, trauma-death interval investigation can facilitate the post-mortem creation of an osteological or biological profile of an unknown individual during life. Evidence of fracture can suggest limps or deformities during life, and knowing the approximate 'age' of a fracture can deepen the understanding of the course of an individual's life. The knowledge that, for example, the individual suffered from a broken leg two years prior to a fractured finger, can greatly reduce the number of possible identities presented for the unknown remains. Similarly, such information can significantly facilitate the search for ante-mortem medical records and radiographs, by giving investigators an indication of the antiquity of the injury in the individual's lifetime. Ante-mortem medical records and X-rays represent the 'jackpot' of the identification lottery, as they provide a point of comparison and reference between a named individual and unknown remains.

An application of trauma-death interval estimation with unfortunately increasing relevance today is that of compensation claims after accident. An issue that came to light after the Pan Am Flight 103 crash in Lockerbie, Scotland in 1988, was that of the survival times of the victims and their possible rights to compensation. Professor Anthony Busittil testified that it was likely that some victims were conscious or aware of their surroundings and their ordeal in the few seconds before their death (Auode, 2000 e-reference[1]). Any investigation into the presence or absence of vital response to trauma, especially of histological features present in the first few minutes after fracture, may help to determine the worth of such compensation claims. It would also serve to give bereaved relatives comfort and peace of mind, if reassured that their loved one died quickly before regaining consciousness. This may be achievable through the careful charting and categorisation of the body's immediate cellular responses to trauma.

This research project has tried to take an alternative approach to the animal analogue models that have traditionally fuelled research into the temporal analysis of fracture healing (Oni, 1995; Raekallio and Mäkinene, 1967); not only by using human fracture samples, but also by retrospectively examining the extent of healing visible in samples of known time since trauma. The use of human material was pursued in an effort to make the results more applicable in a forensic context, and to reduce the need for extrapolation

[1] e-reference. Cited at end of literature references, using the conventions stipulated by the Harvard Citation Guide (Scott, 1998).

and conversion based on animal lifetimes and metabolic rates. However, there has been considerable sacrifice in the reproducibility and standardisation of fractures caused by using human forensic samples.

In order to find appropriate histological samples of fractured bone to use for the research, the autopsy records of the Medico-Legal Centre in Sheffield were scrutinised. Any case submitted to the Medico-Legal Centre between 1992 and 2002 where a fracture was present was examined. Only cases where there was adequate information regarding the date of the trauma believed to have caused the fracture and the date of the death of the individual, accompanied by a formalin-fixed, wax-embedded histological sample of the appropriate bone could be used. Samples of the fractured bone had been taken in each case for histological analysis as part of the standard forensic investigation into the cause of death of the individual. No cases less than two years old could be used, as these remained *sub judici*. A total of 29 individuals and 52 fractures were found to fit these research criteria. The research therefore is strongly retrospective in its outlook, and no samples other than those originally taken at autopsy were used for any research purposes.

This raises the issue of the ethical procedures taken in the study. When the project was started in 2001, it was common practice to use archived residual fixed material for this type of research. The tissue was obtained lawfully under the Coroner's rules, and all samples were anonymised. All samples were taken by a Home Office registered forensic pathologist, as part of the routine collection of tissue for investigative purposes. At the time of autopsy, the pathologist did not envisage the use of the tissues for research purposes and the issue of consent would not have arisen. The samples were taken at the Medico-Legal Centre in Sheffield, which is a non-NHS premises, and as the individuals autopsied there are not NHS patients, there was no formal requirement for NHS ethical committee approval. In addition, the retrospective nature of the selection of appropriate cases, often as much as ten years after the autopsies, would have made approaching families and relatives for consent very difficult in the majority of cases, should it have been deemed necessary. As a result of these factors, in 2001 when the project was started, it was not apparent that ethical approval was necessary in order to continue with the research. However, during the course of the research, there was increasing public concern about ethical issues following a number of well-publicised incidents concerning the use and misuse of post-mortem tissue. This made it apparent that the ethical basis of the research needed reconsideration. Guidance from the South Sheffield Research Ethics Committee was sought immediately (see Appendix 01), outlining the circumstances of the research and the problems with gaining consent, but at the time of submission, the results of the Committee's deliberation was unknown.

This research project aims to build upon the previous work in fracture dating, by combining techniques known to be effective in this field with newer, more experimental immunohistochemical methods in order to attempt to estimate the trauma-death interval. Samples of human bone of known trauma-death interval were examined, and the histological features and protein expression visible compared to time since fracture, in an effort to find features that correlated in any way with the trauma-death interval. Perls' Prussian Blue stain was used to test for the presence of haemosiderin granules in the bone tissue and extracellular matrix, as this has been recognised as an indicator of length of time since trauma previously (Iancu, 1992; Vanezis, 2001). CD68 was chosen as an immunohistochemical marker, as it is a well-known to be present in macrophages, which are abundant during the inflammation and resorption stages of fracture healing. Bone sialoprotein was chosen as a complementary immunohistochemical marker, as it is expressed in osteoblasts and osteocytes, active during the bone formation stages of the healing process. The availability and relative inexpense of these markers also contributed to their use.

This project aims to answer a few simple questions: Is it possible to accurately chart and quantify histological changes during the early stages of fracture healing? Are there any clear correlations between the histological or immunohistochemical features examined and the trauma-death interval? Would it be possible to extrapolate backwards and predict the trauma-death interval from the histological appearance or the specific immunoreactivity of a fracture section? The working hypothesis is that the answer to these questions is 'yes', and the null hypothesis is that there is no significant correlation between any of the examined features and the trauma-death interval, and that no predictions of trauma-death interval from histology slides of fractures would be possible. An attempt has been made to answer these questions through original research and experiment using samples of human bone fractures of known trauma-death intervals.

Before the methodology and results of the present study are presented, it is necessary to build an understanding of the context of this work within the existing framework of forensic trauma analysis. In order to guide the reader toward an understanding of the motives, expectations and limitations of this work, a broad background is given, addressing such fundamental questions as: what is bone? how is it composed? what is its histological structure? as well as what are fractures? and how are they detected? The stages of fracture healing are also described on a microscopic level. An immunohistochemical outline of the healing process is included, illustrating the relationship between the various proteins expressed at different times throughout the process, and how their fluctuating levels can be used to estimate the time since the fracture occurred. In addition, the factors that are believed to influence the rate of bone healing are examined, as these impact significantly on the observations and results obtained. The reader is then guided through the

pilot research (Chapter 02), the experimental methodology of the study proper (Chapter 03), and the bisected results and analyses (Chapters 04 and 05). A discussion of the significance of the empirical results, the implications of the findings in the context of the previous research, and the limitations of the research is given in Chapter 06. The final conclusions are presented in Chapter 07.

Introduction

Bone is the principal calcified tissue of vertebrates, and functions to protect and support the soft tissues of the body. Despite its strength and rigidity, it is dynamic and flexible, and so has been the subject of mechanical and microscopic investigation for decades. The application of histological methods to the tissue of bone has been very successful, and implemented in a variety of scientific pursuits. Bone histology has a wide range of applications, in the fields of clinical and forensic pathology, as well as that of identification sciences. It is used mainly to diagnose tumour and metabolic bone diseases in living patients, but also has functions in the post-mortem examination. This introductory chapter aims to provide the reader with a detailed image of the macroscopic and microscopic structure of bone and an understanding of the physical components of bone with key roles in the processes associated with fracture healing.

Histology is the science of cells, the cellular structure and the extracellular matrix of tissues, and their combined functions (Junqueira *et al.* 1995; Janssen, 1984). The word histology is derived from the Greek *histo*, meaning web or tissue, and *logos*, meaning study. Unlike almost any other medical discipline, histology takes a direct approach to the recording of cellular data, and in so doing has promoted the recognition and understanding of natural and pathological changes to the tissues of the body (Janssen, 1984). Histological techniques have been successfully utilised by the fields of chemistry, physiology, immunology and pathology, to produce new disciplines of histochemistry, histophysiology, immunohistochemistry and histopathology. Tissue is examined using light or electron microscopy, which has meant that there has been a chronological correlation between the development of the discipline and advances in microscope technology.

Introduction to bone as a tissue

Bone constitutes almost all of the hard, mineralised component of the skeleton in most species (Pritchard, 1972a). Yet, it is a highly vascular, living, dynamic mineralised connective tissue, and is remarkable for its hardness, resilience and capacity to regenerate, as well as its highly specialised growth mechanisms (Soames, 1995). The bones of the adult human body are the 206 individual organs of the skeletal system, which are actually composed of not only bone tissue, but also of cartilage, fat, connective tissue, haematopoietic bone marrow, nerves and vessels (Gurley and Roth, 1992). Like all other connective tissues, bone consists of cells and an intercellular matrix. The matrix is composed of organic materials, such as collagen fibres, combined with an inorganic mineral component, which makes up about 60% of its dry weight in mature bone (Gurley and Roth, 1992; Pritchard, 1972a; Soames, 1995). The inorganic element of bone consists of mainly inorganic

crystalline salts, which are principally composed of calcium and phosphate. Calcium and phosphate molecules combine to form crystals of hydroxyapatite, the chemical formula for which is:

$Ca_{10}[PO_4]_6[OH]_2$ hydroxyapatite

The collagen and mineral salts work in combination to strengthen the bone (Lujan and White, 2002). The fibres of collagen have great tensile strength, so can endure stretching forces, while the salts, which possess physical properties similar to marble, can have impressive compressional strength. These combined properties, intrinsic to the biphasic structure of bone, in addition to the degree of bonding between the collagen fibres and the crystals, provide bone with its unique characteristics of extreme tensile and compressional strength, coupled with flexibility and elasticity. The tensile strength of bone approaches that of reinforced concrete or traditional cast iron (Soames, 1995), while the compressional strength far exceeds that of the best man-made reinforced concrete (Lujan and White, 2002). However, despite these strengths, bone suffers from a weak resistance to torsional or twisting forces.

The primary function of the bones and the skeletal system is to provide mechanical shape and support to the body, as well as allow movement (Soames, 1995). Bones have been compared to man-made levers, supporting columns, arches, struts and girders (Soames, 1995). Bones are not only similar to these structures in external shape and internal architecture, but also in their uses and functions (Soames, 1995). They provide the resistance against which muscles can act, as well as function mechanically to protect the delicate soft tissues of the body, such as the brain, heart, lungs and other organs (Gurley and Roth, 1992). Bones also have an important metabolic function, as a reservoir for calcium, phosphate and other ions. Because bone is intensely vascularised in comparison to cartilage or other connective tissue, the mineral salts can be removed from the bone and distributed easily around the body to wherever they are needed (Marieb, 2001; Soames, 1995). Equally, minerals can be taken up by the bone, should they be required for remodelling or other purposes. Bones also provide host sites for the haematopoietic tissue, or the bone marrow. Marrow is found in the numerous small spaces between the trabeculae in all cancellous bone, and even in the larger Haversian canals of lamellar bone. It differs in composition in different bones, and at different ages of the skeleton. It occurs in two forms, yellow and red marrow (Bannister, 1995).

The macroscopic structure of bone

Bones are rigid, lightweight organs with a high tensile strength (Gurley and Roth, 1982; Soames, 1995), and this is reflected in their macroscopic structure. The mechanical functions of bones, coupled with their microscopic organisation, contribute to the gross appearance of bones. Wolff described this relationship between the morphology of the bones and their function, and the response of bones to mechanical stress, in his law of 1892, which states,

"..every change in the form and function of bones, or in their functions alone, is followed by certain definite changes in their internal architecture and equally definite changes in their external conformation in accordance with mathematical laws." Wolff, 1892

There are four categories into which all bones can be placed with regard to their morphology. Long bones are the tubular bones of the limbs – the humeri, ulnae, radii, femorae, tibiae and fibulae. The bones of the hands and feet, including the metacarpals, metatarsals and phalanges are also classified as long bones. As their name suggests, they are considerably longer than they are wide. Short bones are roughly cuboid in shape, and good examples of these are the carpals of the wrist, and the cuneiforms of the ankle (Marieb, 2001). Sesamoid bones are categorised as short bones, and are defined as those that form within a tendon. The patella is such a sesamoid bone, and others can develop pathologically, for example within the tendons of the first metacarpal or metatarsal (thumb and big toe). Flat bones are thin, flattened and usually slightly curved in shape. Most of the bones of the calvarium are flat, as are the bones that make up the sternum and the scapulae. All other bones that are not easily categorised are lumped together in the all-encompassing class of irregular bones. This includes the vertebrae and the bones of the pubis, ischium and ilium (Marieb, 2001).

Bone is further classified into lamellar, or mature bone and woven or immature bone. This is dependent on the organisation of collagen fibres within it (Biswas and Iqbal, 1998). In mature, lamellar bone, the collagen fibres appear in a regular, parallel arrangement, and have a highly organised infrastructure. This organisation makes it mechanically strong (Biswas and Iqbal, 1998). In contrast, immature, woven bone is composed of irregularly organised coarse collagen fibres and a large number of osteocytes. Woven bone has a low mineral content, which makes it mechanically weak. However, what it lacks in strength, it compensates for in the speed with which it is formed. This makes it the first type of bone to develop in the embryo and after fractures, but it is gradually remodelled and replaced with the stronger lamellar bone (Biswas and Iqbal, 1998). Immature bone will be discussed later in the chapter.

Mature lamellar bone

Mature bone tissue is classified on the basis of its gross and microscopic structure into compact bone, which constitutes the bone cortex, and fine and coarse cancellous bone, which form the central regions of mature bones (Gurley and Roth, 1992). Every bone of the skeleton has a dense outer layer which looks smooth and solid to the naked eye (Marieb, 2001). This external layer is the compact or cortical bone. Internal to this is cancellous bone, which has a honeycomb structure of small needle-like or flat struts, called trabeculae, which is derived from the Latin for 'little beams'. All bones have trabeculae in differing amounts, which are not only resistant to mechanical stresses, but are also the sites of bone

marrow production. The numerous small spaces between the trabeculae are occupied by marrow, which is either hematopoietic or adipose. The trabecular architecture of most bones is conducive to lightness without loss of strength, and is an economic structure in terms of biological materials (Soames, 1995).

In the adult skeleton, every long bone is composed of three distinct components. The diaphysis is the central shaft of the long bone, which forms the long axis of the bone. It is constructed of a relatively thick collar of compact bone, which surrounds a central medullary cavity (Marieb, 2001). At each end of the diaphysis, there is an epiphysis. In many cases, they are more expanded than the diaphysis of the bone. Epiphyses are also composed of an external compact bone shell, with an internal cancellous core. There is a particularly high concentration of cancellous bone at the epiphyses, as cancellous bone provides the greatest amount of elastic strength, and the epiphyses are subject to the greatest forces of compression within the skeleton (Lujan and White, 2002). Epiphyses either articulate with another bone, or form the distal extremity of the skeleton, as in the case of the phalanges of the hands and feet. Those that meet a joint with another bone are covered with a thin layer of articular or hyaline cartilage. This cushions the opposing bone ends during joint movement, and so absorbs stress. The diaphysis is separated from the epiphyses by the epiphyseal line. In adults, this is a remnant of the epiphyseal plate, which is a disc of hyaline cartilage that grows during childhood and puberty to lengthen the bone (Marieb, 2001). These are often clearly visible on radiographs of growing children. The metaphysis is a small portion of bone that connects the diaphysis to the epiphyseal line, or to the epiphyseal plate in juvenile skeletons. Short, irregular and flat bones of the skeleton also have a simple macroscopic structure. They consist of cancellous bone covered in endosteum, sandwiched between thin plates of compact bone, externally covered with periosteum. The internal cancellous bone is termed the diploë. Because these bones are not tubular or cylindrical in shape, they have no diaphysis or epiphyses. They contain bone marrow between the trabeculae, but there is no marrow cavity.

An examination of the cross-section of bones shows that the morphology of most bones is designed to provide a maximum strength to weight ratio (Gurley and Roth, 1982). The cortex is a plate or tube, made up of sheets of compact or cortical bone, which is strengthened by spicules of coarse cancellous bone. The spicules follow the lines of maximum force and stress, as predicted by Wolff's law (Gurley and Roth, 1982). The size and thickness of the cortex also varies according to the relative stress placed on different areas of the bone. Cross struts connect the trabeculae following the lines of stress for added support (Gurley and Roth, 1982). In the case of the femoral head and neck, the cortex on the medial side of the bone is thicker than that on the lateral side, since this weight-bearing region is under more mechanical stress (Gurley and Roth, 1982). Growth, modelling and remodelling after trauma or pathology are also affected by the phenomenon described by Wolff's law. The medullary cavity is

internal to the compact bone, and less dense. The medulla is composed of cancellous bone and the soft tissues, such as nerves, blood vessels, adipose tissue and the hematopoietic elements.

Periosteum and endosteum

The external and internal surfaces of bone are covered by layers of bone forming cells and connective tissue called the periosteum and the endosteum. The periosteum covers the outer surface of the bone. Its outer layer contains blood vessels, nerves and lymphatics (Biswas and Iqbal, 1998), as well as collagen fibres and fibroblasts (Junqueira *et al.* 1995). Bundles of periosteal collagen fibres, called Sharpey's fibres, penetrate the bone matrix, binding the periosteum to the bone. The inner, more cellular layer of the periosteum is composed of flattened cells with the potential to divide by mitosis and differentiate into osteoblasts or osteoprogenitor cells (Junqueira *et al.* 1995). The endosteum lines all the internal surfaces of cavities within bone (Junqueira *et al.* 1995). It lies on the interface between the compact bone and the medullary cavity, and between the trabeculae in cancellous bone. It is composed of a single layer of flattened osteoclasts, macrophage-like cells, osteoprogenitor cells, and active osteoblasts, as well as a small amount of connective tissue (Gurley and Roth, 1992; Junqueira *et al.* 1995). It is therefore considerably thinner than the periosteum (Junqueira *et al.* 1995). The principal functions of the periosteum and endosteum are to provide nutrition to the osseous tissue, and to replenish the bone with a continuous supply of new osteoblasts for the growth and repair of bone (Junqueira *et al.* 1995).

The microscopic structure of compact bone

Compact bone is usually limited to the cortices of mature bones, and is of extreme importance in providing their strength (Soames, 1995). Its thickness and architecture varies between bones, reflecting their overall shape, position and functional roles (Soames, 1995). Compact bone appears dense and smooth to the naked eye, but microscopic examination reveals a complex structure. It is made up of densely packed cylindrical 'systems', called osteons, which are circular or oval in cross section, and run as parallel columns along the long axis of the bone. Between the osteons are lamellae, which encircle the osteons in concentric rings, and fill up the spaces where the osteons do not tessellate. This configuration of cellular systems gives rise to the hard, dense and tough nature of compact bone.

Osteons

Osteons are also termed Haversian systems after their discovery and description by Clopton Havers in 1691. Each osteon is a long, often bifurcated cylinder which runs parallel to the long axis of the diaphysis of the bone (Junqueira *et al.* 1995). It consists of a central canal surrounded by concentrically arranged lamellae. The canal in the centre of the osteon carries blood vessels, nerves and loose connective tissue around the whole bone, and are formed when bone matrix is laid down

around the pre-existing blood vessels (Junqueira *et al.* 1995). There are also channels, which travel transversely through the osteon columns and perforate the concentric lamellae. These are named Volkmann's canals, and allow communication between osteons and the periosteum, the marrow cavity and each other (Junqueira *et al.* 1995). Each osteon is separated from the adjacent one and from the interstitial lamellae by a cement line which stains darkly when dyed with haematoxylin (Revell, 1986). Straight or smoothly curved cement lines mark stages when osteon formation has stopped, whereas irregularly shaped, indented lines indicate site of new bone formation after resorption. These are sometimes referred to as 'reversal' lines (Revell, 1986).

There is great variability in the diameter of the osteons. Each central canal is surrounded with between four and 20 concentric lamellae, depending on the age of the osteon (see Figure 01: 01: 01). Successive concentric layers of lamellae are deposited gradually, starting at the periphery and working inwards towards the central canal. The innermost lamella is therefore the most recently formed (Junqueira *et al.* 1995). Under plane polarised light, the lamellae of osteons appear to alternate between bright and dark layers (Junqueira *et al.* 1995). This is thought to be due to the differential orientation of the collagen fibres in each alternate layer (Junqueira *et al.* 1995; Pritchard, 1972a). In each lamella, the collagen fibres run parallel to each other in a helical, spiralling course vertically up the osteon column. The lamellae appear to alternate between a clockwise and anti-clockwise direction in adjacent layers. This organisation provides the bone with great strength, despite its low weight (Junqueira *et al.* 1995). In addition to the concentric lamellae around the osteons, there are three other types of lamellae found in compact bone; inner circumferential lamellae, outer circumferential lamellae and interstitial lamellae.

Figure 01: 01: 01 A paraffin section of fixed, decalcified cortical bone, stained with haematoxylin and eosin stain, seen at x30 magnification. The Haversian system is clearly visible, as are the osteocytes trapped in the lacunae between the concentric lamellae.

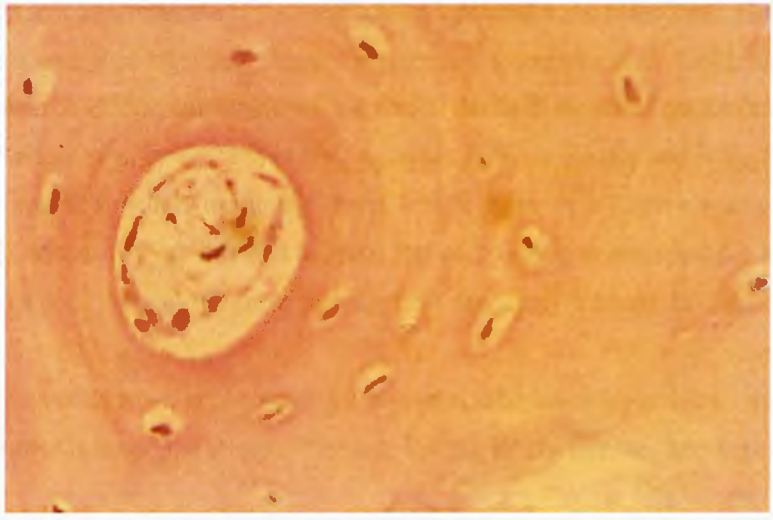

Inner circumferential lamellae are located on the inner border of the compact bone, at the interface with the internal medullary cavity. The unicellular endosteum separates them from the cancellous bone of the medulla. The outer circumferential lamellae lie in several layers immediately beneath the periosteum, which is the outer surface of the bone (Junqueira *et al.* 1995). Between the concentric lamellae surrounding each osteon, cells called osteocytes occupy small cavities called lacunae.

Osteocytes

Osteocytes, which are derived from osteoblasts, lie in the lacunae situated between the lamellae of osteons (Junquiera *et al.* 1995). Only one osteocyte occupies each lacuna. They are generally spidery in shape with a plump cell body and many long, fine branching cytoplasmic processes (Pritchard, 1972a). These processes are housed in thin, cylindrical channels of matrix known as canaliculi. Osteocytes vary wildly in size, shape and cytoplasmic detail, as well as in the density and regularity with which they are packed in the matrix (Pritchard, 1972a). Their abundance and concentration is usually dependent on the type of bone they are in (Gurley and Roth, 1992). In mature, lamellar bone, they are relatively sparsely distributed in between the concentric lamellae, and are small and spindle-shaped. Contrastingly, in immature, woven bone, osteocytes are randomly distributed throughout the matrix, and are large, and plump or spherical spindles (Gurley and Roth, 1992).

The exact functions of osteocytes are not yet clear (Soames, 1995). It is widely thought that they play an essential role in maintaining bone, and that their death leads to the resorption of the matrix by osteoclast activity (Soames, 1995). It has also been suggested that they are involved in signalling the requirement to resorb microdamaged compact bone, and to repair fractured trabeculae with microcallus (Soames, 1995). They may also act as local sensors of the mechanical and chemical state of the bone, and can initiate resorption or addition of the matrix at the surface accordingly (Soames, 1995). Osteocytes may also be responsible for the exchange of ions with the bone matrix and the extracellular spaces (Gurley and Roth, 1992). The long, dendritic processes of the osteocytes extend through the canaliculi of the bone, crossing lamellae but not the cement lines. They connect via gap or nexus junctions with the processes of the neighbouring osteocytes and osteoblasts (Gurley and Roth, 1992). Molecular exchange takes place along the processes (Junqueira *et al.* 1995), and it is thought that, under certain conditions, osteocytes are involved in the rapid release of calcium and phosphorus from the mineralised bone, by a process called 'osteotic osteolysis' (Gurley and Roth, 1992). In doing so, they may manufacture and resorb the martix around them, in a manner which is observable histologically (Pritchard, 1972a). It is also believed that each osteocyte is responsible for the life of a section of bone around it, about 100 μm in diameter in all directions (Pritchard, 1972a).

The life span of an osteocyte is not known, but it is thought to be extremely variable, ranging from only a few days to over a decade in length (Pritchard, 1972a). Empty lacunae, and lacunae containing

pyknotic remains of osteocytes, are often found after injury to the bone, especially in elderly individuals (Pritchard, 1972a). Empty lacunae are an indicator that the osteocytes and therefore the bone matrix immediately surrounding them is dead (Pritchard, 1972a). Osteocyte death is followed by the resorption of the matrix by osteoclasts in adjacent living tissue (Junqueira *et al.* 1995), but it is not clear how long the dead bone persists before it is reabsorbed (Pritchard, 1972a).

Osteoclasts

Osteoclasts are large, multinucleated cells with many branched processes (Biswas and Iqbal, 1998), found at sites where bone is in the process of physiological or pathological resorption (Hancox, 1972). They are 40 to 100 μm in diameter, with an average of 10 to 15 nuclei, although the number may actually range from about two to as many as 100 (Gurley and Roth, 1992). Because osteoclasts are mobile, their shape can look variable in fixed tissue histological sections. The cells may be flattened against the bone in the form of a thin, plate-like cytoplasmic layer, or the cytoplasm may be 'bunched' up, so that the osteocyte appears as a roughly spherical mass (Hancox, 1972). The cell bodies may be divided into lobes, or show processes or branches (Hancox, 1972), which are often quite irregular and vary in thickness and shape (Junqueira *et al.* 1995).

Osteoclasts are derived from mononuclear, hematopoietic progenitor cells. They are thought to arise primarily by fusion of the progenitor cells, to have the ability to constantly acquire or shed nuclei, and to be phagocytic (Biswas and Iqbal, 1998; Gurley and Roth, 1992). With these properties, osteoclasts are largely responsible for bone resorption (Gurley and Roth, 1992). It is thought that their activity is stimulated by the secretion of paracrine and possibly autocrine factors by osteoblasts or the osteoprogenitor cells (Gurley and Roth, 1992). Lymphokines, leukotrienes, prostoglandins and other osteoclast stimulating factors have been suggested as the messengers for osteoclast stimulation and activation (Gurley and Roth, 1992). Under normal conditions, active osteoclasts are directly apposed to the surface that is to be reabsorbed. After a short period of reabsorption, they are found in small troughs, called Howship's lacunae (Biswas and Iqbal, 1998; Gurley and Roth, 1992), which are produced as a result of localised osteoclast attacks on the bone matrix (Hancox, 1972). Howship's lacunae are quite easily identifiable at low magnifications as saucer-like depressions or deep pits on the bone surface (Hancox, 1972). The osteoclasts may be still visible within the lacunae, or they may have disappeared, in which case the lacunae are subsequently filled with new bone or connective tissue (Hancox, 1972).

Osteoclasts contain numerous mitochondria and vacuoles, many being tartrate-resistant acid phosphotase-positive lysosomes (Soames, 1995). The granular endoplasmic reticulum is relatively sparse considering the size of the cell, and they have extensive perinuclear Golgi apparatus (Soames, 1995). At the site of bone resorption, there are numerous transport vesicles and vacuoles between the

Golgi stacks and the surface of the osteoclast cell (Soames, 1995). The surface of the osteoclast is highly folded with leaf and finger-shaped processes, which form a ruffled membrane or border, fanning out from the osteoclast surface to the bone surface (Hancox, 1972; Junqueira *et al.* 1995; Soames, 1995). Around the perimeter of the ruffled membrane is a well-defined clear zone, which is devoid of organelles, but rich in actin microfilaments (Junqueira *et al.* 1995; Soames, 1995). This zone is a site where the osteoclast is firmly attached to the bone matrix, which serves to create a microenvironment for bone resorption (Junqueira *et al.* 1995).

Evidence of the involvement of osteoclasts in bone resorption is provided by visualisation techniques such as autoradiography and time lapse video recordings (Hancox, 1972; Väänänen *et al.* 1998). Hancox cites experiments where small pieces of calvarium bone were filmed *in vitro.* It appeared possible to see the bone matrix disappearing around the osteoclasts. Bone appeared to 'melt away', and apparently 'dissolved' beneath the osteoclasts (Hancox, 1972). Also clear was that osteoclasts were mobile, and exhibited a back and forth sliding motion against the resorbing surface (Hancox, 1972). Autoradiographic studies (Arnold and Jee, 1957) convincingly showed that plutonium injected into dogs became incorporated into newly formed bone deposited by osteoblasts, and subsequently was resorbed by osteoclasts (Hancox, 1972). Autoradiographic preparations showed isotope 'hot spots' within the osteoclasts, indicating that they had taken in labelled material from the adjacent bone (Hancox, 1972). This is now known to consist of products of bone resorption, taken up by the osteoclast's cytoplasm, in order to be digested further, and then transferred to blood capillaries (Junqueira *et al.* 1995).

Osteoclast activity is thought to be stimulated by a number of differing factors. Agents released by osteoblasts and a variety of other cells, such as macrophages and lymphocytes, appear to prompt osteoclasts to resorb bone (Soames, 1995). A rise in the concentration of calcium within the osteoclast leads to the inactivation of the cell, whereas a reduction in the intracellular calcium levels stimulates the cell into action (Soames, 1995). Various factors such as parathyroid hormone and calcitriol ($1,25(OH)_2$ vitamin D3) are also involved in bone resorption (Hancox, 1972; Soames, 1995).

The exact method by which osteoclasts resorb bone is not known (Revell, 1986; Soames, 1995). The sequence of events in the process of degradation of the organic and inorganic components of the bone matrix is a matter for debate. Hydroxyapatite crystals or collagen fibres may be removed first, or both components may be resorbed simultaneously (Revell, 1986). It has been proposed that osteoclasts can only attack bone after its organic lining has been removed by osteoblasts or bone lining cells, revealing the mineralised surface (Soames, 1995). The demineralisation of the hydroxyapatite occurs locally where the ruffled border of the osteoclast approaches the bone surface. It is generally accepted that the dissolution of the mineral is a result of the targeted secretion of acid through the ruffled border

into the closed compartment of a resorption lacuna, which is separated from the extracellular matrix by the sealing zone (Väänänen *et al.* 1998). The low pH value is achieved and maintained in the resorption lacuna by the action of a high number of proton pumps at the ruffled border membrane (Väänänen *et al.* 1998). There is also much evidence to suggest that osteoclasts can degrade collagen and other organic components of the unmineralised or demineralised matrix, perhaps by the secretion of lysomal and non-lysomal enzymes, such as collagenase, gelatinase or cysteine proteases (Soames, 1995). Väänänen *et al.* (1998) have found that several proteolytic enzymes are also expressed by osteoclasts, such as matrix metalloproteinases (types 1 and 9) and cathespin K, and that these seem to play a central role in bone resorption (Väänänen *et al.* 1998). Matrix metalloproteinase 9 is found in high concentrations in osteoclasts, and is likely to act on type I collagen, either with interstitial collagenases or cathepsins, to induce a complete degradation of type I collagen (Väänänen *et al.* 1998). It is also thought that metalloproteinases are associated with the migration and attachments of osteoclasts (Väänänen *et al.* 1998).

The ruffled border is then thought to be involved in the transfer of material loosened by osteoclast activity from the bone edge into the osteoclast cell interior (Hancox, 1972). The ruffled border is essential for the activity of osteoclasts, and therefore for efficient bone resorption. The hereditary disease osteopetrosis is characterised by heavy, dense bones, often referred to as 'marble bones'. The osteoclasts in osteopetrotic bone lack ruffled borders, and so the process of bone resorption is defective (Junqueira *et al.* 1995).

When bone resorption has finished, it is possible that osteoclasts dissociate into mononuclear cells, possibly with the potential of fusing to form active osteoclasts again if suitably stimulated (Soames, 1995). The lifespan of an osteoclast nucleus has been estimated to be about 16 days, but some researchers (Jaworski *et al.* 1981) claim that *in vivo*, osteoclasts can live up to seven weeks.

Osteoblasts

Osteoblasts are basophilic, roughly cuboid mononuclear cells, measuring about 15 – 30 μm in diameter (Soames, 1995). They are differentiated, non-meiotic cells which arise from osteoprogenitor cells, and possibly from the de-differentiation of osteocytes when these are released from bone during its resorption. Ultrastructurally, osteoblasts have features typical of protein secreting cells, such as a pale, euchromatic, oval nucleus, away from the secreting surface, an extensive granular endoplasmic reticulum, large Golgi complex and numerous secretory vesicles (Soames, 1995). The nucleus of the osteoblast is usually found in one end of the cell, furthest from the bone surface, and the secretory vesicles and secretory surface are orientated towards the adjacent bone (Soames, 1995). Osteoblast cells contain prominent bundles of actin, myosin and other cytoskeletal proteins, which are associated with the maintenance of cell shape, motility and attachment. Their plasma membranes have many

extending processes, which reach between the cells and make contact with neighbouring osteoblasts and osteocytes at intercellular junctions (Soames, 1995). These processes become more prominent as the amount of matrix surrounding the cell increases (Junqueira *et al.* 1995). It is through the cytoplasmic processes that the activity of quite large groups of osteoblasts can be co-ordinated (Soames, 1995). For example, osteoblasts arrange themselves side by side to form a single-celled layer which covers the forming surfaces of growing or remodelling bone (Soames, 1995). They can be found in a variety of different formations, with their long axes parallel to the bone surface, or lying obliquely and overlapping like roof tiles (Pritchard, 1972b). The surfaces of osteoblasts are rich in alkaline phosphatase activity, located at the plasma membrane (Soames, 1995). In conditions of rapid bone formation or turnover, such as after trauma, some of this enzyme reaches the blood stream, and is detectable in blood samples (Soames, 1995).

Osteoblasts are the bone cells responsible for the synthesis, depostion and mineralisation of the organic components of the bone matrix, known as osteoid, which is composed primarily of type I collagen, small amounts of type V collagen, proteoglycans and glycoproteins (Junqueira *et al.* 1995; Soames, 1995). They also synthesise various macromolecules including the gamma-carboxyglutamic acid (GLA)-containing protein osteocalcin, matrix GLA-protein, as well as osteonectin, latent proteases and growth factors (Soames, 1995). Collagen production occurs in much the same way as in fibroblasts, initially in the granular endoplasmic reticulum, and later in the Golgi apparatus, before it is secreted out of the cell to the extracellular matrix (Soames, 1995). Secretion of the matrix components occurs at the cell surface, which is in contact with the older bone matrix (Junqueira *et al.* 1995). Secretion produces an osteoid layer of new, uncalcified matrix between the osteoblast layer and the previously formed bone, in a process known as bone apposition (Junqueira *et al.* 1995). Osteoid consists of coarse collagen fibres containing foci of initial calcification, and so the interface between the osteoid layer and the mineralised bone matrix is referred to as the 'calcification front' (Revell, 1986). The process of bone apposition is completed by subsequent deposition of calcium salts into the newly formed matrix (Junqueira *et al.* 1995). Osteoblasts mineralise the organic matrix by utilising alkaline phosphatase, which is present in osteoblasts which are actively forming bone, and the adjacent tissue (Revell, 1986; Soames, 1995).

There is also evidence to suggest that osteoblasts play an indirect but significant role in bone resorption, through hormone regulation (Soames, 1995). They bear receptors for parathyroid hormone and $1,25(OH)_2$ vitamin D3 and other resorption stimulants (Soames, 1995). During bone *deposition*, osteoblasts may inhibit osteoclast activity, or fail to stimulate them, but during bone *resorption*, in the presence of parathyroid hormone, osteoblasts release various agents which prompt osteoclasts to remove osseous tissue (Soames, 1995).

Once the skeleton has matured, and bone growth in length and width has stopped, osteoblasts virtually disappear from the periosteum. However, when an adult bone is subjected to trauma, stress or infection, irritants, vascular disturbances, or any other unusual pressures, osteoblasts reappear in the periosteum (Pritchard, 1972b). This evidence suggests that cells with the potential to multiply and differentiate into osteoblasts are present throughout life, but lying dormant in the periosteum until activated by an appropriate stimulus. Such cells have been termed osteoprogenitor cells (Pritchard, 1972b; Soames, 1995).

Osteoprogenitor cells

Osteoprogenitor cells are derived from pluripotential stromal cells present in the bone marrow and other connective tissues (Soames, 1995). They can proliferate and differentiate into osteoblasts prior to bone formation (Soames, 1995). The stromal cells are of mesenchymal origin, and resemble young fibroblasts. They are responsible for all bone formation during early development (Soames, 1995). It is thought that there may be two types or stages of osteoprogenitor cell, committed osteoprogenitors and inducible osteoprogenitors (Soames, 1995). Committed osteoprogenitors are only found associated with bone, and are completely dedicated to bone formation (Soames, 1995). Conversely, inducible osteoprogenitors are found in connective tissue and are probably able to differentiate and specialise into various connective tissue cells, such as fibroblasts, chondroblasts, osteoblasts, or myoblasts and adipose cells, depending on the nature of the stimulus (Soames, 1995). Cells that have differentiated into a particular type of cell may be able to revert to the original osteoprogenitor cell and then specialise again into osteoblasts (see Figure 01: 01: 02) (Soames, 1995).

Figure 01: 01: 02 A paraffin section of fixed, decalcified, compact bone stained with Martius Scarlet Blue stain, seen at x20 magnification. Osteons are visible, with cement lines (arrows) separating adjacent osteons. These cement lines are thought to represent the residual organic matrix laid down as the osteons formed.

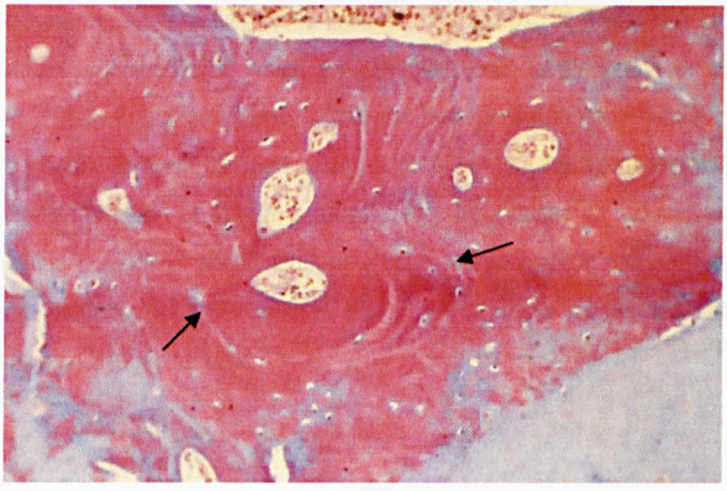

Bone lining cells

Bone lining cells are, like osteocytes, "retired" or quiescent osteoblasts (Martin *et al.* 1998). These are the osteoblasts that were not incorporated into the newly formed bone, and instead remained on the surface once bone formation had ceased (Martin *et al.* 1998). As bone matrix production stops, the bone lining cells become quiescent, and epithelial-like, flattened against the resting surfaces of bone, particularly in the mature skeleton (Martin *et al.* 1998; Soames, 1995). Although they cover the surface of the bone, they do not form a continuous, gap-free barrier over the bone (Martin *et al.* 1998). They maintain contact with each other and with adjacent osteocytes through gap junctioned processes (Martin *et al.* 1998; Soames, 1995). They also appear to maintain their receptors for parathyroid hormone, estrogen and other chemical messengers; and, like osteocytes, they are thought to be responsible for transfers of mineral in and out of bone (Martin *et al.* 1998). Bone lining cells form the outer boundary of the marrow tissue, on the endosteal surface of marrow cavities, and are also present on the periosteal surface of bones (Soames, 1995). They also line the vascular system within osteons (Soames, 1995). They are thought to play an active role in regulating the differentiation of osteoprogenitor cells. They also may control the access of osteoclasts to the bone surface, and maintain mineral balance (Soames, 1995). It has also been suggested that they can sense mechanical strain, and may secrete collagenase to remove osteoid from the surface of bone, in order to prepare surfaces for osteoblastic resorption (Martin *et al.* 1998; Soames, 1995).

The origin of bone cells

Until recently, it was thought that osteoclasts and osteoblasts were derived from a common precursor (Revell, 1986). However, it is now becoming increasingly apparent that the two main bone cell types are derived from different cell lineages (Revell, 1986). It is now thought that the osteoclast is descended from the haematopoietic system, and the osteoblast from the stromal cell system (Revell, 1986). However, a close relationship exists between bone and bone marrow formation, and it seems likely that bone and bone marrow stromal tissue influence haematopoiesis (Revell, 1986).

Osteoblasts originate from connective tissue cells (see Figure 01: 01: 03). Their immediate precursor cells are known as preosteoblasts, which are fibroblast cells located near osteoblastic and bone surfaces (Revell, 1986). Fibroblasts derived from the stroma of non-bone tissues such as spleen or lymph node, do not usually form calcified tissue, unless an inducing agent is present (Revell, 1986). Cartilage and bone formation in skin and muscle may be induced by agents such as transitional (bladder) epithelium, decalcified bone matrix or a bone morphogenetic protein (Revell, 1986). Those cells that require induction in order to form bone and cartilage are termed inducible osteogenic precursor cells or osteoprogenitor cells.

Figure 01: 01: 03 Schematic diagram showing osteoblast ontogeny. (After Marcus *et al.* 2001).
(Sample images from www.academicpress.com/oste/gfx/marcus_02_int_0203.jpg)

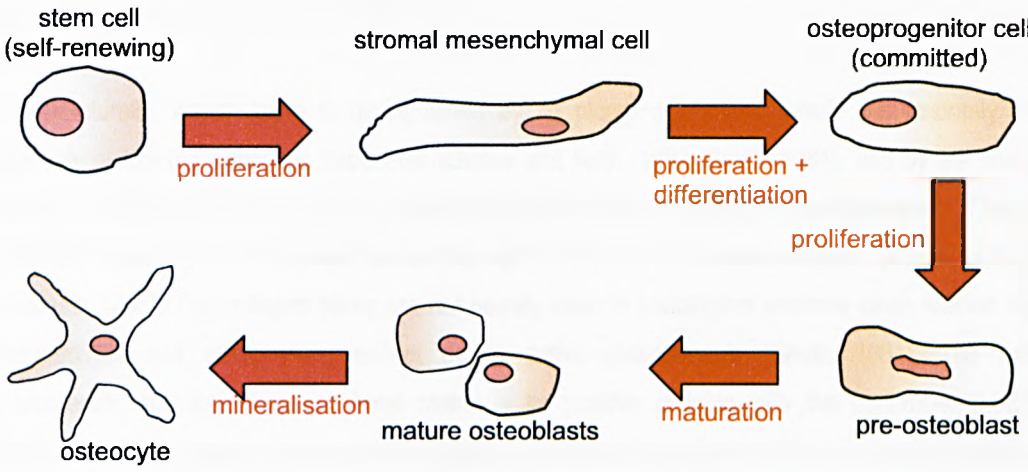

The microscopic structure of cancellous bone

Under the microscope, both compact bone and the trabecullae separating the cavities of the cancellous bone have the same basic histological structure (Junqueira *et al.* 1995). The organisation of cancellous or trabecular bone is basically lamellar (Soames, 1995). The bone is in the form of branching and anastomosing curved plates, tubes and bars of different widths and lengths (Soames, 1995). Their thickness ranges from about 50 to 400 µm thick, and each trabecula is wrapped in endosteal tissue (Gurley and Roth, 1992; Soames, 1995). In general, bone lamellae are oriented parallel to the adjacent bone surface, and there is the same arrangement of cells and matrix as is found in circumferential and compact, osteonic bone. Only the thickest trabeculae contain small osteons, which contain capillaries, but otherwise there are no blood vessels within the cancellous bone matrix. Bone cells have to rely on the canalicular diffusion from adjacent medullary cavities for their blood supply (Gurley and Roth, 1992; Soames, 1995). In immature, woven bone, calcified cartilage may be present in the cores of the trabeculae, but this is generally replaced by bone during subsequent remodelling (Soames, 1995).

Immature woven bone

Woven, primary, or immature bone is found in many sites in the skeleton, whether infant, juvenile or adult. It is seen in the embryo, in growing pre-pubertal bone, and in malformed bone, such as in *osteogenesis imperfecta*, rickets and scurvy (Gurley and Roth, 1992). It is also found at sites of periosteal injury and fracture - in the form of fracture callus - and at sites of bone repair, such as the involcrum of osteomyelitis or the reaction to bone tumours (Gurley and Roth, 1992). Woven bone is generally a fine cancellous bone, architecturally arranged in a close network of trabeculae and spicules

(Gurley and Roth, 1992; Sevitt, 1981). This is because it is formed within and around a vascular mesh, causing the trabeculae to have a honeycombed or sponge-like arrangement (Sevitt, 1981). The trabeculae are small, and the network is relatively small compared to that of the lamellated trabeculae of mature cancellous bone (Sevitt, 1981).

Ultrastructurally, woven bone is distinguished by its plump osteocytes, which are randomly and unevenly distributed within the trabeculae (Gurley and Roth, 1992; Sevitt, 1981), and by the coarse bundles of fibres in its matrix. These form an intertwining pattern, giving it the appearance of woven material, especially when viewed under the light microscope between crossed polarising filters (Soames, 1995). The collagen fibres are not usually seen in histological sections when stained with haematoxylin and eosin stain, except during active osteogenesis (Sevitt, 1981). The most characteristic reaction of woven bone matrix is its positive staining with the periodic-acid-Schiff reaction, which contrasts to the negative reaction of lamellar bone (Sevitt, 1981). During its formation, new woven bone can appear in two forms. One kind is characterised by a relatively homogenous condensed matrix, with trabeculae lined with well-defined osteoblast membranes (Sevitt, 1981). The other kind is characterised by a much more fibrillar matrix, and few lining osteoblasts. It is thought that the fibrillary component of woven bone is derived from condensations of pre-formed connective tissue fibrils in the osteogenetic field (Sevitt, 1981).

Woven bone is the immature bone formed during rapid osteogenesis by very active osteoblasts in foetuses, and during the active growth period in children (Sevitt, 1981; Soames, 1995). In adults, its formation is stimulated by fracture, growth factors, or prostaglandin E_2 (Soames, 1995). Nearly all the bone in fracture callus is woven (Sevitt, 1981). Woven bone always acts as a temporary or provisional structure that is, if normal circumstances persist, removed and replaced with more solid and stable lamellar bone through the process of ossification and remodelling.

Bone histogenesis

There are two distinct ways in which new bone can be formed (Junqueira *et al.* 1995). Bone matrix secreted by osteoblasts can be directly mineralised in a process termed intramembranous ossification, or bone matrix can be deposited on a pre-existing framework of cartilage or woven bone, in a process called endochondral ossification (Junqueira *et al.* 1995). The two processes result in an identical bone microstructure, and both compact and cancellous bone can be produced by either method (Biswas and Iqbal, 1998). After ossification, immature bone grows and is continuously remodelled by osteoblasts and osteoclasts, which is sustained through into skeletal maturity (Biswas and Iqbal, 1998).

Intramembranous ossification

Intramembranous or mesenchymal ossification is so called because it takes place between 'membranes' of condensed mesenchymal tissue, and is the origin of most flat bones (Biswas and Iqbal, 1998; Junqueira *et al.* 1995; Soames, 1995). The frontal and parietal bones, as well as parts of the occipital, temporal, mandibular and maxillary bones of the skull, and the clavicle, are all formed by intramembranous ossification (Junqueira *et al.* 1995). Intramembranous ossification is essentially the direct mineralisation of a highly vascular connective tissue, which spreads outwards from a primary ossification centre (Soames, 1995). At the primary ossification centres, mesenchymal osteoprogenitor cells differentiate into osteoblasts, and proliferate densely around the capillary network, and a fine mesh of collagen fibres and ground substance appears between cells and around the blood vessels (Biswas and Iqbal, 1998; Soames, 1995). The central osteoblast cells enlarge, and secrete eosinophilic matrix, the earliest form of new bone, which appears in fine strips between the cells (Soames, 1995). These strips or ribbons of bone rapidly extend and fuse into a fine, delicate mesh, which encloses blood vessels (Soames, 1995). Mesenchyme cells become osteoblasts, and proliferate to form an incomplete polarised osteoblast layer in contact with the primitive, eosinophilic bony matrix (Soames, 1995). The osteoblast layer secretes osteoid constituents from the surface facing away from the blood vessels, and also forms numerous matrix vesicles (Soames, 1995). These are the loci of the earliest crystal formation of salts, such as hydroxyapatite, in newly forming bone (Soames, 1995). The crystal formation extends into the surrounding matrix, and permeates the network of collagen fibres, forming the distinctive lacework appearance of woven bone (Soames, 1995). Layers of calcifying matrix are continually added to these primitive trabeculae, and some osteoblasts become enveloped within the matrix, stuck in small capsules or lacunae (Biswas and Iqbal, 1998; Soames, 1995). These osteoblasts trapped in matrix become known as osteocytes. These new osteocytes retain intercellular contact with neighbouring cells by means of their cytoplasmic processes, and as these elongate, matrix condenses around them to form canaliculi (Soames, 1995).

As the processes of matrix secretion, calcification and osteoblast enclosure continues, the trabeculae thicken, and the intermediate vascular spaces narrow (Soames, 1995). This persists in areas destined to become compact bone until all the vascular channels have been surrounded by primary osteons that later, with lamellation, become secondary osteons (Soames, 1995). In areas that will eventually become cancellous bone, the process of matrix secretion slows and the spaces between the trabeculae become occupied with haematopoietic tissue (Soames, 1995). During these changes, mesenchyme collects on the external surface of the bone to form a fibrovascular periosteum, and bone is laid down by new osteoblasts differentiating from osteoprogenitor cells deep in the periosteum (Biswas and Iqbal, 1998; Soames, 1995). This acts as an advancing front of matrix deposition that entraps periosteal vessels and osteoblasts which become osteocytes, progressively forming the outer surface of the bone (Biswas and Iqbal, 1998; Soames, 1995). Overall growth results from a

continuation of these processes, with fine shaping and modelling due to varying rates of resorption and deposition in different areas, dependent on the shape and structure of the bone (Soames, 1995).

Endochondral ossification

Endochondral ossification is the process of forming bone over an existing cartilage framework. It takes place within a piece of hyaline cartilage with the shape and morphology of a small version of the bone to be formed (Junqueira *et al.* 1995). This type of ossification is principally responsible for the formation of most human bones, especially the long bones, including the metacarpals and metatarsals.

The cartilaginous model is surrounded by vascular condensed mesenchyme or perichondrium, similar to that which precedes and surrounds intramembranous ossification centres (Soames, 1995). The first phase of endochondral ossification is characterised by hypertrophy and deconstruction of the chondrocytes within the primitive diaphysis (Junqueira *et al.* 1995). During this phase, the chondroblasts enlarge greatly, their cytoplasm becomes vacuolated, and they accumulate glycogen (Soames, 1995). As the cells and their lacunae enlarge, the cells degenerate, leaving distended and sometimes merged lacunae with calcified walls, separated by septa of the calcified cartilage matrix (Junqueira et al. 1995; Soames, 1995). The large empty lacunae are known as primary areolae (Soames, 1995). In the second phase, osteoprogenitor cells deep in the perichondrium surrounding the centre of the model become osteoblasts and form a peripheral layer of fenestrated bone (Soames, 1995). This periosteal collar, formed by intramembranous ossification, is a thin-walled tube enclosing the central shaft, which gradually increases in diameter and extends towards the ends of the diaphysis of the bone model (Soames, 1995). The periosteal collar overlying the calcified lacunae is invaded from the deep periosteal layers by osteogenic buds, which consist of osteoprogenitor cells, osteoclasts and blind ended blood capillaries (Junqueira *et al.* 1995; Soames, 1995). The osteoclasts excavate the newly formed bone, and continue to erode the walls of the primary lacunae, resulting in larger, irregular, communicating spaces called secondary areolae (Soames, 1995). Blood vessels and osteoprogenitor cells from the periosteal collar penetrate through the holes made by the osteoclasts into the calcified cartilage matrix and proliferate, giving rise to osteoblasts (Junqueira *et al.* 1995). The lacunae then fill with embryonic medullary tissue, composed of vascular mesenchyme, osteoblasts, osteoclasts, haemopoietic and marrow stromal cells (Soames, 1995). The osteoblasts attach themselves in a continuous layer to the delicate walls of the calcified cartilage, and rapidly synthesise bone matrix (Junqueira *et al.* 1995; Soames, 1995). Layers and layers of bone are formed, enclosing young osteocytes in lacunae, and narrowing the perivascular spaces (Soames, 1995). As the formation of the subperiosteal bone continues, deposition on to the calcified cartilage stops (Soames, 1995). Giant, phagocytic, multinucleated cells similar to osteoclasts resorb the calcified cartilage remnants, which can be distinguished histologically as they are basophilic, whereas the new bone tissue is acidophilic (Junqueira *et al.* 1995). This creates a primitive medullary cavity (Soames, 1995).

The replacement of the calcified cartilage with the newly formed bone matrix starts in the middle of the diaphysis of the bone, at the primary ossification centre (Biswas and Iqbal, 1998; Junqueira *et al.* 1995). Rapid growth of the periosteal collar and of the region of ossification extends longitudinally along the diaphysis towards the two epiphyses of the long bones. A medullary cavity is formed in the centre of the diaphysis by the osteoclasts which are continuously active, resorbing bone and calcified cartilage (Junqueira *et al.* 1995). Secondary ossification centres are formed in the centre of each epiphysis of the long bones (Junqueira et al. 1995). The function of these centres is similar to that of the primary centre, but their growth is radial not longitudinal (Junqueira *et al.* 1995). However, there is no periosteal collar formed, as the articular cartilage has no perichondrium (Junqueira *et al.* 1995).

Once the cartilage of the whole diaphysis has been replaced with bone matrix through endochonral ossification, there are only two areas of the bone where cartilage remains (Junqueira *et al.* 1995). These are the articular cartilage, which persists throughout adult life, and is found between the epiphyses and the joints where the bone articulates with the two (or one) adjacent to it, and epiphyseal cartilage, which connects the epiphyses to the diaphysis (Junqueira *et al.* 1995). As the cartilage of the epiphyseal plate grows, it is replaced continuosly by newly formed bone matrix, mainly from the diaphyseal primary ossification centre (Junqueira *et al.* 1995). This is known as the growth plate.

Growth plate

The growth plate is an organised region of rapid growth situated between the epiphysis and the diaphysis of a long bone, which grows in all dimensions (Soames, 1995). On the side of the plate closest to the epiphysis is a zone of hyaline cartilage, made up of relatively quiescent stem cells, called the resting zone (Junqueira *et al.* 1995; Martin *et al.* 1998; Soames, 1995). These stem cells are not really 'resting', but are dividing very slowly to produce chondrocytes for the rest of the growth plate (Martin *et al.* 1998). Closer to the diaphysis is the proliferative zone, where there is a region of active mitotic chondrocytes, which divide rapidly and form numerous longitudinal columns or palisades (Junqueira *et al.* 1995; Soames, 1995). They also become disclike, so that they look rather like a stack of coins in cross section (Martin *et al.* 1998) (see Figure 01: 01: 04). They produce proteoglycan, type II collagen and other molecules needed for the surrounding extracellular matrix (Martin *et al.* 1998). The hypertrophic cartilage zone contains large chondrocytes whose cytoplasm accumulates glycogen as the cells mature (Martin *et al.* 1998; Soames, 1995). They secrete copious amounts of matrix, increasing the volume of the surrounding tissue. They also undergo *hypertrophic* changes, increasing their intracellular volume (Martin *et al.* 1998). It is thought that the chondrocytes in this zone are in the early stages of *apoptosis* (programmed cell death), and so degenerate and die. They stop producing cartilage matrix, and start producing molecules that prepare the adjacent cartilage for calcification (Martin *et al.* 1998). The death of the chondrocytes leaves lacunae separated only by thin septa of cartilage matrix (Junqueira *et al.* 1995; Soames, 1995). The longitudinal walls between the

chondrocytes become impregnated with hydroxyapatite crystals, and these compose the calcified cartilage zone (Junqueira *et al.* 1995; Soames, 1995). The calcified portions enter the ossification zone and are invaded by vascular mesenchyme, accompanied by osteoblasts, osteoclasts, chondroclasts, haemopoietic and marrow stromal cells, from the primary ossification centre of the bone (Soames, 1995). Eventually, bone matrix deposition, bone formation and osteocyte enclosure occurs on the surfaces of the longitudinal cartilage walls (Soames, 1995).

Figure 01: 01: 04 A paraffin section of fixed, decalcified bone stained with haematoxylin and eosin stain, seen at x10 magnification. The epiphyseal growth plate is visible, showing the proliferative zone of active, mitotic chondrocytes lying in columns. These produce proteoglycans and type II collagen.

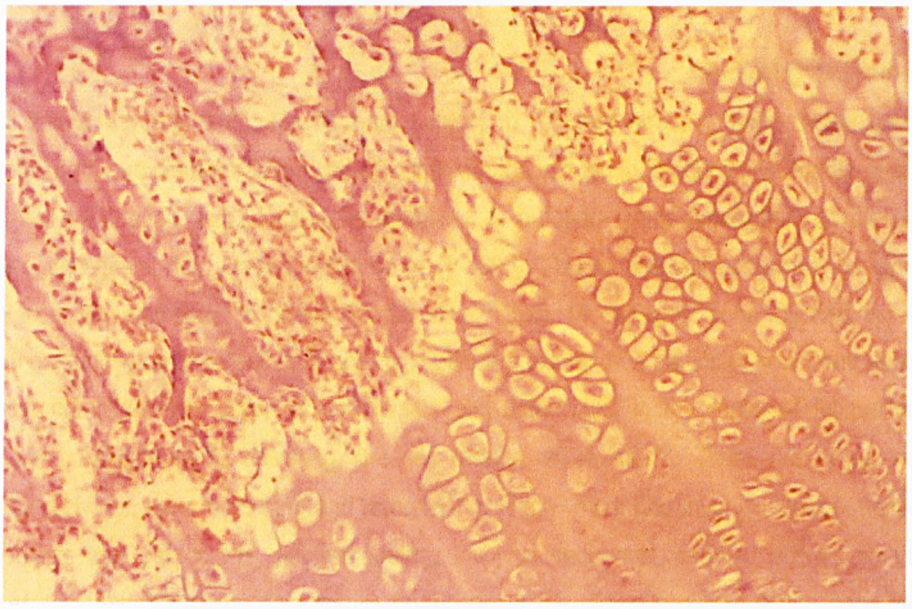

In summary, growth of a long bone occurs by proliferation of chondrocytes in the epiphyseal plates adjacent to the epiphysis. At the same time, chondrocytes of the diaphyseal side of the plate hypertrophy, their matrix becomes calcified, and the cells die. Osteoblasts then deposit a layer of osteoid on to the cartilage mesh network (Junqueira *et al.* 1995). Because the rates of the two opposing processes of proliferation and destruction are approximately equal, the epiphyseal plate does not change in thickness (Junqueira *et al.* 1995). Instead, it is displaced away from the diaphysis, which results in lengthening of the bone (Junqueira *et al.* 1995). There is also concurrent internal erosion and remodelling of the new bone tissue and, as further subperiosteal bone deposition continues towards the epiphyses, the bone also grows in diameter (Soames, 1995). The medullary cavity also extends longitudinally and transversely as this process advances (Soames, 1995).

As a child matures, its bones eventually reach their adult length, and the growth-promoting function of the epiphyses is no longer required. Throughout an individual's infancy and adolescence, the epiphyses of different bones 'fuse' by ossification to the diaphyses of the long bones. The age at which this fusion occurs varies from bone to bone, but not remarkably from individual to individual. The closure of the various epiphyses occurs in a specific, predictable sequence, which allows the forensic or archaeological examiner to estimate the skeletal age of an individual by observing which of the epiphyses have fused and which have not. For example, the inferior pubic ramus of the pelvis fuses to the ischial ramus at the age of about 6 to 8 years. The ilium, ischium and pubis unite to form the complete hip bone at the age of about 14 years. So, if an individual showed evidence of the former instance of fusion, but not of the latter, it would be possible to surmise that the individual's age was between 6 and 15 years old.

Modelling and remodelling

As long bones develop, and they become subject to different stresses and mechanical strains, increased length and diameter alone cannot cope with the varying load conditions (Martin *et al.* 1998). Bones must be shaped and sculpted, or *modelled*, in order to adapt successfully to the changing conditions, and retain their shape (Junqueira *et al.* 1995). This means that bone must be removed in some places, and deposited in others (Martin *et al.* 1998). Modelling of bone involves osteoblastic activity in conjunction with osteoclastic activity in different places on a particular bone, and remodelling entails the complimentary action of osteoblasts and osteoclasts in the repair of fatigue damage, fracture, and adjustment to changing stresses (Martin *et al.* 1998). There are some important distinctions between bone modelling and remodelling. Firstly, modelling involves independent actions of osteoblasts and osteoclasts, but remodelling involves sequential, coupled actions by the cells (Martin *et al.* 1998). Modelling also results in change of the shape and size of the bone, whereas remodelling does not usually affect size or shape (Martin *et al.* 1998). The rate of modelling is greatly reduced once an individual has reached skeletal maturity, but remodelling occurs throughout life, although it has slightly diminished capability as maturity is reached (Martin *et al.* 1998). Modelling at a particular site is continuous and prolonged, whereas remodelling is sporadic, with each episode having a clear beginning and end (Martin *et al.* 1998).

Modelling

Modelling, or change in general shape, occurs in all growing bones (Soames, 1995). Modelling in cranial and long bones has been particularly well studied (Junqueira *et al.* 1995; Martin *et al.* 1998; Soames, 1995). For example, as a child grows, the bones of the skull must increase in size to accommodate the growing brain (Martin *et al.* 1998). This enlargement cannot simply be accomplished by addition of bone at the suture lines between the cranial bones, because the curvature of the calvarium needs to change as well (Martin *et al.* 1998). Resorption on the inner surface and formation

on the outer surface is required for proportionally correct increases in cranial size (Martin *et al.* 1998). Modelling also occurs in bones at the metaphysis, which is the area where the diaphysis starts to bulge to form the epiphysis. As a child's bone grows, the expanded diameter of the metaphysis has to be reduced, so that this area can become the shaft of the bone, thus elongating the diaphysis (Martin *et al.* 1998). This change is accomplished by osteoclasts working continuously on the periosteal surface of the metaphysis, and is particularly important in bones with a wide, flaring metaphysis, such as the proximal tibia (Martin *et al.* 1998). In other bones, such as the metacarpals and metatarsals, this action is unnecessary, as longitudinal growth and diametric growth of the epiphysis is coordinated (Martin *et al.* 1998). Modelling also functions to increase the diameter or alter the curvature of long bones (Martin *et al.* 1998). The diameter of a long bone is increased by the complimentary deposition of bone matrix by osteoblasts on the periosteal surface of the bone and of bone resorption from the endosteal surface of the bone by osteoclasts (Martin *et al.* 1998). This process of 'diaphyseal drift' may be employed to alter the curvature of a long bone. This works as osteoblasts add bone matrix to the periosteal surface and the opposite endosteal surface, and osteoclasts erode bone from the remaining endosteal and periosteal surfaces (Martin *et al.* 1998). This creates a gradual shift of the diaphysis to one side relative to the ends of the bone (Martin *et al.* 1998). Tetracycline marking techniques have emphasised the malleability and mutability of bone, including mature compact bone (Soames, 1995). A single section can be seen to contain osteons in any stage of their life cycle; from the recently formed, or already forming, to resorbing or mature and quiescent osteons (Soames, 1995).

Remodelling

The process of remodelling removes a portion of older, lamellar bone and replaces it with newly formed woven bone. It occurs throughout life, in the form of major bone repair after fracture, or continuous repair of microscopic damage and prevention of fatigue fracture (Martin *et al.* 1998; Soames, 1995). It depends on delicate geometric balances between deposition and removal (Soames, 1995).

Remodelling is accomplished by teams of osteoclasts and osteoblasts, known by some researchers as basic multicellular units (BMUs) (Martin *et al.* 1998). A basic multicellular unit consists of approximately ten osteoclasts and several hundred osteoblasts. There are three principal stages of remodelling, undertaken by BMUs (Martin *et al.* 1998). These are *activation*, *resorption* and *formation* (Martin *et al.* 1998). Osteoclasts are activated by chemical or mechanical stimuli, which cause them to form and start to remove bone at a particular part of the skeleton (Martin *et al.* 1998). On bone surfaces, osteoclasts resorb bone in little troughs around themselves, and so give the surface of the bone a pitted appearance. In compact bone, however, osteoclasts move through the cortex at a speed of about 40 to 50 µm per day (Martin *et al.* 1998; Soames, 1995), leaving a hollow, cylindrical tunnel approximately 200 µm in diameter behind them (Martin *et al.* 1998). This is termed a cutting cone, and

is produced by the concerted action of a team of about nine osteoclasts (Soames, 1995). Blood vessels are also present within the cutting cone, as they are required to supply nutrients to the osteoclasts at the head of the tunnel, as well as to the osteoprogenitor cells which differentiate into osteoblasts when bone formation takes place (Martin *et al.* 1998). The action of the osteoclasts is closely followed by that of osteoblasts, which fill in the space left by resorption through the concentric deposition of bone matrix around blood vessels, to form secondary osteons or Haversian systems (Soames, 1995). This forms a closing cone, which consists of about 4000 osteoblasts per mm^2 (Soames, 1995). The concentric deposition of lamellae occurs on the internal walls of the resorption tunnels, which narrows the vascular channels (Soames, 1995). A hypermineralised, basophilic cement line marks the site of reversal from the process of resorption to that of deposition (Soames, 1995). The formation of bone is much slower than resorption. The resorption period is about three weeks, whereas the formation phase lasts about three months in a healthy adult in normal conditions (Martin et al. 1998). Therefore, the total remodelling period can take up to four months to complete (Martin *et al.* 1998). The rate of remodelling varies according to age in humans. It is very high in children, where the activation frequency of basic multicellular units can be as high as $40/mm^2$/year in a newborn infant (Martin *et al.* 1998). The activation frequency of BMUs falls with age, to a BMU activation frequency of less than $1/mm^2$/year in the 75 year old (Martin *et al.* 1998).

Remodelling can also occur on endosteal and periosteal surfaces (Martin *et al.* 1998). This process is likely to be responsible for the radial growth of long bones with age observed in both children and adults (Martin *et al.* 1998). This expansion would involve increased formation and reduced resorption on the periosteal surface, accompanied by the reverse process on the endosteal surface (Martin *et al.* 1998).

Applications of bone histology

The histological examination and analysis of bone material has many applications in the fields of clinical and forensic pathology and identification sciences. Perhaps the most common application of bone histology is the examination of bone biopsies to enable the diagnosis of tumours, infection or metabolic bone disease (Page, 1982). Such evaluations of bone sections involve histomorphometric analyses, which allows for the quantitative assessment of amount of bone, bone density and mineralisation, as well as the rates of bone formation and resorption (Gurley and Roth, 1992). These studies are most useful in evaluating metabolic bone disease such as osteoporosis, osteomalacia, rickets and renal osteodystrophy (Gurley and Roth, 1992). They can measure the changes in these diseases with time, and have been used extensively to correlate with radiological assessments of bone mineral density. They also have been used successfully to evaluate the results of therapeutic intervention (Gurley and Roth, 1992; Page, 1982).

In the field of identification science, bone histology has proved extremely valuable. If bones of unknown origin are discovered, histomorphometric analyses are valuable for distinguishing between animal and human bones (Janssen, 1984). The accurate distinction relies on the difference in diameter of the Haversian systems. The region of the proximal femoral diaphysis is thought to yield the most significant results. The canal width is measured after maceration and decalcification of 10 to 15 µm thick sections, stained with thionin and examined in a projection microscope (Janssen, 1984). In humans, the central sections of bone contain Haversian canals which are, on average, larger and wider than those of animals, with narrower canals in the peripheral areas. Animal bone shows an irregular composition of both wide and narrow Haversian canals, distributed randomly across the section (Janssen, 1984). Therefore, the number of canals per visual field is lower in humans than in animals. The bone most similar to humans is found in horses, although it has a different lamellar pattern (Janssen, 1984). Histological studies of bone can also be used to determine the age at death of unknown individuals for the purpose of identification (Cho *et al.* 2002; Stout, 1986). Analysis of the degree of mineralisation of older and younger osteons from cross sections of compact bone with the use of microradiography can facilitate the estimation of age (Janssen, 1984). The best results are usually provided by samples taken from the femur or the sternal ends of the ribs, or a combination of as many samples as possible (Dudar *et al.* 1993; Stout, 1988; Thompson, 1981). Also, the diameter of Haversian canals is thought to correlate in a predictable manner with the chronological age of humans (Janssen, 1984; Thompson, 1981).

In a forensic context, the histological examination of bone can sometimes aid the determination of the cause of death of an individual, as histological evidence of certain trauma can be seen. For example, burning, electricity lesions and radiation injuries leave clear histological indicators in bone, which can be detected and identified (Janssen, 1984). The presence of drugs can also be detected histologically in bone (Schiwy-Bochat and Lemke, 1999). The event of drowning can also be diagnosed histologically, as fresh of salt-water diatoms are readily identified from samples of bone marrow (Pollanen, 1997).

Introduction

Now that the basic macroscopic and microscopic nature of bone has been examined, we can turn our attention to understanding the occurrence and mechanisms of fracture. Fractures are the most common of all types of trauma, and appear frequently in archaeological skeletons as well as in forensic cases. Fractures are of great importance to forensic anthropologists, as they leave clues to the nature of the impact, the weapon used, the sequence and force of blows, and of course about the timing of the trauma.

Fractures occur when the mechanical strength and elasticity of bone is overwhelmed. Fracture is the result of unusual, undue or excessive stress applied to one or more bones (Schwartz, 1995). The stress can be dynamic or static. Chronic or static stress is that which gradually impinges on the bone over an extended time period, and eventually causes a 'fatigue' fracture by weakening the bone slowly. Fatigue fractures are associated with the onset of a new, repetitive activity. They are often seen in new military recruits during their initial training (Ortner and Putschar, 1985). The onset of vigorous activity triggers an attempt by the bone to increase its mechanical strength through the process of bone remodelling, according to Wolff's law (Ortner and Putschar, 1985). However, the initial part of the process is resorption by osteoclasts. Abnormal physical activity accelerates the rate of resorption, which occurs at about ten times the rate of bone deposition by osteoblasts (Ortner and Putschar, 1985). This creates microcracks which accumulate and coalesce, severely weakening the bone, which eventually succumbs to fracture. Fatigue fractures tend to be closed and non-displaced, with little disruption of the periosteum or intramedullary vasculature, and no soft tissue damage (Tami *et al.* 2003). In contrast to fatigue fractures, where the bone is weakened by the onset of continued high stress, insufficiency fractures occur after normal or moderate pressure is applied to bone with already decreased strength and resistance (Soubrier *et al.* 2003). They are most commonly seen in elderly women with post-menopausal osteoporosis. Insufficiency fractures are particularly common in the pelvic ring, including the sacrum and acetabulum, but can occur in all bones of the lower limbs (Soubrier *et al.* 2003).

Dynamic, or sudden, acute stress is the most common traumatic condition in skeletal material (Ortner and Putschar, 1985); and appears most often in modern orthopaedic settings. It is also the form of trauma that characterises fractures in a forensic context. Fortunately for the forensic anthropologist, each type of dynamic force results in characteristic, recognisable fractures (Ortner and Putschar, 1985). However, some fractures are the result of one or more combined forms of stress. The types of stress that might be

produced in a traumatic injury are compression, torsion (twisting), bending and shearing (Ortner and Putschar, 1985; Shwartz, 1995). These types of forces give their names to the types of fractures they cause. The type of force and impact dictates the shape and morphology of the fracture to such an extent that it is usually easy to distinguish which type of fracture was caused by which type of force (Mays, 1998). This section aims to give the reader a brief overview of the majority of different types of fractures and the types of forces that cause them, and an understanding of the wide variety of mechanisms that cause fracture.

Types of fracture

The majority of long bone fractures affect the diaphysis of the bone, and are described simply by their shape and angle. Fractures can also be classified by the types of forces which cause them.

Transverse fractures

Transverse fractures are simple linear fractures that cut across the shaft of the bone at a 90° angle. They can be caused by tension forces, which act at either end of the diaphysis to 'pull' the bone apart longitudinally. This results in a transverse fracture with rough, jagged edges. Such fractures are associated with the dislocation of a joint and the subsequent increase in tension from the tendons, which can cause the tubercle from which the tendon originates to separate from the diaphysis of the bone.

Spiral fractures

Spiral fractures are caused by torsion forces, which twist the bone. If one end of the bone is immobile, the torsion force will ultimately lead to a spiral fracture. Spiral fractures tend to occur at high speeds, and are commonly associated with skiing, where the lower leg is rigidly fixed and the body twist during a fall (Erskine, 1959; Ortner and Putschar, 1985). Spiral fractures are particularly common in the humerus, and have also been associated with many arm-focussed activities, such as arm-wrestling, ball-throwing, javelin, shotput and snowball-throwing (Reed and Mueller, 1998). They are thought be the result of torsional stress concentrated on the middle to distal humerus, and are not usually associated with pathological disease. Spiral fractures in individuals with habitual over-use of their humeri can also be the result of chronic stress. Spiral fractures have even been found in the proximal phalanx as a result of finger-wrestling (van der Lei *et al.* 1992). These fractures can sometimes be confused radiographically with compression fractures, as the break follows the natural course of mechanical weakness in the bone shaft.

Compression fractures

Compression fractures are caused by sudden impaction, and have a variety of patterns. Pure compression can result in a diagonal break of a long bone diaphysis at a 30° angle and a chattered fracture surface (Mather-Saul, 1997). Compression forces are applied to the vertebral column and the long bones in falls on to the feet from a great height. Excessive compressional forces can cause the diaphyses of the long bones of the legs to bulge, with associated cracking of the cortical bone (Schwartz, 1995). Compression fractures are best illustrated in the vertebral column, where forced flexion of the spine can result in the crushing of a vertebral body by the neighbouring vertebrae (Mays, 1998). The trabecular bone of the vertebral body is crushed, giving the vertebra a distinctive wedge-shaped appearance.

Flexion fractures

Flexion or bending fractures are extremely common, and are caused when a combination of compression and tension forces are applied to the bone simultaneously in different planes. They can also be caused by falls onto the feet from a height (Schwartz, 1995). In much the same way as a pencil can be bent more and more until it eventually snaps, the long bones are capable of enduring bending forces until a specific point. The younger the bone, and the higher the collagen content, the more it will bend before finally breaking. In young bone, fractures caused by excessive bending forces are known as 'greenstick fractures', as the pliable, collagen-rich bone acts much like a young, flexible 'green' twig under bending forces, and does not break completely. Greenstick fractures are incomplete fractures which do not extend all the way through the bone, and do not break the bone into two or more fragments. In adults, the bone is more rigid and brittle as a result of a decrease in collagen content, and more prone to complete fractures. The fracture is caused when the outside, convex side of the diaphysis lengthens under the forces of tension, and the concave side is forced to shorten through compression. The maximum stress occurs at a discrete point on the concave side and this is the initiation point of a transverse fracture (Ortner and Putschar, 1985). If the bone is older and less flexible, the bending force pushes a triangular shaped wedge of bone out of the diaphysis on the convex side of the bend. The wedge of bone which is displaced is narrowest on the side that the bone is being compressed and broadest where the bone is being stretched through tension forces (Schwartz, 1995).

Shearing fractures

Shearing fractures are not always distinguishable from bending fractures, but occur when opposing forces are applied to the bone in slightly different planes. One end of the diaphysis of the long bone is held static, while the other end is subjected to a sudden dynamic force, which causes one end of the bone to be

shifted sideways. A common example of a shearing fracture is a Colles' fracture of the distal radius, which results from a fall onto the wrist. The static force is applied by the floor and the dynamic force by the weight of the falling body. The distal end of the radius is sheared off and displaced backwards (Ortner and Putschar, 1985).

Comminuted fractures

When high-energy, violent impact shatters a bone into more than three fragments, the fracture is termed comminuted. Comminuted fractures are often open and communicate with the external environment, and are difficult to reduce successfully. Open, surgical reduction is invariably necessary, and treatment of comminuted fractures can involve metal implants such as plates or screws, wires or pins. The introduction of autograft material between the fragments may be necessary to promote fracture healing. Fractures that are severe enough to expose the break to the outside are termed *compound* fractures, and pose a serious risk of infection.

Skull fractures

The primary function of the skull is to protect the brain, and fracturing is one of the ways in which it performs this function. A skull fracture greatly decreases injury to the underlying brain caused by a blow to the head by dispersing the traumatic force evenly. There is a wide variety of skull fracture types, which are characteristic of the type of force applied. Skull fractures can be linear, depressed, comminuted or diastatic.

Linear fractures

Linear fractures are the most common type of skull fracture. In-bending of the skull at the point of impact, and the out-bending of the adjacent area exert a tensile stress on the outer table of the skull (Gean, 1994). If the critical physical threshold of the bone's capacity to withstand these stresses is breached, fracture occurs. Linear fractures are narrow, straight or curved lines of disruption to the bone, which appear to radiate out from a depression made in the cranium by blunt force trauma. Linear fractures are generally caused by blunt objects impacting with low velocity and low levels of force (Mather-Saul, 1997). Ring fractures are distinctive linear fractures of the base of the skull, which surround the foramen magnum. They are specifically the result of immense compression force that accompanies a fall onto the top of the head, the feet or the bottom of the spine from a height. The force pushes the spinal column up through the foramen magnum, and dissipates in the posterior cranial fossa around the point of entry. Hinge fractures are also very distinctive linear fractures, which course across the posterior cranial fossa from one temporal

bone to the other, sometimes completely separating the skull into two distinct pieces. Hinge fractures are particularly associated with motorcycle accidents, where impact is most often to the side of the head.

Depressed fractures

A blow to the head with a blunt instrument such as a baseball bat or the head of a hammer can compress the bone and cause a localised depression of the outer table of the skull. The blow is usually of sufficient force to damage the inner table of the skull. The inner table is often more displaced than the outer table in a depressed skull fracture, and can even become detached (Gean, 1994; Schwartz, 1995). The area of depression often faithfully registers the shape of the impacting object, so much so, that it is sometimes possible to identify the weapon with a high level of accuracy (Maples and Browning, 1994). The force of the blow radiates outwards from the point of impact, causing such bending and distortion of the bone that linear fractures are initiated distant to the point of impact, and spread back towards it, to appear ultimately as though they are radiating from the depression like spokes from the centre of a wheel. The effect of a depression fracture on the skull is similar to that of a bullet or stone hitting a pane of glass – a conical field is produced, where the affected area of the internal surface is larger than that of the external surface (Schwartz, 1995). Depressed fractures are often accompanied by a degree of comminution, in cases where the inbending results in fragmentation (Gean, 1994). Fragments of bone from the centre of the depressed area may even impinge on the dura and brain tissue. Depressed fractures of the skull are very common, and can be the result of any combination of velocity and force of impact, and can be caused by both severe blunt or penetrating trauma in which a large amount of energy is dissipated over a short period of time and within a small area (Gean, 1994; Mather-Saul, 1997).

Diastatic fractures

The term 'diastatic' refers to fractures with separated margins. It is usually applied in the case of infants, where, instead of fracturing bone, the force of the impact travels along the suture line, separating it. Diastatic fractures are particularly common in infants and children, before complete suture closure (Tomsick *et al.* 1978). They also occur in adults, when a linear fracture extends into a suture. Normal variations in suture width, especially of the lambdoid and squamosal sutures sometimes hinder the diagnosis of diastatic fractures.

Compound fractures

If the bone fragments created by a fracture pierce the skin, and expose the fracture site to external pathogens, it is referred to as an open or compound fracture. There are two types of compound fracture – external and internal. The external type is typically associated with depressed, comminuted skull fractures, and is usually caused by sharp force, penetrating injury (Gean, 1994). The internal type is caused by blunt

force trauma, and refers to fractures that communicate with internal air spaces such as the sinuses or a mastoid air space or the middle ear. Both types of open fractures are at increased risk of infectious complications such as meningitis, osteomyelitis, empyema or even brain abscess (Gean, 1994). Obviously, healing is compromised in the compound fracture by the potential introduction of infectious pathogens (Ortner and Putschar, 1985).

Fracture aetiology

The most common cause of dynamic fracture in adolescents and non-elderly adults is undoubtedly road traffic accidents. In infants and children, physical abuse at the hands of adults is the primary cause of mortality and morbidity, and in the elderly, fractures to the upper limb, pelvis, femora and ribs are most commonly fall-related and compounded by conditions such as osteoporosis and pneumonia (DeGoede *et al.* 2003).

Road traffic accidents

Motor vehicle accidents are far and away the greatest aetiological factor behind blunt and sharp force trauma injuries and fractures. On the road, cyclists, pedestrians and motor vehicle passengers are particularly at risk (Marks, 2003; McCarthy and Gilbert, 1996). Injuries to pedestrians are disproportionately more common in children, the elderly and the intoxicated (Bowley and Boffard, 2002). Pedestrians hit by motor vehicles exhibit characteristic injuries, such as fractures to the tibia and fibula caused by lateral impact from motor vehicle bumpers. The ensuing impact with the vehicle windscreen causes torso and head injuries, and the impact with the ground can produce fractures of the head and spine (Bowley and Boffard, 2002). In the case of motor vehicle passengers and drivers, distinctive patterns of injury can sometimes allow investigators to reconstruct the events of the crash. For example, full-on, frontal collisions are characterised by multiple injuries, initially to the knees and ankles, with associated femoral fractures and hip dislocations, and then subsequent injuries to the chest, head and cervical spine, as the body impacts with the windscreen, dashboard or steering column (Bowley and Boffard, 2002; Härtl and Ko, 1996). Lateral collisions tend to cause compressive pelvic injuries, whereas rear impact affects the head and cervical spine, causing whiplash injuries and fractures of the cervical vertebrae.

Even the safety measures introduced into vehicles contribute to the fractures caused by motor vehicle collisions. Airbags are thought to reduce the number of injuries caused by motor vehicle accidents, and have been stated as improving chances of survival after crash by up to 30% (Bowley and Boffard, 2002; Reath *et al.* 1989). However, children have been adversely affected by the introduction of passenger airbags as a safety precaution, as the increase in the occurrence of passenger-side airbags has been

paralleled by a concurrent rise in airbag-associated injuries (Bandstra and Carbone, 2001; Hollands *et al.* 1996).

Falls

In the UK, falls from heights represent the third most common cause of accidental death, accounting for approximately 5000 deaths per year (Teh *et al.* 2003). In the United States, falls are second only to motor vehicle accidents as the leading cause of injury (Pipas *et al.* 2002). The injuries sustained from free-falls from heights represent a unique form of blunt trauma. Victims often have multiple injuries, and fractures to the extremities, spine and head are especially common. The injuries sustained by fallers can be classified as deceleration-type injuries or direct impact injuries (Teh *et al.* 2003).Deceleration injuries primarily affect the internal organs, as they continue to move inside the body even after impact with the ground. Direct impact injuries are predominantly fractures. The orientation of the body at the point of impact greatly affects the pattern and distribution of injuries, as well as the prognosis for survival (Teh *et al.* 2003). Falls onto the feet tend to cause flexion forces to be distributed through the axial skeleton, resulting in pelvic, spinal and even skull fractures. Spinal injuries tend to be compression or burst fractures, and the lumbar and thoracic vertebrae are most frequently affected (Teh *et al.* 2003). Fractures to the ribs are common too, although seem to be more predominant in individuals who have deliberately jumped from a height rather than fallen accidentally. This is thought to be because jumpers attempt to break their falls using their dominant right sides, resulting in fractures to their right arms and ribs, whereas fallers tend to fall more randomly, and therefore show a more even distribution of injuries (Teh *et al.* 2003). Sternal fractures can occur with direct, chest-first, or indirect feet-first or bottom-first landings. Indirectly, they are caused when hyperflexion of the neck slams the mandible into the sternum. Similarly, pelvic fractures can be caused by the indirect transfer of forces from the feet, up through the lower leg bones and through the femur. These are seen more often in jumpers rather than fallers, due to the higher percentage of victims who land on their feet (Teh *et al.* 2003).

Pipas *et al.* (2002) have conducted research into the most common aetiological factors resulting in fractures from falls. In the USA, there is clear seasonal variation in the frequency of falls, with the greatest number occurring in the winter months. One specific cause of winter-related falls is clearing snow from rooftops. Such falls cause fractures to the head, vertebral column, and upper and lower extremities (Pipas *et al.* 2002). Icy conditions are also particularly hazardous to children and the elderly. Elderly women are the demographic section most vulnerable to fracture as a result of a fall. Post-menopausal osteoporosis leaves their bones brittle and weak, and unable to resist even small impacts. Fractures to the neck of the

femur are particularly common as a result of a trip or slip, even on soft impacting surfaces such as carpet or grass.

Sports and other activities

Obviously, fractures can be caused by a huge variety of activities, which are not all high speed or high impact sports. A few sporting activities are particularly associated with trauma, such as skiing and horse-riding, but fracture can even result from completely sedentary pastimes, such as sitting under a tree in a park (Escoffery and Shirley, 2001). Skiing represents an important cause of traumatic head injury and skull fracture in otherwise healthy adults (Diamond *et al.* 2001). Skull fractures can be caused by falls, collisions with other skiers or by striking an object at high speed. In Diamond *et al.*'s study (2001) of ski-related head injuries on the Colorado traumatic brain injury database, only 24% of the skiers studied sustained skull fractures, but this thought to be fewer than has been presented elsewhere (Shorter *et al.* 1996). Other sporting activities such as horse riding are also aetiological factors of head injury and fracture. In a study of paediatric patients, the Modified Injury Severity Score of equestrian injuries was exceeded only by that of pedestrians hit by cars (Temes *et al.* 1997). Head injuries and skull fractures are the most common horse-related cause of hospitalisation or death. Blunt force trauma caused by falling from the horse is thought to be the main cause of fracture, but injuries also result from horse kicks, bites, trampling or dragging. Torsion fractures of the leg bones can be caused if the foot is fixed in the stirrup, but the body is being dragged along the ground.

Child abuse

The distinction between accidental and abusive fractures in young children is vital, as failure to recognise the signs of abuse can have fatal consequences (Taitz *et al.* 2004). Fortunately, child abuse or non-accidental injury is associated with some specific patterns and types of fractures that can facilitate the recognition of abuse. Fractures of the extremities are the most common skeletal injuries occurring in abused children (Taitz *et al.* 2004). Fractures of the metaphyses of the long bones are highly specific of child abuse, to the point of being pathognomonic (Thomsen *et al.* 1997). Metaphyseal fractures appear on radiographs as either 'bucket-shaped' or corner lesions, depending on the orientation of the X-ray film. They represent a series of transverse microfractures across the metaphyses of the long bones, and when found in conjunction with cortical thickening and subperiosteal bleeding, are highly indicative of non-accidental injury. Metaphyseal fractures are caused by indirect dynamic trauma, such as shaking, pulling, twisting and torsion forces (Thomsen *et al.* 1997). By far the most important radiological sign of foul play is multiple fractures at different stages of the healing process, indicating many distinct, separate trauma incidents (Cashman and Bell, 2002). Ribs are recognised as the most common site of fracture in abused

children, and spiral fractures of the long bones, especially the humerus, are also recurrent (Thomsen *et al.* 1997). Kleinman *et al.*'s study (1995) of 31 infants suspected to be the victims of child abuse, found 51% of the fractures to involve the ribs, and 89% were metaphyseal. Pelvic fractures occurring in the absence of serious, well documented accidents are considered highly suspicious for child abuse (Starling *et al.* 2002). Femoral fractures in non-ambulant children are also thought to be virtually diagnostic of child abuse. Indeed, any fractures in non-ambulant children are recognised as meriting further investigation (Taitz *et al.* 2004).

Conclusions

It is clear that there are as many different types of fractures as there are mechanisms that cause them. The shape, extent, pattern and distribution of fractures are usually very indicative of the forces and types of impact that have caused them, and forensic investigators can use this phenomenon to their advantage. For example, the patterns of injury seen on people who have jumped from heights are distinct from those seen on victims of accidental falling, and certain activities produce typical, almost diagnostic fracture patterns. We have seen that fractures belie their aetiology and can be used to support accusations of suicide, for example, or physical abuse. However, this capacity of investigators to 'read' fractures and make inferences about their causal factors relies heavily on the ability to detect fractures in both living and dead individuals. Without accurate visualisation techniques, the informative qualities of fractures are lost.

Introduction

The suspicion of the presence of a fracture has to be confirmed before any clinical assessment of the fracture can be made. The majority of long bone fractures are obvious to the patient and the emergency room staff, but fractures of the skull, ribs, vertebrae and digits may be difficult to detect. For example, patients with clinically obvious skull fractures represent only a tiny fraction of the millions who visit hospital each year after recent head injury (Jennett, 1980). It is the function of imaging techniques in the evaluation of the patient to demonstrate both the direct pathological and the secondary effects of fracture, and to provide sufficient information to guide patient care, management and, if necessary, surgery (Jones, 1997).

The role of imaging in trauma evaluation has increased over the last thirty years, particularly with the advent of computed tomography (CT) in 1972 (Kelly *et al.* 1988), and the introduction and more widespread use of magnetic resonance imaging (MRI) and sonography as diagnostic methods. However, each weapon in the ever-enlarging armoury of techniques at the disposal of accident and emergency units has its own strengths and weaknesses, as has been appreciated by many researchers (Goh *et al.* 1997; Hendler and Hershkop, 1998; Hendrich *et al.* 1995; Lloyd *et al.* 1996). The most commonly used imaging techniques for identifying and classifying fractures are conventional radiography, computed tomography, bone scintigraphy, and more recently, ultrasonography and dual-energy X-ray absorptiometry (DEXA). Magnetic resonance imaging, although not used specifically for the diagnosis of skull fractures, is a very important tool in the assessment of head injury, and so is appraised here. In order to assess the relative utility of the most common bone imaging techniques, it is necessary to understand the basic premise of how each works, and to examine the applications, practical considerations, and the advantages and disadvantages of each.

Conventional radiography

The value of conventional radiology in the diagnosis, localisation and classification of fractures is controversial. It used to be the 'gold standard' of imaging techniques for identifying both cranial and postcranial fractures (Hendrich *et al.* 1995), and McRae (1994) states that radiographic examination of suspected fractures is mandatory. He claims that they generally give a clear indication of the presence of a fracture, and provide a sound basis for treatment planning (McRae, 1994). Conventional radiography is also of value as documentation of multiplicity of injuries, especially in children with suspicion of abuse

(Mogbo *et al.* 1998) (see Figure 01: 03: 01). They are particularly useful in the diagnosis and assessment of skull, vertebral and scapular fractures (Kleinman, 1998).

Figure 01: 03: 01 An example of a radiograph used as a document of an eggshell fracture in a child suspected of abuse. (Image courtesy of www.vh.org).

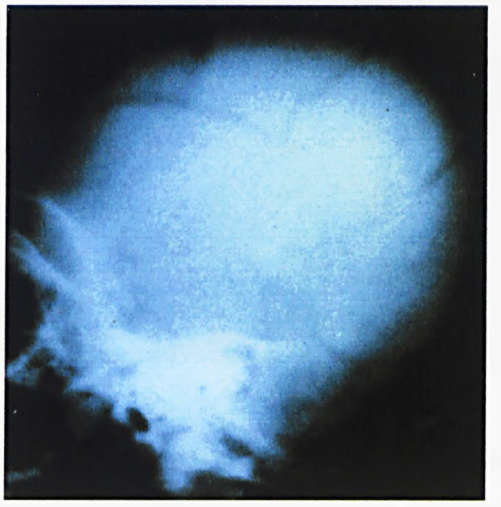

However, conventional radiography is now viewed by most researchers as only having a limited role in head injury evaluation (Cummins, 1997; Jones, 1997; Lloyd *et al.* 1996). Some maintain that plain skull X-ray films provide a good, simple method of demonstrating fractures of the cranial vault (Moseley, 1979), particularly linear fractures (Gean, 1994) (see Figure 01: 03: 02). However, as a skull fracture in isolation has few clinical consequences, except in the case of a depressed fracture (Hofman *et al.* 2000), an increasing number of radiographers are turning to CT scanning as a means of demonstrating more clinically significant intracranial trauma (Gean, 1994; Hofman *et al.* 2000).

Figure 01: 03: 02 A plain film radiograph of a linear skull fracture in the parietal bone of an adult. (Image courtesy of www.trauma.org)

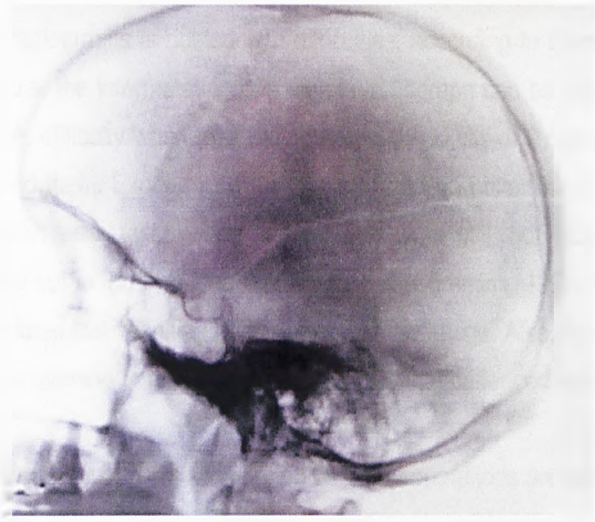

X-rays are man-made ionising radiation, identical to gamma rays in their high frequency and short wavelength. X-rays are produced in an X-ray tube when electrons are accelerated across a vacuum. A radiograph is produced when X-rays pass from the tube, through the patient, onto photographic film (Weir and Murray, 1998). X-rays are absorbed to a variable degree by different body tissues depending on their density. Black areas on the radiograph indicate structures of low density, such as air in the lungs, through which the X-rays easily pass to blacken the film. Radio-opaque white areas indicate structures of high density, such as bone, which absorb X-rays so fewer pass through to the film (Roberts *et al.* 1998). The way in which X-ray films are produced is associated with many of the disadvantages of the technique. Many accident and emergency departments still obtain skull plain films for any injury to the skull, no matter how trivial (DeLacey *et al.* 1980; Gean, 1994; Jennett, 1980). This overuse of radiographs contributes not only to rising health care costs, but also to increased doses of radiation. All ionising radiations, such as X-rays, have a potential for harm, even in small doses (Weir and Murray, 1998). Exposure to X-rays creates some risk for patients, but especially for radiographers, who are particularly vulnerable. Exposure to radiation can have effects which manifest immediately, or are not exhibited for years or generations. Erythema, or 'radiation burn' can often be seen immediately after examination, and was the first unit used to measure radiation dosage (Ehrlich *et al.* 1999). Longer term effects are less easy to predict or identify. Documented latent effects of low doses of ionising radiation include cataract formation and an increased risk of malignant disease (Ehrlich *et al.* 1999). Genetic mutations, affecting future generations, are associated with exposure of the gametes to ionising radiation, which necessitates the use of lead shields

during pelvic examinations. Radiation exposure poses specific risks to the developing embryo, which restricts its use on pregnant women (Ehrlich *et al.* 1999).

The use of plain skull radiographs is riddled with difficulties, according to Cummins (1997). For even the most experienced doctors, the interpretation of a simple radiograph can be problematic. Weber and Folio (1976) demonstrated this difficulty when they radiographed the skulls of 9 cadavers, fractured their crania and then re-radiographed them. Experienced radiologists fared no better than juniors at the interpretation of the radiographs, which were taken when the subjects were still, but most emergency radiographic examinations are carried out in far from ideal circumstances (Cummins, 1997). Patients may be confused or drunk and unable to keep still, resulting in a useless blurred image. Also, over half of all radiographs of fractures are taken in the evening or at the weekend, often by inexperienced staff (Cummins, 1997).

In infants suspected to be victims of child abuse, epiphyseal separations are very difficult to diagnose with radiographs because of limited ossification of the cartilaginous epiphyses (Kleinman, 1998), and cross-sectional imaging is often required as a double-check method to fully characterise the injury (Kleinman, 1998). Sonography or magnetic resonance imaging is often required in cases where fractures are not always visible. Greenstick fractures of the wrist in children are also often over-looked on radiographs, due to a lack of care in studying the images (McRae, 1994). Radiography has also recently been recognised as a poor technique with which to measure fracture healing. It was found to show poor correlation with biomechanical testing and histological techniques of assessing healing (Blokhuis *et al.* 2001).

A small number of modern researchers still champion X-ray radiography as a method of diagnosing fractures, despite the swing in popularity towards CT scanning. The radiation doses from X-rays are tiny in comparison to those from CT examinations. For example, the radiation dose from a chest radiograph is approximately the equivalent of 3 days background radiation; but the dose from a CT scan of the chest and abdomen can be as much as 450 times that of a chest radiograph – equivalent to about 4 years of natural background radiation (Weir and Murray, 1998)! Gean (1994) suggests that CT scans can be less sensitive than plain radiographs in diagnosing linear skull fractures, and that true plain films sometimes can be used more successfully to localise the weapon in penetrating injuries. Cummins (1997) describes how depressed skull fractures can be seen clearly on plain films as a curvilinear area of double density due to overlapping bone fragments. He also states that X-ray films are often better at depicting cranial vault fractures than CT scans, especially when the fracture runs parallel to the CT section. Jones (1997) maintains that plain films still have a role in the management of minor and moderate head injuries, especially in departments where CT scanning is not available 24 hours a day. Also, the development of

powerful portable radiograph machines now ensures excellent quality films in most emergency departments (Cummins, 1997).

Computed tomography (CT)

Computed tomography is primarily used in the diagnosis and assessment of head injury and skull fracture, but also plays a valuable role in the imaging of post-cranial fractures and bone pathology. The detailed structure of bone can be easily visualised with CT, and CT scanning allows the very early diagnosis of skeletal metastatic disease (Kreel and Meive, 1979). The display of complex facial, skull and pelvic fractures and pathology is greatly facilitated (Kreel and Meive, 1979). Resnik *et al.* (1992) concluded that although plain film radiography was sufficient to identify virtually all pelvic fractures and dislocations, plain radiographs alone were not accurate enough to detect fracture fragments within the hip joint, and CT was recognised as the only way to accurately identify such intra-articular fracture fragments found in association with acetabular fractures (Resnik *et al.*, 1992).

Computed tomography (CT) is fast becoming the first and only examination for head-injured patients, especially those with medium to high risk of intracranial injury (Jones, 1997), and, more recently, even for those with minimal head injury (Nagy *et al.* 1999). It is said to have revolutionised neuro-radiological techniques, and displaced older conventional methods such as air encephalography and angiography (Kreel and Meive, 1979). CT, like conventional radiography, uses X-rays, but differs in that it can be used to produce a three-dimensional representation of anatomical structures (Weir and Murray, 1998). The X-ray tube revolves around the patient and detectors pick up the emergent beam (Roberts *et al.* 1998). X-rays are emitted at predetermined intervals – usually between one and four seconds – as the tube revolves around the body, producing images of 'slices' of specified thickness through the body. Consecutive 'slices' can later be reconstructed to form a three-dimensional image (Roberts *et al.* 1998) (see Figure 01: 03: 03).

Figure 01: 03: 03 An example of how computed tomography images can be used to reconstruct a three-dimensional image of the skull, showing skull fractures. (Image courtesy of www.rctradiology.com)

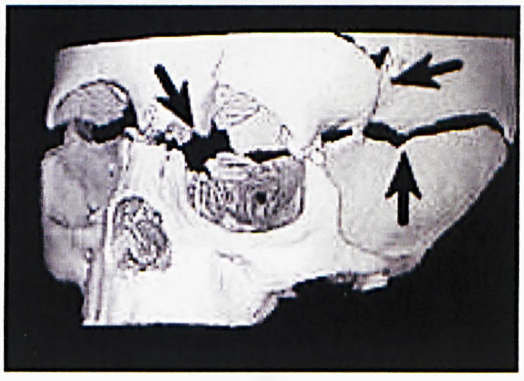

As the X-ray beam passes through the body, the tissues attenuate, or absorb and scatter, the X-rays. Each type of tissue attenuates the X-rays to a different degree, and these values are computerised to give a pixelated image in varying shades of grey. In comparison to plain radiographs, the visual grey scale is enhanced, improving organ visualisation and definition (Roberts *et al.* 1998). The image can be manipulated to include detail of tissue with widely varying densities, so that bone and soft tissue can be visualised together. Also, lower contrast agent concentrations - sometimes needed for increasing definition for plain radiographs - are necessary for CT, because the image and contrast is enhanced by the digitisation (Roberts *et al.* 1998).

For the examination of skull fractures and head injury, CT does not show all skull vault fractures, particularly those parallel to the CT sections, but that it does reveal depressed fractures and fractures of the base of the skull, which cannot always be seen on plain skull X-ray films (Jones, 1997. See Figure 01: 03: 04). Goh *et al.* (1997) also advocate the use of CT scans to demonstrate suspected basal skull fractures, as clinical features and radiological evidence are not always reliable. CT scanning is important because it reveals intracranial haematomas, which, if missed, are very costly in terms of mortality and morbidity (Goh *et al.* 1997). Tanrikulu and Erol (2001) favourably compare CT to conventional radiography for the assessment of midfacial fractures, especially zygomatic fractures, as the exact position of the major articulations of the zygomatic bone can be seen more easily with CT, which facilitates treatment.

Figure 01: 03: 04 An example of a CT scan showing a clinically significant depressed skull fracture. (Image courtesy of www.rad.usuhs.mil/rad)

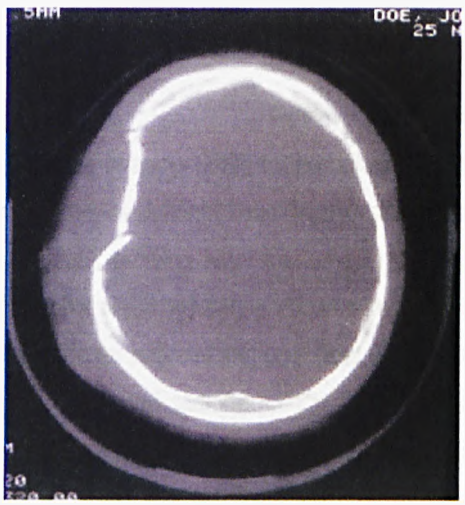

However, CT has its challengers. Gean (1994) asserts that CT is not always useful in the evaluation of head trauma in children suspected of abuse, as linear fractures may often be invisible in CT scans because of the relatively thin, incompletely ossified skulls of children. The American College of Radiology specifically advises that all children under 2 years old with head trauma should have a CT scan (Mogbo *et al.* 1998), but Mogbo *et al.* (1998) dispute this recommendation. They claim that the routine imaging of head-injured children is unnecessary, and could lead to excessive exposure to ionising radiation. They also suggest that CT does not alter the clinical management, clinical outcome or legal outcome of the head injury, and that magnetic resonance imaging (MRI) may be more useful than CT in depicting soft tissue trauma of clinical significance (Mogbo *et al.* 1998). Another disadvantage of CT imaging is that the sensitivity of a scanner to changes in tissue attenuation is limited by random fluctuations present in the scanned data. A small change in the attenuation of a tissue may not be detected if it is smaller than the ubiquitous random fluctuations present (Pullan, 1979). When compared to techniques such as MRI and ultrasonography, CT has not been entirely successful (Ellis *et al.* 2000; Kelly *et al.* 1988; Kreel and Meive, 1979; Mogbo *et al.* 1998). The capital outlay and running costs of CT scanners are about ten times that of ultrasound scanners, and the number of patients seen daily is approximately a third of that of an ultrasound scanner (Kreel and Meive, 1979). This means that CT is vastly more expensive per examination than ultrasound. Ellis *et al.* (2000) deride CT imaging by saying that although it remains the preferred imaging technique for acute head injury, it can fail to show the severity of craniocerebral trauma. Inappropriate algorithms and artefacts may obscure injuries located near the base of the skull. A fracture on a CT scan may look deceptively benign, because the fracture margins do not appear greatly depressed and the cortical contusion beneath the fracture may appear trivial (Ellis *et al.* 2000). They declare that MR imaging surpasses CT in depicting cranial burst fractures and associated intracranial injuries in children (Ellis *et al.* 2000).

Magnetic resonance imaging (MRI)

The application of magnetic resonance imaging (MRI) to the detection of fractures is primarily through its use as a method of diagnosing and evaluating head injury, skull fractures and intracranial trauma. Recently, it has been used to assess growing skull fractures in children (Ellis *et al.* 2000). Magnetic resonance imaging is unlike conventional radiography and computed tomography because it does not use ionising radiation, which makes it safer for patients and operators (Ehrlich *et al.* 1999; Roberts *et al.* 1998). MRI combines a strong magnetic field and radiofrequency (RF) energy to study the distribution and behaviour of hydrogen protons in fat and water (Weir and Murray, 1998). The proton in the nucleus of each hydrogen atom in the body acts as a tiny magnet. Normally, the magnetic moments of the protons are randomly arranged, but when the patient is placed in the strong magnetic field of the MR machine, these

magnetic moments align, either with or against the field lines of the magnet, creating a magnetic vector. Radiofrequency energy is used to rotate the protons while they are influenced by the magnetic field. When the RF energy is switched off, the protons 'flip' back to their original position, and as they do so, they emit a small radiofrequency signal. These signals are detected by the antennae in the MRI machine, and digitised, amplified and spatially organised. The resulting image is displayed on the operator's console (Weir and Murray, 1998). MR imaging provides excellent imaging of the soft tissues of the nervous system, and so is especially valuable in the diagnosis of many types of pathology, including brain and spinal cord tumours (Ehrlich *et al.* 1999) (see Figure 01: 03: 05).

Figure 01: 03: 05 An example of a MRI scan of an adult head. It is a particularly effective technique for demonstrating soft tissue trauma and pathology. (Image courtesy of www.rubomed.com)

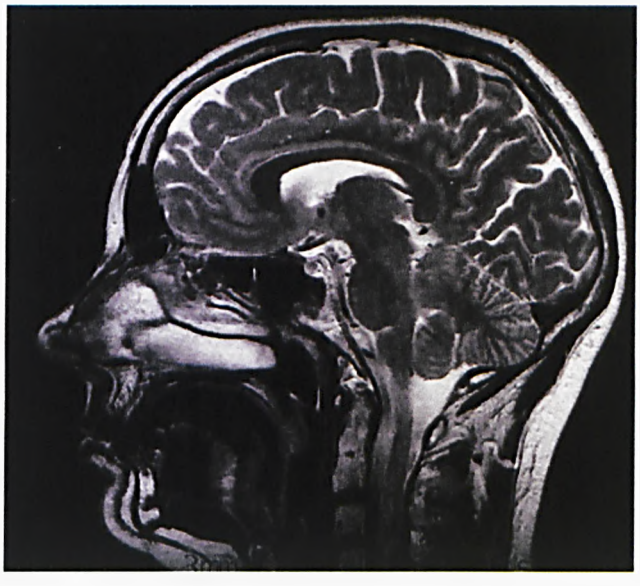

The multi-planar capacity of MRI allows images of the body to be taken in several planes while the patient is in one position, and is recognised as a great advantage of this technique (Roberts *et al.* 1998). When used to detect intracranial trauma, magnetic resonance images are unencumbered by artefacts from adjacent bone (Kelly *et al.* 1988), which is an indication that MRI is not an ideal technique to use when looking at postcranial bone fractures and evidence of healing. However, it recently has been found to be valuable in improving the early diagnosis of skull fracture in children, as it reveals the site of the injury – the dural cortical surface – much more clearly than CT (Ellis *et al.* 2000). It has been successful in showing evidence of temporal bone fractures, but only when these contained blood or cerebro-spinal fluid. It was not superior to CT, which demonstrated the full extent of the fractures (Zimmerman *et al.* 1987).

Although MRI is not associated with any recognised biological hazard, there are considerable limitations to its use. It is not a safe technique for patients with pace-makers or other electroinductive implants, including aneurysm clips, neurostimulators, orthopaedic protheses, intra-uterine devices or artificial heart valves (Ehrlich *et al.* 1999; Weir and Murray, 1998). This property of MR scanning underlies its major current limitation as an emergency procedure. Logistic problems are encountered with patients whose condition necessitates extensive monitoring or life support equipment (Kelly *et al.* 1988). As loose metal objects and metal equipment cannot be taken in the examination room, it is impossible to scan such patients using magnetic resonance imaging. These factors greatly reduce the number of individuals who can be examined safely using MRI, and so CT scanning remains the screening procedure of choice, especially in emergency departments (Ehrlich *et al.* 1999; Kelly *et al.* 1988). Rare problems can occur, such as patient allergy to the paramagnetic contrast media used, and claustrophobia within the enclosed space of the gantry (Ehrlich *et al*, 1999).

Ultrasonography

Ultrasonography as a diagnostic technique for identifying fractures and bone disease is a relatively recent addition to the medical imaging armoury. In 1979, Kreel and Meive maintained that ultrasonography had 'no part to play' in the diagnosis of skeletal disease or the imaging of bone (Kreel and Meive, 1979); yet in the last decade, it has become more and more popular as an alternative to plain film radiographs (Caruso *et al.* 2000; Hendrich *et al.* 1995; Maffulli and Thornton, 1995; Steiner and Sprigg, 1992; Yoshioka *et al.* 1997; Young *et al.* 1990). Pulse-echo ultrasonic diagnostic methods depend primarily on the measurement of the time delay between the transmission of a brief pulse of high frequency ultrasound and the reflection of its echo from tissue interfaces in the body (Wells, 1979). As the sound beam travels through the tissues, it is attenuated and reflected. The reflection of sound waves back to the receiver produces the image (see Figure 01: 03: 06).

The texture of the image is dependent on the differences in acoustic impedance between different tissues (Wells, 1979). Sophisticated hardware has been developed that converts the pulse-echo system into a real-time two-dimensional sectional image, analogous to the sectional image of CT (Weir and Murray, 1998). Fluid is a good conductor of sound, and air is not (Roberts *et al.* 1998), as it attenuates and reflects ultrasound strongly. This necessitates the use of a liquid coupling medium, such as a gel or oil, which is smeared on the skin to ensure effective transmission of the ultrasound between the probe and the patient (Wells, 1979).

Figure 01: 03: 06 An example of an ultrasound image of a bone fracture.
(Image courtesy of www.worldwidefeet.com)

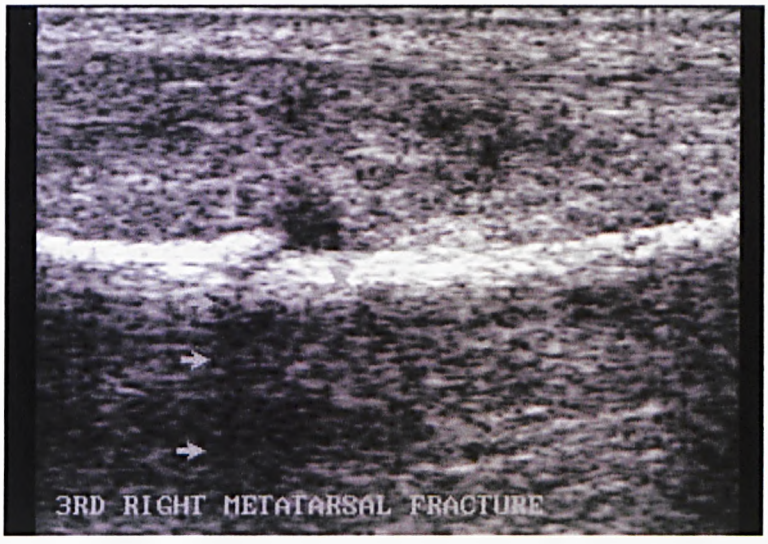

Ultrasonographic scanning (US) has been used recently in the diagnosis of fractures of the sternum (Hendrich *et al.* 1995), and high-resolution, real-time US for fractures of the clavicle, humerus and femur (Maffulli and Thornton, 1995). Ultrasound scanning has also been used to aid diagnosis of fractures in infancy, separation of epiphyses and pathologies such as osteomyelitis (Steiner and Sprigg, 1992). Monitoring of new bone formation at the distraction site of bone-lengthening procedures such as the Ilizarov technique is an important application of sonography (Caruso *et al.* 2000; Leitgeb *et al.* 1990; Young *et al.* 1990). Hendrich *et al.* (1995) used ultrasonography to demonstrate and diagnose sternal fractures, and found that, by using criteria such the presence of a disruption to the bony outline, and the formation of an echo-free area, they could corroborate radiological findings, and even detect fractures where plain films could not (Hendrich *et al.* 1995). Sonography *should* have a theoretical advantage over conventional radiography in its sensitivity. While radiography can only show a cortical gap in the orthograde projection, the ultrasound transducer can be adjusted very easily to highlight the greatest disruption of the bony outline (Hendrich *et al.* 1995). Ultrasonography has also proved invaluable in assessing callus formation and healing in long bone fractures (Caruso *et al.* 2000; Hendrich *et al.* 1995; Leitgeb *et al.* 1990; Maffulli and Thornton, 1995; Young *et al.* 1990), which is discussed later.

The advantages of sonography over conventional radiography, CT and MRI are mainly concerned with the practicalities of its use. The handling of the sonographic device is very easy to learn, but does require a

trained professional. The positioning of a severely-injured patient for a radiographic examination is sometimes difficult, but ultrasound scanning can be performed easily with the patient lying down (Hendrich *et al.* 1995). With patients undergoing limb-lengthening, the external metal fixators create problems for positioning the X-ray tube, and they preclude the use of MRI (Steiner and Sprigg, 1992). Ultrasound scanning provides a useful alternative in these cases. Ultrasonography does not use ionising radiation, which makes it an ideal diagnostic technique for children and pregnant women (Roberts *et al.* 1998).

The main disadvantage of ultrasound, like CT, is that if the extent of the displacement of bone is greater than one antero-posterior thickness, it cannot be detected (Hendrich *et al.* 1995). Also, training of technicians to use ultrasound equipment and to interpret sonographic images takes longer than that for radiologists, and the individual ability of the technician has a greater influence on the quality of the image than with CT or conventional radiography (Kreel and Meive, 1979). As ultrasound waves are strongly reflected and attenuated by body tissues, the beam may be badly distorted, and can reverberate between reflecting surfaces, causing multiple reflection artefacts on the image (Wells, 1979). Also, it is much more difficult to determine the exact position of structures within the body using ultrasonography than with conventional radiography or CT, where true axial images are possible (Kreel and Meive, 1979).

Dual energy X-ray absorptiometry (DEXA)

Two other bone imaging techniques are worth mentioning. Dual energy X-ray absorptiometry (DEXA) and bone scintigraphy can both be used to localise and evaluate fractures. DEXA uses low energy X-rays passed through bones to measure the calcium content of the bones (www.spine-health.com). Its miniscule radiation dose and high accuracy means that it is currently the modality of choice for assessing bone mineral density (www.vig.com.au). Although it is most commonly applied to monitor bone density levels in patients with osteoporosis, DEXA has been used to locate areas of low bone density such as fractures in the early stages of healing, and to predict future fracture risk.

Bone scintigraphy

Bone scintigraphy is one of the most commonly performed studies in nuclear medicine, and is especially useful for diagnosing and locating stress fractures (Hendler and Hershkop, 1998) (see Figure 01: 03: 07). The unstable radioactive isotope Technetium (^{99m}Tc) methylene diphosphonate is the radio-pharmaceutical agent used most often for scintigraphy. Once injected into the patient, the phosphate compounds enter into the same chemical reactions as their stable counterparts, and bind to bone by chemiadsorption to the hydroxyapatite crystal. Because they are metabolised in the body the same way as ordinary phosphate compounds, and are detectable using a gamma camera, the appearance of activity on the scan usually

reflects osteoblastic activity in the bone (Hendler and Hershkop, 1998). Scintigraphy is used to detect fractures when the results of plain films are normal or equivocal. For example, rib fractures can be difficult to assess on plain X-ray films, but are easily demonstrated with scintigraphy. Although fractures are not always visible immediately on scintigraphy scans, 95% of scans are positive for fracture within 24 hours, and 100% are positive within 72 hours (Hendler and Hershkop, 1998). The high sensitivity of scintigraphy to detect small changes in bone formation and bone blood flow mean that it is a method that is both more sensitive and more specific than the standard methods. ^{99m} Tc-labelled compounds have also been used to study fracture healing (Hughes, 1984).

Figure 01: 03: 07 An example of a bone scintigraphy scan of a patient exhibiting a stress fracture of the right distal tibia (black arrows). (Image courtesy of www.unipd.it)

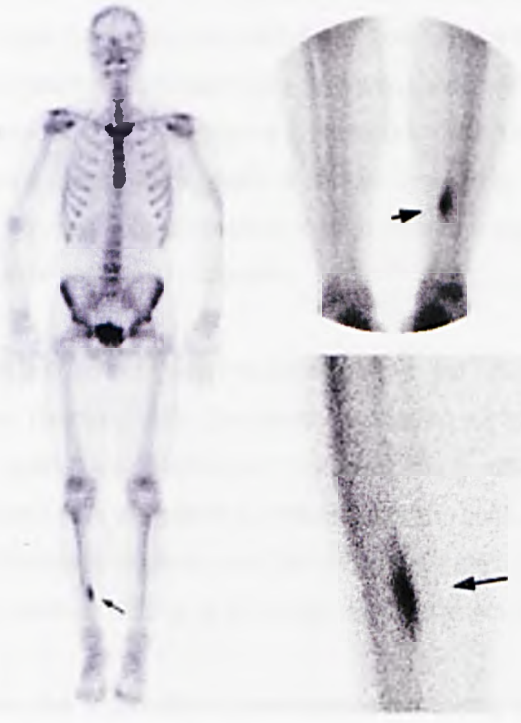

The diagnosis of skeletal injury in child abuse has been aided by the development of bone scintigraphy and an increased use of radiopharmaceuticals and especially bone avid polyphosphate compounds (Kleinman, 1998). In the hands of radiologists and technologists with strong training and experience with paediatric training, scintigraphy is a valuable technique for assessing skeletal injury. Although plain radiography is sufficient for most fractures, certain images demand cross sectional imaging (Kleinman, 1998).

Scintigraphy is a superior method for the diagnosis and assessment of rib fractures, acute non-displaced long bone fractures and subperiosteal haemorrhage (Kleinman, 1998).

Fracture healing

The assessment of bone fracture healing is a key application of the bone imaging techniques discussed here. It is clinically important to be able to evaluate the rate of union of a fracture, especially in long bones, and to know whether surgery and further intervention is required. Conventional radiography, ultrasound and bone scintigraphy are the imaging techniques used most commonly to evaluate fracture healing. Radiography is the method universally used to demonstrate fracture healing, but can only be used once calcification starts to take place (Maffulli and Thornton, 1995), as the only indications of fracture healing on a plain film are hard callus formation and greater bone density implied by increased radio-opacity. Thus conventional radiography cannot be used to visualise the repair process until 30 – 40 days after the fracture, once the radio-opaque hard callus has formed and bone density has increased (Caruso *et al.* 2000). Young *et al.* (1990) agree that plain radiographs cannot be used to detect new bone formation until a significant quantity has been laid down, and they are inadequate to determine the rate at which new bone production occurs in the early stages. Radiography is thought by some to be a very crude method of assessing the relatively simple parameters of presence of callus, new bone and subsequent bony union, as these features cannot always be seen on a radiograph.

There is a good correlation between magnetic resonance images and histological events in tibial shaft fracture healing (Maffulli and Thornton, 1995). The tissues surrounding the fracture site gradually develop signs corresponding to the calcified area (Maffulli and Thornton, 1995). It would theoretically be possible to evaluate fracture healing using DEXA to measure to gradual increase in bone density. However, in practice in many hospitals, once a fracture is diagnosed and the limb put into plaster, the assessment of healing and bone density becomes extremely difficult, as the plaster may appear almost as white as the bone itself.

Ultrasonography has proved very successful in demonstrating the healing of bone fractures. Histologic studies suggest that one of the earliest changes during new bone formation is the development of small blood vessels. The capillaries surrounding the fracture site show signs of neoangiogenesis, which is accompanied by osteoblast proliferation in the first week after trauma. This process can be identified on grey-scale sonography about three weeks after fracture (Caruso *et al.* 2000). Serial ultrasound scanning allows the study of the fracture healing process *in vivo*, with apparent good matching between images and the known histology of fracture healing (Maffulli and Thornton, 1995; Steiner and Sprigg, 1992). Colour Doppler sonography has been used to monitor the first stages of fracture callus formation, even earlier

than is possible with grey-scale sonography (Caruso *et al.* 2000). The sonographic appearance of new bone consists of echogenic foci within the cortical gap, which become aligned in the longitudinal plane, and increase in number and size until they coalesce as echo-dense bone, which does not allow transmission of the ultrasound beam (Young *et al.* 1990). Sonography is valued especially during Ilizarov limb-lengthening procedures, as new bone formation is detectable between one and three weeks after surgery – up to seven weeks earlier than with conventional radiography – which allows closer management of the delicate balance between healing and distraction of the bone segments (Young *et al.* 1990). Sonographic callus diagnosis can also focus on the texture of the callus in relation to adjacent muscle tissues (Leitgeb *et al.* 1990). Hendrich *et al.* (1995) have also suggested that sonographically visible echo-free zones, which indicate the presence of a haematoma, may be useful in the differentiation between fresh and old fractures in a short interval.

Bone scintigraphy has also been used effectively to study fracture healing. It is possible to distinguish between viable and non-viable experimental bone grafts by the degree of their radionuclide uptake (Hughes, 1984). This helps to differentiate between the clinically significant conditions of delayed union and non-union of a fracture. The rate of radioactive isotope uptake by the patient can be used to assess changes in bone blood flow and vascularisation, which are important indicators of progress in fracture healing. The measurement of radionuclide uptake by scintigraphy appears to be a reliable method of quantification of the rate of bone formation, something which has not been possible with ultrasonography or other techniques so far (Hughes, 1984; Maffulli and Thornton, 1995).

Conclusions

When faced with an injured patient, doctors have an impressive range of diagnostic imaging techniques at their disposal. However, it is clear that each method has its own particular strengths and weaknesses, which have to be balanced efficiently in order to provide a cost-effective, safe and accurate diagnosis. There are no incontrovertible guidelines for the use of bone imaging techniques, and their use is left to the discretion of the individual doctor. It is also clear that the most appropriate imaging techniques for diagnosing and examining fractures are independent and distinct from the most suitable method for the assessment of fracture healing.

For the majority of postcranial fractures, conventional radiography remains the technique of choice employed by emergency rooms and orthopaedic consultants. It remains the 'gold standard' for confirming the presence of a fracture and describing the extent of trauma. Resnik *et al.* (1992) showed that, for pelvic fractures at least, conventional radiography successfully accounted for 81% of fractures, and treatment

was not affected by any loss of information due to the use of this technique. It continues to represent a relatively inexpensive and generally reliable imaging technique, with acceptable risks to patients. The low radiation dose of a single x-ray in comparison to that of a CT scan helps to keep conventional radiography popular. However, more and more practitioners are recognising the benefits of computed tomography, and the use of these scans as the first port of call to look at a fracture is increasing.

For patients exhibiting cranial fractures, computed tomography appears to be most the most effective imaging technique for the evaluation of cranial fractures. It demonstrates almost the full array of fracture types, and can reveal intracranial trauma, which is usually more clinically significant. CT images are typically detailed and clear, with digitally enhanced contrast, and can show bone and soft tissue simultaneously. The sectional images can be combined to produce a true three-dimensional reconstruction of the head, which may facilitate surgery as structures can be pinpointed exactly. CT remains more capable at demonstrating the majority of cranial fractures than conventional radiography and MRI, and continues to be the first choice examination in most emergency departments.

In the evaluation of fracture healing, ultrasonography and scintigraphy are undoubtedly the most valuable of the imaging techniques. Ultrasound is beginning to be recognised as extremely effective as a tool for assessing callus formation and new bone growth in long bone fractures (Caruso *et al.* 2000; Maffulli and Thornton, 1995; Steiner and Sprigg, 1992). It is also especially helpful in aiding the management of treatment in Ilizarov limb-lengthening procedures (Young *et al.* 1990). Colour Doppler sonography may be useful in the diagnosis and evaluation of skull fractures, especially in growing fractures in children, as it can exhibit brain protrusions through the bony defects (Yoshioka *et al.* 1997). However, it does not appear that much research has been undertaken to investigate the use of sonography (Colour Doppler or grey-scale) in the assessment of cranial fracture healing. Bone scintigraphy is a technique with few contraindications that is valuable in the diagnosis and evaluation of fractures. It is also, more importantly, one of the few techniques that allow quantification of healing rate, by assessing changes in bone blood flow and vascularisation around the fracture site (Hughes, 1984). Its only limitations are that it exposes the patient to radiation and is only possible to do *in vivo*. Studies in fracture healing are lacking, as it is not ethically feasible to biopsy patients in order to provide serial correlation of radiographic images with histological samples (Maffulli and Thornton, 1995), so ultrasonography and scintigraphy are prized additions to the arsenal of imaging methods for research and diagnostic purposes.

Introduction

Fracture healing has been described as one of the most remarkable of all biological processes in the body (Doblare *et al.* 2003; McKibbin, 1978). Unlike skin and other soft tissues, bone healing can be so complete that it results not in a scar (Martin *et al.* 1998; Webb and Tricker, 2000), but in the reconstitution of tissue indistinguishable from the original pre-trauma tissue. Fracture healing is a spontaneous process that, in favourable conditions, can result in the full reconstitution of the injured tissue and restoration of strength and function (Doblare *et al.* 2003; Soames, 1995; Szachowicz, 1995). It is a complex, carefully choreographed ballet of immigration, differentiation and proliferation of a wide range of cells including inflammatory cells, angioblasts, fibroblasts, osteoblasts and osteoclasts. This section aims to furnish the reader with an understanding of the predictable cellular processes involved with fracture healing, and the stages of healing which can be monitored with immunohistochemical techniques.

Fracture healing can be either primary or secondary. Primary healing occurs only in cases where the fracture gap is very small and the bone fragments are stable and immobile. Osteoprogenitor cells in the periosteum proliferate and differentiate into osteoblasts and secrete osteoid into the extra-cellular matrix adjacent to the fracture site. This form of healing is straightforward, without the preliminary development of fibrous tissue or cartilage (Funk *et al.* 2000; Soames, 1995).

Secondary fracture healing

The majority of human fractures are repaired by secondary fracture healing. It is more efficacious than primary healing, and provides a stronger bridge between the bone fragments. Secondary healing occurs when the fragments of bone are not stable and the gap size is moderate or large. This takes the form of endochondral ossification, where a cartilaginous callus is formed, calcified and eventually replaced by bone. The formation of a cartilage collar is stimulated by the movement of the fragments, and it serves to increase the stiffness of the bone at the fracture site, and therefore increase stability (Doblare *et al.* 2003). Secondary fracture healing is traditionally described as a series of phases, which occur in sequence but which also overlap (Nicoll *et al.* 1998). The introduction of cellular and molecular biology techniques has allowed clearer visualisation of this process, and, on a microscopic level, it can be seen as a smooth continuum of cellular events (Funk *et al.* 2000; Webb and Tricker, 2000). The phases of secondary fracture healing are generally accepted as the inflammation phase; soft callus formation phase; hard callus formation phase and the remodelling phase (Biswas and Iqbal, 1998; O'Connor and Cohen, 1998; Soames, 1995).

The inflammation stage is triggered by the trauma itself. Inflammation begins immediately after fracture, and typically lasts for about four days (Soames, 1995). Initially there is bleeding from the damaged bone ends, periosteum and the ruptured blood vessels, and a haemorrhage quickly fills the gap between the fragments. The amount of blood that is lost from the circulation is often under-estimated, and in severe fractures of the femoral shaft or pelvis, it can amount to a litre or more (Sevitt, 1981). The role of the initial haematoma in the process of fracture healing is debated. Some researchers believe that it plays an active role in promoting fracture healing, as its fibrin network is thought to act as a scaffold for fibrocellular invasion, while others have claimed that the haematoma hinders bone repair and fracture union (Sevitt, 1981). There is also research to suggest that fracture union takes place normally in individuals with haemophilia, unless the fracture is unstable or badly positioned, which implies that the haemorrhage does not significantly affect the repair (Flatmark, 1964).

The haematoma acts as the source of haematopoietic cells and platelets that initiate the inflammatory cascade (Webb and Tricker, 2000). This is characterised by a predomination of neutrophils, lymphocytes, basophils, monocytes, platelets, mast cells and some macrophages (Oni, 1997a; Webb and Tricker, 2000). These circulating cells appear within minutes of the injury, and are attracted to the site by chemotaxis (Oni, 1997a). The clotting function of the platelets helps to stabilise the haematoma, and they release growth factors from their alpha granules, which include platelet-derived growth factor (PDGF) and transforming growth factor beta (TGF-β). PDGF has been shown to be a potent mitogen and regulator of all mesenchymal cells, including osteoblasts (Bostrom *et al.* 2000; Webb and Tricker, 2000). It stimulates cell replication and collagenous and non-collagenous protein synthesis. These growth factors also play a role in chemotaxis and angiogenesis (Bostrom *et al.* 2000; Webb and Tricker, 2000). To the swelling caused by the haematoma is added a proteinous, fibrin-rich, inflammatory exudate, which accumulates on either side of the fracture gap (Sevitt, 1981). This exudate is thick and highly eosinophilic, so is easily seen on histology slides stained with haematoxylin and eosin.

Vascular damage causes the fracture site environment to become hypoxic and acidic, which precipitates localised necrosis, or death of the surrounding bone cells (Junqueira *et al.*, 1995; Sevitt, 1981; Soames, 1995; Webb and Tricker, 2000). The hypoxia causes a drop in the pH level of the fracture site, from 7.4 to as low as 5.2, which returns to pre-fracture levels at about two weeks after injury (Devlin, 2003) (see Figure 01: 04: 01). Mast cells, polymorphonuclear leucocytes, neutrophils and macrophages appear at the site of injury and are stimulated by the low pH to release cytokines that initiate the healing process (Sevitt, 1981; Soames, 1995). Cytokines have a variety of functions, and serve to regulate haematopoietic cellular proliferation and differentiation in the early healing phase (Webb and Tricker, 2000). Some cytokines may stimulate the proliferation of reparative cells such as

osteoblasts, endothelial cells and even chondroblasts (Soames, 1995), and others have angiogenic functions, which facilitates healing, as the re-establishment of a rich blood supply is vital.

Figure 01: 04: 01 Graph showing changes in pH value at the fracture site in relation to time elapsed since trauma. (After Devlin, 2003).

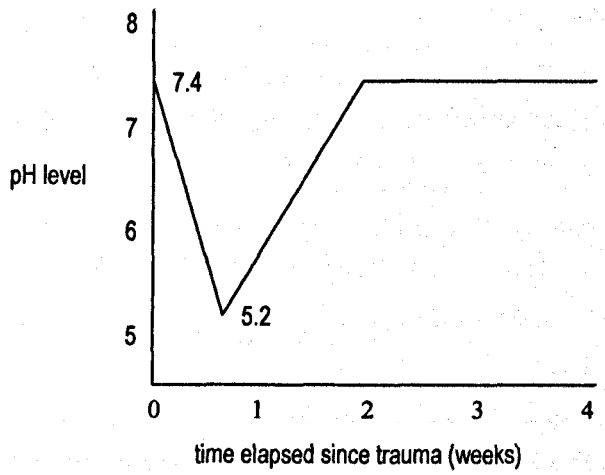

The necrotic areas become more evident as the initial haematoma gradually disappears due to lysis and phagocytosis (Sevitt, 1981). Necrotic compact bone is characterised histologically by empty lacunae, and is easy to distinguish microscopically. It extends some distance away from the site of the fracture, and can be measured to assess the progress of the fracture healing process. This histomorphometric measurement was used to quantify the effect of haemorrhagic shock on osteocyte necrosis after closed bone fracture by Wichmann *et al.* in 1996. Macrophages, easily visualised using immunohistochemical stains such as CD68, erode and resorb necrotic bone and remove tissue debris from the fracture site through the process of osteoclasis (Junqueira *et al.* 1995; Sevitt, 1981; Soames, 1995). Osteoclasts, which are bone-specific macrophages, also work to clear the site of dead bone, as they are stimulated into action by the ambient acidic environment (Soames, 1995). It is thought that the macrophages may also secrete factors which stimulate collagen production, which may be beneficial in the fracture healing process (Soames, 1995). Macrophages also infiltrate the fracture area and help to remove the extravasated red cells and collagen fragments by phagocytosis and by degrading haemoglobin to haemosiderin. Haemosiderin particles are stained blue by Perls' Prussian Blue stain, which reacts with the ferric iron of haemosiderin to produce the blue compound ferric ferrocyanide, visible on histology slides.

Unequivocal microscopic signs of cell proliferation are first seen a few days after injury in most human fractures, either in the periosteum or the medulla or both (Sevitt, 1981). Reparative activity is first

visible in fractured ribs after about three or four days after injury, and appears slightly later in the medulla of femoral fractures, especially complicated pertrochanteric fractures (Sevitt, 1981). Cell proliferation is characterised by an increase in abundance of osteogenic or osteoprogenitor cells, which migrate to the fracture site from the peripheral regions of the fractured bone (Devlin, 2003). As the haemorrhage subsides, minute vessels sprout from undamaged capillaries and grow towards the fracture site. Vasoactive substances such as nitric oxide and enthothelial stimulating angiogenesis factor cause this neo-vascularisation (Borrill *et al.* 2001).

Bone healing depends on the development of a highly specialised vascular and cellular tissue, which has the potential to form bone, cartilage or fibrous tissue (Sevitt, 1981). It originates from the periosteum and the medulla some distance away from the fracture, and migrates slowly towards the fracture site. This mass of proliferating, migrating, differentiating and matrix-producing cells, termed a *blastema* by Pritchard (1964), is osteogenic in nature. It is composed of osteogenic cells of mesenchymal origin, which have the potential to differentiate into osteoblasts, chondrocytes and fibroblasts; other connective tissue cells such as histiocytes and lymphocytes; and small blood vessels. It is referred to by most pathologists and clinicians as *osteogenic granulation tissue* (Sevitt, 1981). New granulation tissue usually appears in isolated pockets which grow, coalesce and spread to involve more and more of the marrow surrounding the damaged areas. Blood vessels and the accompanying cells migrate into the damaged marrow at the same time, and then into the fibrous exudate in the fracture gap (Sevitt, 1981). This provides the ideal environment for subsequent callus formation.

The soft callus phase begins any time between two days and two weeks after fracture (www.orthoteers.co.uk). The process of rapid soft callus formation and its subsequent remodelling is critical to successful bone healing (Ford *et al.* 2002). Soft callus formation occurs at and overlying the fracture site through the process of endochondral ossification (Webb and Tricker, 2000). The soft callus serves to increase stability between the bone fragments by bridging the gap between them, and its formation is stimulated by movement of the fragments and inhibited by immobility brought about by rigid fixation (Sevitt, 1981; Webb and Tricker, 2000). By increasing the stability between the fragments, it works to increase the likelihood of eventual union (Soames, 1995). In cases where the medullary cavity is destroyed by intramedullary reaming, soft callus becomes the only way that provisional bridging can be achieved (Sevitt, 1981).

Soft callus is also referred to as periosteal callus, due to its periosteal origin (Oni, 1997b). The role of the periosteum in fracture healing becomes clear, as it is the source of the undifferentiated mesenchymal cells which migrate towards the fracture site, where they transform into cartilage-producing chondroblasts (Ito *et al.* 2001). At first, the proliferating part of the periosteum is only a few cells thick, but it soon becomes a thick layer of highly cellular tissue. This periosteal proliferation takes

place on both sides of the fracture gap, and starts where the marrow and periosteum are undamaged and viable, eventually moving towards the fracture site. As a consequence, the area of damaged periosteal layer immediately adjacent to the fracture site is the last to be colonised by callus. Periosteal activity is most prolific where the overlying soft tissue is thick, as the callus blood supply is derived from the overlying soft tissues (Sevitt, 1981). Evidence of this can be seen is callus formation around tibial fractures, which is concentrated on the posterior aspect of the bone, and very little callus is formed anteriorly (Sevitt, 1981). The proliferating callus tissue separates the outer fibrous layer of the periosteum from the cortex. The fibrous periosteum forms a sealed capsule for the expanding callus masses, which enlarge outward and toward each other, eventually fusing to form a bridge between the bone fragments (Sevitt, 1981). Because of the vital role it plays in chondro- and osteo-genesis, preservation of the periosteum is essential for successful fracture healing, and in surgery, all measures are taken to preserve its integrity and function.

Chondrocytes also proliferate, and become the predominant cell type in the soft callus phase (Webb and Tricker, 2000). Histologically, the soft callus appears as a dense cluster of chondrocytes, surrounded by a cartilaginous matrix (Ford *et al.* 2003). Those cells in the non-cartilaginous matrix are receptive to Alcian blue stain, and are visible within their lacunae at early stages of the soft callus phase. As the chondrocytes hypertrophy, intracellular vesicles appear, enlarge and release their contents into the extra-cellular matrix through exocytosis (Webb and Tricker, 2000). These vesicles contain the three components required to allow cartilage calcification – proteases, phosphates and calcium (Webb and Tricker, 2000).

As the soft callus matures, new matrix is formed at the cartilage edge (Ford *et al.* 2003). The Alcian blue-staining cartilage matrix of the soft callus gradually disappears and is replaced by new cartilage composed primarily of type I collagen (Ford *et al.* 2003). It is thought that the chondrocytes in the centre of the cartilage undergo apoptosis or 'cell suicide', but those around the edges of the cartilage were found not to exhibit the classic features of this form of cell death (Ford *et al.* 2003). Instead, they shrink within their lacunae and eventually disappear, which possibly occurs due to the absence of phagocytic cells in the cartilage tissue (Ford *et al.* 2003). The gradual replacement of the chondrocyte-rich soft callus by non-collagenous extra-cellular matrix heralds the start of the hard callus phase.

During this stage of fracture healing, the external periosteal and internal endosteal soft callus are gradually converted into woven bone primarily by the process of endochondral ossification (Soames, 1995). An exception to this occurs if the bone fragments have been surgically immobilised with a compression plate, in which case intramembranous ossification dominates (Soames, 1995). Both the cellularity and vascularity in the immediate environs of the fracture increase, as does the pH value gradually (Soames, 1995). Osteoclastic activity continues to remove necrotic bone and debris from the

fracture site, and chondrogenesis and osteogenesis persist until firm bony union is reached (Soames, 1995). The ossification of the hyaline cartilage of the periosteal callus surrounding the fracture gap and the callus in the medullary cavity often takes place contemporaneously with the deposition of new callus cartilage by osteogenic cells (Sevitt, 1981). This means that endochondral ossification and new cartilage formation can occasionally be seen in the same histology slide. At first, the new woven bone forms in a thin layer adjacent to the cortex, and this is accompanied by the formation of new trabecular bone concentrated around the clumps of cellular proliferation distant from the actual fracture site (Sevitt, 1981). Appositional formation broadens the trabeculae, and then new lamellar bone is deposited on their surfaces, giving the new bone a more compact structure (Sevitt, 1981).

Several matrix proteins are involved in this process of mineralisation. In particular, bone sialoprotein (BSP) is closely linked with the formation of hydroxyapatite crystals during mineralisation (Cuisinier, 1996). BSP is a phosphorylated protein which is spatially and temporally associated with the nucleation processes of bone crystals. It is produced in large quantities by cells in the osteoblastic cell lineage, and its three-dimensional structure facilitates the nucleation of the hydroxyapatite mineral (Cuisinier, 1996). It is actively involved in the process of mineralisation, and its presence in osteoblasts can be monitored immunohistochemically.

The process of mineralisation starts approximately three to four weeks after trauma, and the resulting gradual increase in radio-opacity is visible radiographically. This continues for approximately two to three months in healthy adults (Soames, 1995). In children, bony union is achieved much sooner, and a good rule of thumb for determining the healing period in children is that union occurs just after the same number of weeks as the child's age (O'Connor and Cohen, 1998). For example, a fractured femur in a three year old may take four weeks to unite, or nine weeks in an eight year old child. In an adult, however, a fractured femur may take between three and six months to unite (O'Connor and Cohen, 1998).

Immunohistochemical studies of nuclear activity during the soft and hard callus stages of repair have shown that the two processes begin at roughly the same time, but the duration of the former is prolonged as maturation of the callus involves more stages (Webb and Tricker, 2000). The end result of the two processes is the stabilisation of the fracture with a bony bridge, which is classified as the point of union (Webb and Tricker, 2000). Remodelling starts during the repair phase, and may continue for many years.

The final stage of the fracture healing process is that of remodelling the bone. This stage overlaps with the hard callus formation phase, and can continue for several years after the original fracture (Soames, 1995). It involves the gradual replacement of the woven bone of the hard callus with permanent,

mature lamellar bone (Soames, 1995). The method of remodelling differs according to the type of bone in which it occurs. In cancellous bone, the processes of bone deposition and apposition take place on the surface of the trabeculae. This is sometimes referred to as 'creeping substitution' (McKibbin, 1978). In compact bone, an orderly sequence of events is observed, as the replacement of osteons is a more complicated procedure. Osteoclasts gouge out a tunnel in necrotic bone, through which a blood vessel passes. This carries osteoblasts to the surface of the lamellar bone, where they can deposit layers of osteoid to build a new osteon (McKibbin, 1978).

Remodelling also refers to the continuous process of adapting bone to the stresses placed on it, in accordance with Wolff's law. After the fracture has been satisfactorily bridged, it is necessary for the newly-formed bone to adapt to its new functional demands. Osteoclasts remove excess bone from the exterior of the periosteal collar and from the callus between the fracture ends, so that the external lump of callus is thinned and the medullary cavity is restored across the fracture site (Junqueira *et al.*, 1995; Soames, 1995). If the fracture has united at an angle, new bone is incorporated on the concave aspect of the bone, while resorption takes place on the convex side, gradually straightening the bone (Catto, 1980). As the vascularity at the fracture site returns to normal, so does the oxygen supply (Soames, 1995).

Bone remodelling after fracture is a long process, and in adults, evidence of its continued action can still be seen up to seven years after trauma. However, it is usually so efficient that often no physical or functional evidence of the fracture can be seen years after the trauma. It is considered to be complete when the fracture can no longer be identified structurally or functionally (Soames, 1995). Remodelling is achieved much faster in children than in adults, although attempts to accelerate the rate of remodelling in adults have had measured success. The success of surgical intervention depends largely on the location of the fracture. Exposure to physical agents such as ultrasonic waves, pulsed electromagnetic waves or even direct current have also been tried (Soames, 1995).

Primary bone healing is a more recently recognised phenomenon than secondary fracture healing (Devlin, 2003). It occurs only in very stable or immobilised fractures, when the ends of the bone fragments are in contact with one another. It was first observed in compression arthrodesis, where the cancellous surfaces of the femur and tibia are held in perfect anatomic reduction with compression clamps, allowing no movement of the bone fragments (Catto, 1980; DePuy Ace Orthopaedics Inc. 2001). Healing occurs without the development of an external callus bridge joining the fragments. The necrotic ends of the cortical bone are not resorbed, but blood vessels enter the osteons, and subsequently, osteoblasts and osteoclasts are carried directly to the centre of the fracture site. Osteoclasts form fast-moving cutting cones, which cross the fracture site, and osteoblasts deposit layers of new bone to form new osteons involving both bone fragments, thus bonding them together.

This is the first stage of primary healing, as is termed 'gap healing'. If primary healing is successful, bone union is achieved within a few weeks. However, the fragment ends are frequently partially devascularized. So, over time, both the repair tissue in the fracture gap and the avascular cortical areas have to be substituted by viable haversion remodeling via BMUs. This constitutes the second stage of direct healing (DePuy Ace Orthopaedics Inc. 2001). Pitfalls of direct bone healing involve the influence of the gap width, and possible damage created by over compression and delayed revascularization (DePuy Ace Orthopaedics Inc. 2001). The strength and integrity of the bone after primary healing is often poor in comparison to that achieved by secondary bone healing.

Immunohistochemical outline of fracture healing

As seen in the previous section, the processes of repair and regeneration in bone echo those of early development, and can be seen to follow a predictable sequence of events. It is this reliability that allows backward extrapolation from an evaluation of the stage of repair to a determination of the age of a fracture.

The organic matrix of mineralised tissues such as bone consists mainly of collagens and non-collagenous matrix proteins, arranged in a well-organised network (Derkx *et al.* 1998; Sommer *et al.* 1996). The nature of the non-collagenous matrix proteins determine the specific properties of the various mineralised tissues. For example, bone, dentin and cementum contain collagen type I, cartilage contains collagen type II, and enamel contains hardly any collagen at all (Sommer *et al.* 1996). The non-collagenous proteins (NCPs) comprise approximately 10% of the total bone protein content. A wide variety of such proteins have been identified, including osteocalcin, osteonectin, bone sialoprotein, decorin and biglycan (Derkx *et al.* 1998). The knowledge of the role of these non-collagenous proteins and their effects on bone metabolism is fairly limited, and relies heavily on localisation studies in animals (Derkx *et al.* 1998). It is currently thought that these proteins play a role in the regulation of mineralization (Derkx *et al.* 1998; Irie *et al.* 2002); in the attachment of osteoblasts and osteoclasts to the bone matrix; and the attraction of cells toward the bone matrix.

These proteins are expressed in a tightly controlled, predictable pattern. Their expression is sequential, and depends on the location and differentiation stage of the mesenchymal cells which produce them (Sommer *et al.* 1996). Some experimental studies have been carried out in order to elucidate the timing of the expression of bone matrix proteins and proteinases during the process of bone remodelling and fracture repair (Bord et al. 1996; Pinero et al. 1995). The presence and activity of these bone matrix proteins can also be monitored through the expression of genes encoding for bone morphogenetic proteins (BMPs), which regulate the production of some bone matrix proteins (Sykaras and Opperman, 2003; Young, 2003). *In situ* hybridisation and immunolocalisation have been shown to

be the most effective techniques at determining the stages of bone formation and the proteins expressed at each stage.

Impact

The process of fracture healing is triggered by the impact of the trauma itself. The impact has two principal effects on the reparative process. There is immediate damage to cells local to the area of impact, which sensitises them to incoming stimuli (imc.gsm.com, 2004). The cell destruction also causes the release of enzymes, biochemical messengers and cell components that initiate the process of induction.

Inflammation

The inflammatory stage begins within hours of the fracture and continues for several days until it is replaced by the developing soft callus (imc.gsm.com, 2004). There is often periosteal disruption, cortical bone displacement and separation, and disruption of vessels at the fracture site, which causes extrusion of blood into the fracture gap. Extruded blood, cellular debris and fragments of tissue envelope the fracture site in a hematoma. The acidic conditions of the inflammation stage help to activate latent forms of growth factors such as TGF-ß1, which stimulates cartilage and bone formation (Sykaras and Opperman, 2003). TGF-ß1 is an important, multifunctional regulator of bone formation, which has been shown to down-regulate alkaline phosphatase, osteocalcin and osteopontin (Sykaras and Opperman, 2003).

The inflammatory phase is characterised by extensive cell proliferation. Cell proliferation during fracture healing has been examined in experimental mouse models using immunohistochemistry with proliferating cell nuclear antigen (PCNA) monoclonal antibody (Li *et al.* 2002). Proliferation of undifferentiated mesenchymal cells was evident in the initial stages of healing, between 2 and 4 days after fracture, in the periosteum and the tissue immediately surrounding the fracture site (Li *et al.* 2002). Cell proliferation levels peaked on day 8 after fracture, and then declined in the latter stages of healing (Li *et al.* 2002).

Alkaline phosphatase has been localised in fracture healing during the earliest stages of osteogenic cell differentiation (Pinero *et al.* 1995). It is an early marker expressed by pre-osteoblasts and osteoblasts, as well as lining cells (Pinero *et al.* 1995). Definitive osteonectin immunostaining is observable in newly differentiated osteoblasts, but not in the intercellular unmineralised matrix (Ishigaki *et al.* 2002). This suggests that osteonectin is synthesised and secreted by newly differentiated osteoblasts, and is incorporated subsequently into the new mineralised matrix (Ishigaki *et al.* 2002).

Bone sialoprotein and osteopontin are expressed in osteoblasts later than alkaline phosphatase, at about the time of matrix synthesis (Roach, 1994; Sommer *et al.* 1996). These proteins are also expressed by hypertrophic chondrocytes (Sommer *et al.* 1996). Osteocalcin is subsequently detected in osteoblasts and mature osteocytes (Sommer *et al.* 1996).

In situ hybridization localisation of genes encoding for the bone morphogenetic protein 4 during fracture healing have revealed that BMP-4 is not expressed in (murine) ribs without fracture, but it is detected in the early stages of healing between 12 and 72 hours after trauma (Nakase *et al.* 1994). BMP-4 was expressed in cells of the proliferating periosteum, the medullary cavity and the surrounding soft tissue (Nakase *et al.* 1994). This suggests that BMP-4 production is triggered by the trauma and is expressed in the callus-forming tissue (Nakase *et al.* 1994).

The devascularized ends of the bone at the fracture site are necrotic, and osteoclastic resorption is prompted by the action of non-collagenous matrix proteins. Osteocalcin is necessary for the recruitment of osteoclast progenitor cells to the sites of resorption, and facilitates their differentiation into osteoclasts for the resorption of necrotic bone littering the fracture site (Roach, 1994). The osteoclastic resorption of bone debris usually lags behind the replacement of the haematoma by reparative vascular tissue (imc.gsm.com, 2004).

Callus formation

Markers of bone resorption such as osteocalcin are thought to increase as callus is formed. Ohishi *et al.*'s (1998) study of the changes in biochemical markers during fracture healing in human osteoporosis patients showed that osteocalcin concentrations in blood serum increased gradually from the first two weeks after admission, after which callus was visible radiographically (Ohishi *et al.* 1998).

Hadjiargyrou *et al.* (2000) identified the gene for the growth factor CYR61 that is known to stimulate chondrogenesis and angiogenesis during the callus formation phase of healing. Elevated levels of the gene, and hence, the protein expression, are found as early as 3 days after fracture, and rise dramatically at day 7 to day 10, and decline eventually between days 14 and 21 (Hadjiargyrou *et al.* 2000). The highest peak of expression coincided with chondrogenesis, and was approximately ten times higher than the levels of CYR61 found in intact femora (Hadjiargyrou *et al.* 2000). It is thought that CYR61 plays an important role in cartilage and bone formation and may act as a regulator of fracture healing (Hadjiargyrou *et al.* 2000).

Mineralisation phase

Bone sialoprotein and osteopontin are important for the initiation of mineralisation (Roach, 1994). Both are localised just ahead of the mineralisation front, and play an essential role in mineralisation. BSP

levels increase gradually in line with increasing mineralisation, and it is believed to act as a crystal nucleator (Roach, 1994). Osteopontin levels also increase in intensity towards the mineralisation front, peaking just prior to mineralisation, which relates to its function as an inhibitor of inappropriate crystal formation (Roach, 1994). In fact, inhibition of osteopontin synthesis has been linked to increased mineralisation (Roach, 1994). Osteopontin is expressed in the latter stages of bone healing, in osteoblasts and continues to be expressed in mature osteocytes (Pinero *et al.* 1995). Osteonectin is present in all cells of the periosteum, but does not appear in the matrix until a relatively late stage (Roach, 1994).

The distinctive woven bone of the hard callus stage is characterised by the loose packing of collagen, as result of its rapid formation. The packing density of the collagen and the distribution of osteopontin is thought to reflect the speed of bone formation (Irie *et al.* 2002). Intense immuno-reactivity for osteopontin has been demonstrated in experimentally-induced woven bone, which suggests that osteopontin levels are increased with rapid bone formation and loose, irregular packing of collagen fibres. Once lamellar bone has gradually replaced the woven bone, the expression of osteopontin and other non-collagenous proteins is significantly reduced (Irie et al. 2002; Sykaras and Opperman, 2003).

Osteopontin, osteocalcin and bone sialoprotein appear to have dual roles, as they function to regulate mineralisation and resorption. Osteonectin seems only to act as a negative regulator of crystal growth (Roach, 1994).

Resorption phase

Non-collagenous bone matrix proteins are also associated with resorption activity during the resorption phase of fracture healing. Osteopontin, osteocalcin and bone sialoprotein are found localised at the cement lines in compact bone, which provides evidence for their role in resorption (Roach, 1994). Bone sialoprotein is more strongly expressed than osteopontin at the cement lines in human bone, and both proteins are thought to mediate the attachment of osteoclasts to the matrix, and aid resorption in that way (Roach, 1994; Sommer *et al.* 1996). Although osteopontin and bone sialoprotein are not expressed in active osteoclasts, the matrix adjacent to the ruffled border of mature osteoclasts has been observed to immunostain for these proteins and alkaline-phosphatase. This suggests that these proteins are liberated from the mineralised matrix by the action of the osteoclasts (Pinero *et al.* 1995).

A basic outline of the changes in immunohistochemically visible proteins during fracture healing is given in Table 01: 04: 01. It provides the basis for the estimation of the trauma-death interval from the immunolocalisation of the non-collagenous proteins expressed at different stages of the healing process.

Table 01: 04: 01 Table showing the expression pattern of different proteins during the fracture healing process.

Time since trauma (days)	Stage of healing	Protein(s) expressed	Nature of protein expression	Function or effect of expression	Reference
1-7	Inflammation: cell proliferation	alkaline phosphatase	found in osteoblast precursors, + later in osteoblasts	marks the intense cell proliferation of undifferentiated cells produced in response to trauma	Pinero *et al.* 1995
		CD68	expressed by tissue macrophages	found in tissue exudates that forms part of the acute inflammatory response	Lydyard *et al.* 2000
		proliferating cell nuclear antigen (PCNA)	positive expression, peaking on day 7/8	active proliferation of undifferentiated mesenchymal cells	Li *et al.* 2002
1-7	Inflammation: resorption	osteopontin	found in osteoblasts	facilitates the attachment of osteoclasts to the matrix	Reinholt *et al.* 1990
		bone sialoprotein	found in osteoblasts	facilitates the attachment of osteoclasts to the matrix	Roach, 1994
		CD68	expressed in osteoclasts	marks resorption of necrotic bone fragments	Lydyard *et al.* 2000
7-14	Soft callus formation	CYR61	elevated levels day 3-5, highest peak of expression day 7-10	stimulates chondrogenesis and angiogenesis during soft callus formation	Hadjiargyrou *et al.* 2000
		osteocalcin	gradual increase after 7 days	due to initiation of callus formation at the fracture site	Ohishi *et al.* 1998
		bone sialoprotein	found in callus matrix	marks the transition of chondrocytes into osteoblasts	Oni, 1995

16-24	Hard callus formation	osteopontin	intensely expressed in woven bone + osteoid	acts as an inhibitor of excess mineralisation	Roach, 1994
		proliferating cell nuclear antigen (PCNA)	dramatic decline in expression at day 16	reflects change in major cell activity from cell proliferation to callus ossification and remodelling start	Li *et al.* 2002
from 24	Mineralisation front	osteopontin	peaks just before mineralisation	acts as an inhibitor of excess mineralisation	Roach, 1994
from 28 (week 4)	Mineralisation	bone sialoprotein	increases in line with mineralisation	acts as a crystal nucleator	Roach, 1994
		osteonectin	only present in fully mineralised bone	acts as a negative regulator of crystal growth	Roach, 1994
from 56 (week 8) continues for years	Remodelling	osteocalcin	significantly elevated levels, present in the mineralised matrix	recruits pre-osteoclasts to sites of resorption, + facilitates their differentiation into osteoclasts, and acts as a chemo-attractant for osteoclasts. Reflects accelerated bone remodelling at the fracture site	Ohishi *et al.* 1998; Roach, 1994; Sommer *et al.* 1996
	Remodelling: resorption	bone sialoprotein	found at cement lines + adjacent to ruffled border of osteoclasts	facilitate the attachment of osteoclasts to the matrix	Pinero *et al.* 1995
		osteopontin			
		osteocalcin			
		CD68	expressed by macrophages: osteoclasts	involved in resorption of bone	Lydyard *et al.* 2000

Introduction

Fracture healing is a process that is susceptible to a multitude of internal and external parameters. Healing rate and the overall success of healing is influenced by a wide variety of factors, which can be local or systemic. Systemic factors are those which affect the whole body, and include age, sex, hormonal activity, nutrition, disease, drug intake and activity such as exercise. Local factors are those concerned with the immediate surroundings of the trauma. Bone healing rate and prognosis is related to the severity of the trauma, and any localised infection, the extent of damage to the vascular system, as well as the type of bone fractured, the degree of immobilisaton, and the fixation method used (Borrill *et al.* 2001). These factors complicate the study of healing rates and the possible estimation of the trauma-death interval, as they increase the number of variables that have to be considered in any scientific study. It is unlikely that any single body of research can accurately account for all of them as many can be subtle and difficult to quantify. However, it is important to understand the demands made on the fracture as it heals and the many ways in which the successful union of the fracture pieces can be hampered. This section is intended to briefly introduce the reader to some of the more important factors affecting fracture healing.

Age

It is well established that the age of the injured individual affects the rate of union of a fracture and the reestablishment of pre-fracture strength and structure. Children are known to recover from fractures much more rapidly than adults, as can be seen from their average healing times (see Table 01: 05: 01).

Table 01: 05: 01 Average healing times for individuals of different ages after fracture of the femoral mid-shaft. (Futrell, 2003)

Age at time of fracture (years)	Time period until clinical union (weeks)
Newborn (0)	3
Child (8)	8
Adolescent (12)	12
Adult (20)	20

The speed of fracture healing in children is due to the thickness of a child's periosteum. The periosteum is a major source of undifferentiated mesenchymal cells that possess the potential for chondrogenesis during

cartilage repair and in fracture healing. In children, the periosteum is thick, and allows faster healing because it is highly vascular and active. Reduction of fracture fragments is also aided by the thicker periosteum, which often remains intact, and can be used by a surgeon to reduce fracture angulation easily (Nuzzo, 2002). The thick periosteum also serves to impart stability on the fragments in addition to a cast. With age, the chondrogenic potential of periosteum declines significantly (O'Driscoll *et al.* 2001). This means that older periostea are unable to supply the fracture site with enough osteoprogenitor cells to meet the demand, and this slows and decreases the effectiveness of the fracture healing process.

Gene expression during fracture healing is also affected by age, which may be the cause of delayed healing in older individuals. In a study of gene expression in rats after femoral fracture, Desai *et al.* (2003) concluded that although both young and old rats exhibit genes controlling extracellular matrix, osteoblasts, bone morphogenic protein, inflammation, cytokine, and receptor genes, young rats reached radiographic union up to 4 weeks earlier than adult rats. Adult rats showed deficient gene expression for genes controlling bone morphogenetic proteins, and transforming growth factor-beta before union was achieved (Desai *et al.* 2003).

One of the other major factors that decreases the healing potential of elderly adults is concerned with the age-related reduction in the production and release of the reproductive hormones oestrogen and testosterone. Both of these hormones – especially oestrogen – have a very strong influence on bone regowth and formation, and their decline in old age is catastrophic for bone health and regeneration potential after a fracture.

Hormonal activity

Oestrogen

Oestrogen plays a role in decreasing bone turnover (Khan *et al.* 2001). Osteoblasts have oestrogen receptors, which suggests that the hormone directly affects the formation of bone (Khan *et al.* 2001; Majeska *et al.* 1994). When oestrogen binds directly to the osteoblast receptor, it increases the production of type I collagen and transforming growth factor ß (TGF-ß). Oestrogen also acts by controlling the production of cytokines, prostaglandins and other growth factors, which act as powerful stimulators of bone resorption and osteoclast formation (Khan *et al.* 2001). Oestrogen may also have an indirect effect on bone via the action of the kidney, by increasing renal retention of calcium. It may also stimulate the production of calcitonin, which in turn limits bone turnover and bone loss as well as increasing renal calcium retention (Khan *et al.* 2001).

The positive effect that oestrogen has on bone formation and calcium retention helps to explain why the single greatest factor affecting bone health in women is the onset of the menopause and the subsequent rapid decline in oestrogen production. The dramatic decline in oestrogen production upsets the delicate balance between bone formation and resorption, as osteoblast activity is curtailed, but osteoclast activity is unhindered. Osteoclasts tend to live longer after the menopause, and so bone loss proceeds unchecked. Post-menopausal hormone replacement therapy has been found to greatly protect against loss of bone density (Hannan *et al.* 2000).

Oestrogen production is also important for bone maturation and mineralisation in men, and clinical cases of individuals with abnormal oestrogen receptors on their osteoblasts have been found to exhibit low bone mineral density and incomplete epiphyseal closure (Khan *et al.* 2001).

Testosterone

Testosterone may contribute to the accumulation of bone mass and hence the higher average bone size in men than women. It is thought to contribute to periosteal bone apposition, and is positively associated with bone mineral density (Khan *et al.* 2001). It plays a complementary role to oestrogen in maintaining bone health and fracture healing potential, and declines with age gradually rather than drastically as oestrogen does in women after the menopause.

Corticosteroid hormones

Glucocorticosteroid hormones promote trabecular and cortical bone loss due to several mechanisms. They directly cause osteoblasts and osteoclasts to decrease bone formation and increase bone resorption, as well as inhibiting the gastrointestinal resorption of calcium (Khan *et al.* 2001). Corticosteroid hormones are predominantly found in anti-inflammatory drugs (see below) prescribed for pain in patients with rheumatoid arthritis or transplant patients for example (Khan *et al.* 2001). The action of glucocorticosteroid hormones has a deleterious effect on fracture healing, and can lead to delayed healing and non-union.

Parathyroid hormones

There is new evidence to suggest that parathyroid hormones (PTH) may be able to reverse the detrimental effects of oestrogen loss on bone, as they positively stimulate the activity of osteoblasts (Whitfield *et al.* 2000). Injections of PTHs into ovariectomised mice appear to stimulate cortical bone growth, increase trabecular thickness and build cortical bone strength. Experiments on rats and cultured rat and human cells, PTHs seemed to cause a dramatic accumulation of osteoblasts and stimulated pre-osteoblast proliferation by causing quiescent bone lining cells to revert to active osteoblasts. They also appeared to

increase the life span of osteoblasts by preventing programmed cell death or apoptosis (Whitfield *et al.* 2000). While this evidence suggests that PTH may be the answer to delayed fracture healing and osteoporosis, the non-osteogenic function of PTH cannot be ignored. In animal studies, the injections of PTH also stimulated osteoclast activity and kick-started resorption, but this was over-shadowed by the bone-forming function of the hormone (Whitfield *et al.* 2000). PTHs have been shown to accelerate fracture healing in both normal and osteoporotic bones. Daily injections of the hormone can increase the volume of callus around rat tibial fractures by as much as 95% (Whitfield *et al.* 2000).

Nutrition

Healing of broken bones is extremely energy-expensive to the body. The greater the severity of the injury, the larger the demand made by the body on the calorific reserves, and so the period immediately after trauma is often associated with a marked loss of the body's reserves of nitrogen, sulphur and phosphorous (Kakar and Einhorn, 2004). Patients are required to increase their daily calorific intake, by as much as three times, as the metabolic demands can exceed 6000kcal per day (Kakar and Einhorn, 2004). If this nutritional demand is not met, then the success of the healing process and the patient's health can be seriously adversely affected (Kakar and Einhorn, 2004).

The phosphorous contained - in the form of phosphoric acid - in carbonated drinks such as cola is thought to increase the body's need for calcium by interfering with calcium absorption. When the demand for calcium exceeds the calcium intake through diet, the reserves of calcium in the bones are sacrificed, increasing bone loss and fragility (NIH ORBD, 2001). Sodium and caffeine also increase the demands on the body's calcium reserves by increasing calcium urinary excretion and by reducing calcium absorption from the diet (NIH ORBD, 2001).

Body weight

Obesity may precipitate the occurrence of such fractures as Colles' or other wrist fractures, as the weight can put extra strain on the bones. Once a fracture has occurred, obesity is a risk factor for delayed healing or even non-union, and can induce re-fracture (Breuckmann, 2000). However, obesity may have a positive effect on overall bone health, by yielding metabolically active steroid hormones and storing of sex hormones. It appears to be negatively correlated with osteopathy (Marc, 2004). Obesity has also been cited as a factor in preventing fracture, by providing the bones with a soft tissue cushion that sustains the impact of a fall or other trauma. Indeed, low body weight, especially in post-menopausal women has been recognised as a contributing factor to increased fracture risk.

Diabetes

Diabetes mellitus adversely affects the healing rate of fractures. Clinical studies have shown that fractures in both insulin and oral hypoglycaemic-controlled diabetes sufferers take longer to heal than those of non-diabetic patients (Loder, 1988). Diabetes interferes with bone formation and causes delayed fracture healing by affecting the expression of genes which regulate osteoblast activity (Lu *et al.* 2003). Lu *et al.* (2003) showed that diabetic experimental animals produced enough immature mesenchymal tissue but failed to adequately express the genes which regulate osteoblast differentiation, and therefore exhibit decreased levels of bone formation and delayed fracture healing. The lack of insulin in patients with type 1 diabetes may be disadvantageous for osteoblast activity and collagen formation. On the contrary, hyperinsulinaemia can have a positive effect on bone mass or can even cause increased osteogenesis in the spine in elderly patients with type 2 diabetes. In both cases a stimulating effect of insulin on bone can be confirmed (Marc, 2004).

Drug Intake

The intake of readily available drugs, such as nicotine, alcohol or non-steroidal anti-inflammatory drugs (NSAIDs), has an effect on the long-term prognosis after fracture. Knowledge of their effect on fracture healing is based on a combination of experimental animal research and clinical studies.

Smoking

Smoking appears to have major effects on bone function, risk of fracture and bone healing after fracture (Moore *et al.* 1994). A small number of experimental studies using animal analogues have confirmed that nicotine intake impairs fracture healing, by diminishing osteoblast function, causing tissue ischaemia and necrosis, and decreases oxygen tension (Hollinger *et al.* 1999). Clinical research has shown that 80% of individuals with impaired osseous healing were smokers (Jones and Trippet, 1992). Hollinger *et al.*'s study on the success of rat parietal bone defects confirms that nicotine ingestion hinders bone regeneration, although the osseous healing was less affected by nicotine in the early stages (14 days) than in later stages of healing (28 days). There is evidence to suggest that nicotine disrupts the renewal of osteoid-producing cells by causing peripheral vasoconstriction at the recipient sites, which reduces the potential osteoblast progenitor cell pool (Hollinger *et al.* 1999). This decreases osteoblast activity and produces an inhospitable environment for bone repair (Hollinger *et al.* 1999). Smoking has been associated with delayed healing and even non-union, resulting in four times as many pseudoarthroses after spine fusion in smokers than in non-smokers (Hollinger *et al.* 1999). Schmitz *et al.* (1999) conducted a clinical trial examining the effect of smoking of the healing rate of tibial shaft fractures, in which they found that the time taken to reach clinical healing point was significantly longer in patients who smoked, and non-union was

more prevalent among smokers. They also observed a 69% delay in radiographic union in smokers, and a significant difference in healing time between smokers and non-smokers whose fractures were fixed with intramedullary nailing or external fixation (Schmitz *et al.* 1999). Smoking is also thought to inhibit oestrogen production, leading to bone loss, fragility and increased risk of fracture or osteoporosis (McCardell, 2002).

Alcohol consumption

Many epidemiological studies suggest that heavy alcohol consumption, especially in adolescence and early adulthood has a detrimental effect on bone formation and renewal, and can dramatically increase the risk of osteoporosis in later life (Simpson, 2003). Although alcohol appears to have an effect on the performance of osteoblasts, by slowing bone turnover, the actual mechanisms by which alcohol affects bone are poorly understood (Simpson, 2003). Samson (1998) suggests that chronic alcohol consumption impairs osteoblast activity, as his studies on experimental rats show that most bone cell parameters remain relatively normal in alcohol-fed rats, except for decreased wall thickness, which is an indication of reduced bone formation by osteoblasts. Other experimental research on animals has shown unequivocally that chronic alcohol consumption has a detrimental effect on bone health, and leads to decrease in bone weight and mineral density (Dyer et al. 1998; Turner *et al.* 2001). In Reed *et al.*'s (2002) study examining the effect of alcohol consumption and exercise on rats, cancellous and periosteal bone formation rates were found to be significantly decreased in the alcohol-fed rats versus rats on the normal diet. Alcohol-fed rats exhibited a significant reduction in trabecular thickness in the tibial metaphysic, and lower cortical bone density. Exercise appeared to have no significant effect on cancellous or cortical bone measurements. These results suggest that heavy alcohol consumption weakens the skeleton, reduces bone density and increases the incidence of endurance-exercise-related bone injuries (Reed *et al.* 2002).

Prescription drugs

There is some data to suggest that non-steroidal anti-inflammatory drugs (NSAIDs) have a detrimental effect on fracture healing (Giordano *et al.* 2003; Schmidt and Templeman, 2002). NSAIDs are thought to have an effect on bone healing as they inhibit cyclo-oxygenases, which are essential for prostaglandin production. Prostoglandins are vital in the fracture healing process, as they mediate inflammation and influence the balance between bone formation and resorption, especially during fracture repair (Moore *et al.* 1994). Recent papers indicate that NSAIDs retard bone formation *in vitro* and one study has demonstrated a strong association between NSAID use and non-union of femoral shaft fracture (Giannoudis *et al.* 2000). Burd *et al.* (2003) also noted a significantly greater occurrence (26% vs 7%) of non-union of long bone fractures in patients receiving the NSAID indomethacin after surgery than those who received no drug. Although NSAIDs are effective pain-killers, they have been shown to negatively

affect fracture healing, and are associated with delayed healing, non-union of long bone fractures and mechanically weaker callus (Burd *et al.* 2003).

Exercise

Exercise seems to be a double-edged sword with regard to fracture healing. Mild exercise is required to stimulate and encourage bone formation and remodelling, by placing strains on the bone which promote bone deposition by osteoblasts. Exercise of the whole body or the affected part also helps to increase blood supply to the fracture, and oxygenate the blood, which is vital for fast fracture healing. However, the resumption of exercise too early after a fracture can do more harm than good. Too much exercise is known to cause stress or fatigue fractures, which occur when repetitive activity causes the muscles to tire and lose their ability to absorb shock. The shock is transferred to the bone, causing tiny cracks. Running has been reported to increase the risk of fatigue fractures (Reed *et al.* 2002), and the tibiae are most at risk. The familiar term 'shin splints' refers to a very mild form of stress fracture. Once a stress fracture has occurred, a return to exercise too early can delay or even prevent a full recovery.

Socio-economic status

Socio-economic status is a complex variable that is notoriously difficult to define and quantify. Elliot *et al.* (1996) attempted to assess the link between socio-economic status (SES) and bone mineral density (BMD) and risk of osteoporosis, which is obviously linked with fracture risk and success of healing. SES was defined using a hierarchical occupation index, which attempted to account for differences in education and income. They observed statistically significant higher bone mineral density values in the lower SES categories, which they felt were not explained by any of the other known risk factors for lower BMD and osteoporosis. Increased physical activity and higher calcium intake amongst lower SES men were suggested as possible reasons for the difference seen, but these factors could not account for all differences found (Elliot *et al.* 1996).

Because socio-economic status is an umbrella term for such an enormous number of sub-factors, it is virtually impossible to use it as a realistic variable in a scientific analysis of differences in a specific subject such as fracture healing. It encompasses a wide variety of behaviours, environments, medical and health-related circumstances and attitudes, which all interact with each other to varying degrees. As such, it remains an abstract concept that researchers can appreciate and infer, but one that eludes accurate scientific definition.

Severity of trauma

The severity of the fracture and the extent of the surrounding damage are the most influential factors governing the speed and success of recovery. This is because these factors dictate the healing environment of the fracture. Retarded healing is expected in fractures associated with extensive bone and soft tissue injury. Severe trauma usually means that the wound is open and the fracture compound, which can adversely affect the healing process as infection is likely and difficult to prevent. It is harder to immobilise and reduce a severe comminuted fracture, and so excess movement between the fragments can hinder callus formation and subsequent union of the pieces.

The vascular damage associated with severe trauma can critically affect the healing process. Successful healing is dependent on a healthy blood supply to the affected area, and prolonged damage to this can cause localised ischaemia and necrosis. The head of the femur, the proximal scaphoid and the body of the talus are particularly prone to avascular necrosis as a result of damaged blood supply (Parker, 2004).

Severe trauma can result in damage to the bone marrow, periosteum and soft tissues surrounding the fracture. This is particularly disastrous for the healing process, as these tissues are the source of healthy mesenchymal cells which later differentiate into osteoblasts and osteoclasts.

Type of bone fractured

The type and location of the fractured bone, as well as the type of fracture has a significant effect on the healing outcome. For example, fractures of the diaphysis of long bones tend to develop more callus, and therefore take longer to heal, than metaphyseal fractures or those of small, irregular bones. Fractures of the phalanges, scaphoid, calcaneous, skull, and those of intra-articular surfaces develop minimal to no callus at all. This difference is due to the extent of periosteal cover of the bone (McKinley *et al.* 2000). Spiral fractures of long bones tend to heal more quickly than simple transverse fractures. This is due to the relatively large surface area of active fracture site in a spiral fracture.

Degree of immobilisation

Immobilisation of a fracture site can be done internally or externally. The primary goal of immobilisation is to maintain the realignment of a bone long enough for healing to start and progress. The gap size and movement between fracture pieces are fundamental factors that influence the rate and success of fracture healing. It is well established that a small amount of movement between the fragments is desirable and conducive to accelerated bone healing, but also that too much movement is counter-productive, and can decrease accumulation of bone in the fracture gap (Borrill *et al.* 2001). Rib fractures are particularly

vulnerable to excess movement, as they are constantly moving with breathing. It is extremely difficult to immobilise a rib fracture, and so rib fractures may have extended healing times. This may affect the results seen in this study, but it may be impossible to quantify or control for the effect. Kenwright *et al.* (1986) found increased bone mineral content in the fracture gap with movement of 0.5mm, but decreased bone mineral content in the fracture gap with movement of 2.0mm. Claes *et al.* (1998) investigated the influence of osteotomy gap size and interfragmentary motion on the success of fracture healing in sheep analogues, and reported that increasing gap sizes delayed the healing process, and increasing movement stimulated callus formation but not tissue quality.

Mobilisation of a fracture too early in the healing process can have adverse effects on fracture outcome and return to pre-trauma function. Solanki *et al.* (2000) showed that patients treated with early mobilisation physiotheraphy after radius and ulna fractures had significantly lower performance ratings on simple gripping and pinching exercises than those treated normally (Solanki *et al.* 2000).

Method of fixation

The method of fixation of a fracture influences the rate of healing and the eventual outcome because they dictate the rigidity of the fracture, the movement between the fragments and the blood flow around the fracture site. This is not so important in the earliest stages of healing, where, according to Mark *et al.* (2004), the characteristics of periosteal and intramedullary bone formation are similar and not influenced by rigidity and fracture environment. However, in the latter stages of healing, histological and morphometric analyses show that less fixation rigidity and an increased fracture gap can lead to slightly delayed fracture healing, by demanding more endochondral bone formation (Mark *et al.* 2004).

According to Lewallen *et al.* (1984), both compression plates and external fixators are equally effective at *inducing union of tibial fractures (in a standard canine model), but that bones mended with external fixators* exhibited higher bone porosity, less intra-cortical bone formation and more resorption than their compression fixation counterparts. The callus was also less mature after 120 days post-fracture on the externally-fixed bones than the compression-fixed ones (Lewallen *et al.* 1984).

Conclusions

It appears that the fundamental factor contributing to the rate and success of fracture healing is the health and activity of the periosteum. It is the main basis of advanced healing in children compared to adults, and is an indirect reason why smoking, NSAIDs and alcohol have a detrimental effect on fracture healing. As we have seen, if the periosteum is damaged, through severe trauma or restricted blood supply, osteoblast

differentiation and proliferation are seriously affected and fracture healing may be delayed or not occur at all.

This is obviously not an exhaustive list of the local and systemic factors that influence bone healing after fracture. It is also important to note that these sources of variation act in conjunction with each other, and no single factor exists in isolation. Any investigation of fracture healing has to take into consideration the extensive range of variables that affect the process. However, it would be impossible to design a range of experiments that could accurately account for the complex interaction between such variables, and as a result, the majority of clinical, and even animal studies, are limited in their scope.

02 : PILOT STUDY

"To look backward for a while is to refresh the eye, to restore it, and to render it the more fit for its prime function of looking forward." Margaret Fairless Barber

Introduction

In order to isolate the sample population on which to base the research project, it was necessary to scrutinise the autopsy records from the Medico-Legal Centre and concentrate on those cases where individuals had exhibited a fracture and where there was a known time of fracture and time of death (so that trauma-death interval could be calculated). It was initially anticipated that there would be a significant number of cases exhibiting skull fractures, as these constitute a considerable proportion of the forensic cases processed by the Medico-Legal Centre each year (Lumb, 2001). The autopsy archive confirmed the significant presence of skull fractures in the cases submitted, and a pilot study was undertaken in order to investigate the nature and distribution of skull fractures from forensic cases from the Medico-Legal Centre from 1992 to 2002. It was thought that this retrospective study would aid an assessment of the feasibility of estimating the trauma-death interval, by highlighting the variety of fractures exhibited, and their pattern and distribution among individuals of different age, sex and ethnicity. The study was used to provide a contextual framework for the fractures, by providing information about the aetiology of fractures, including the impacting object and cause of death, fracture location and types, as well as the distribution of fractures within the population and the relative survival times. It was hoped that an understanding of when and why fractures occur could be achieved, and insight into the factors affecting fracture distribution and outcome gained.

A secondary goal of this evaluative study was to assess the information recorded by pathologists in their autopsy reports, in order to tailor the project research objectives to the information available. For example, the time since trauma was often recorded by pathologists in days or even weeks rather than hours, which limited from the outset the precision of predictions of trauma-death interval from histological evidence. The relative frequencies of different types of fractures in the population, and the availability of histological samples of fractures were also assessed during the retrospective study.

Head injury

Severe head injury is the most frequent cause of mortality and morbidity in individuals under the age of 45 in developed countries (Akang *et al.* 2002; Baethmann *et al.* 1998). The causes of severe head trauma are

as diverse as the individuals who exhibit them, but three major aetiological factors stand out as far more frequent than any other origin. These are road traffic accidents and falls, and in infants, non-accidental injury. Road traffic accidents account for more than half of the severe head and facial injuries in England and Wales each year. On average, 4,000 individuals die per annum and 8,000 more are severely disabled or injured; the majority of whom are young people, pedestrians and cyclists (Jones, 1997). A recent study by McCarthy and Gilbert (1996) of cyclist deaths in and around London, showed that 54% of cyclist deaths were caused by head injury.

Falls have been generally under-appreciated as a mechanism of injury in adults (Helling *et al.* 1999) and children (Plunkett, 2001) until recently. However, in the UK, falls from heights represent one of the most common causes of accidental death, accounting for approximately 5000 deaths a year (Teh *et al.* 2003). The category includes falls from a height, falls from standing, falls from beds or chairs, and falls from moving vehicles. There is also an important category of individuals who jumped from a height in suicide attempts.

Physical abuse is the leading cause of serious head injury in infants (Kairys *et al.* 2001), and one of the most common causes of death to infants and children in Britain (www.forensicpsychology.co.uk). Bruce and Zimmerman (1998) reported that 80% of death from head trauma in infants and children under the age of two years were the result of non-accidental injury. Correspondingly, a significant proportion (just over 5 %) of the sample population examined were victims of child abuse, and of these twelve cases, all except one was under one year of age.

Skull fractures are not always found in association with head injury, but occur in approximately two thirds of severe cases (Jennet, 1980). Although skull fractures are far less clinically significant than intracranial injury, they are interesting to study from a medico-legal perspective. Skull fractures are recognised as evidence of a considerable force having been applied to the head, and can be caused in a variety of ways. What makes them forensically valuable is the manner in which skull fractures can give the investigator insight into the force and direction of the impact, the nature of the impacting surface of weapon, and the sequence of blows. An investigation into the distribution and pattern of skull fractures may have implications not only in the medico-legal arena, but also in clinical trauma management and improving safety devices and procedures.

Sample population

The study was based on a retrospective analysis of the cases of single or multiple skull fracture referred to the Medico-Legal Centre, Sheffield, UK between 1992 and 2002 inclusive. Any case where the phrase 'skull fracture' was found in the autopsy report was examined, providing that enough information pertaining to the individual, the type of fracture and the aetiology of the trauma was available. Details relevant to the individual, such as age at death, sex, ethnic origin, weight and build, were extracted from the records. Information pertaining to the trauma, such as date of trauma and date of death, aetiology of the fractures, weapon or impacting object, and type and location of skull fractures was also recorded. Clinical details such as toxicology and medical treatment were also included. Cases without adequate clinical or post-mortem records were excluded from the data. The information obtained was entered into a SPSS statistics programme file, and statistically analysed.

There were 221 cases where single or multiple skull fractures were recorded in the autopsy records taken by the Home Office Pathologists at the MLC between 1992 and 2002. These cases consisted of 167 male (75.56%) and 53 (23.98%) female individuals. The sex of one individual was unascertainable or unrecorded. The ages of the individuals ranged from 10 days to 93 years old (n = 218, mean = 38.36 years, s.d. = 23.12 years). As can be seen in Figure 02: 01, the data roughly conforms to Gaussian normality. However, there is a clear over-representation of individuals under five years of age, with the majority of these under 12 months old.

Figure 02: 01 A histogram representation of the distribution of ages within the sample population, compared to the Gaussian normality curve.

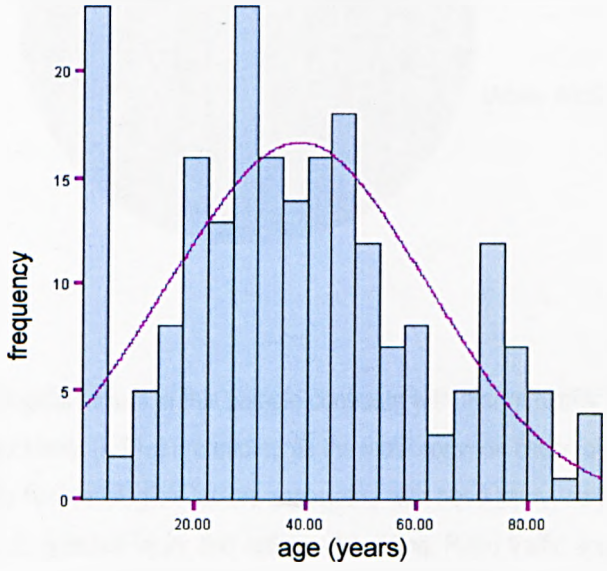

This peak in frequency of skull fracture in under-five year olds corresponds to the number of victims of repeated child abuse and non-accidental injury. Non-accidental injury is defined as active physical violence towards an infant or child, that should be viewed as one part of child abuse, which may occur in isolation or in combination with other forms of child abuse including neglect, sexual or emotional abuse (Forensic Psychology Practice Ltd, 1999).

The distribution of ethnic origins in the sample population shows that the majority of individuals (81%) are white, with a small contribution to the sample made by mixed race, Asian, Afro-Caribbean or Indo-Pakistani individuals. This ethnic mix is approximately typical of a northern English sample, and corresponds quite well with the ethnic composition of Sheffield. According to statistics from the Government Census in 2001 (www.sheffield.gov.uk), 91.2% of the population of Sheffield are White, 3.69% are Indo-Pakistani, 4.6% are Asian or Asian British, and 1.01% are of Afro-Caribbean origin. The 9.05% of cases where ethnic origin was unascertainable or unrecorded helps to account for any discrepancy between the true composition of the city and that observed in the sample population (see Figure 02: 02).

Figure 02: 02 A pie chart showing the percentage composition of the cases by ethnic origin.

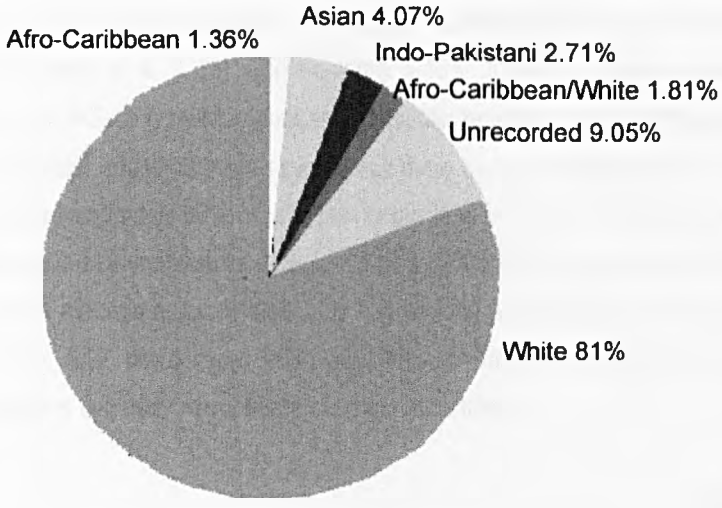

Fracture Aetiology

The spread of aetiological factors in this sample contrasts with that of similar studies (Akang *et al.* 2002), where road traffic accidents (RTAs) are quoted as the most common cause of fatal skull fracture. Akang *et al.* (2002) quote only five aetiological factors associated with head injury, namely road traffic accident, fall from a height, assault, gunshot injury and collapsed building. Road traffic accidents account for 83.8% of

injuries in their study. In the present study however, the majority of fatal skull fractures were caused by inter-personal assaults and falls. This is simply attributed to the nature of the cases referred to the Medico-Legal Centre for autopsy. The Home Office Pathologists at the MLC are called upon to examine cases of homicide and suspicious death, whereas victims of accidental falls and road traffic accidents are more routinely seen by pathologists at local district general hospitals. This element of pre-selection clearly influences the sample, which shows an obvious bias toward inter-personal assaults and violent causes of skull fracture. In addition, many difficult and legally contentious cases are referred to the experts at the MLC from outside the boundaries of Sheffield and South Yorkshire. These factors suggest that the sample is not wholly representative of the true distribution of skull fractures in Sheffield and its immediate surroundings. A more representative picture of the nature of skull fracture incidence in South Yorkshire could be obtained from an analysis of routine Coronal records, which would provide an interesting comparison to the present study.

Falls

Falls represent the largest aetiological category, and so it was deemed necessary to divide the category into more descriptive subsets. These included falls from standing; falls down stairs; falls from a height; falls from bed and falls from a moving vehicle. It has long been recognised that falls present a serious risk to older individuals, as fall-related injuries and their various sequelae tend to be more life-threatening with advancing age (DeGoede *et al.* 2003). Approximately 5-15% of falls in community-dwelling older adults result in serious injury, including head trauma, fractures, disclocation or acute soft tissue injury (DeGoede *et al.* 2003). Among older adults, falls are seven times more likely to be fatal than for those younger than 65 years old. Also, approximately 60% of fatal falls occur in older adults, principally due to complications such as pneumonia due to immobilisation (DeGoede *et al.* 2003). In this sample, adult individuals over 65 years old survived on average approximately only half as long as adults aged between 18 and 65 years (survival mean <=65: 8.37 days, mean >65: 4.69 days. p=0.412). Although this was not statistically significant, these figures generally mirror those of other researchers.

Falls from a low height

Falls from a low height are gradually being recognised as an important cause of injuries, including skull fractures. Helling *et al.* (1999) have analysed the severity and pattern of injuries resulting from low falls, and have found falls represent a common cause of injury not only in the elderly, but in younger individuals too. They demonstrated that the majority of sufferers of low fall injuries are aged between 25 and 40 years old. Low falls cause significant injuries, most commonly to the head and spine, and in the study by Helling *et al.* (1999), 35% of patients suffered serious head injury, and 64.2% of fatalities were as a direct result of

head injury. Plunkett (2001) drew attention to the potential of falls from heights as low as 2 feet to cause fatal head injury in children and infants. He also showed that low fall injuries are often associated with a lucid interval and bilateral retinal haemorrhage, which have until recently been regarded as very strong diagnostic indicators of inflicted abuse (Plunkett, 2001). This may suggest that misdiagnoses of abuse are more common than expected.

'Jumpers' and 'Fallers'

An important distinction has to be made between victims of accidental fall from a height and those who intentionally jumped from a height. Teh *et al.* (2003) compared the skeletal injuries sustained by so-called 'fallers' and 'jumpers', and discovered that although both were subjected to the same deceleration-type and direct impact injuries, there were clear differences in the pattern of fractures exhibited. In Teh *et al.*'s study (2003), jumpers sustained more rib fractures, particularly on their right, and more pelvic and lower limb fractures, but fewer skull fractures. In accordance with Teh *et al.*'s study (2003), the jumpers in the MLC sample population exhibited fewer skull fractures than accidental fallers. In this sample, 18 individuals (8.1%) fell from a height, and 3 individuals (1.4%) jumped. The jumpers only sustained one significant skull fracture each, whereas one third of the fallers sustained two skull fractures and several individuals sustained a third. The majority (38.9%) of fractures sustained by fallers was linear, whereas the jumpers exhibited only comminuted or undisplaced fractures (see Figure 02: 03).

Figure 02: 03 A graph showing the distribution of different types of fractures sustained by those individuals who jumped or fell from a height.

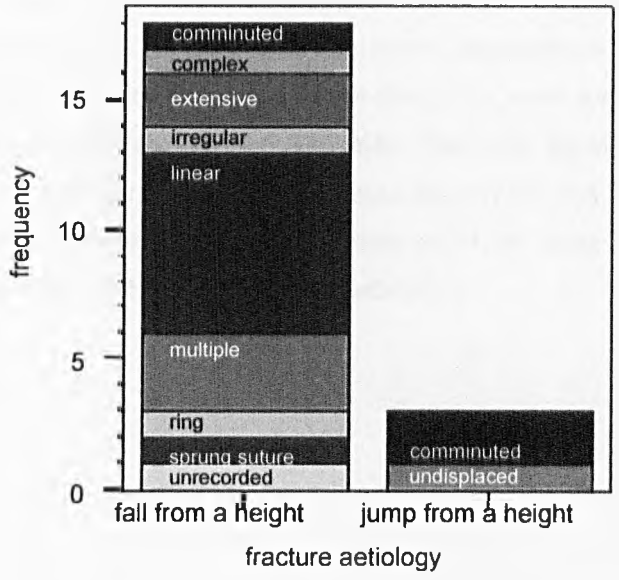

Teh *et al.* (2003) proposed that the difference in fracture pattern between jumpers and fallers reflects the tendency for jumpers to jump from greater heights than fallers, and to fall feet-first, attempting to break their falls using their (dominant) right sides.

Television 'tip-over'

One interesting case in the sample appears to be evidence of a relatively recent, but increasingly common, phenomenon. A 19 month old girl was playing in her family home with her sister, when the large television toppled and fell on top of her, causing fatal crush injuries. There is a significant mortality rate associated with this mechanism related to severe head injuries (Scheidler *et al.* 2002). Jea *et al.* (2003) have also noted this phenomenon, and discovered that skull fractures are the most common type of head injury sustained from falling television sets, especially in infants and children less than two years of age. This 'television tip-over' is becoming a more and more significant source of paediatric head injury and death, and is likely to increase in frequency unless substantial improvements are made in television stand safety measures and child supervision within the home.

Blood-alcohol level

The intake of alcohol and drugs is undoubtedly a significant contributor to the occurrence of head injury and skull fracture. A high level of inebriation was found to be prevalent throughout the adult cases, and certainly compounded the severity of outcomes. For example, it is unlikely that falls down stairs would have constituted such a significant (9.5%) aetiological factor, without the complication of alcohol. All but one of the individuals who fell down the stairs was intoxicated.

Of the 151 individuals over the UK legal drinking age of 18, 63 (41.72%) were reported to have alcohol in their blood. Of these, 16 (25.4%) had their exact blood alcohol concentration (BAC) recorded as over the legal driving limit of 80mg/cl. Out of 35 legal minors, two individuals (5.71%) were recorded as having a blood alcohol concentration over the legal driving limit. Mean survival time can be seen to have been influenced by blood alcohol concentration. The mean trauma-death interval for those individuals with a BAC of over the legal limit of 80mg/cl was only 0.8 days (s.d.=1.15 days), whereas those with a low BAC survived on average 4.32 days (s.d.=12.45 days). This result was not quite statistically significant to the 95% confidence level (p=0.081).

Trauma-death interval

An analysis of the time elapsed between the fracture and death, or the 'trauma-death interval', can aid an understanding of the severity of skull fractures and the probable outcome of different types of fractures in clinical cases.

Figure 02: 04 Graph showing the relative frequencies of the different trauma-death intervals within the sample, and a curve emphasising the gradient.

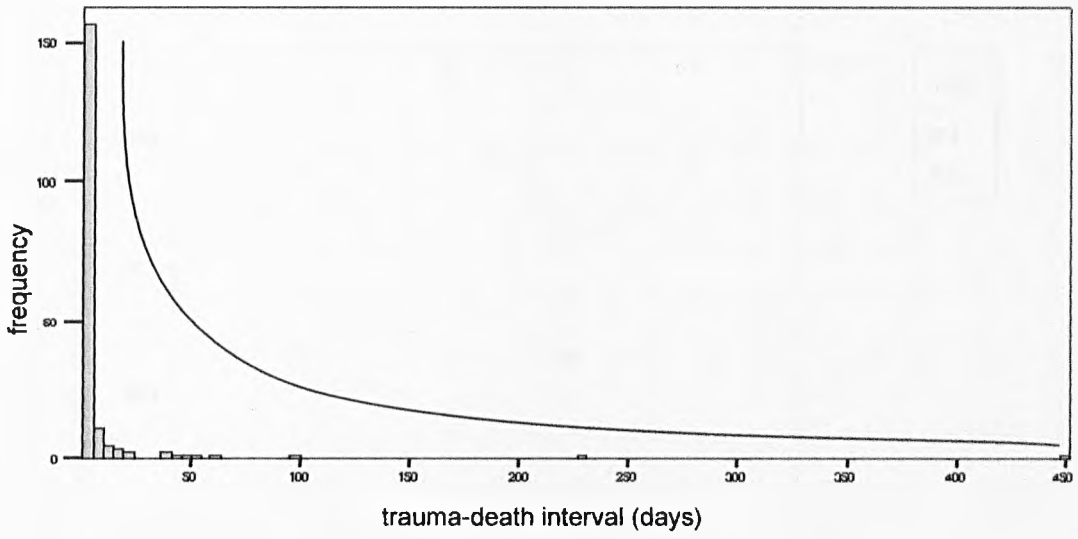

The steep gradient to the graph (see Figure 02: 04) demonstrates that the vast majority of individuals survived only a short period. 38% of individuals did not survive longer than 24 hours. The mean survival time for the whole sample was 7.6 days. Only 8 individuals (3.62%) survived longer than 3 weeks. The maximum survival time was 452 days, in the case of a 41-year-old female assault victim, who died of broncho-pneumonia and complications after skull fracture. The mean survival time of individuals under 18 years of age was not significantly different to that of adults (Student's t test at 95% significance level, p=0.934). However, the maximum survival period was considerably lower for infants and children. There was no significant difference between the mean survival times for infants under one year of age and other children (Student's t test at 95% significance level, p=0.755).

The relationship between age and trauma-death interval was examined. It was expected that the youngest and oldest individuals in the sample would exhibit the shortest survival times, and that the young to middle-aged adults would have survived the longest. However, the pattern which is seen is one of consistency across the ages, with equally short survival times in every age group. Figure 02: 05 below shows a scatter-graph of trauma-death interval plotted against age, with colours denoting sex (the sex of one individual was

not recorded, and is denoted as an orange circle). The overlapping symbols, which make it difficult to distinguish individuals clearly, is indicative of low variability between individuals, and a general homogeneity of survival times. However, we can see that the majority of the 'outliers' are male. This has been tested and is not statistically significant (Student's t test at 95% significance level, p=0.576), but is nonetheless interesting to note.

Figure 02: 05 A scattergraph showing the relationship between age, trauma-death interval and sex.

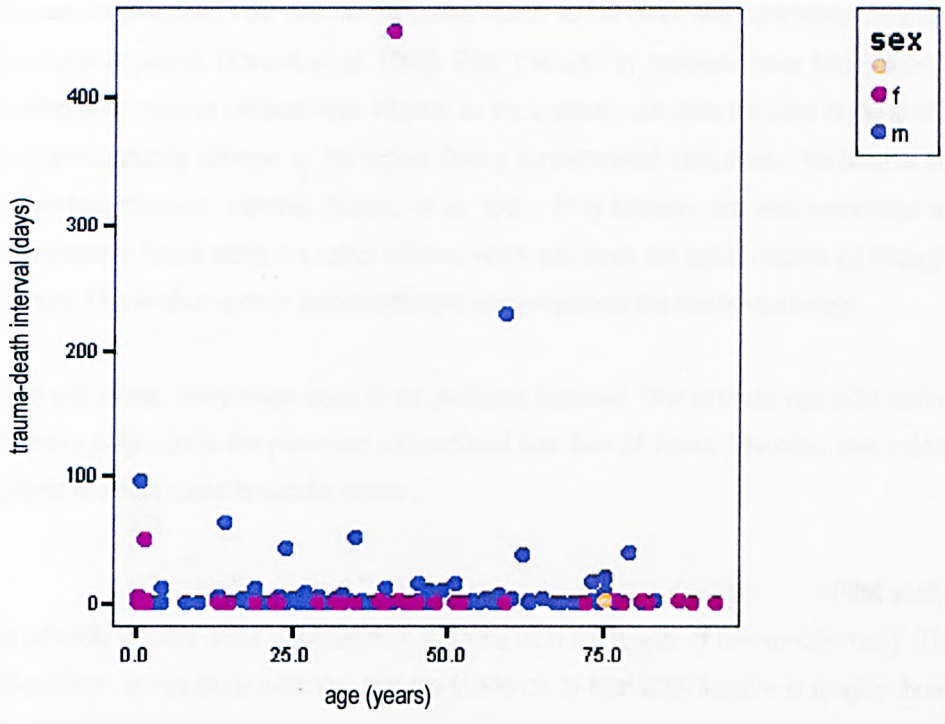

Fracture patterns

Although the range of skull fracture patterns seen in the sample was extensive, some basic patterns were visible. Fractures involving the right parietal, right temporal and occipital bones were found to be particularly common (10.9%, 9.5% and 19.45% respectively). They are indicative of inter-personal assaults, as are fractures to the orbital roof and mandible. This pattern complies with what would be expected, given that punches across the face from a right-handed assailant would send a victim falling backwards and to the right.

Linear fractures were by far the most prevalent, comprising 57.22% (218) of the entire sample of fractures (n=381). They generally appeared in combination with other fractures. Comminuted and depressed

fractures were the next most commonly occurring (7.7% and 7.2% respectively). As expected, in child and infant cases, sprung sutures were common. This is because, in developing skulls, the sutures have not yet fused, and form natural pathways along which force can be transmitted. Out of the seven cases of sprung sutures, 5 (71.4%) were under 16 years of age. In the twelve cases of non-accidental injury, linear and sprung suture fractures comprised 79.2% (19/24) of the fractures seen.

It is interesting to study the combinations of skull fractures associated with different causes of fracture. For example, fractures of the base of the skull, either ring fractures around the foramen magnum, or hinge fractures which extend from one middle cranial fossa[1] to the other, are particularly common in victims of motorcycle accidents (Konrad *et al.* 1996). Ring fractures in motorists have been clearly identified as resulting from massive whiplash-type injuries, as the ligaments between the base of the skull and the spine are biomechanically stronger in this region. During supramaximal axial stress, the base of the skull, being the weakest structure, ruptures (Konrad *et al.* 1996). Ring fractures are also associated with excessive compressional forces along the spinal column, which can force the spinal column up through the foramen magnum. This is often seen in suicide attempts and jumps onto the feet from a height.

In two individuals, every single bone in the skull was fractured. One of these was a 29 year old male who fell from a height on to the pavement and survived less than 24 hours. The other was a 44 year old man involved in a high-speed helicopter crash.

Pilot study discussion

It is possible to draw some generalised inferences from the results of this specific study. The element of self-selection in this study indicates that the incidence of fatal skull fracture is roughly three times more common in male individuals than in female individuals. This has been observed in similar studies, such as that by Prat and Calatayud-Maldonado (1998). The age distribution of the sample appears to follow Gaussian normality broadly, except for the noticeable peak in the under-five age group. This corresponds to the significant number of infants who were the victims of abuse or non-accidental injury. There are also significant peaks in fatal skull fracture frequency which correspond to the age categories 25 to 30 and 70 to 75 years. Drugs and alcohol intake is clearly a contributing factor to the frequency and severity of skull fractures in the sample population. 41.7% of inter-personal assaults (25/60) were compounded by the presence of alcohol in the victim's blood. The mean blood alcohol concentration for the whole sample

[1] Hinge fractures can also occur in the frontal or posterior cranial fossae, but are generally more common in the middle cranial fossae involving the foramen magnum.

(n=221) was 84.41mg/cl, which is just over the legal driving limit, and only 151 individuals were over the legal drinking age. 5.71% of minors were also found to have alcohol in their blood.

It can be seen that, in the sample population, young, working-age, white male individuals are most prone to fatal skull fracture. They are most likely to be involved in a road traffic accident, fall or inter-personal assault, and the intake of alcohol and drugs greatly increases the likelihood of death after such trauma. The survival period is short, with an average trauma-death interval of just over a week. This may be an indication of the severity of the injuries sustained, or may reflect the standard of trauma care available in the region.

A very important sub-section of skull fracture sufferers is the children and infants who were victims of non-accidental injury or child abuse. They constituted 34.29% of the children under 18 years old in the sample. This demographic group is at extremely high risk, and it is hoped that with further research into the patterns of fractures exhibited by abused children, it may be possible to recognise non-accidental injury in a living child more easily, and attempt to prevent more individuals becoming fatality statistics.

The most pertinent conclusions that can be made on the basis of this population-specific retrospective study are:

- male individuals are approximately three times more likely to suffer from skull fractures than female individuals.
- children under five years old, young adults (5-30 years old), and older adults (75-80 years old) are at the highest risk.
- in this sample population, inter-personal assault appears to be the most common cause of skull fracture, followed by falls and road traffic accidents.
- the average blood alcohol content was over the legal limit. Alcohol and drug use clearly increase the risk of sustaining a skull fracture.
- the average trauma-death interval was 7.6 days, although the majority of individuals did not survive longer than 24 hours.
- out of 35 individuals under the age of 18, 34.29% were victims of non-accidental injury and repeated abuse at the hands of adults.

These conclusions do not contradict what is already known about skull fracture patterns and their distribution within the population. The incidence of injuries caused by inter-personal assaults seemed surprising at first, but can be attributed to the unusually high number of violent cases referred to the

Medico-Legal centre from outside the Sheffield region. This creates an artificial bias towards inter-personal assaults and falls caused by assaults as aetiological factors leading to skull fracture. The numbers of infants exhibiting skull fractures as a result of non-accidental injury and the effect of blood-alcohol concentration on fracture occurrence also do not signify new findings to the forensic community. As such, this retrospective study acted as confirmation that the Medico-Legal Centre sample population investigated is representative of a typical population, and that the cranial and post-cranial fractures are not significantly unusual in pattern, distribution or aetiology.

As an evaluative pilot study, the retrospective analysis of skull fractures from the Medico-Legal Centre served to highlight a few considerations for the project proper.

The main conclusion drawn was that it was necessary to obtain samples from a range of fractured bones, in order to have a statistically viable sample size. In the majority of skull fracture cases investigated during the process of the retrospective study, no histological samples of the fracture site of the fractured bone were taken. Histology samples were only available for four of the individuals exhibiting skull fractures. This directed the research towards fractures of the post-cranial skeleton, which were well-represented in the autopsy archive. The post-cranial fractured bones most commonly present in the records were ribs and femora, and histological samples were more often taken from these fractures. Once these fractures were included in the sample, a viable sample size was achieved. The final composition of bone types in the sample was as described in Figure 02: 06 below.

Figure 02: 06 A pie-chart showing the relative percentages of fractures of different bones in the sample population. (n = 29).

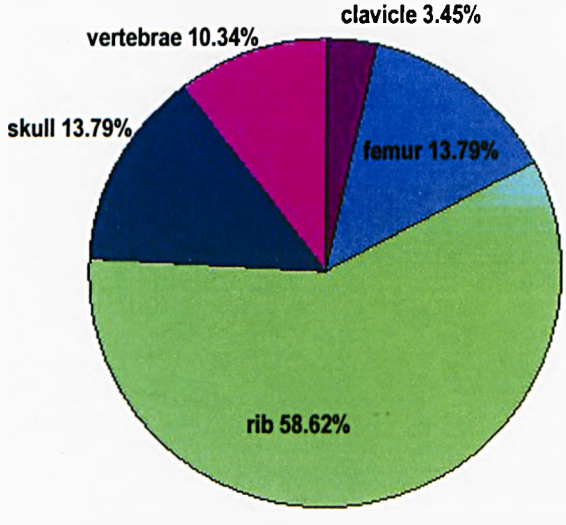

Thus, the results of the evaluative study of skull fractures directed attention towards the assessment of healing rates in rib fractures, and contributed to an appreciation of the potential applications of this research in the diagnosis and evaluation of fractures in suspected child abuse cases.

Another outcome of the study was the realisation of the necessity to standardise pathologists' autopsy reports, and to improve the routine histology sampling procedures. Samples of bone are taken infrequently, as bone is rarely the main focus of a pathologist's report, and often it is only examined to confirm findings from other organs. As a result, little attention is given to noting information on which the project was based, such as details of the exact location from which the bone sample was taken. For example, a report might state that "3 x rib" samples were taken, which is especially unhelpful in cases with multiple rib fractures of different ages. It was also found that even when a fracture is mentioned in the report, and bone histology blocks have been taken, the two did not always correspond. For example, in cases of suspected child abuse, if the infant exhibits multiple skull fractures, a sample of un-fractured rib is often taken to rule out rickets. This was a potential source of confusion, and suggests that measures should be taken by pathologists to accurately describe the samples they take, to facilitate data collection for research projects in the future.

03 : MATERIALS AND METHODOLOGY

"We are what we repeatedly do."

Aristotle (384BC – 322BC)

Introduction

As a result of the information gathered during the pilot study about the availability and suitability of tissue samples, and the amount of information obtainable from the pathologists' reports, the archive database at the Medico-Legal Centre was interrogated, and a working sample population identified. The composition of the sample population is fully described below, as are the complete methods used, from extraction of bone samples from the deceased, through the staining procedures, to the qualitative and quantitative histomorphometric analysis. The statistical analyses performed are also outlined.

Sample population

The working sample population was composed of 29 individuals, with an age range of between 1 month and 98 years of age, and a mean age of 53.4 years (n = 29, s.d. = 34.25) (see Figure 03: 01). See Appendix 02 for a table showing the raw sample population data.

Figure 03: 01 Age distribution of the sample population, with a curve indicating Normal distribution.

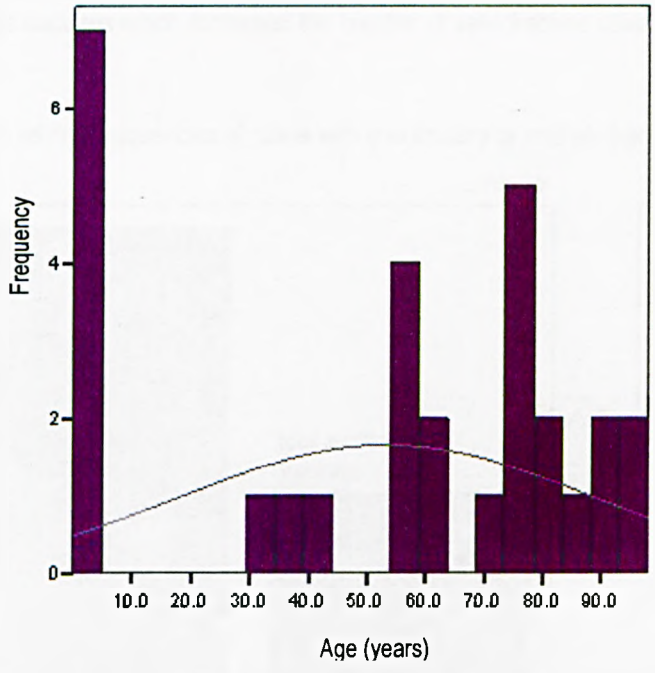

The distribution of the sexes was approximately even, with 15 male individuals (51.7%) and 14 female individuals (48.3%). 55.2% of the sample population was described as being of 'White' origin, 6.9% of

'Asian' descent, and 3.4% 'Afro-Caribbean'. Ethnic affiliation was unknown or unrecorded in 34.5% of cases (see Figure 03: 02).

Figure 03: 02 Sex and ethnic affiliation distribution of the sample population.

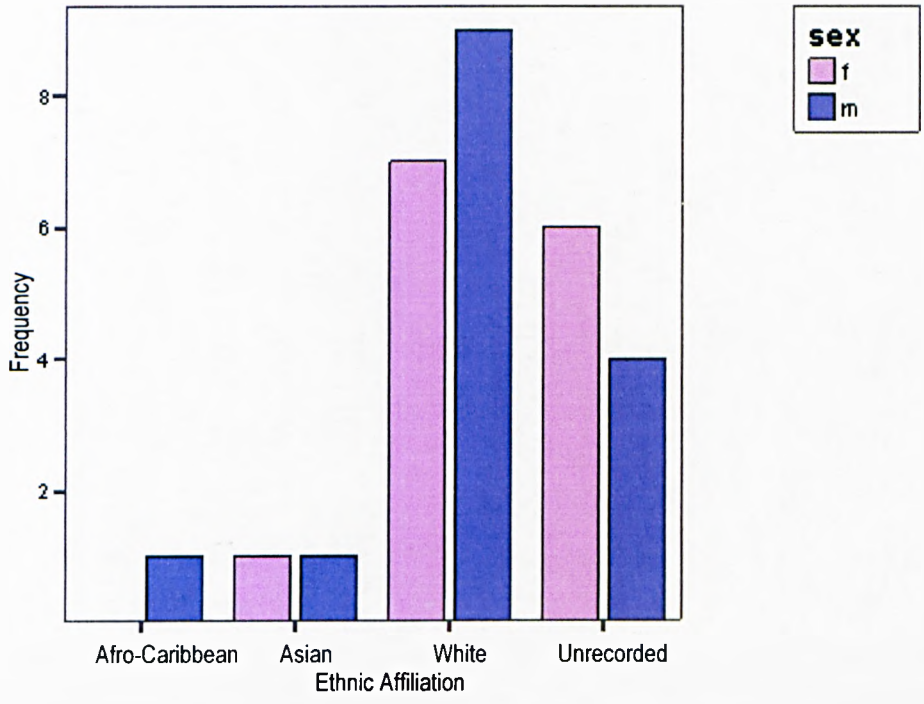

Although the sample population consisted of only 29 individuals, 15 of these individuals exhibited additional multiple fractures which increased the number of valid fracture cases to 52 (see Figure 03: 03).

Figure 03: 03 The relative frequencies of cases with one fracture or multiple fractures.

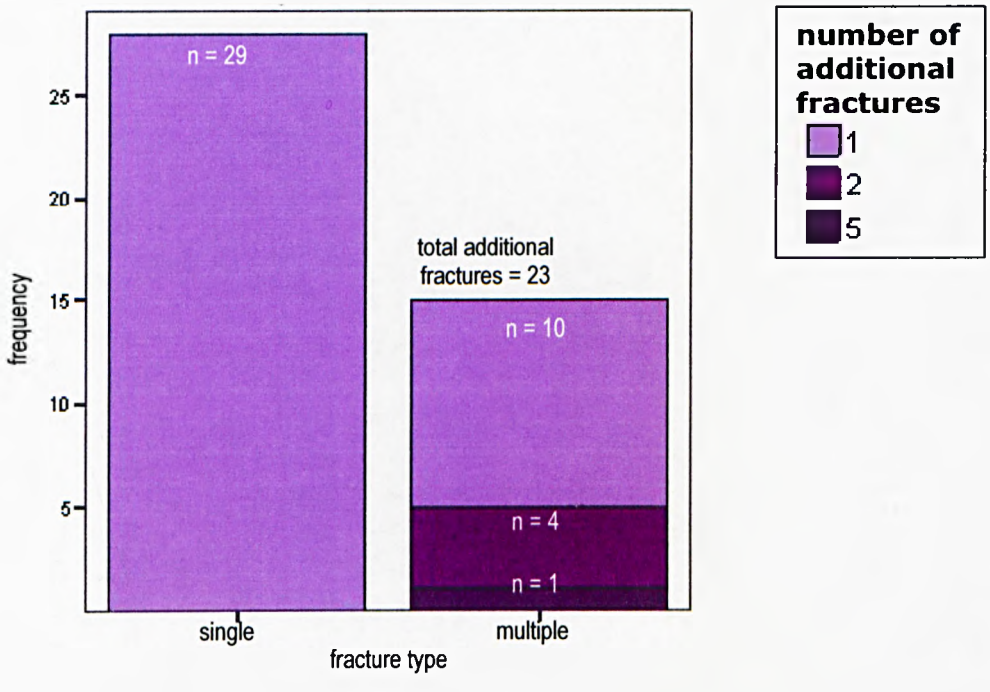

The fractures exhibited by individuals in the sample originated from a wide range of aetiologies (see Figure 03: 04), including abuse or non-accidental injury (20.7%), assault (13.8%) and falls (31%). Road traffic accidents also constituted 6.9% of the causal factors. A significant proportion of the fractures were inflicted post-mortem (10.3%), a phenomenon that is thought to occur during handling of the corpse, and is hence commonly referred to as an 'undertaker's fracture'. These are most likely to affect the cervical vertebrae or the ribs and sternum.

Figure 03: 04 The relative frequencies of different forms of trauma aetiology represented by the sample cases.

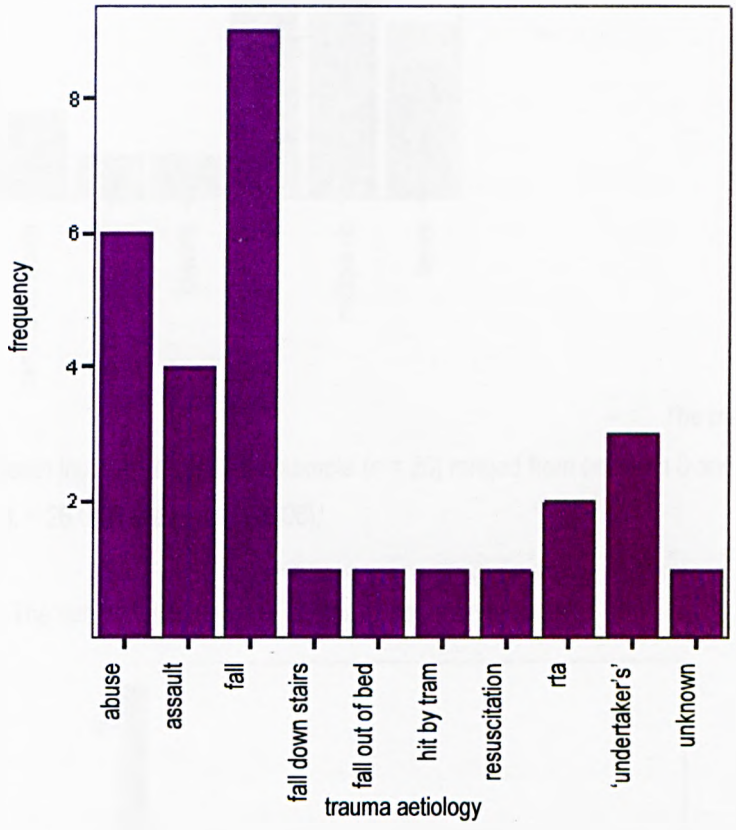

Figure 03: 05 shows the relative distribution of primary fractures affecting different bones, and the locations of the secondary fractures associated with them.

Figure 03: 05 The relative occurrence of fractures of different bones, and any secondary fractures associated with them.

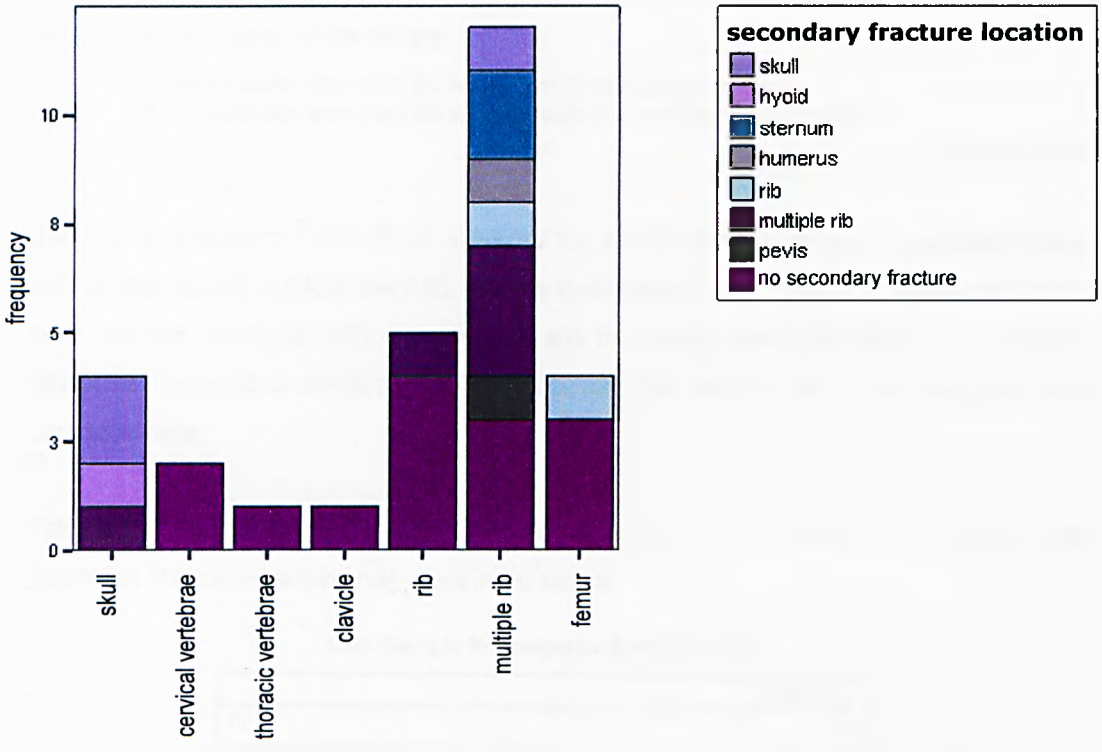

The trauma-death interval

The trauma-death interval values of the sample (n = 26) ranged from between 0 and 120 days (mean = 15.9 days, s.d. = 26.04) (see Figure 03: 06).

Figure 03: 06 The relative distribution of trauma-death interval values.

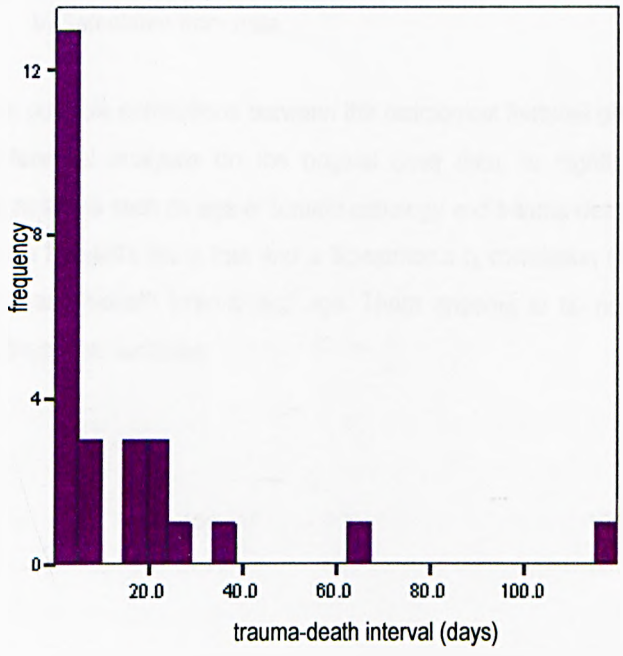

In order to compare variables against the trauma-death intervals (tdi) of the sample, it was necessary to determine whether or not the distribution of these values conformed to normality. The One Sample Kolmogorov-Smirnov test for single variables was used to scrutinise the distribution of tdi values in the sample. The hypotheses of this test are:

> H0: the population from which the sample results follows the Normal law
> H1: the population from which the sample results does not follow the Normal law
>
> (Statsoft, 2003a)

The results, tabulated in Table 03: 01, show that the p value for the numerical trauma-death interval data (termed tdinum) was less than 0.05, and was therefore significant to the 95% confidence level. As such, the null hypothesis (H0) was rejected, and the values were recognised as not normally distributed. Subsequent statistical analyses concerning this variable had to be done using non-parametric tests.

Table 03: 01 Results of the One Sample Kolmogorov-Smirnov test to determine the nature of the distribution of trauma-death interval values in the sample.

One-Sample Kolmogorov-Smirnov Test

		TDINUM
N		28
Normal Parameters[a,b]	Mean	15.904
	Std. Deviation	26.045
Most Extreme Differences	Absolute	.271
	Positive	.230
	Negative	-.271
Kolmogorov-Smirnov Z		1.380
Asymp. Sig. (2-tailed)		.044

a. Test distribution is Normal.

b. Calculated from data.

Before assessing the possible correlations between the histological features observed, it was possible to perform some statistical analyses on the original case data, to highlight any association or correlation between variables such as age or trauma aetiology and trauma-death interval. Table 03: 02 shows the results of a Kendall's tau-b test and a Spearman's r_s correlation coefficient test (for non-parametric data) for trauma-death interval and age. There appears to be no statistically significant correlation between these two variables.

Table 03: 02 Results of a Kendall's tau-b and a Spearman's r_s correlation coefficient test to determine any correlation between age and trauma-death interval.

Correlations

			AGE	TDINUM
Kendall's tau_b	AGE	Correlation Coefficient	1.000	.254
		Sig. (2-tailed)	.	.076
		N	29	26
	TDINUM	Correlation Coefficient	.254	1.000
		Sig. (2-tailed)	.076	.
		N	26	26
Spearman's rho	AGE	Correlation Coefficient	1.000	.365
		Sig. (2-tailed)	.	.066
		N	29	26
	TDINUM	Correlation Coefficient	.365	1.000
		Sig. (2-tailed)	.066	.
		N	26	26

Figure 03: 07 shows the scatter-plot for the two variables.

Figure 03: 07 Scatter-plot showing the relationship between trauma-death interval and age. (Spearman's correlation coefficient r = 0.365 , n = 26, p = 0.66).

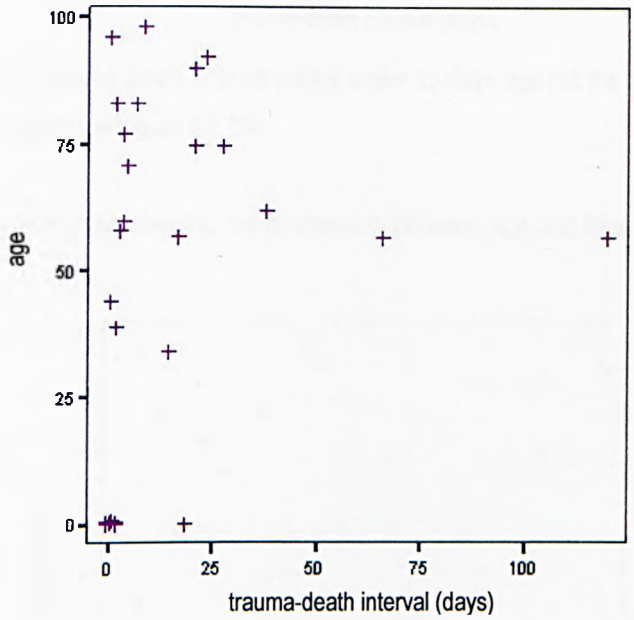

Four individuals (13.8%) from the sample population had trauma-death intervals of over 25 days, ranging from 28 to 120 days. It was thought that these 'out-lying' values might mask any correlations or skew correlation analyses between the trauma-death interval and other variables. By ignoring those cases with tdi values greater than 25 days, it was thought that clearer relationships between the trauma-death interval and other variables may become visible.

The graph of the frequency distribution of the trauma-death interval values under 25 days (Figure 03: 08) suggests that the sample is not normally distributed, and that non-parametric tests should be performed.

Figure 03: 08 Distribution of trauma-death interval values under 25 days in the population sample, with a normal distribution curve included for comparison.

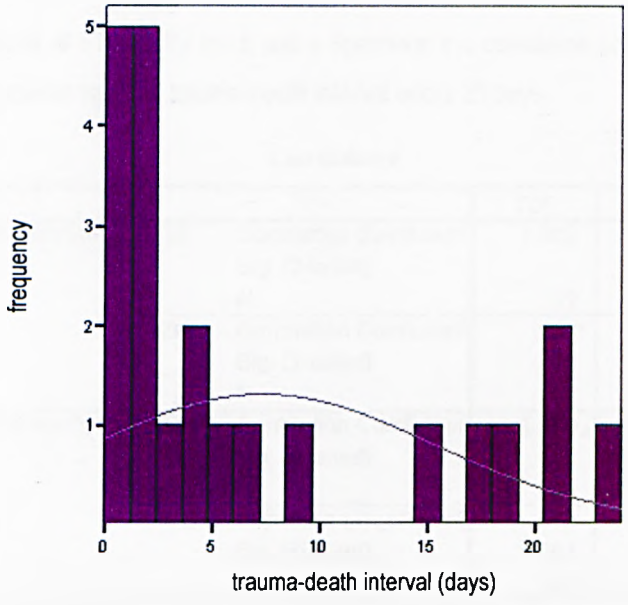

A scattergraph of the trauma-death interval values under 25 days against the ages of the individuals in the sample was plotted (see Figure 03: 09).

Figure 03: 09 A scattergraph showing the relationship between age and trauma-death interval values under 25 days.

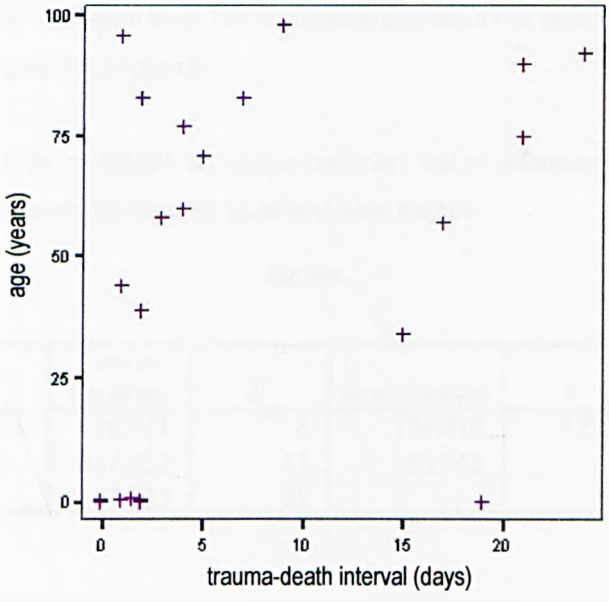

Kendall's tau-b and Spearman's r_s correlation coefficient tests were carried out to assess the level of correlation between trauma-death interval values under 25 days and age (see Table 03: 03). The Kendall's tau-b test gives a p value of less than 0.05, which suggests that there is a statistically significant correlation (to the 95% confidence level) between these variables. This means that when the trauma-death interval is under 25 days, there is a statistically significant positive correlation with the age of the individual.

Table 03: 03 Results of a Kendall's tau-b and a Spearman's r_s correlation coefficient test to determine any correlation between age and trauma-death interval under 25 days.

Correlations

			TDI	AGE
Kendall's tau_b	TDI	Correlation Coefficient	1.000	.340*
		Sig. (2-tailed)	.	.031
		N	22	22
	AGE	Correlation Coefficient	.340*	1.000
		Sig. (2-tailed)	.031	.
		N	22	25
Spearman's rho	TDI	Correlation Coefficient	1.000	.417
		Sig. (2-tailed)	.	.054
		N	22	22
	AGE	Correlation Coefficient	.417	1.000
		Sig. (2-tailed)	.054	.
		N	22	25

*. Correlation is significant at the .05 level (2-tailed).

An analysis of variance (ANOVA) test was performed to assess any difference in the means of trauma-death interval values under 25 days in each of the different fracture location categories (see Table 03: 04 and Figure 03: 10), to determine if the location of fracture had any bearing on survival time. The p value generated by the ANOVA test was greater than 0.05, so the correlation is not statistically significant to the 95% confidence level. The relationship between these variables and the trauma-death interval will be discussed in Chapter 06.

Table 03: 04 Results of an ANOVA correlation coefficient test to determine any correlation between trauma-death interval under 25 days and location of bone fracture.

ANOVA

TDI

	Sum of Squares	df	Mean Square	F	Sig.
Between Groups	416.841	4	104.210	1.869	.162
Within Groups	947.852	17	55.756		
Total	1364.693	21			

Figure 03: 10 Graph showing trauma-death interval (under 25 days) means for each location of bone fracture. (Error bars show standard deviation +/- 1.0).

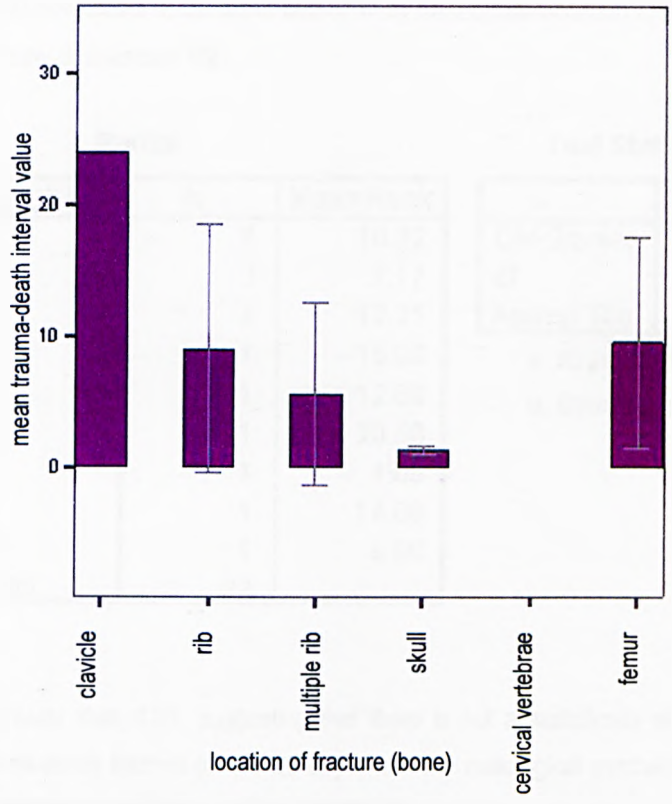

The non-parametric Kruskal-Wallis test confirms this result, as the p value generated is greater than 0.05 (see Table 03: 05).

Table 03: 05 Results of a Kruskal-Wallis test to determine any correlation between trauma-death interval under 25 days and location of bone fracture.
(BONE_CAT categories: clavicle 1, rib 2, multiple rib 3, skull 4, cervical vertebra 5, femur 6)

Ranks

	BONE_CAT	N	Mean Rank
TDI	1	1	22.00
	2	4	11.50
	3	11	10.32
	4	2	5.00
	6	4	15.38
	Total	22	

Test Statistics[a,b]

	TDI
Chi-Square	6.469
df	4
Asymp. Sig.	.167

a. Kruskal Wallis Test

b. Grouping Variable: BONE_CAT

Another Kruskal-Wallis test was performed to assess any difference in the means of trauma-death interval values (under 25 days) in each of the different fracture aetiology categories (see Table 03: 06), to determine if the aetiology of fracture had any bearing on survival time.

Table 03: 06 Results of a Kruskal-Wallis test to determine any correlation between trauma-death interval values under 25 days and the aetiology of bone fracture. (AET_NUM categories: abuse 1, assault 2, fall 3, fall downstairs 4, fall out of bed 5, hit by tram 6, resuscitation 7, road traffic accident 8, 'undertaker's fracture' 9, unknown 10)

Ranks

	AET_NUM	N	Mean Rank
TDI_25	1	6	10.92
	2	3	7.17
	3	7	12.21
	4	1	18.00
	5	1	12.50
	6	1	20.50
	7	1	4.00
	8	1	17.00
	10	1	8.50
	Total	22	

Test Statistics[a,b]

	TDI_25
Chi-Square	6.745
df	8
Asymp. Sig.	.564

a. Kruskal Wallis Test

b. Grouping Variable: AET_NUM

The p value is greater than 0.05, suggesting that there is not a statistically significant relationship between the trauma-death interval (under 25 days) and the aetiological mechanism of fracture. The nature of the relationship will be discussed in Chapter 06.

Materials Used

Samples of human bone tissue routinely taken during post-mortem examinations at the Medico-Legal Centre Sheffield were decalcified and prepared as blocks of paraffin-embedded tissue in order to facilitate histological examination under the microscope. See Appendix 03 for a comprehensive list of the materials used.

Dissection at autopsy

Approximately matchbox-sized samples of human bone tissue were taken as a matter of routine during post-mortem examinations at the Medico-Legal Centre, Sheffield. These were placed into plastic containers containing 10% buffered formalin solution, in order to preserve and fix the tissues until the 'cut up' procedure. The period of fixation was unspecified, as samples were processed as soon as possible, but within no set time-frame. An estimate of the average fixation time is approximately one week (Newsome, 2004).

Decalcification

Decalcification is undertaken on the majority of bone samples, as these often prove too dense and difficult to cut to go straight to the 'cut up' procedure. Infant ribs and small bones such as fingers or

carpals may be soft enough to be processed immediately. Bone samples that required decalcification were placed in plastic tubs and 4M formic acid poured over them to cover them adequately. Formic acid was chosen as the decalcifying agent over EDTA, as the latter is known to only be efficient on samples less than 3 cm thick. The softness and extent of decalcification of the bone tissues was monitored every few days, to prevent over-decalcification. The time taken to satisfactorily decalcify the samples varied considerably with the thickness and density of the sample (Newsome, 2004), the location of the bone and the age of the individual. This means that the decalcification stage of the experimental procedure was un-standardised, but this could not be avoided, as this was carried out by the MLC technical staff years in advance of the project. Decalcification precluded the use of certain staining techniques (outlined below), such as Von Kossa's stain, which can be used to highlight areas of mineralisation in histological samples of bone.

"Cut up" procedure

During the 'cut up' procedure, the blocks of tissue were cut by a pathologist into pieces that clearly demonstrated the specific pathology of interest, and that would fit into standard white plastic (Cell Path System II) cassettes. The tissue pieces are placed in the plastic cassettes, and covered with metal 'clip on' covers. The cassettes are numbered with the unique individual FP (Forensic Pathology laboratory) number, and the number and specimen in each cassette is recorded and filed. This numbering system is double-checked by the pathologist and the technician. The cassettes were then ready for processing.

Tissue Processing

Cassettes containing pieces of tissue are removed from the formalin bath and placed in a metal basket, which was placed inside the Shandon Hypercenter XP processor. The lid was tightly clamped down. The processing programme is automated and regulated by computer, so all that is required is to select the preferred programme on the screen. Each programme is tailored to cater for differentially fixed tissues. The programs are chosen according to the extent of tissue fixation, as this changes the length of processing required. For bone tissue samples, the longest available program (number 4) is selected, as approximately 64 hours are required for the solutions to adequately penetrate the bone tissue.

The metal basket containing the tissue-filled cassettes was submerged in a succession of different reagents in order to dehydrate, clear and prepare the tissues for embedding. The tissues are placed first in a 70% formalin solution, and then in a series of alcohol baths of gradually increasing purity. This serves to remove any formalin or water from the tissue. A 'clearing' agent is then used to remove any traces of the alcohol, and to prepare the tissue for embedding. The clearing agent must therefore be miscible with both the dehydrating agent (alcohol) and the embedding medium (paraffin wax). The

tissue-filled cassettes are swamped with xylene, which serves as the clearing agent. After this, the tissue-filled cassettes are placed into a bath of molten paraffin wax for a period of eleven hours (Mason, 2004). The molten paraffin wax is kept under a vacuum, which aids the impregnation of the tissues with the wax. After this, they are ready to be embedded in paraffin wax blocks.

Embedding

The tissue-loaded cassettes were taken out of the metal basket and immediately placed in the wax bath of the Raymond A Lamb Blockmaster II 'embedding centre'. The wax bath is filled with molten plain paraffin wax, kept at a constant temperature of 65°C. This is just above the melting point of wax, to ensure that the wax stays in a molten liquid state throughout the embedding process. The metal moulds are available in 4 different standard sizes, and the most suitable size was chosen for each block. The metal mould was filled slightly with molten wax poured from the wax dispenser, and this was allowed to cool by placing it on a cold plate briefly. This was carried out to reduce the occurrence of artefacts or defects in the wax embedding. Heated tweezers were then used to transfer the tissue blocks from the plastic cassettes into the metal moulds. The tissue samples were placed in the metal moulds with the cutting edge or 'face' of the tissue section 'face' down. A plastic cassette was then placed on top of the metal mould, and topped up with wax from the wax dispenser, which is at a constant 70°C. The cassettes are immediately placed on a cool plate, which ensures the rapid cooling of the paraffin wax. This 'quick cooling' helps to reduce the size of the crystals formed during the wax-hardening process, which in turn facilitates cutting. A scalpel was used to crack the block out of the metal mould, and to trim off any wax stuck to the outside of the plastic cassette. The metal covers and moulds were then put in the 56°C incubator to melt the wax, and were cleaned in the finish cycle of the processor before being used again. The blocks of paraffin-embedded tissue were trimmed on a 'sledge-based' microtome, which was used to remove the excess wax until the 'full face', or whole surface, of the tissue was exposed, ready for cutting into sections.

Cutting sections from paraffin wax blocks

Before sections could be cut from the paraffin-embedded tissue blocks, it was necessary to cool them and sometimes to carry out localised surface decalcification on the sections of bone. Bone is a notoriously difficult tissue to cut on a microtome. A Raymond A Lamb cold plate, constantly kept at a temperature below 0°C (average temperature was -1.2°C) was used to bring the temperature of the block down. This ensured that the paraffin remained solid and did not melt at all, which facilitates the cutting of thin sections. The hardened blocks of tissue embedded in paraffin wax encased in plastic cassettes were placed in the 'chuck' of the Slee Mainz Cut 4060 rotary microtome. Tiny adjustments were made to bring the blade clamp up to the tissue block. The angle of the blade clamp could also be adjusted to ensure that the full face of the paraffin block was squarely against the blade. The blades used for cutting the bone sections were Feather S35 blades. The microtome was set to cut 5µm slices

of the block. The advance handle was rotated rapidly in order to bring the tissue block against the cutting edge of the blade repeatedly. After each full revolution of the advance handle, the chuck automatically adjusted so that the tissue block was advanced by 5µm uniformly. The thin tissue sections were carefully separated from each other, and occasionally uncurled with a short sharp breath. Blowing on the sections was done to briefly heat the wax and flatten out any creases. Sections were lifted from the microtome with a fine paintbrush and gently floated on the surface of a bath of pre-warmed distilled water at a temperature of 45°C. From the bath, the sections were then 'floated' on to glass slides. The identifying FP number was written on the slide in pencil, which survives the washing and staining procedures, in order to maintain continuity and ease of reference. Eight sections of each block were cut, and four were mounted on to standard BDH Laboratory Supplies Premium Microscope glass slides, and the remaining four were mounted on to BDH Laboratory Supplies Polysine Microscope glass slides. These are treated with Polysine, which provides superior adhesion of the tissue section to the slide, which was necessary if the sections were to survive the relatively aggressive immunohistochemical heating and washing procedures. The slides were then positioned vertically in stainless steel draining racks, and placed in an incubator with an ambient temperature of 57°C overnight, and then relocated to an incubator at 37°C until they were dry.

Staining

Several stains were used in order to emphasise and highlight different features present at the fracture sites of the specimens. Tinctorial stains such as Haematoxylin and Eosin, and Perls' Prussian Blue stain were used in order to highlight histological features associated with fracture healing, such as bone cells and haemosiderin granules, on the fracture sample sections.

Haematoxylin and Eosin

One section from each sample was stained with Haematoxylin and Eosin (H+E) stain. This was done using a Shandon Linistain GLX staining machine. The slides were mounted on a mobile rack which moves at a constant speed of 1mm per second. First, the slides moved slowly underneath a heated metal plate, which warmed and dried the section, slightly melting the wax surrounding the section. This facilitates the staining by removing the fine coating of wax that coats the section. The slides are gently dropped into narrow baths of varying solutions that serve to hydrate, wash and stain the sections. The table below (see Table 03: 07) shows the sequence and duration of chemical baths used to stain the sections with Haematoxylin and Eosin. The technique is the one favoured by the Department of Forensic Pathology histology laboratory for decalcified bone sections.

Table 03: 07 The sequence and duration of chemical baths used in H+E staining.

Number of baths	Time bathed (seconds)	Bath	Purpose
4	120	xylene	removes the wax and water from the tissues
4	120	100% alcohol	removes the xylene from the tissues
1	30	water	wash
6	360	Mayer's haematoxylin	stains the nuclei of the cells blue-purple
1	30	water	wash
1	30	2% acetic acid	removes excess haematoxylin to reduce background staining
1	30	water	wash
1	30	water with a few drops of sodium hydrogen carbonate	changes the colour of the nuclei from purple to blue (blueing agent)
1	30	Water	wash
1	30	0.2% eosin	stains the cytoplasm of the tissue different shades of pink
1	30	water	wash
4	120	100% alcohol	dehydrates the tissues
1	30	alcohol/xylene mixture (50%/50%)	removes the alcohol, so that a xylene-based mountant is useable
1	30	xylene	removes alcohol from the tissues

Positive and negative controls in the conventional sense were not done to check the validity of the Haematoxylin and Eosin staining. A test slide containing samples of lung, liver, kidney and heart tissue was passed through the above procedure every morning. The test slide was examined under the microscope to confirm that the haematoxylin had stained any nuclei in the tissue blue-purple, and that the eosin had stained the cytoplasm of the cell and surrounding tissue different shades of pink. If this occurred satisfactorily, the staining was deemed successful and subsequent staining runs were performed. If the staining was too dark or not specific, the amounts of reagents in the Shandon Linistain GLX staining machine were adjusted to compensate accordingly.

Perls' Prussian Blue stain

Perls' Prussian Blue is a simple tinctorial stain that emphasises the presence of haemosiderin in tissues. In histological sections, ferric iron in the form of ferric hydroxide ($Fe(OH)_3$)) is unmasked from compounds such as haemosiderin by hydrochloric acid. The ferric iron then reacts with potassium ferrocyanide to produce an insoluble blue compound, ferric ferrocyanide or Prussian Blue (Lumb,

2000). Haemosiderin has been recognised as being of forensic importance for over a century (Vanezis, 2001), and as a break-down product of blood often associated with old haemorrhage, it has become one of the classic indicators of age of a wound. Haemosiderin-laded macrophages have been seen in histological sections of the skin and sub-cutaneous tissue as early as 24-48 hours after a wound, but more commonly after about four to eight days (Vanezis, 2001).

The method used to stain the fracture slides with Perl's Prussian Blue is outlined below:

1) 10 ml of 2% potassium ferrocyanide was carefully added to 10 ml of 2% hydrochloric acid and the mixture was dropped on to prepared bone fracture sections mounted on standard glass slides.
2) The solution was left for 25 minutes, and then tipped off.
3) The slides were rinsed in distilled water, and the excess water was then tipped off again.
4) Filtered 1% Neutral Red counter-stain was then dropped on to the slides and left for one minute before being tipped off.
5) Slides were then passed through the final eight baths of the Linistain machine, and mounted with xylene-based mountant.

The action of the hydrochloric acid releases the ferric iron from its attachments to the protein, facilitating its reaction with the potassium ferrocyanide. The ferric iron present in the tissue reacts with the dilute potassium ferrocyanide to produce an insoluble blue compound called ferric ferrocyanide, or Prussian Blue. It is usually visible in tissue sections as small granules stained blue, and not present in fractures immediately after trauma. It begins to appear later as the haemorrhage associated with the trauma begins to break down.

The positive control sample used was a section of liver taken from an individual with haemochromatosis, which is a pathological condition that increases the amount of haemosiderin in the tissues. It is not standard practice in the Forensic Pathology laboratory to include a negative control on runs of slides stained with Perls' Prussian Blue. A negative control would have to be done with a tissue known not to express haemosiderin.

Immunohistochemical staining

Immunohistochemistry and immunocytochemistry are extremely valuable techniques for specialised bone and cartilage studies (Gruber and Ingram, 2003). Such procedures are performed to obtain specific types of information about bone cells, such as osteoblasts and osteoclasts, bone matrix and bone formation and mineralisation. No single stain or technique is exhaustive in the information it reveals, and so a variety of staining or localisation procedures has to be employed.

CD68 is a 110kDa transmembrane (Type 1) glyco-protein made up of 354 amino acids, which is expressed in virtually all macrophages, and a variety of other cells, such as dendritic cells, inflammatory neutrophils and basophils and mast cells (Goyert, 1999). It plays a role in the phagocytic activities of macrophages, in cell to cell and cell to pathogen interactions and in intracellular lysosomal action (Goyert, 1999). The monoclonal antibody anti-CD68 is primarily used as a macrophage marker. CD68 was chosen as one of the proteins to examine in relation to fracture healing as it marks osteoclasts, which play an active role in the resorption of necrotic bone after fracture. It is also widely available and relatively inexpensive, which improves the reproducibility of the study. The primary monoclonal (mouse-derived) anti-human anti-CD68 antibody (DAKOCytomation) was used as a macrophage marker (DAKO, 1999).

Two runs of 26 slides were undertaken, to stain the 52 available fracture sample slides. The sample was split in such a way so that it was possible to mount all the slides on one rack and to keep transition periods between one treatment and the next minimal. Approximately 30 slides was the maximum number of slides with which it is easy to work given the immunohistochemistry staining equipment available at the Medico-Legal Centre. A positive and a negative control section were included in each run. Both control sections were taken from diseased lung from individuals with bronchi-pneumonia, which exhibited a high concentration of inflammatory cells and therefore macrophages.

Sections on Polysine-coated slides mounted in stainless steel draining racks were de-waxed and washed in a series of baths. They were placed in a xylene bath for five minutes, and then transferred to three consecutive baths of 100% alcohol, for five minutes in each bath. The xylene serves to remove the paraffin wax and any water in the tissues, and the alcohol stage is necessary in order to remove the xylene. Slides were then placed in a bath of distilled water for approximately five minutes in order to remove traces of alcohol. This is necessary so that any water-soluble reagent can be applied to the tissues.

Three solutions were made up in 20ml vials in the following manner:

1) 3% Hydrogen peroxide solution: 1ml of refrigerated and shaken 30% hydrogen peroxide solution was pipetted into a 20ml vial and 10ml of distilled water was added, and the mixture shaken.
2) DAB solution: One tablet of 3,3diamino-benzidine (DAB) was dropped into an empty 20ml vial and 10ml of tris-buffered saline (TBS), with pH value 7.6 was added. The mixture was shaken and stored in a refrigerator until required.
3) Primary antibody solution: Calculations were done to determine the correct volume of primary antibody and TBS to use in order to make up a 1 in 100 strength dilution. 3 drops of diluted primary antibody solution were required for the staining, so this volume (0.084ml) (Mason, 2004)

was multiplied by the number of slides in each run (including the positive control) to find the required volume of solution. This amount was then rounded up to the nearest half millilitre and a solution of 1 in 100 made up. For example:

0.084 x 27 = 2.27 ml

2.27 ml rounded up to 2.5 ml.

1 in 100 dilution made with 25µl CD68 and 2475µl of TBS.

Appropriate safety measures were taken throughout. These included wearing laboratory coat and latex gloves to prevent contact between the reagents and skin. The DAB tablets and solution were treated with extreme caution, as it is known to be a potent carcinogen, so care was taken to ensure that the DAB solution was not flushed down the laboratory drain but into the specially filtration system called 'DABout'. This filtered the toxic DAB out of the solution and decontaminated the water, which could then be flushed normally.

Once the slides were de-waxed and washed, they were placed in a purpose-made condensation chamber which contained three rubber racks. The negative control was placed at the end of one row of slides, to act as a reminder not to place primary antibody on it. They were flooded with distilled water to wash off any last traces of xylene, and to keep them hydrated.

A PAP-pen (DAKOCytomation, 1-bromopropane) was used to draw around each section on each slide. This is to restrict the outward flow of the reagents dropped in solution onto the slides, so that the reagent covers the section only. In so doing, it minimises the amount of reagent necessary.

Enough 3% hydrogen peroxide solution to cover each section was then dropped on to each slide with a hand-dropper. The purpose of the hydrogen peroxide solution is to block the endogenous peroxidase activity (see Figure 03: 11). The lid of the condensation chamber was then placed over the slides, and the solution was left on the slides for exactly five minutes. After five minutes, the hydrogen peroxide solution was washed off the slides by rinsing them three times in tris buffered saline. After the first rinse in TBS solution, the slides were tipped immediately to allow the solution to run off. TBS was then put on the slides again, and left for a period of five minutes minimum. This is to ensure adequate rinsing of the hydrogen peroxide solution. A third quick rinse in TBS was done before the next stage.

Two drops of DAKOCytomation Protein Block were dropped on to each slide and left under the lid of the condensation chamber for five minutes. This serves to mask any endogenous proteins on the section. After this, the slides were tipped but not rinsed. A tissue was used to carefully dab away any excess moisture from the section.

Figure 03: 11 A schematic diagram showing the process of immunohistochemical labelling of CD68+ macrophages.

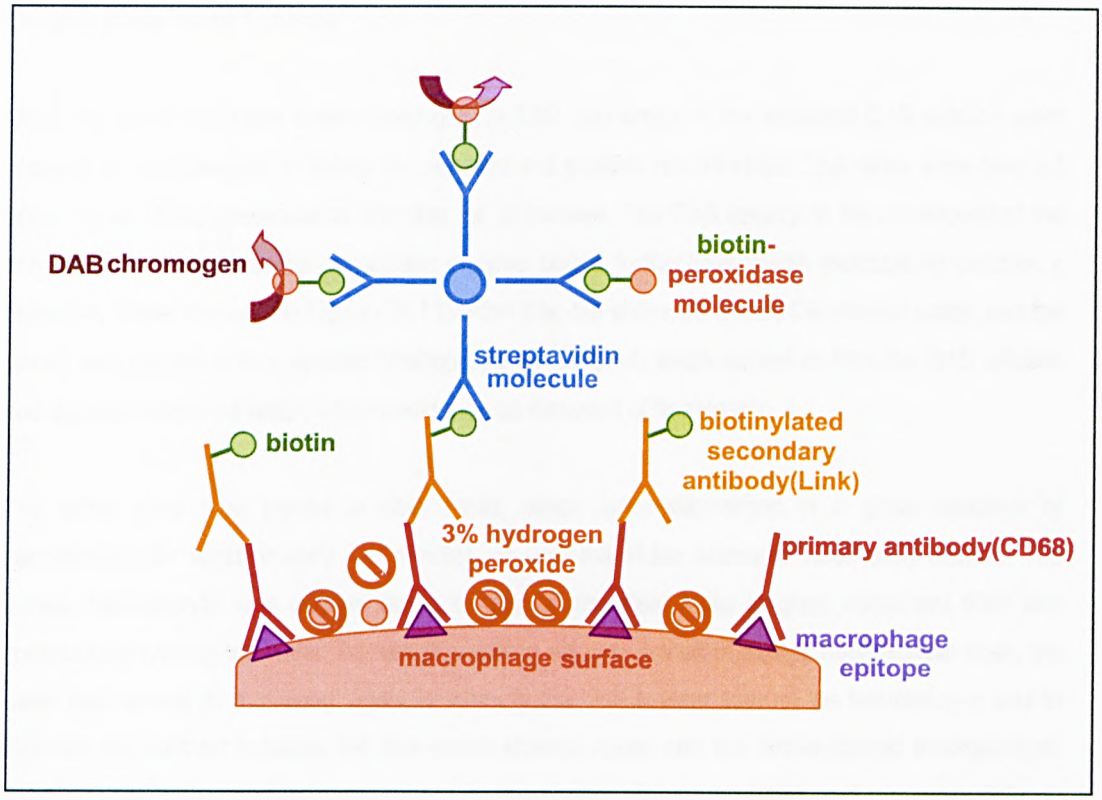

Three drops of the primary antibody were then dropped on to each slide using a hand pipette. It was dropped on to the positive control slide, but not on to the negative control slide, which was covered in TBS only. The primary antibody was left on the slides for 60 minutes exactly. During this time, the antibody molecules bound to the epitopes of the antigens present on the surface of the macrophages in the fracture section (see Figure 03: 11). After one hour, the slides were tipped and rinsed in TBS three times. The same procedure of a quick rinse followed by a five-minute rinse, followed by a quick rinse was done.

Two drops of DAKOCytomation Link Antibody were dropped on to each slide (including the negative and positive control slides), and left under the condensation chamber lid for 20 minutes. After 20 minutes exactly, the lid of the condensation chamber was lifted, and the slides were tipped and rinsed three times in TBS solution, again with the 'quick-slow-quick' rinse procedure.

Two drops of DAKOCytomation Streptavidin Solution were dropped on to each slide (including the negative and positive control slides), and left under the condensation chamber lid for 20 minutes. Again, after 20 minutes, the slides were tipped and rinsed with TBS, using the 'quick-slow-quick' rinse

procedure. During the second five-minute rinse with TBS, the vial of 3% hydrogen peroxide solution was removed from the refrigerator, and shaken. 75µl was pipetted out and added to the vial containing the DAB tablet and TBS solution. The vial was then shaken, which serves to facilitate the activation of the DAB. It was left for 1 minute.

Once the slides had been rinsed thoroughly in TBS, two drops of the activated DAB solution were dropped on to each slide, including the negative and positive control slides. The slides were then left under the lid of the condensation chamber for 10 minutes. The DAB solution is the chromogen of the process, and reacts with the peroxidase enzyme bound to the Streptavidin molecule to produce a distinctive brown colour (see Figure 03: 11). After this, the slides were rinsed in distilled water, and the run-off was poured in to a specific filtration system (DABout) which served to filter the DAB solution and decontaminate the water, which could then be disposed of harmlessly.

The slides were then placed in steel racks, which were submerged in a glass container of haematoxylin for approximately five minutes, or until the slides appeared adequately stained. The excess haematoxylin was washed away, by placing the steel racks in glass containers filled with continuously running tap water. As well as washing away all traces of excess haematoxylin stain, the water also served as a 'blueing' agent to intensify the blue nuclear stain of the haematoxylin and to increase the contrast between the blue-purple-stained nuclei and the brown-stained macrophages. After this, the racks of slides were placed in the alcohol and xylene baths in the reverse order to previously, in order to dehydrate and clear the tissues once more, and make it possible to use a xylene-based mounting agent. The slides were then mounted with cover-slips and DPX (di-butylphalate) synthetic mounting agent.

Bone Sialoprotein

Bone sialoprotein (BSP) is a sialic, acid-rich glyco-protein, with an approximate weight of 70 – 80 kDa, and is found in the extra-cellular matrix of bone. Besides osteocalcin, osteopontin and osteonectin, it is one of the major non-collagenous proteins, constituting roughly 12% of all the non-collagenous proteins in bone (Calbiochem, 2003; Fisher *et al.* 1990). It is expressed in cells in the osteoblast lineage, including mesenchymal cells, osteoblasts and osteocytes. It is believed to mediate endothelial cell attachment and migration, and promotes angiogenesis (Barou *et al.* 2002). As a marker of osteoblasts and osteocytes, the anti-bone sialoprotein antibody was chosen to complement the action of the CD68 antibody. Osteoblasts secrete osteoid which undergoes mineralisation and gradually forms bone, and are particularly active during the remodelling stages of fracture healing. CALBIOCHEM Monoclonal Human Anti-Bone Sialoprotein, (mouse-derived) was used (CALBIOCHEM, 2004).

In order to determine the optimum working dilution and antigen-retrieval procedure for the bone sialoprotein (BSP) tests on fractured bone samples, it was necessary to do some preliminary pilot tests. These tests were also performed to find the best positive control to use. As time and equipment were restricted, an evolutionary approach to the pilot tests was taken. As bone sialoprotein is known to be bone-specific (CALBOCHEM, 2004), it was necessary to use bone sections. The majority of bone histology samples taken at or submitted to the Medical-Legal Centre are pathological in origin, but it was possible to find a small sample of 'normal' (non-pathological) samples by interrogating the Department of Forensic Pathology histology database, which contains records of the autopsy cases reviewed at the MLC over the last ten years. The sample of normal bone histology samples consisted of 11 individual cases. The majority of these samples were taken during autopsy as a precautionary measure in cases where an infant was suspected to be the victim of child abuse. Samples were taken from unfractured bones in infants with one or multiple fractures to investigate the possibility of osteogenesis imperfecta or any other pathological condition that might have contributed to the occurrence of fractures.

Using the same techniques as previously described, six sections of each block were cut, and four were mounted on glass polysine-coated slides for immunohistochemical staining, and two were mounted on standard glass microscope slides. After this, they were prepared for antigen retrieval and staining by de-waxing and washing as before.

In order to determine whether antigen retrieval was necessary for the BSP staining procedure, one complete set of samples (11 slides) was subjected to the citrate-buffer antigen retrieval technique perfected by the technicians at the Department of Forensic Pathology (Mason, 2004), and one complete set of slides was not subjected to any method of enhanced antigen retrieval before the immunohistochemical BSP staining was performed. The citrate-buffer antigen retrieval techniques comprised the following steps:

1) A large microwaveable container (two litre margarine or ice-cream tub) was filled to the half-way mark with citrate antigen retrieval buffer.
2) The slides with the tissue sections on them were placed in a plastic rack and lowered into the citrate buffer solution until they were adequately covered. The tub and slides were placed in the standard household microwave.
3) The microwave was switched on and set to microwave on full power for 12 minutes.
4) After 12 minutes of heating, the microwave was turned off and the contents of the tub 'rested' inside the microwave for two minutes.

5) The contents of the microwave were then heated again for two minutes, rested for two minutes, heated for two minutes, rested for one minute and finally heated again for one minute.
6) The tub was removed from the microwave and allowed to cool for ten minutes.
7) The slides were then removed from the citrate buffer solution and washed in cold water.

Both complete sets of sections (22 normal bone sections and four normal bone control sections) were then ready to be stained with BSP. The control sections were included to ensure that the immunohistochemical staining procedure had been performed correctly. As with the CD68 staining controls, the positive control was taken through each stage of the staining process including the primary antibody; whereas for the negative control, the primary antibody stage was omitted. Because no information could be obtained from the antibody manufacturer or in the research literature about the most appropriate working dilution of bone sialoprotein to use, or which controls to use, it was necessary to try several different dilutions of the BSP primary antibody. It was thought that it was best practice to start with a low dilution (i.e.: a high concentration of antibody), to ensure that sufficient staining was obtained. If staining seemed adequate, then higher and higher dilutions (less and less antibody) could be tried. The first stain dilution attempted was a 1 in 25 dilution. The specific quantities of antibody and TBS were calculated in the same way as previously described for the CD68 antibody.

Once the slides were examined after being stained, counter-stained and mounted, it was decided that the pre-treatment with the citrate buffer antigen retrieval technique was unnecessary. It rendered some sections useable as the heating and cooling regime was too vigorous, and many of the sections were lost altogether. It was also determined that the 1 in 25 BSP dilution was much stronger than was necessary and the intensity of the chromogen expression was too high. It was difficult to discern individual cells and there was a very high level of background staining which made the sections un-interpretable.

A second dilution pilot test was then performed by staining another complete set of normal bone sections (11 slides, two controls) with BSP in a 1 in 100 dilution. For this test, only non-pre-treated sections were used. Again the dilution was deemed too strong, as background staining was still high, although considerably better than the previous dilution. It was decided that a 1 in 200 dilution of primary antibody would be sufficient for the immunohistochemical staining of the sections of fractured bone.

Tests

The bone sialoprotein immunohistochemical staining was carried out using exactly the same procedure as was used for the CD68 antibody, except with the BSP as the primary antibody. A 1 in 100 dilution

was used, and 50 slides of fractured bone sections were stained. Two runs of 25 slides each were carried out, with a negative and positive control for each. Normal bone sections were used as the positive and negative controls. Proof of a successful immunohistochemical staining procedure was a positive slide exhibiting immuno-positive cells stained brown by the DAB chromogen and a negative control exhibiting no immuno-positive cells. Photographs of the respective control slides are presented in Chapter 04.

Digital Photography

Colour digital photographs were taken of each slide using a Fuji S1 Pro digital camera mounted on a BH-2 Olympus microscope. A photograph of the fracture site, or sites, of each section stained with each stain was taken using a x10 magnification objective (see Appendix 04). The fracture site was deemed to be the area surrounding the gap between the main bone fragments. Using x10 magnification, it was sometimes difficult to take a clear photograph of the area closest to the fracture site, because the gap between the fragments appeared to take up most of the view through the viewfinder. Also, at that magnification, it was sometimes impossible to capture the whole of the fracture site in the photograph, so one side of the fracture site had to be chosen (see Figure 03: 12). Despite these limitations, the x10 magnification was found to be the most appropriate, in order to ensure that it was possible to visualise both the fracture site and the bone cells satisfactorily.

Figure 03: 12 A schematic diagram of a fracture site, showing the typical area captured using x10 magnification. (Image courtesy of Cruess and Dumont, 1975).

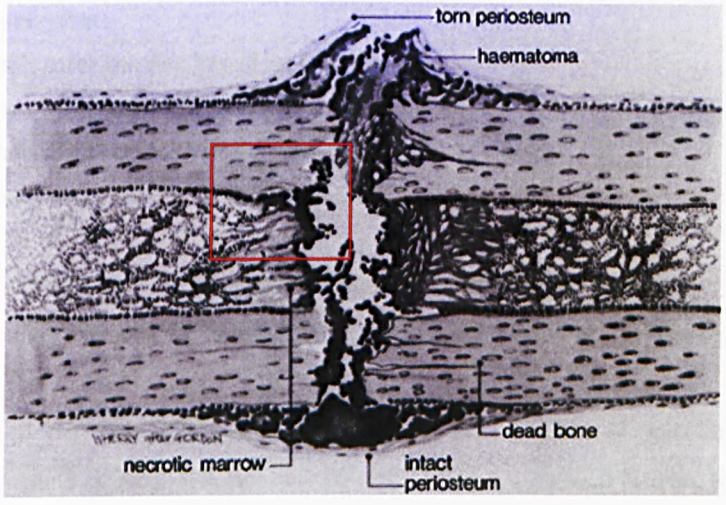

Also, a daylight blue filter was placed in the light path, below the condenser of the microscope for some photographs, in order to enhance the detail visible on the photograph, and to increase the contrast between the section and the background. It was found that the addition of a daylight blue filter was not necessary for all slides, so its use remained on an ad-hoc basis. The exposure time on the

camera was also adjusted between photographs in order to ensure the highest quality pictures. The optimum exposure time was generally determined through trial and error, and varied between 60th and 1000th of a second. The resultant digital photographs were then transferred to computer, and compact disc.

Image Analysis

The photographs were used for two different types of analysis. The first was semi-qualitative, semi-quantiative observation by human observers (see Chapter 04 for results), and the second automated histomorphometric analysis using computer software (see Chapter 05 for results).

Qualitative image analysis

Several semi-quantitative observations of histological phenomena were made by the author and by three other independent observers (see inter-observer agreement below). The histological assessments made were:

estimated percentage cover of the immuno-positive cells
estimated size of the immuno-positive cells
dispersal of the immuno-positive cells

The percentage cover of the immuno-positive cells in relation to the whole photograph was measured in a semi-quantitative fashion, using a category coding system. Observers were asked to assess the approximate percentage cover of the DAB-stained immuno-positive cells by assigning each slide a number on a scale between 0 and 4. The numbers represented the following categories:

0 : no cells visible
1 : the cells cover less than 25% of the background
2 : the cells cover between 26 and 50% of the background
3 : the cells cover between 51 and 75% of the background
4 : the cells cover over 76% of the background

The average size of the cells was estimated by the author in μm^2, by comparing them to cells of known size measured during the collection of the quantitative data using *Scion Image* (see below).

The distribution of the immuno-positive cells over the fracture site is of potential interest in the investigation of fracture healing. This can only be observed in a qualitative fashion, as it relies on the description of features and cells in relation to others. An attempt was made by the author to describe the immuno-positive cell dispersal using a combination of terms for the *nature* of the dispersal, such as clustered, evenly dispersed, lining the compact bone, and in Howship's lacunae, with terms for the *location* of the cells, such as throughout the slide, in or adjacent to compact bone, in the bone marrow

or extra-cellular matrix, around adipose globules, or concentrated around the fractured ends of the bone (see Table 03: 08).

Table 03: 08 A table showing the categories assigned to describe the different aspects of cell dispersal at the fracture site.

Category number assigned	Nature of the dispersal ('how')	Location of the dispersal ('where')
0	none	at fractured ends of bone
1	scattered	in the extra-cellular matrix
2	evenly	lining the compact bone
3	clustered	in the bone marrow
4	few	throughout the fracture site
5	dense	around the cartilage
6		around the adipose globules
7		around the red blood cells

These categories were also combined to produce amalgamated categories, each with a unique number denoting the distinctive combination of the location ('where?') and nature ('how?') variable.

example: a case where the dispersal of the CD68 positive cells were placed in:

location category 2 (compact bone) and
nature category 4 (few in Howship's lacunae)
} combined category 24

These methods were also used to describe the percentage cover of the inflammatory cells with nuclei stained blue by the haematoxylin. As the immunohistochemically-stained slides were counter-stained with haematoxylin, the nuclei of most other cell types present at the fracture site were stained a deep blue-purple colour. Two distinct types of cells with blue-stained nuclei were visible on the majority of the fracture site photographs (see Figure 03: 13). The small round cells are lymphocytes, which predominate during the process of chronic inflammation (Underwood, 2000). Also present are elongated, spindle-shaped fibroblasts, which very common in most types of connective tissue. They play an active role in the healing process, and are responsible for secreting collagen, which eventually forms into cartilage and callus. During their active phase, fibroblasts appear larger, and their nuclei become euchromatic, or less densely stained (King, 2004).

Figure 03: 13 Photograph of a fracture site stained with CD68 and a haematoxylin counter-stain, showing the two distinct types of cells with blue-stained nuclei. (Objective magnification x10)

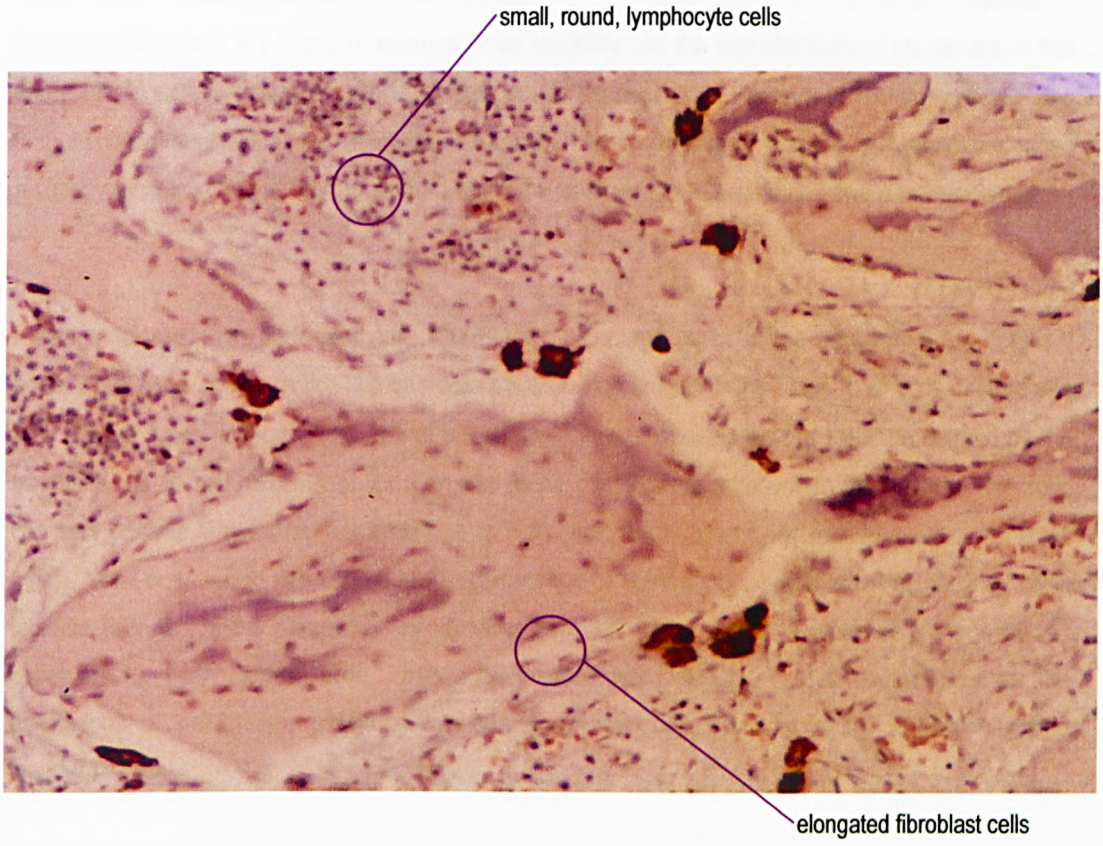

Inter-observer agreement

In order to increase the accuracy and reliability of the qualitative data collected, three additional independent observers were recruited to make assessments of the percentage cover of different cells visible on the photographs of the fracture sites. They were asked to view .jpeg images of the fracture sites of the CD68-stained and BSP-stained slides using PaintShopPro 5 as viewing software. They were given a recording form (see Appendix 05) on which to record their estimates of percentage cover of each type of cell. The cells they were asked to assess were the brown DAB-stained immuno-positive cells, small round cells with blue-stained nuclei (lymphocytes), and elongated cells with blue-stained nuclei (fibroblasts). They were asked to give a number on a scale of 0 to 4 to indicate the level of percentage cover. The scale is described below:

0 : no cells visible

1 : the cells cover less than 25% of the background

2 : the cells cover between 26 and 50% of the background

3 : the cells cover between 51 and 75% of the background

4 : the cells cover over 76% of the background

This choice of this type of semi-quantitative, categorical scale was based on the methodology of similar studies and recommendations from pathology researchers (Cross, 2001; Martiniakova *et al.* 2003). Cross (2001) raises the issue of the experience of the observers in measuring and 'eyeballing' histology slides as a key factor in assessing their reliability and the reproducibility of the results. In this study, the four independent observers had varied experience of looking at histology slides and immunohistochemical staining reactions. Observer 1 was the author, Observer 2 an experienced histology technician in the Department of Forensic Pathology, and Observers 3 and 4 were novices.

Compact bone

Similar analyses were performed to estimate the percentage cover of the background by compact bone, both living and necrotic. The characteristics of the compact bone close to or at a fracture site may aid the determination of the age of a fracture. The devascularisation of the area caused by the trauma leads to the necrosis of the compact bone immediately adjacent to the fracture. Necrotic compact bone is obvious histologically due to distinctive empty osteocyte lacunae (Wichmann *et al.* 1996). Semi-quantitative estimations of the percentage of compact bone with intact osteocytes within lacunae (living) and the percentage of compact bone exhibiting empty lacunae were made by the observers for each fracture slide. These observations were performed at the same time as the estimations of percentage cover of the immuno-positive cells, for the sake of continuity and standardisation.

Red blood cells

The earliest stages of fracture healing are characterised by haemorrhage and inflammation. Red blood cells spill out of the disrupted blood vessels and swamp the damaged area, but their presence at the fracture site is short-lived. The percentage cover of the background by red blood cells was also estimated using the same method, at the same time as the other observations were being made.

Quantitative image analysis

The automated, computerised histomorphometric analysis was performed using the *Scion Image Beta 4.02* (*for Windows 95 to XP*) freeware analysis program for histomorphometric analysis (Scion Corporation. www.scioncorp.com). After much trial and error, and consultation with an expert (Stewart, 2004), it was decided that in order to gain the best resolution of images, and the highest contrast between histological features, it was necessary to make several amendments to the photographs before histomorphometric analysis could be carried out.

Preparing images for analysis

The following procedure was applied to all images:

1) The digital photographs were converted into .tiff format from their original .jpeg format, as Scion Image only recognises .tiff files.
2) The .tiff format image was opened in Indexed Colour RGB image (see Figure 03: 14), and the colour channels were scrolled through using the (>) key (see Figure 03: 15). This was done as it was found, especially for the images of the samples stained with CD68 and BSP, that the software could more easily differentiate between cells and the 'background', or intercellular matrix, if the photographs were split into their component channels (red, green and blue). Through trial and error, the blue channel was found to afford the most contrast.

Figure 03: 14 A 'screen grab' of the *Scion Image* program, showing the image of an immuno-stained slide (CD68, x10 magnification) opened as a .tiff format image.

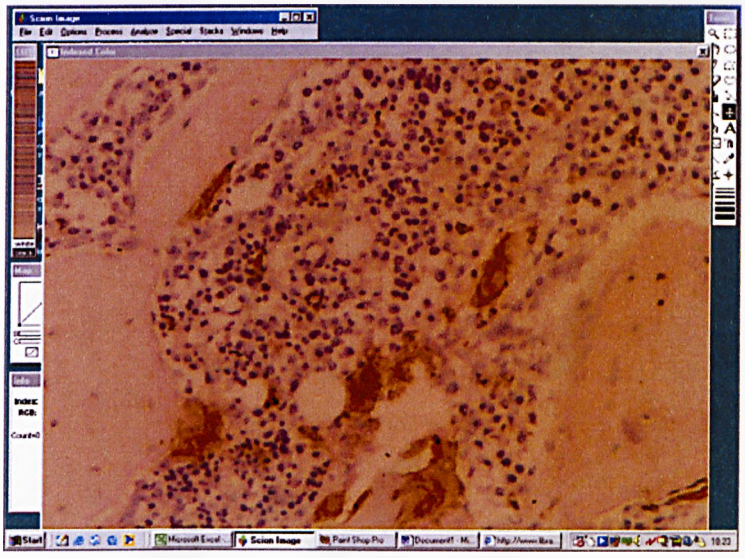

Figure 03: 15 A 'screen grab' of the *Scion Image* program, showing the image of an immuno-stained slide once the blue channel had been selected.

3) Once the blue split channel picture was opened in *Scion Image*, it was possible to adjust the threshold levels of the image. Thresholding was used to segment an image into areas of interest and areas of background. The image was displayed in black and white, with objects on interest coloured black, and what the program interprets as background coloured white (see Figure 03: 16). This was done by selecting Options, Threshold and adjusting the threshold scale until only the immuno-positive cells appeared black and the rest of the image was white.

Figure 03: 16 A 'screen grab' of the *Scion Image* program, showing the image of an immuno-stained slide once the Threshold level had been selected (Arrow indicates the adjustable Threshold level).

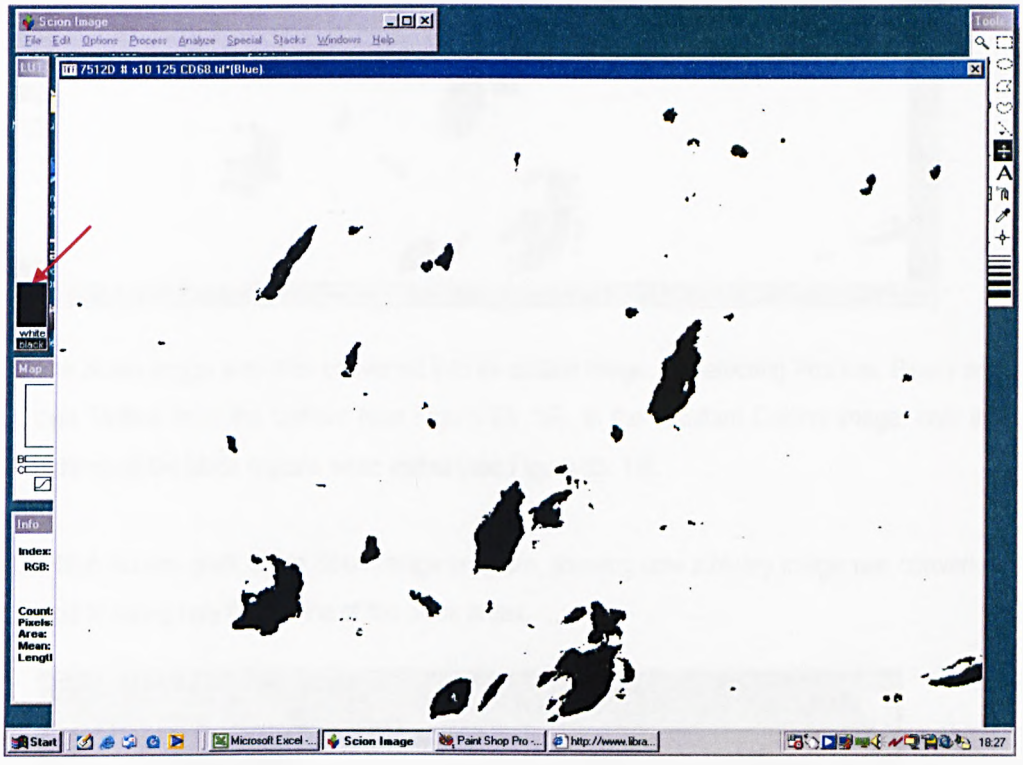

4) The image was then made into a binary image, by selecting Process, Binary, Make Binary from the taskbar (see Figure 03: 17). This turned the image into one with only two true colours – black and white.

Figure 03: 17 A 'screen grab' of the *Scion Image* program, showing how a black and white threshold image was converted into a binary image.

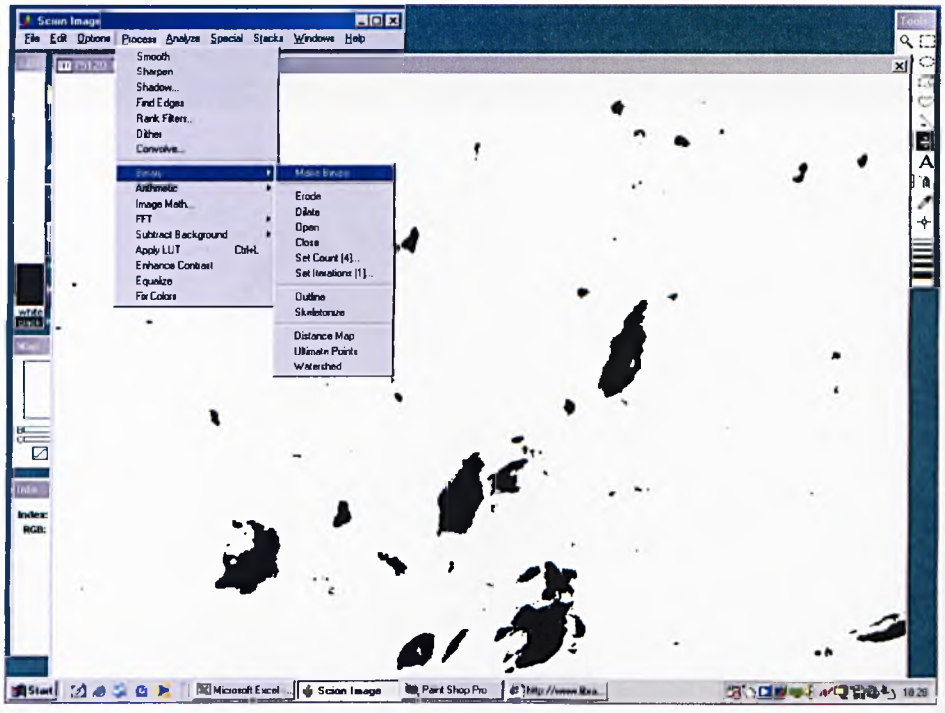

5) The binary image was then converted into an outline image, by selecting Process, Binary and then Outline from the taskbar (see Figure 03: 18). In the resultant Outline image, only the outlines of the black regions were visible (see Figure 03: 19).

Figure 03: 18 A 'screen grab' of the *Scion Image* program, showing how a binary image was converted into an image showing only the outline of the black areas.

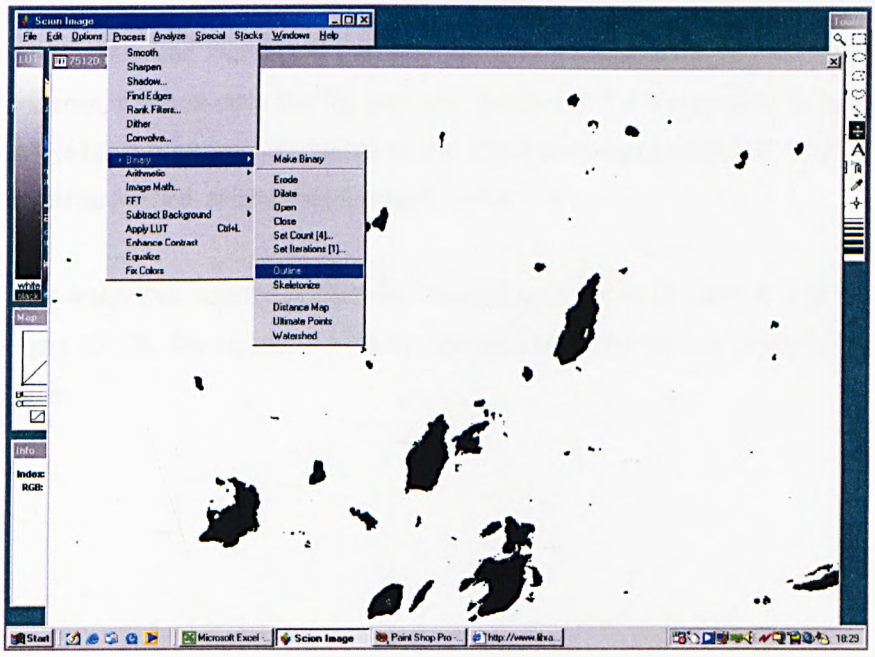

Figure 03: 19 A 'screen grab' of the Scion Image program, showing the result of converting the binary image into an image showing only the outline of the black areas.

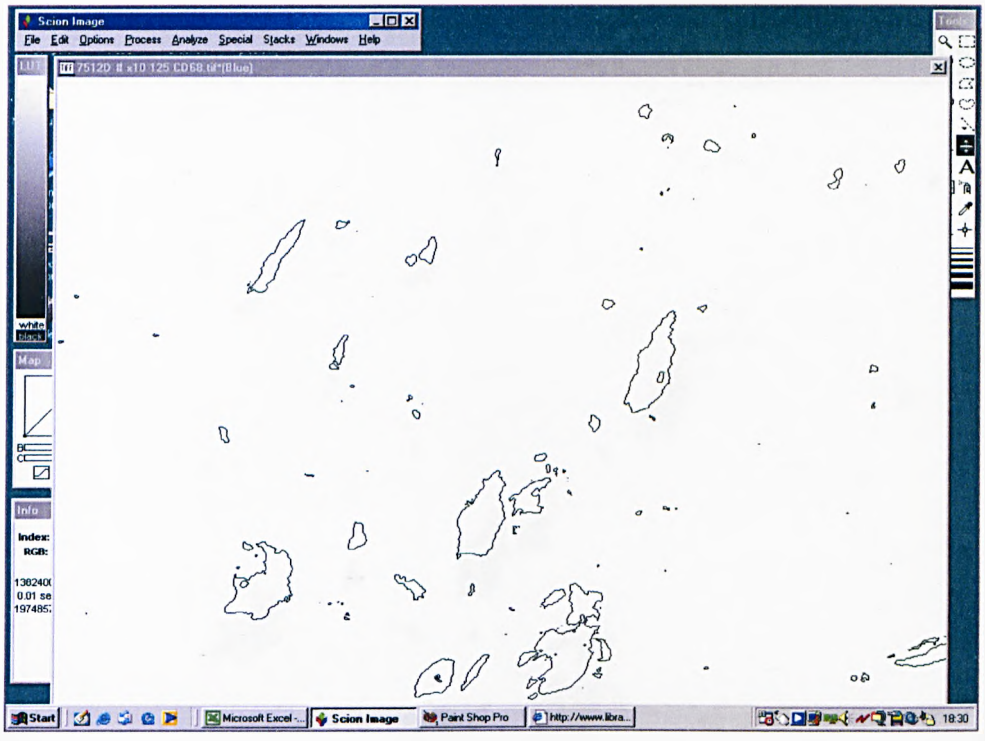

6) Once the image had been converted into an image where the areas of immuno-positive staining were now outlined on a white background, it was possible for the Scion Image software to count the outlined areas and perform histomorphometric measurements.

7) To count the outlined areas, Analyse, Count Particles was selected. It was necessary to state some preferences, such as the minimum particle size that would be counted. After some trial and error, it was decided that the minimum particle size (i.e: the smallest outlined area) that should be counted was 100 (arbitrary units). Other preferences stated were that the particles should be labelled, and the measurement counter reset.

8) *Scion Image* then counted and labelled the particles, turning them grey as it progressed (see Figure 03: 20). The number of particles was displayed in the Info box in the bottom left hand corner.

Figure 03: 20 A 'screen grab' of the *Scion Image* program, showing the result of the counting and labelling of the black areas. Black areas were turned grey as the software counted them.

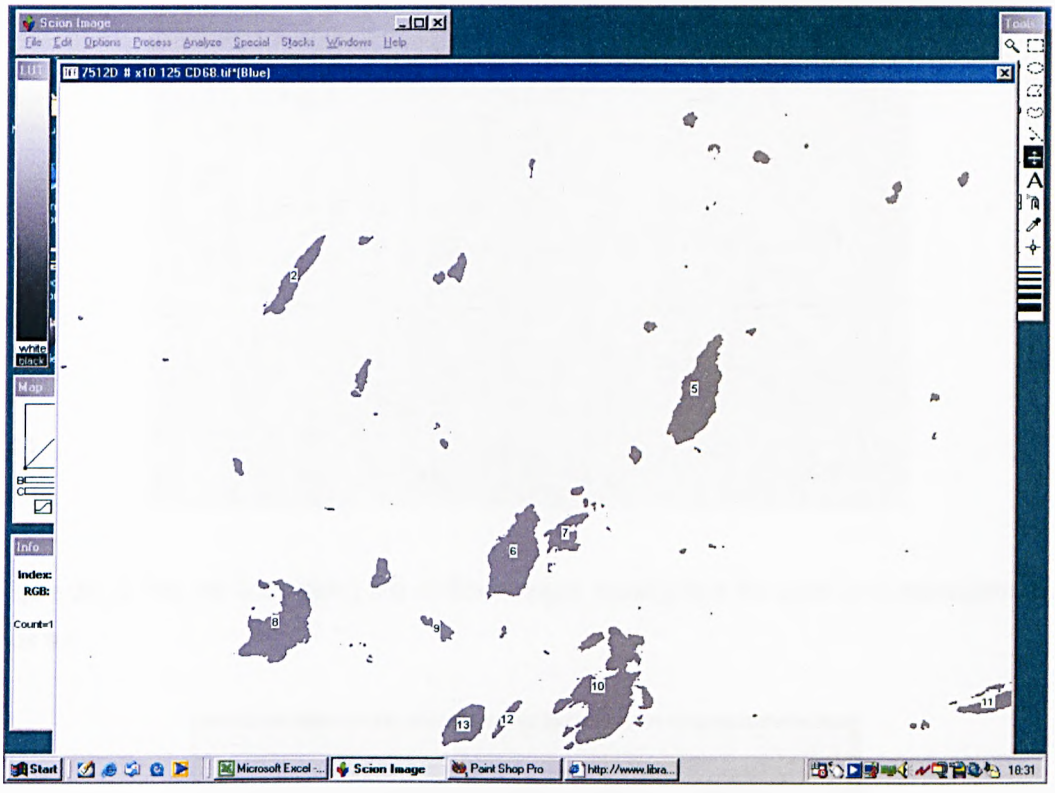

Scaling

All of these eight steps were followed for the image of each immuno-stained slide. Before it was possible to perform any histomorphometric measurements using the *Scion Image* software, it was necessary to establish a scale. This was done by taking a photograph of a graduated haemocytometer of known dimensions in exactly the same way as the slide photographs were taken, with x10 magnification (see Figure 03: 21). This image was then opened with the *Scion Image* program, and the known distance measured on the screen with the line measuring tool. The line indicated on Figure 03: 21 was measured three times using the line measurement tool, and consistently was shown to be 103 pixels long. This number was entered into the Analyse, Set Scale dialog box (see Figure 03: 22) in order to set the scale for all subsequent measurements.

Figure 03: 21 Image of a haemocytometer taken through the microscope (x10 magnification) that was used to calibrate the Scion Image software. The distance between the arrow tips is 50µm.

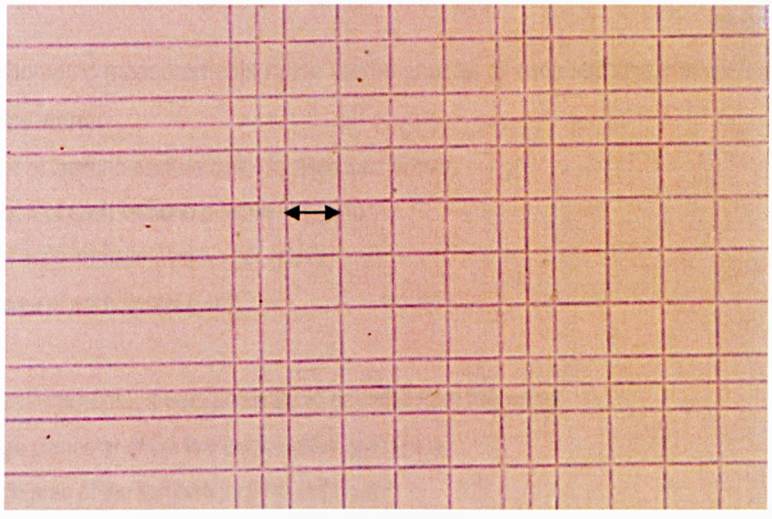

Figure 03: 22 The Set Scale dialog box on *Scion Image*, showing how the scale for all measurements was set.

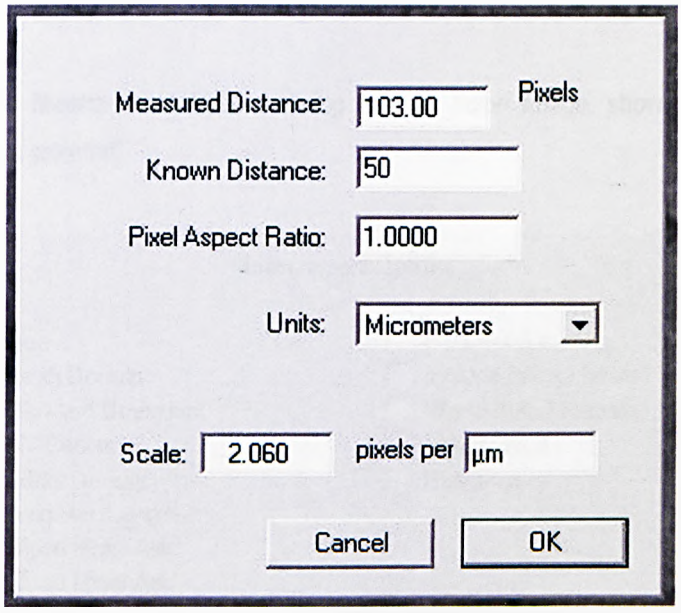

The total area measurement of the whole photograph was also measured, so that data for the percentage cover of immuno-stained cells could be calculated. Once the scale had been set, this was done by selecting Edit, Select All, so that the whole area of the image was highlighted, and then selecting Analyse, Measure. This was repeated three times to account for any unobservable error. The total area of each image was found to be 325761.15µm^2. Once these preliminary preparations had

been made, it was possible to take the histomorphometric measurements of the images of the immuno-stained histology sections of fractured bone samples.

Image measurement

The histomorphometric measurements made on the images of each immuno-stained histology section of fractured bone were:

number of immuno-positive cells (as described above)

perimeter of each immuno-positive cell (μm)

area of each immuno-positive cell (μm^2)

total area of each image (μm^2)

From these measurements, it was possible to calculate the following:

average perimeter of the immuno-positive cells (μm)

average area of the immuno-positive cells (μm^2)

cover of immuno-positive cells over the background (%)

In order to carry out these measurements, the Analyse menu was selected, the Measurement Options dialog box opened, and the tick-boxes for particle area and particle perimeter were ticked (see Figure 03: 23).

Figure 03: 23 The Measurement Options dialog box on *Scion Image*, showing how the above measurements were selected.

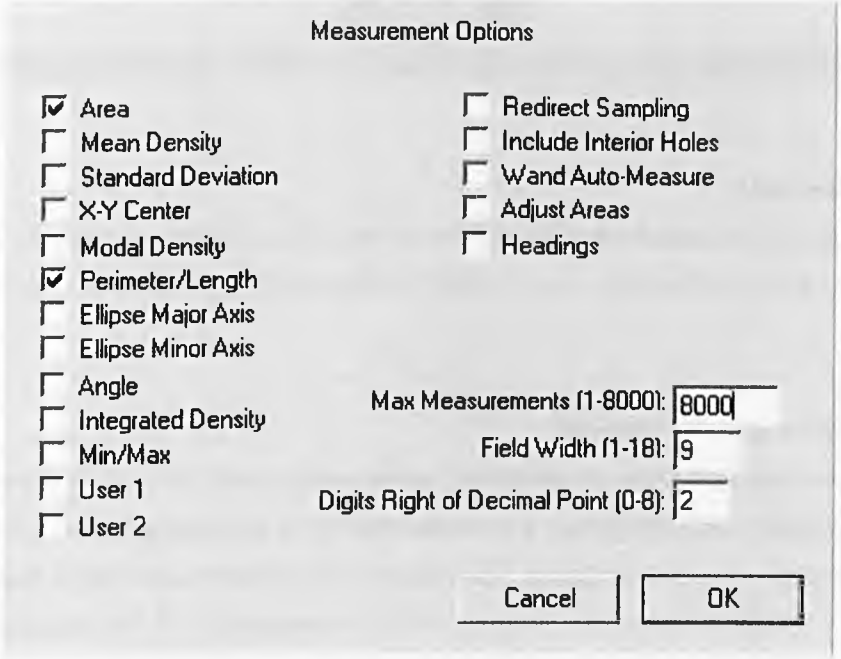

For each image, the *Scion Image* software automatically carried out these measurements according to the scale already set. The results of the measurements could be seen by selecting the Analyse menu and Show Results (see Figure 03: 24). This data could then be exported into a Microsoft Office Excel spreadsheet.

Figure 03: 24 A 'screen grab' of the *Scion Image* program, showing the results of the measurement of the grey immuno-positive areas.

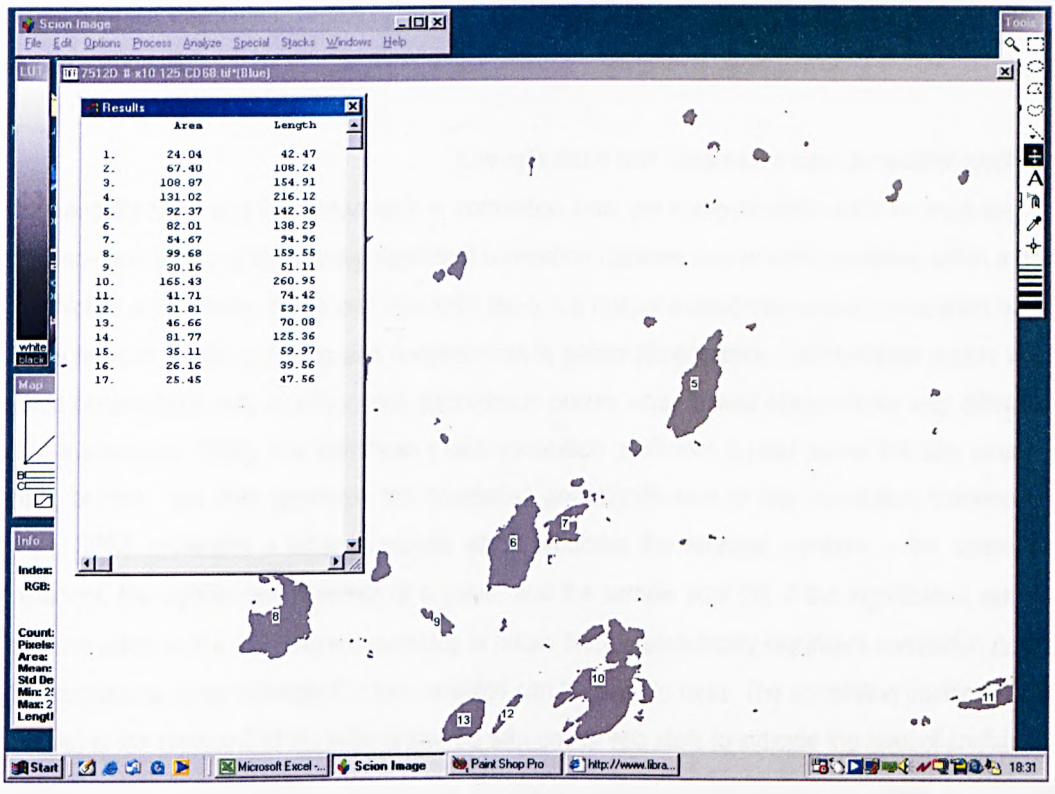

Statistical analyses

The data generated by the image analysis was imported into a Microsoft Office Excel spreadsheet, and from there into a SPSS (version 10) spreadsheet, where it was subjected to a variety of statistical analyses.

One-sample Kolmogorov-Smirnov test

The One-sample Kolmogorov-Smirnov test is used to test whether the data in the sample was normally or not normally distributed according to the Gaussian model of normal distribution. This test serves as a spring-board for other statistical analyses. It allows the choice of a parametric statistical test for normally-distributed data, or a non-parametric test for data that is not normally distributed.

The hypotheses underlying the test are:

H0: the population from which the sample results follows the Normal law

H1: the population from which the sample results does not follow the Normal law

The results generated by the SPSS program are displayed in a table (see, for example, Table 03: 01). The figure given as asymptotic significance value (2-tailed) is the p value of the statistical test. If this number is below 0.05, the result of the test can be seen as statistically significant to the 95% confidence level. This means that the null hypothesis (H0) is rejected, and the data set is assumed to be not normally distributed. Therefore, subsequent statistical analyses concerning this variable should be non-parametric.

Kendall's tau-b and Spearman's rank correlation coefficient

The Kendall's tau-b and the Spearman's rs correlation tests are non-parametric tests for analysing the existence and extent of statistically significant correlation between two or more variables within a data set which is not normally distributed. Kendall's tau-b is a nonparametric measure of association based on the number of concordances and discordances in paired observations. Concordance occurs when paired observations vary together, and discordance occurs when paired observations vary differently (SAS Institute Inc. 1999). The Spearman's rank correlation coefficient (r_s) test places the data values in order, or rank, and then assesses the correlation and significance of any correlation between the ranks. SPSS generates a table of results which tabulates the relevant numbers – the correlation coefficient, the significance (2-tailed) or p value, and the sample size (N). If the significance value in the intersection of the two different variables is below 0.05, a statistically significant correlation (to the 95% confidence level) between the two variables can be seen to exist. The correlation coefficient (the r_s value) in the same cell of the table is starred with one or two stars to indicate the level of confidence associated with the correlation. These two correlation tests were performed in parallel in order to compensate for advantages and disadvantages in their methods. The Spearman's rank test is not especially robust when it comes to small samples, particularly when there are a number of tied ranks (Garland, 1999). Kendall's tau-b is an alternative non-parametric test which can be used instead of or in conjunction with the Spearman's rank correlation test, and is more suitable for larger data sets.

ANOVA

Analysis of variance (ANOVA) tests were performed in order to test for statistically significant differences between the means of two or more variables. This is accomplished by analyzing the variance, by partitioning the total variance into the component that is due to true random error (i.e., within- group *SS*) and the components that are due to differences between means (StatSoft, 2003b). The differences between the means are then tested for statistical significance. If the significance (or p) value is below 0.05, then the differences between the means are taken to be statistically significant to

the 95% confidence level, and not due to chance. This statistical test was particularly useful in analysing the mean trauma-death interval values for a range of variables, in order to see how the survival time was affected by the particular variable.

Kruskal-Wallis correlation test

The Kruskal-Wallis test is a non-parametric alternative to ANOVA. It served as a way to compare the mean trauma-death interval values against the spectrum of variables that were not normally distributed. In some instances, it served to confirm the results of the ANOVA test. The test performs in a similar manner to the ANOVA test, by ordering the mean values for each category, and then assesses the correlation between them, and assigns the difference between them a significance value. If the resultant significance value (or p value) is below 0.05, the correlation between the means is deemed statistically significant to the 95% confidence level.

Multiple regression analysis

Multiple regression analysis was attempted to assess the relative influence of several variables on the trauma-death interval simultaneously. This can be used to determine whether it is possible to more accurately predict the value of a dependent variable – in this case the trauma-death interval – from a combination of variables and not just a single variable. The output from SPSS shows a large tabulated matrix of the different variables and their relative correlations with each other using Pearson's correlation coefficient test. The intersection of each row and column shows the correlation coefficient and significance value for each combination of variables. If the 1-tailed significance (or p) value is below 0.05, the correlation is deemed to be statistically significant to the 95% confidence interval. All the multiple regression analyses were done with the aim of predicting the trauma-death interval, but the detailed matrix allowed analysis of correlation between different variables. The closer the overall R^2 value is to 1.00, the higher the correlation between the dependent variable and the independent variables, and thus the greater the accuracy of prediction of the dependent variable using the independent variable values. The greater the R^2 value, the smaller the contribution of chance to the changes in the dependent variable. The significance value of R is also presented in the ANOVA table of the SPSS output matrix, and represents the confidence level to which any correlations are statistically significant. As usual, if this value is less than 0.05, the correlation can be said to be statistically significant to the 95% confidence level.

Cohen's Kappa

The Cohen's Kappa method was used to assess the extent of inter-observer agreement. It measures the reliability of the observations made by distinct observers, allows calculation of the index of agreement between observers. It also considers the number of observations that would have occurred by chance. In this respect, it is superior to simple analyses that calculate the percentage agreement

between observers. The output is presented in a table that shows a matrix of agreement scores between each observer. The closer the score is to 1.00, the closer the level of agreement between the two observers. Petrie and Sabin (2000) have allocated words to define the strength of agreement between observers. Kappa values over 0.80 are termed 'good', those between 0.61 and 0.80 'substantial', and those between 0.41 and 0.60 'moderate' (Petrie and Sabin, 2000).

Observations and measurements of the data were made in several ways. As outlined above, photographs of the histological slides were scrutinised by human observers and described in a qualitative and semi-quantitative manner using numerical scaling systems and descriptive but discrete classification terms. These observations were then subjected to statistical analyses which are examined in Chapter 04. Quantitative data was obtained through the use of automated computer software that took a variety of measurements from the images of the histological slides. The results of the quantitative histomorphometric data analyses can be seen in the quantitative results chapter Chapter 05. The interpretation of these analyses, as well as the limitations and possible improvements to the methodology will be discussed in Chapter 06.

04 : RESULTS OF QUALITATIVE AND SEMI-QUANTITATIVE OBSERVATIONS

"If scientific reasoning were limited to the logical processes of arithmetic, we should not get very far in our understanding of the physical world. One might as well attempt to grasp the game of poker entirely by the use of the mathematics of probability."

Vannevar Bush (1890 - 1974)

Introduction

Due to the nature of the material under investigation, it was necessary to collect the majority of the data using qualitative observation methods. In the histological analysis of fracture healing, there are fundamental processes that cannot be detected by the mechanical 'eyes' of an image analysis program such as *Scion Image* (*Scion Image Beta 4.02* for Windows 95 to XP, Scion Corporation Inc. See Chapter 05), but that rely on the ability of the human brain to assess such as the spatial relationships between cells or the abundance of one type of cell relative to another. In light of this, the relative abundance of different types of inflammatory cells, their sizes, and their relationship with other histologically-visible features were assessed through human observation. Statistical analyses were performed to determine the nature of the relationship between several histologically-visible features and the trauma-death interval of the sample population. This was done in order to identify any features that might correlate with trauma-death interval, which potentially could be used as predictors of the time elapsed since trauma in a blind test or real anthropological case. Interpretation of these results is given in Chapter 06. Photographs of the fracture slides are given in Appendix 04.

Histology

The histologically-visible features examined on the photographs of the fracture slides, with the intention of comparing their size, abundance and percentage cover of the background to the trauma-death interval values of the sample population, were:

CD68 positive cells
BSP positive cells
Perls' Prussian Blue positive haemosiderin granules
inflammatory lymphocyte cells with haematoxylin-stained nuclei
fibroblast cells with haematoxylin-stained nuclei
compact bone
living compact bone with intact osteocytes
necrotic bone with empty osteocyte lacunae
red blood cells

Perls' Prussian Blue

Perls' Prussian Blue is a simple tinctorial stain that emphasises the presence of haemosiderin in tissues. Haemosiderin-laded macrophages have been seen in histological sections of the skin and sub-cutaneous tissue as early as 24-48 hours after a wound, but more commonly after about 4 to 8 days (Vanezis, 2001). It was hypothesised that a similar pattern of haemosiderin presence would be seen in the fracture samples, as the haemorrhage surrounding the fracture gradually degraded. There are, however, considerable limitations to its use as a prediction tool for the estimation of the post-infliction interval, which shall be discussed in Chapter 06.

The staining was successful in 36 cases (76.6%). Figure 04: 01 and Figure 04: 02 show examples of a positive fracture sample compared to a liver tissue positive control. The presence or absence of blue-black stained haemosiderin granules was recorded in a dichotomous fashion, as either positive or negative. Cases were classified as positive if clear blue-black granules were visible, and the staining was not too light (see Figure 04: 03, Figure 04: 04 to Figure 04: 05 for examples). Thirty-one cases (65.96%) were classified as positive (n = 47), 5 cases (10.64%) as negative. (Eleven cases (23.4%) were unclassifiable due to poor or unspecific staining).

Figure 04: 01 A photograph of a fracture slide with a positive reaction to a Perls' Prussian Blue stain, counter-stained with Neutral Red. (Objective magnification x10).

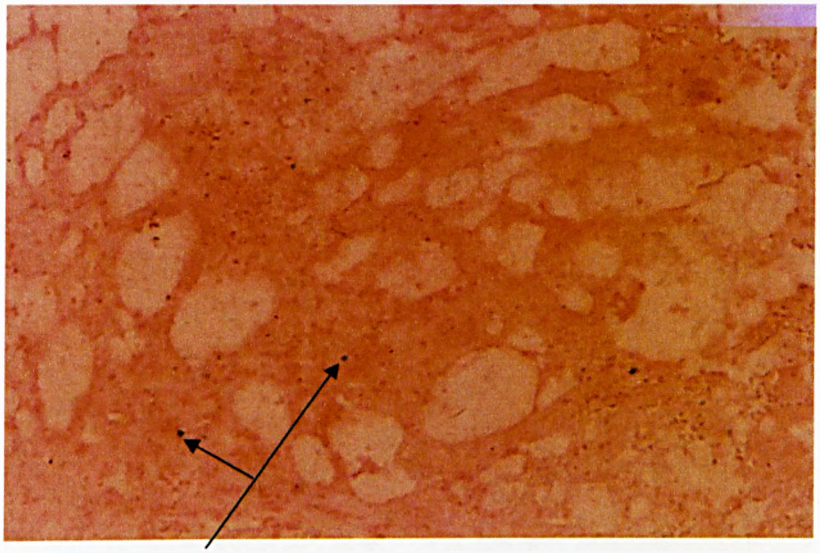

haemosiderin granules stained blue with Perls' Prussian Blue stain

the rest of the tissues have been counterstained with Neutral Red

Figure 04: 02 A photograph of the Perls' Prussian Blue positive control (liver tissue), counter-stained with Neutral Red. (Objective magnification x10).

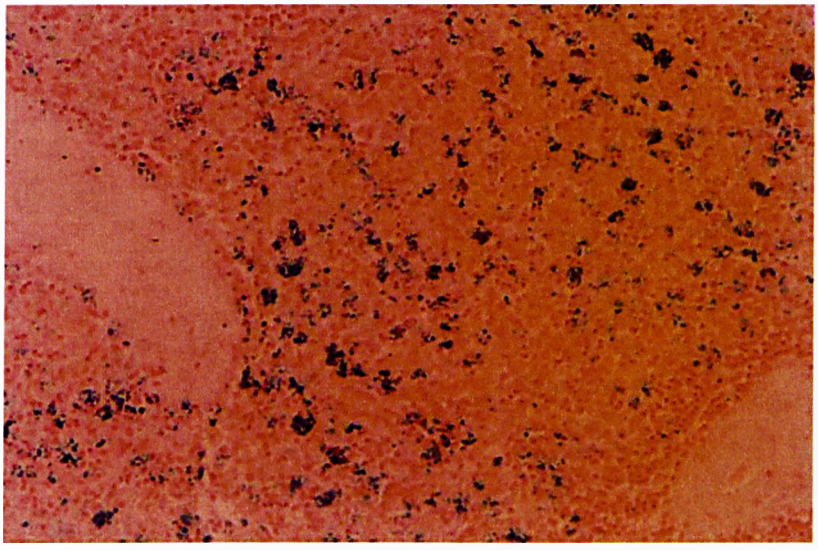

the blue granules are haemosiderin stained blue with Perls' Prussian Blue stain

the rest of tissues have been counterstained with Neutral Red

Figure 04: 03 A photograph of an example of a fracture slide classified as positive for the Perls' Prussian Blue stain. (Objective magnification x10).

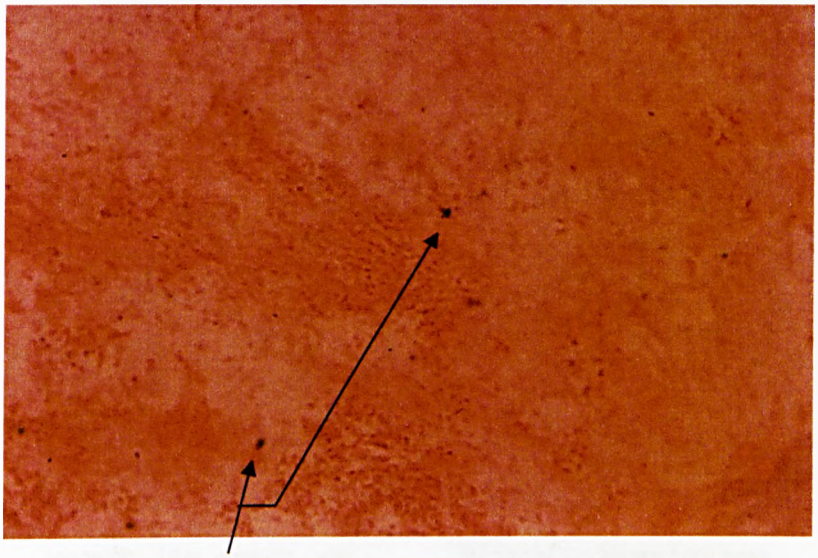

haemosiderin granules stained blue with Perls' Prussian Blue stain

the rest of the tissues have been counterstained with Neutral Red

Figure 04: 04 A photograph of an example of a fracture slide classified as negative for the Perls' Prussian Blue stain. (Objective magnification x10).

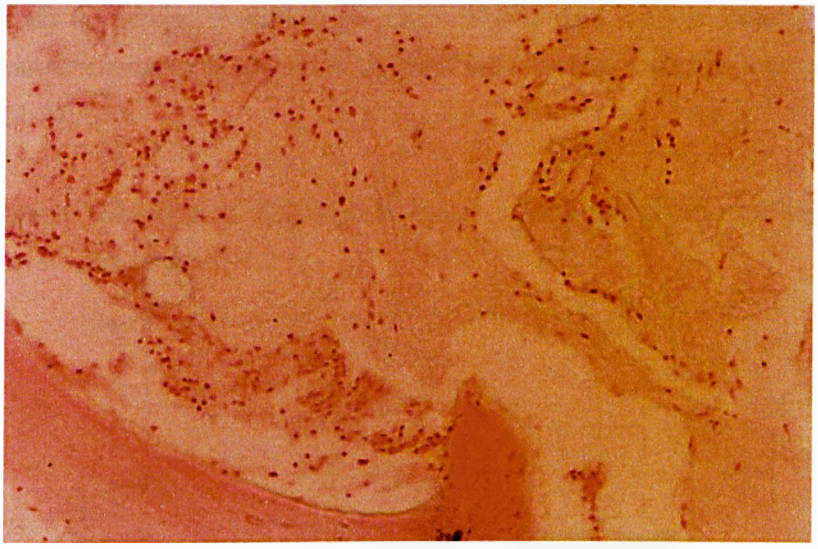

no haemosiderin granules have been stained blue with Perls' Prussian Blue stain

the rest of the tissues have been counterstained with Neutral Red

Figure 04: 05 A photograph of an example of a fracture slide not possible to classify for the Perls' Prussian Blue stain, due to unspecific staining. (Objective magnification x10).

unspecific blue staining with Perls' Prussian Blue stain

the rest of the tissues have been counterstained with Neutral Red

As the full range of trauma-death interval values is not normally distributed, a non-parametric analysis of variance (Kruskal-Wallis) test was performed, to determine if any difference between the mean values of the categories (positive and negative) was statistically significant. When the unclassified cases were included in the test for the sake of completeness, the resultant p value was just under 0.05, making the distinction between the means only just statistically significant to the 95% confidence level (see Figure 04: 06 and Table 04: 01).

Figure 04: 06 Graph showing trauma-death interval means for each classification of Perls' stain. (Error bars show standard deviation +/- 1.0).

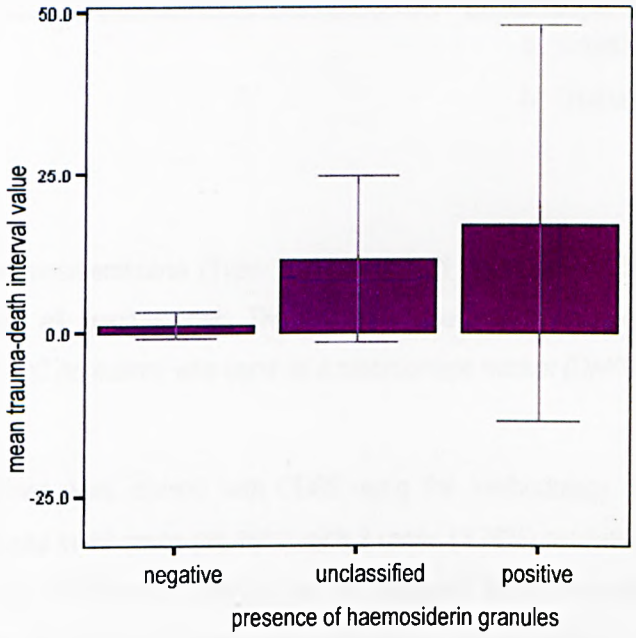

Table 04: 01 Results of a Kruskal-Wallis test to determine any correlation between trauma-death interval and Perls' stain classification.

Ranks

	POSNEG	N	Mean Rank
TDI	0	11	26.95
	1	5	10.00
	2	31	25.21
	Total	47	

Test Statistics[a,b]

	TDI
Chi-Square	6.045
df	2
Asymp. Sig.	.049

a. Kruskal Wallis Test

b. Grouping Variable: POSNEG

However, when the unclassified tdi values were ignored, the p value was reduced to 0.02, which is clearly statistically significant to the 95% confidence level (see Table 04: 01).

Table 04: 01 Results of a Kruskal-Wallis test to determine any correlation between trauma-death interval and Perls' classification, ignoring unclassified values.

Ranks

	POSNEG	N	Mean Rank
TDI	1	5	8.50
	2	31	20.11
	Total	36	

Test Statistics[a,b]

	TDI
Chi-Square	5.313
df	1
Asymp. Sig.	.021

a. Kruskal Wallis Test

b. Grouping Variable: POSNEG

CD68

CD68 is a 110kDa transmembrane (Type 1) glyco-protein made up of 354 amino acids, which is expressed in virtually all macrophages. The primary monoclonal (mouse-derived) anti-human anti-CD68 antibody (DAKOCytomation) was used as a macrophage marker (DAKO, 1999).

Fifty-two fracture slides were stained with CD68 using the methodology described in Chapter 02. Staining was successful in 46 cases (88.46%), with 3 cases (5.76%) exhibiting unspecific staining and three cases showing background staining, which rendered them unusable. It is likely that this inconsistent staining was due to unpredictable variation in decalcification, rather than a fault of the staining process. An example of a successfully stained slide and a positive and negative control are given in Figure 04: 07, Figure 04: 08 and Figure 04: 09 respectively. The CD68 positive cells are seen clearly on the slides as immuno-positive, brown stained cells. The nuclei of the inflammatory cells are clearly visible, stained blue with the haematoxylin counter-stain. The large white areas are adipose globules spilling from the marrow into the fracture site. On the positive control slide (see Figure 04: 08), the immuno-positive cells are clearly visible as intensely brown-stained areas on a light background. The haematoxylin-stained nuclei of inflammatory cells are also clear on the photograph of the positive control slide. The negative control (see Figure 04: 09) was not treated with the primary anti-body, and therefore shows no immuno-positive, brown-stained cells, but only haematoxylin-stained blue cells on a light background.

Figure 04: 07 A photograph of a fracture slide successfully stained with CD68, counter-stained with haematoxylin. (Objective magnification x10).

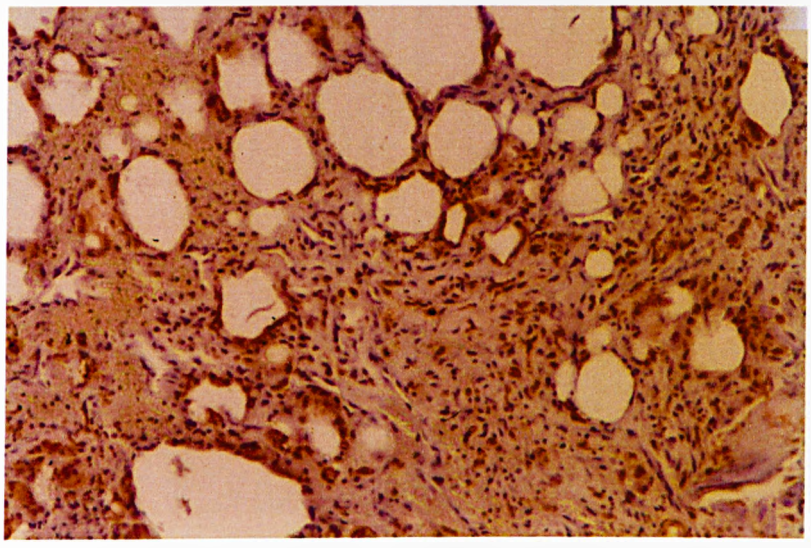

Figure 04: 08 A photograph of the CD68 positive control, counter-stained with haematoxylin. (Objective magnification x10).

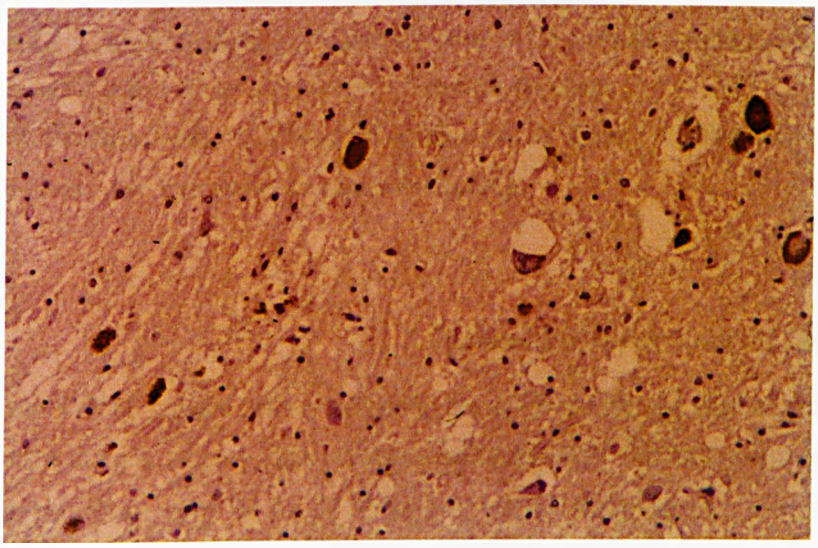

Figure 04: 09 A photograph of the CD68 negative control, counter-stained with haematoxylin. (Objective magnification x10).

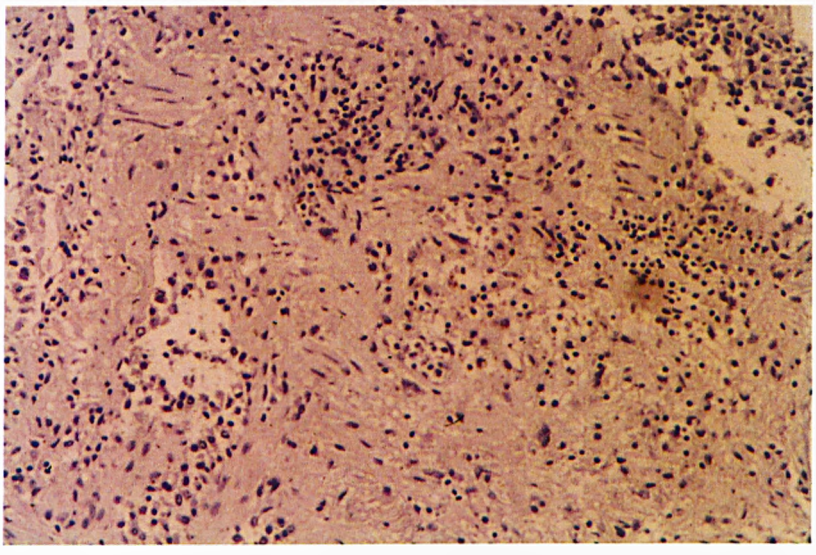

It was hypothesised that variables such as the average size, the percentage cover or spatial distribution of CD68 positive cells would show a correlation with the trauma-death interval values of the sample population. This can be expressed as follows:

H0: there is no statistically significant relationship between the qualitative spatial properties of the CD68 positive cells and the trauma-death interval in the sample population

H1: there is a statistically significant relationship between the qualitative spatial properties of the CD68 positive cells and the trauma-death interval in the sample population

In order to test this hypothesis, qualitative measurements of these variables were taken by four independent observers (see Inter-observer agreement below).

Estimated percentage cover of CD68 positive cells

Percentage cover of CD68 positive cells in relation to the whole photograph was measured in a semi-quantitative fashion, using a category coding system (see Chapter 02). Observers were asked to assess the approximate percentage cover of the CD68 positive cells by assigning each slide a number on a scale between 0 and 4. A scattergraph to show the distribution of cases classified in each category against the trauma-death interval was plotted (see Figure 04: 10).

Figure 04: 10 A scattergraph showing the relative placement of cases into the CD68+ cell percentage cover categories plotted against the trauma-death interval.

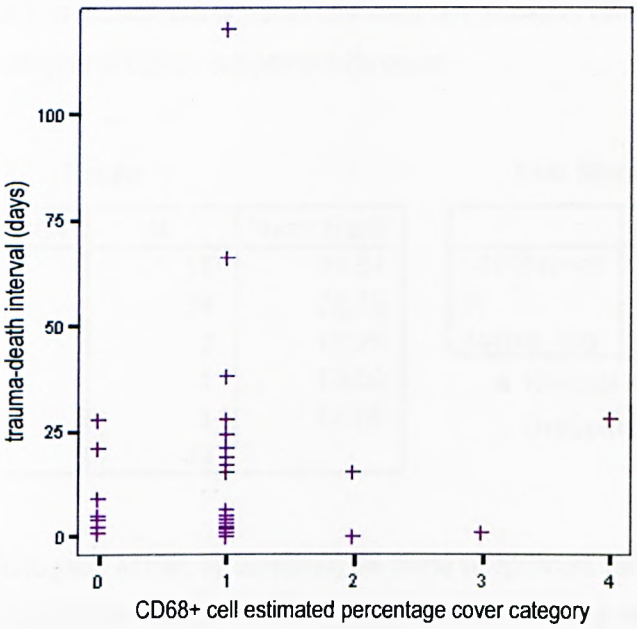

The mean trauma-death interval values for each of the categories were compared using a non-parametric analysis of variance test. A graphical depiction of the variation in the mean trauma-death interval values between the percentage cover categories can be seen in Figure 04: 11.

Figure 04: 11 Graph showing trauma-death interval means for each classification of CD68 positive cell percentage cover. (Error bars show standard deviation +/- 1.0).

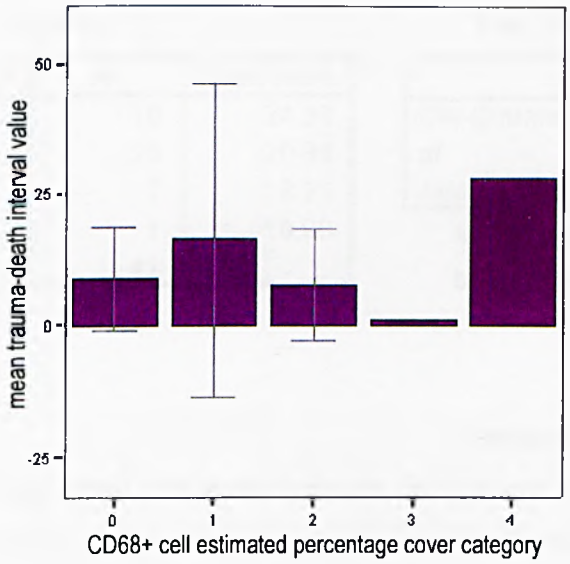

The Kruskal-Wallis test was performed to determine whether there was any significant statistical difference between the tdi mean values in each category (see Table 04: 03). A p value of 0.475 was given, indicating no significant difference.

Table 04: 03 Results of a Kruskal-Wallis test to determine any statistical difference between the mean tdi values for each category of CD68+ cell percentage cover.

Ranks

	CD68_COV	N	Mean Rank
TDI	0	11	26.64
	1	34	24.75
	2	2	18.25
	3	1	10.00
	4	1	44.00
	Total	49	

Test Statistics[a,b]

	TDI
Chi-Square	3.522
df	4
Asymp. Sig.	.475

a. Kruskal Wallis Test

b. Grouping Variable: CD68_COV

The values were interrogated further, by assessing the same independent variable against the trauma-death interval values that were smaller than 25 days. Again, the Kruskal-Wallis test for analysis of variance gave a p value greater than 0.05 (see Table 04: 04), and therefore the alternative hypothesis (H1) for the variable of percentage cover of CD68 positive cells has to be rejected.

Table 04: 04 Results of a Kruskal-Wallis test to determine any statistical difference between the mean tdi values under 25 days for each category of CD68+ cell percentage cover.

Ranks

	CD68TRY	N	Mean Rank
TDI	0	10	24.90
	1	29	20.95
	2	2	18.25
	3	1	10.00
	Total	42	

Test Statistics[a,b]

	TDI
Chi-Square	1.888
df	3
Asymp. Sig.	.596

a. Kruskal Wallis Test

b. Grouping Variable: CD68TRY

Estimated size of CD68 positive cells

The estimated average size of the CD68 positive cells was also compared to the trauma-death interval values for the sample. The average size of the cells was estimated by the author in μm^2, by comparing

them to cells of known size measured during the collection of the quantitative data using *Scion Image* (see Chapter 05).

When compared to the trauma-death interval values of the sample (see Figure 04: 12), a few inferences could be drawn, which are described in Chapter 06. The non-parametric correlation tests (Kendall's tau-b and Spearman's correlation coefficient) confirmed the lack of a significant correlation between these variables (see Table 04: 05). The same tests were attempted using only the trauma-death intervals less than 25 days (see Figure 04: 13). As the spread of tdi values less than 25 days was known to be not normally distributed, non-paramteric correlation tests were performed to quantify the relationship between these two variables (see Table 04: 01). These gave statistically non-significant results.

Figure 04: 12 Scatter-plot showing the relationship between trauma-death interval and estimated CD68 positive cell size. (Spearman's correlation coefficient r =-0.049, n =38, p =0.77).

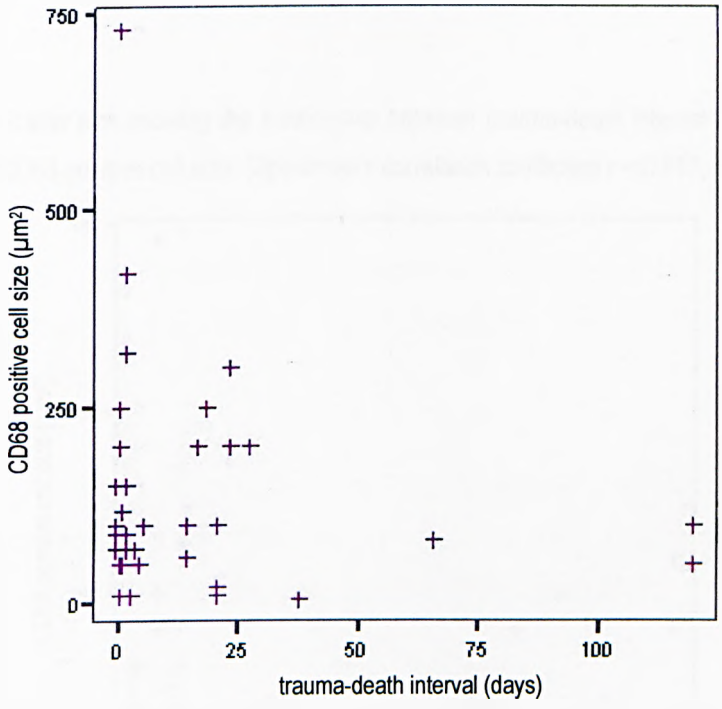

Table 04: 05 Results of a Kendall's tau-b and a Spearman's r_s correlation coefficient test to determine if any correlation exists between the average estimated size of the CD68 positive cells and the trauma-death interval.

Correlations

			TDI	SIZE_NUM
Kendall's tau_b	TDI	Correlation Coefficient	1.000	-.035
		Sig. (2-tailed)	.	.770
		N	49	38
	SIZE_NUM	Correlation Coefficient	-.035	1.000
		Sig. (2-tailed)	.770	.
		N	38	41
Spearman's rho	TDI	Correlation Coefficient	1.000	-.049
		Sig. (2-tailed)	.	.770
		N	49	38
	SIZE_NUM	Correlation Coefficient	-.049	1.000
		Sig. (2-tailed)	.770	.
		N	38	41

Figure 04: 13 Scatter-plot showing the relationship between trauma-death interval values under 25 days and estimated CD68 positive cell size. (Spearman's correlation coefficient r =-0.017, n =42, p =0.926).

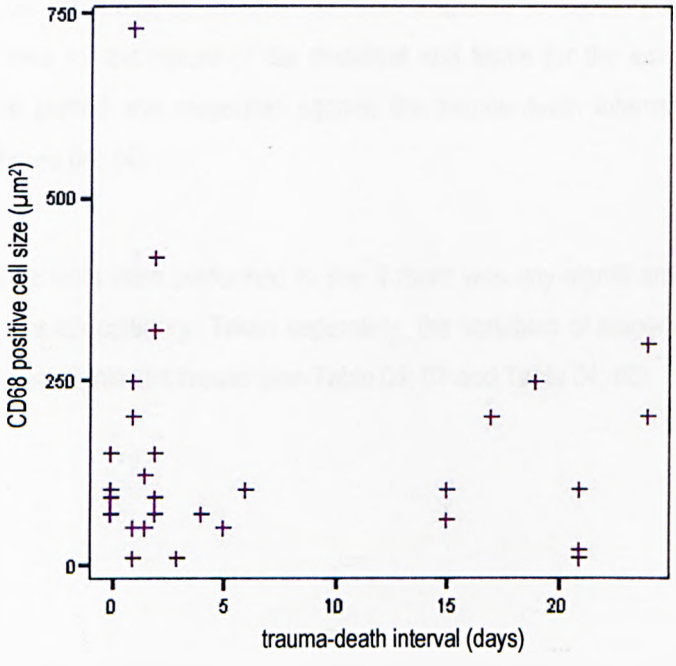

Table 04: 06 Results of a Kendall's tau-b and a Spearman's r_s correlation coefficient test to determine if any correlation exists between the average estimated size of the CD68 positive cells and the trauma-death interval values under 25 days.

Correlations

			TDI_25	SIZE_25
Kendall's tau_b	TDI_25	Correlation Coefficient	1.000	.015
		Sig. (2-tailed)	.	.908
		N	42	32
	SIZE_25	Correlation Coefficient	.015	1.000
		Sig. (2-tailed)	.908	.
		N	32	35
Spearman's rho	TDI_25	Correlation Coefficient	1.000	.017
		Sig. (2-tailed)	.	.926
		N	42	32
	SIZE_25	Correlation Coefficient	.017	1.000
		Sig. (2-tailed)	.926	.
		N	32	35

Dispersal of CD68 positive cells

The distribution of the immuno-positive cells over the fracture site was described using the dual categorical method described in Chapter 02. The dispersal of CD68 positive cells described a combination of terms for the *nature* of the dispersal and terms for the *location* of the cells. These observations were plotted and measured against the trauma-death interval values for the sample population (see Figure 04: 14).

Analysis of variance tests were performed to see if there was any significant difference between the mean tdi values in each category. Taken separately, the variables of dispersal nature and dispersal location did not reveal significant results (see Table 04: 07 and Table 04: 08).

Figure 04: 14 Graph showing the nature (how?) and the location (where?) of the dispersal of the CD68 positive cells against the trauma-death interval values in the sample population.

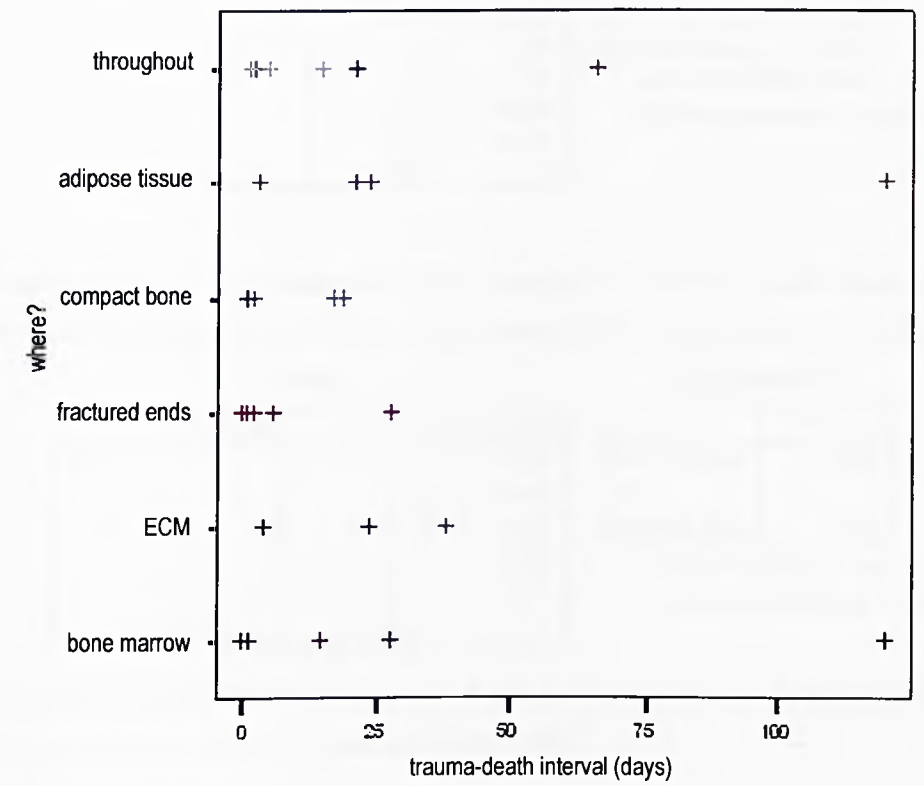

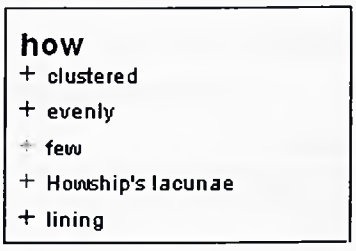

Dot/Lines show Modes

Table 04: 07 Results of a Kruskal-Wallis test to determine if any correlation exists between trauma-death interval and the categories describing the location ('where?') of the dispersal of the CD68 positive cells.

Ranks

	WHERENUM	N	Mean Rank
TDI	0	7	21.29
	2	10	13.75
	3	5	18.90
	4	7	16.71
	5	5	29.40
	6	4	24.00
	Total	38	

Test Statistics[a,b]

	TDI
Chi-Square	8.023
df	5
Asymp. Sig.	.155

a. Kruskal Wallis Test

b. Grouping Variable: WHERENUM

Table 04: 08 Results of a Kruskal-Wallis test to determine if any correlation exists between trauma-death interval and the categories describing the nature ('how?') of the dispersal of the CD68 positive cells.

Ranks

	HOWNUM	N	Mean Rank
TDI	0	21	19.05
	1	9	20.83
	2	1	8.50
	3	3	19.67
	4	4	21.50
	Total	38	

Test Statistics[a,b]

	TDI
Chi-Square	1.288
df	4
Asymp. Sig.	.863

a. Kruskal Wallis Test

b. Grouping Variable: HOWNUM

Despite the amalgamation of the two dispersal categories, there was still no significant difference between the mean trauma-death interval values (see Table 04: 09).

Table 04: 09 Results of a Kruskal-Wallis test to determine if any correlation exists between trauma-death interval and the combined categories describing the location ('where?') and nature ('how?') of the dispersal of the CD68 positive cells.

Ranks

	WHEREHOW	N	Mean Rank
TDI	0	2	22.25
	1	2	22.75
	3	3	19.67
	20	10	13.75
	32	1	8.50
	34	4	21.50
	40	2	13.75
	41	5	17.90
	50	5	29.40
	60	2	21.75
	61	2	26.25
	Total	38	

Test Statistics[a,b]

	TDI
Chi-Square	9.612
df	10
Asymp. Sig.	.475

a. Kruskal Wallis Test

b. Grouping Variable: WHEREHOW

However, when the differences in the means of the trauma-death interval values *less than 25 days* in each of the different amalgamated dispersal categories were analysed using a Kruskal-Wallis analysis of variance test, a statistically significant p value (0.04) was obtained. This is represented graphically in Figure 04: 15 and the results of the test can be found in Table 04: 10 below.

Table 04: 10 Results of a Kruskal-Wallis test to determine if any correlation exists between trauma-death interval values under 25 days and the combined categories describing the location ('where?') and nature ('how?') of the dispersal of the CD68 positive cells.

Ranks

	WHEHOW25	N	Mean Rank
TDI_25	0	1	8.50
	1	2	22.75
	3	3	19.67
	20	9	11.56
	32	1	8.50
	34	4	21.50
	40	2	13.75
	41	3	6.17
	50	4	27.38
	60	1	8.50
	61	2	26.25
	Total	32	

Test Statistics[a,b]

	TDI_25
Chi-Square	18.729
df	10
Asymp. Sig.	.044

a. Kruskal Wallis Test

b. Grouping Variable: WHEHOW25

Figure 04: 15 Graph showing trauma-death interval means (under 25 days) for each classification of combined CD68 positive cell dispersal. (Error bars show standard deviation +/- 1.0).

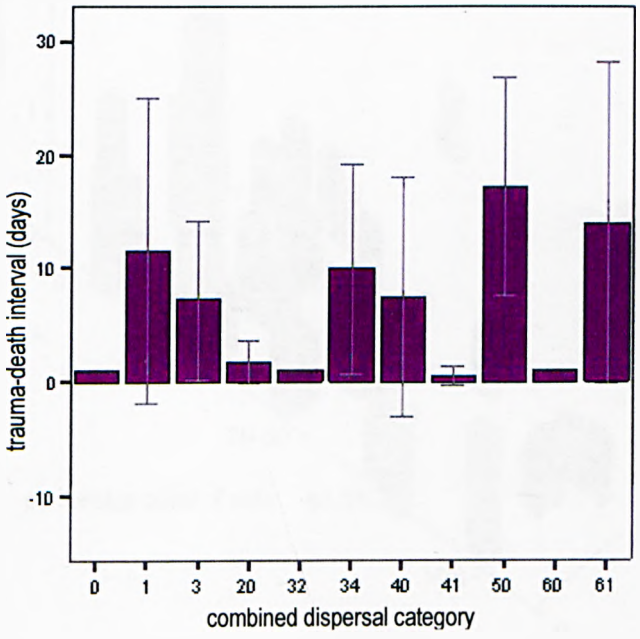

Key

0	clustered throughout
1	evenly dispersed throughout
3	few dispersed throughout
20	clustered at the fractured ends
32	lining compact bone
34	in Howship's lacunae in compact bone
40	evenly in the bone marrow
41	clustered in the bone marrow
50	clustered around adipose tissue
60	clustered in the ECM
61	evenly dispersed in the ECM

Cells with haematoxylin-stained nuclei

The percentage cover of the cells with haematoxylin-stained nuclei was estimated using the same method as was used for the CD68 positive cells (see Chapter 02). Two distinct types of cells with blue-stained nuclei were visible on the majority of the fracture site photographs (see Figure 02: 03) - small round lymphocytes and elongated, spindle-shaped fibroblasts. In order to improve the predictive potential of the study, the ratios of percentage cover of the three types of cells were calculated, and tested for the existence of any correlations with trauma-death interval. As previously, the percentage cover of each type of cell was estimated and classified using the 0 to 4 scale described above. A graphical representation of the changing percentage cover of the CD68 positive cells and the small blue (lymphocyte) cells compared to the trauma-death interval is shown in Figure 04: 16.

Figure 04: 16Three dimensional graph showing the differences in percentage cover of cells with blue-stained nuclei and CD68 positive cells compared to the trauma-death interval.

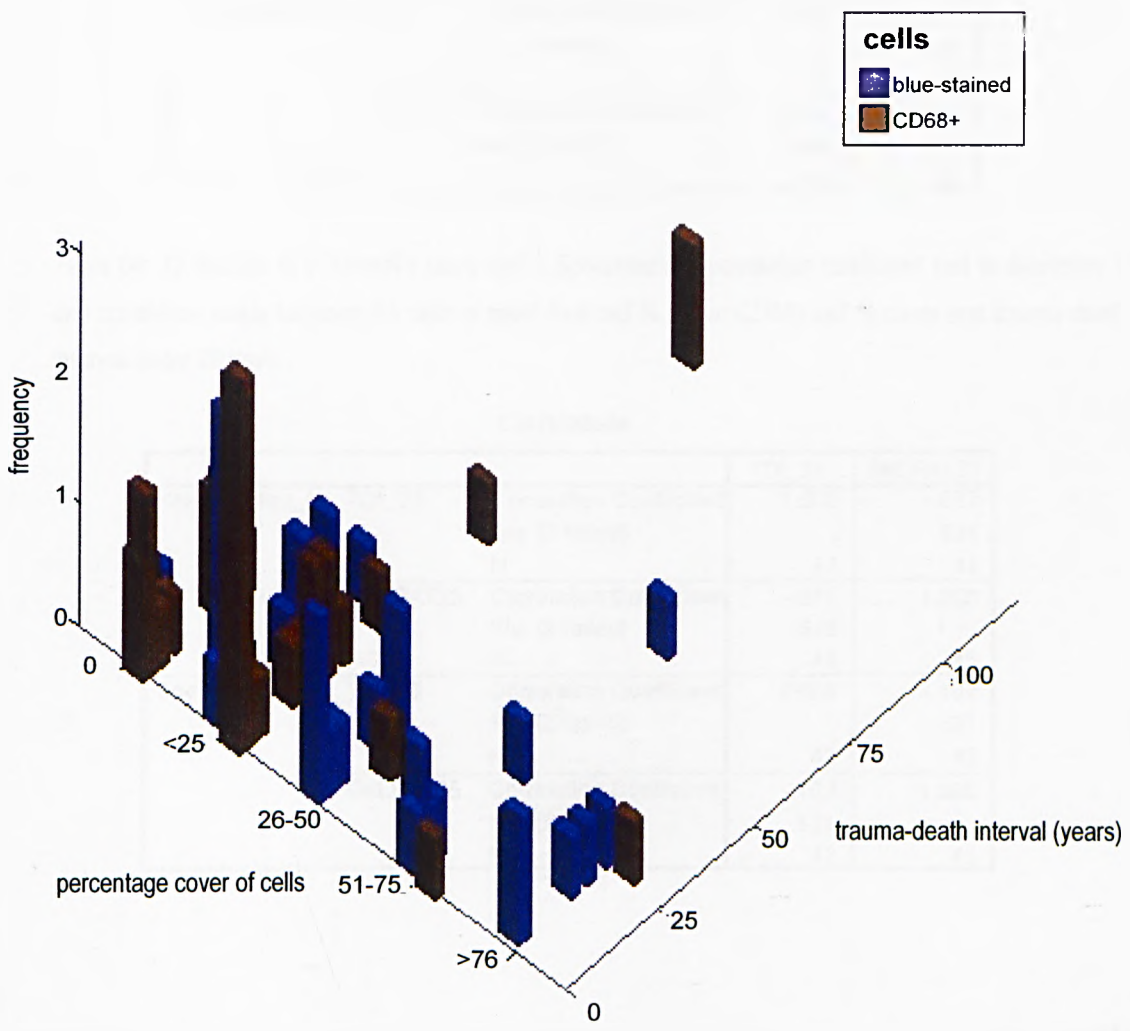

The ratio of *small blue cell % cover: CD68+ cell % cover* did not correlate significantly with the trauma-death interval, nor did the same ratio against the trauma-death interval values under 25 days (see Table 04: 11and Table 04: 12).

Table 04: 11 Results of a Kendall's tau-b and a Spearman's r_s correlation coefficient test to determine if any correlation exists between the *ratio of small blue cell % cover: CD68+ cell % cover* and trauma-death interval.

Correlations

			TDI	RATIO
Kendall's tau_b	TDI	Correlation Coefficient	1.000	-.066
		Sig. (2-tailed)	.	.554
		N	49	49
	RATIO	Correlation Coefficient	-.066	1.000
		Sig. (2-tailed)	.554	.
		N	49	52
Spearman's rho	TDI	Correlation Coefficient	1.000	-.088
		Sig. (2-tailed)	.	.545
		N	49	49
	RATIO	Correlation Coefficient	-.088	1.000
		Sig. (2-tailed)	.545	.
		N	49	52

Table 04: 12 Results of a Kendall's tau-b and a Spearman's r_s correlation coefficient test to determine if any correlation exists between the ratio of *small blue cell % cover: CD68+ cell % cover* and trauma-death interval under 25 days.

Correlations

			TDI_25	SMLRAT25
Kendall's tau_b	TDI_25	Correlation Coefficient	1.000	-.077
		Sig. (2-tailed)	.	.526
		N	42	42
	SMLRAT25	Correlation Coefficient	-.077	1.000
		Sig. (2-tailed)	.526	.
		N	42	45
Spearman's rho	TDI_25	Correlation Coefficient	1.000	-.102
		Sig. (2-tailed)	.	.521
		N	42	42
	SMLRAT25	Correlation Coefficient	-.102	1.000
		Sig. (2-tailed)	.521	.
		N	42	45

The ratio of *small blue cell size: CD68+ cell size* also did not correlate significantly with the trauma-death interval or the trauma-death intervals under 25 days (see Table 04: 13 and Table 04: 14). Figure 04: 17 shows a scatter-plot of the size ratios plotted against the trauma-death interval values under 25 days.

Table 04: 13 Results of a Kendall's tau-b and a Spearman's r_s correlation coefficient test to determine if any correlation exists between the ratio of *small blue cell size: CD68+ cell size* and trauma-death interval.

Correlations

			TDI	SIZE_RAT
Kendall's tau_b	TDI	Correlation Coefficient	1.000	.039
		Sig. (2-tailed)	.	.752
		N	49	35
	SIZE_RAT	Correlation Coefficient	.039	1.000
		Sig. (2-tailed)	.752	.
		N	35	38
Spearman's rho	TDI	Correlation Coefficient	1.000	.051
		Sig. (2-tailed)	.	.771
		N	49	35
	SIZE_RAT	Correlation Coefficient	.051	1.000
		Sig. (2-tailed)	.771	.
		N	35	38

Table 04: 14 Results of a Kendall's tau-b and a Spearman's r_s correlation coefficient test to determine if any correlation exists between the ratio of *small blue cell size: CD68+ cell size* and trauma-death interval values under 25 days.

Correlations

			TDI_25	SIZRAT25
Kendall's tau_b	TDI_25	Correlation Coefficient	1.000	.027
		Sig. (2-tailed)	.	.842
		N	42	30
	SIZRAT25	Correlation Coefficient	.027	1.000
		Sig. (2-tailed)	.842	.
		N	30	33
Spearman's rho	TDI_25	Correlation Coefficient	1.000	.033
		Sig. (2-tailed)	.	.862
		N	42	30
	SIZRAT25	Correlation Coefficient	.033	1.000
		Sig. (2-tailed)	.862	.
		N	30	33

Figure 04: 17 Scatter-plot showing the relationship between the ratio of *blue-stained cell size: CD68 positive cell size* and the trauma-death interval values under 25 days.

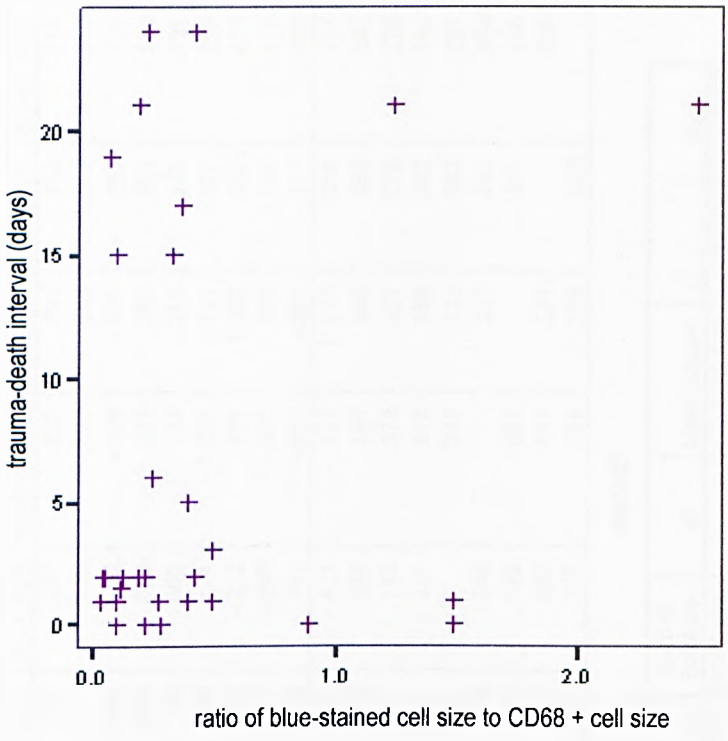

Multiple regression analysis

In order to test the influence of several CD68-related and other histological variables at once on the trauma-death interval, multiple regression analysis was attempted. Multiple regression can aid the understanding of the relationship and interplay between several independent variables on one dependent variable. The trauma-death interval was the dependent variable, as it was hoped that it would be possible to predict tdi from a combination of independent variables related to the spatial characteristics of the CD68+ cells, the compact bone and red blood cells. Table 04: 15 shows a summary of the SPSS output for the standard multiple regression analysis of the trauma-death interval against the variables. Table 04: 40 provides a summary of the relationships between each of the variables and the trauma-death interval. A histogram of the distribution of the standardised error (residual) is also plotted, to show that this fits with Gaussian normality enough to make the multiple regression plausible. The errors for both the dependent and independent variables were assumed to be normally distributed. Table 04: 15 shows the correlation tables of the CD68+ cell, compact bone and red blood cell variables against the trauma-death interval. These correlations will be discussed in Chapter 06. It also shows that the resultant R^2 value is 0.414 (adjusted R^2 value is 0.210), and the significance level of R is 0.088 (see ANOVA table), which is just outside of being statistically significant to the 95% confidence level. The significance level for each of the

Table 04: 15 A summary of the SPSS output showing correlations between the trauma-death interval and the CD68+ cell, compact bone and red blood cell variables, with the R^2 value (n = 32 for all correlations).

Correlations

		TDI	CD68_COV	CD68SIZE	BLUE_COV	BLU_SIZE	WHEREHOW	RBC	BONE_LIV	BONE_NEC
Pearson Correlation	TDI	1.000	-.031	-.149	.012	.037	.200	.391	-.284	-.114
	CD68_COV	-.031	1.000	.079	.200	.115	.197	.249	-.270	.310
	CD68SIZE	-.149	.079	1.000	.382	.190	-.059	-.085	.259	-.136
	BLUE_COV	.012	.200	.382	1.000	-.060	-.039	.286	.293	-.188
	BLU_SIZE	.037	.115	.190	-.060	1.000	.124	-.212	-.240	.131
	WHEREHOW	.200	.197	-.059	-.039	.124	1.000	.321	-.027	-.250
	RBC	.391	.249	-.085	.286	-.212	.321	1.000	.080	-.073
	BONE_LIV	-.284	-.270	.259	.293	-.240	-.027	.080	1.000	-.617
	BONE_NEC	-.114	.310	-.136	-.188	.131	-.250	-.073	-.617	1.000
Sig. (1-tailed)	TDI	.	.433	.208	.474	.421	.137	.013	.058	.267
	CD68_COV	.433	.	.333	.136	.265	.140	.085	.068	.042
	CD68SIZE	.208	.333	.	.015	.149	.374	.321	.076	.228
	BLUE_COV	.474	.136	.015	.	.371	.416	.056	.052	.151
	BLU_SIZE	.421	.265	.149	.371	.	.249	.122	.093	.237
	WHEREHOW	.137	.140	.374	.416	.249	.	.037	.441	.084
	RBC	.013	.085	.321	.056	.122	.037	.	.331	.346
	BONE_LIV	.058	.068	.076	.052	.093	.441	.331	.	.000
	BONE_NEC	.267	.042	.228	.151	.237	.084	.346	.000	.

Model Summary[b]

Model	R	R Square	Adjusted R Square	Std. Error of the Estimate
1	.643[a]	.414	.210	26.9580

a. Predictors: (Constant), BONE_NEC, RBC, CD68SIZE, BLU_SIZE, CD68_COV, WHEREHOW, BLUE_COV, BONE_LIV

b. Dependent Variable: TDI

ANOVA[b]

Model		Sum of Squares	df	Mean Square	F	Sig.
1	Regression	11807.461	8	1475.933	2.031	.088[a]
	Residual	16714.844	23	726.732		
	Total	28522.305	31			

a. Predictors: (Constant), BONE_NEC, RBC, CD68SIZE, BLU_SIZE, CD68_COV, WHEREHOW, BLUE_COV, BONE_LIV

b. Dependent Variable: TDI

Table 04: 15 continued

Coefficients[a]

Model		Unstandardized Coefficients		Standardized Coefficients	t	Sig.	95% Confidence Interval for B	
		B	Std. Error	Beta			Lower Bound	Upper Bound
1	(Constant)	49.500	20.873		2.371	.026	6.321	92.679
	CD68_COV	-8.715	8.729	-.189	-.998	.329	-26.773	9.343
	CD68SIZE	-3.63E-03	.040	-.017	-.091	.928	-.086	.079
	BLUE_COV	.624	5.156	.024	.121	.905	-10.042	11.290
	BLU_SIZE	9.215E-02	.209	.079	.442	.663	-.339	.524
	WHEREHOW	-9.19E-02	.353	-.050	-.260	.797	-.822	.638
	RBC	.922	.364	.482	2.532	.019	.169	1.675
	BONE_LIV	-.426	.154	-.619	-2.771	.011	-.745	-.108
	BONE_NEC	-.323	.173	-.423	-1.867	.075	-.680	.035

a. Dependent Variable: TDI

regression coefficients are shown in the Coefficients table of Table 04: 15. Figure 04: 18, Figure 04: 19, Figure 04: 20, Figure 04: 21, Figure 04: 22, Figure 04: 23, Figure 04: 24 and Figure 04: 25 show simple linear regression scatterplots for each of the CD68+ cell, compact bone and red blood cell variables against the trauma-death interval. A histogram of the distribution of the standardised error (residual) of the trauma-death interval is included (see Figure 04: 26).

Figure 04: 18 Partial regression plot showing linear regression between CD68+ cell size and the trauma-death interval.

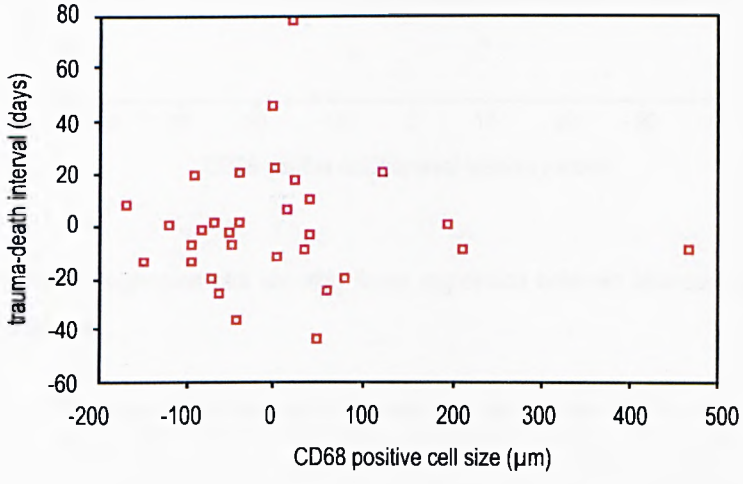

Figure 04: 19 Partial regression plot showing linear regression between CD68+ cell percentage cover and the trauma-death interval.

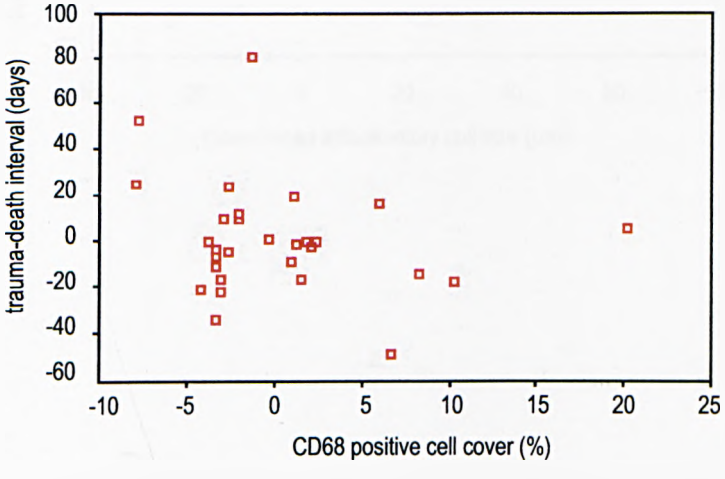

Figure 04: 20 Partial regression plot showing linear regression between CD68+ cell dispersal (category score) and the trauma-death interval.

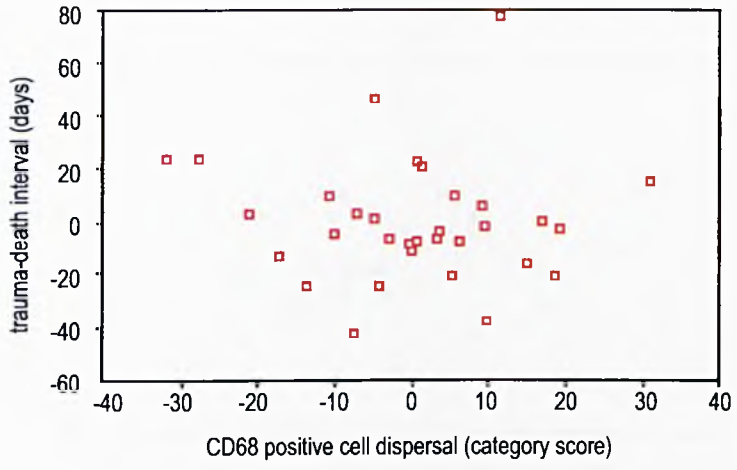

Figure 04: 21 Partial regression plot showing linear regression between blue-stained cell size and the trauma-death interval.

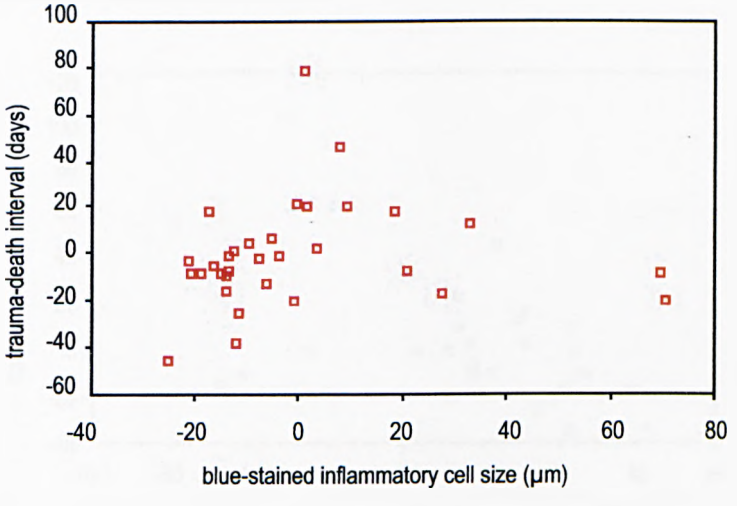

Figure 04: 22 Partial regression plot showing linear regression between the estimated percentage cover of the blue-stained cells and the trauma-death interval.

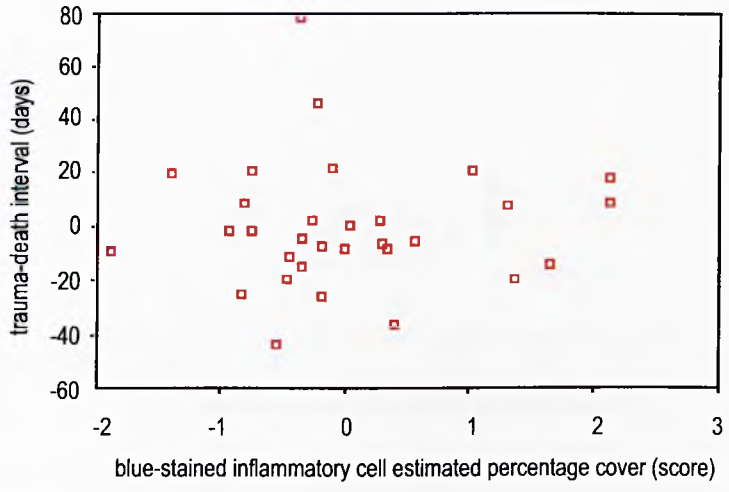

Figure 04: 23 Partial regression plot showing linear regression between the percentage cover of living compact bone and the trauma-death interval.

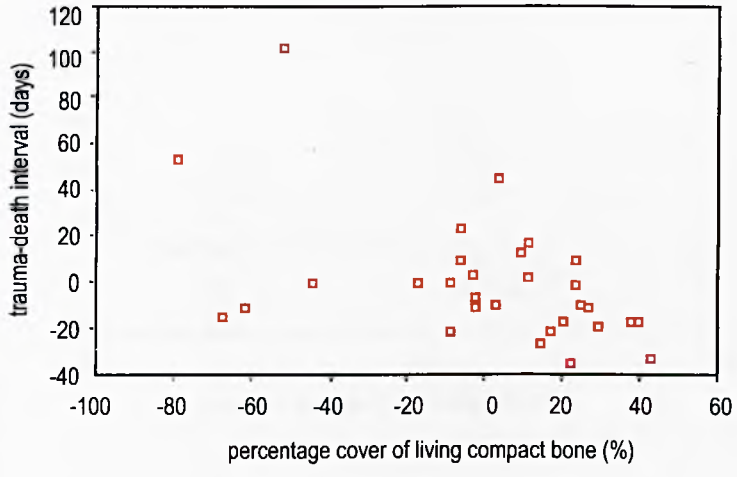

Figure 04: 24 Partial regression plot showing linear regression between the percentage cover of necrotic compact bone and the trauma-death interval.

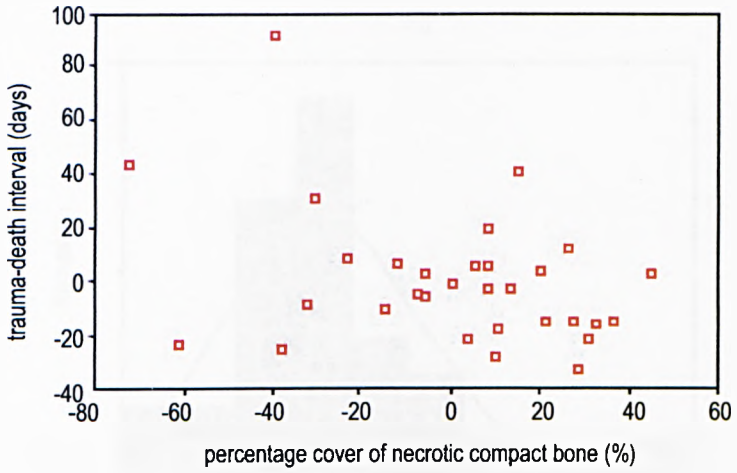

Figure 04: 25 Partial regression plot showing linear regression between the percentage cover of red blood cells and the trauma-death interval.

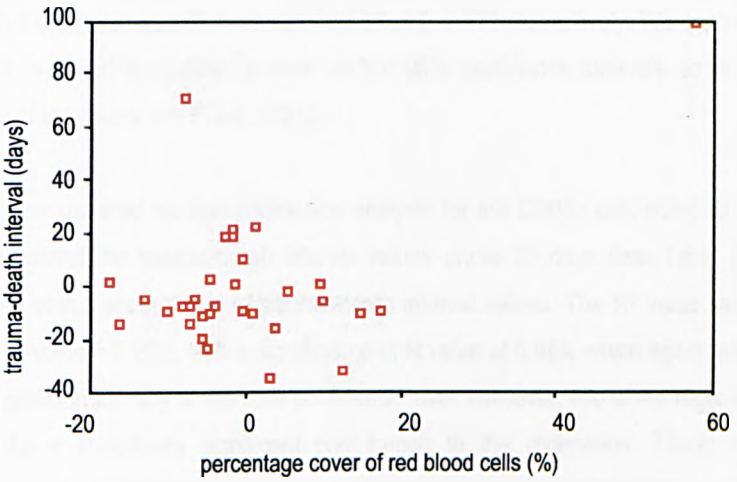

Figure 04: 26 A histogram of the distribution of the standardised error (residual) of the trauma-death interval values. (Standard deviation = 86, mean = 0.00, n = 52).

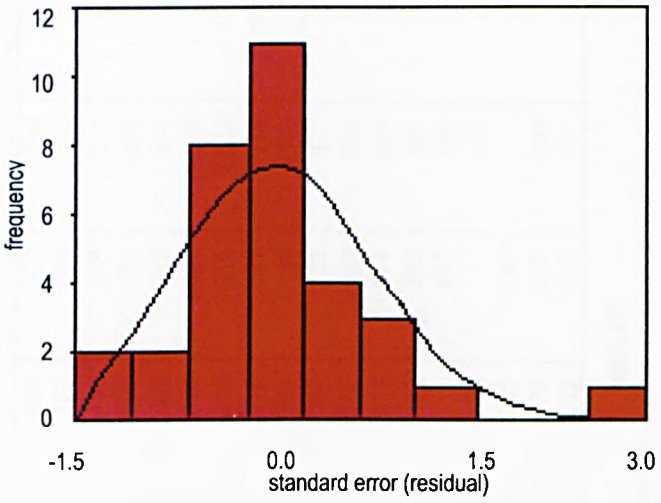

It appears that RBC (% cover of red blood cells) and BONE_LIV (% cover of living bone) contribute significantly to the regression with *t* values of 2.532 and -2.771 respectively. We can see that these values are significant to the 95% confidence level as the 95% confidence intervals do not include zero as a possible value (Tabachnick and Fidell, 2001).

The results of the standard multiple regression analysis for the CD68+ cell, compact bone and red blood cell variables against the trauma-death interval values under 25 days (see Table 04: 16) appear very similar to those of the whole range of trauma-death interval values. The R^2 value was found to be 0.489 (the adjusted R^2 value = 0.262), with a significance of R value of 0.084, which again makes the significance level of the regression just shy of the 95% confidence level. However, two of the regression coefficients are shown to make a statistically significant contribution to the regression. These are BONE_LIV and BONE_NEC, as their *t* values are -3.352 and -2.633 respectively. These values are both significant to the 95% confidence level. This will be discussed further in Chapter 06.

Table 04: 16 A summary of the SPSS output showing correlations between the trauma-death interval values under 25 days and the CD68+ cell, compact bone and red blood cell variables, with the R^2 value (n = 27 for all correlations).

Correlations

		TDI_25	CD68_COV	CD68SIZE	WHEREHOW	BLUE_COV	BLU_SIZE	BONE_LIV	BONE_NEC	RBC
Pearson Correlation	TDI_25	1.000	-.105	.000	.264	.058	.197	-.290	-.119	-.123
	CD68_COV	-.105	1.000	.038	.162	.162	.082	-.264	.174	.403
	CD68SIZE	.000	.038	1.000	-.065	.436	.188	.277	-.208	-.002
	WHEREHOW	.264	.162	-.065	1.000	-.009	.134	-.051	-.336	.349
	BLUE_COV	.058	.162	.436	-.009	1.000	-.049	.314	-.219	.264
	BLU_SIZE	.197	.082	.188	.134	-.049	1.000	-.210	.162	-.160
	BONE_LIV	-.290	-.264	.277	-.051	.314	-.210	1.000	-.712	.003
	BONE_NEC	-.119	.174	-.208	-.336	-.219	.162	-.712	1.000	-.247
	RBC	-.123	.403	-.002	.349	.264	-.160	.003	-.247	1.000
Sig. (1-tailed)	TDI_25	.	.300	.499	.092	.387	.162	.071	.277	.270
	CD68_COV	.300	.	.425	.210	.210	.342	.091	.192	.019
	CD68SIZE	.499	.425	.	.374	.012	.174	.081	.149	.496
	WHEREHOW	.092	.210	.374	.	.482	.252	.401	.044	.037
	BLUE_COV	.387	.210	.012	.482	.	.403	.055	.136	.092
	BLU_SIZE	.162	.342	.174	.252	.403	.	.146	.210	.212
	BONE_LIV	.071	.091	.081	.401	.055	.146	.	.000	.494
	BONE_NEC	.277	.192	.149	.044	.136	.210	.000	.	.107
	RBC	.270	.019	.496	.037	.092	.212	.494	.107	.

Model Summary

Model	R	R Square	Adjusted R Square	Std. Error of the Estimate
1	.699[a]	.489	.262	7.406

a. Predictors: (Constant), RBC, CD68SIZE, BLU_SIZE, BONE_NEC, CD68_COV, BLUE_COV, WHEREHOW, BONE_LIV

ANOVA[b]

Model		Sum of Squares	df	Mean Square	F	Sig.
1	Regression	944.894	8	118.112	2.153	.084[a]
	Residual	987.272	18	54.848		
	Total	1932.167	26			

a. Predictors: (Constant), RBC, CD68SIZE, BLU_SIZE, BONE_NEC, CD68_COV, BLUE_COV, WHEREHOW, BONE_LIV

b. Dependent Variable: TDI_25

Table 04: 16 continued.

Coefficients[a]

Model		Unstandardized Coefficients		Standardized Coefficients	t	Sig.	95% Confidence Interval for B	
		B	Std. Error	Beta			Lower Bound	Upper Bound
1	(Constant)	21.896	7.920		2.765	.013	5.257	38.535
	CD68_COV	-2.856	3.764	-.151	-.759	.458	-10.763	5.051
	CD68SIZE	-2.88E-03	.011	-.051	-.254	.803	-.027	.021
	WHEREHOW	4.816E-02	.112	.090	.429	.673	-.188	.284
	BLUE_COV	2.425	1.500	.331	1.617	.123	-.725	5.576
	BLU_SIZE	2.908E-02	.059	.093	.496	.626	-.094	.152
	BONE_LIV	-.186	.056	-.949	-3.354	.004	-.303	-.070
	BONE_NEC	-.169	.064	-.779	-2.633	.017	-.303	-.034
	RBC	-.325	.195	-.357	-1.664	.113	-.735	.085

a. Dependent Variable: TDI_25

Inter-observer agreement

In addition to the author, three independent observers made assessments of the percentage cover of different cells visible on the photographs of the fracture sites. They estimated the percentage cover of three types of cell visible at the fracture site: the brown DAB-stained immuno-positive cells, small round cells with blue-stained nuclei (lymphocytes), and elongated cells with blue-stained nuclei (fibroblasts). They gave a number on a scale of 0 to 4 (as described previously) to indicate the level of percentage cover. An example of a typical fracture slide stained with CD68, and its classification score is given in Figure 04: 27.

The level of inter-observer agreement was calculated using Cohen's Kappa method as an index of inter-rater reliability and reproducibility (Carletta, 1996; Petrie and Sabin, 2000). The Kappa statistic measures the reliability of the observations made by distinct observers, and allows the researcher to calculate the index of agreement between observers, and take into account the number of agreements that would have occurred by chance. In that respect, it is superior to simple percentage calculations of inter-observer reliability.

Figure 04: 27 A photograph of an example of a fracture slide stained with CD68. All 4 observers gave this slide a classification score for percentage cover of CD68 positive cells of 1 (<25%).

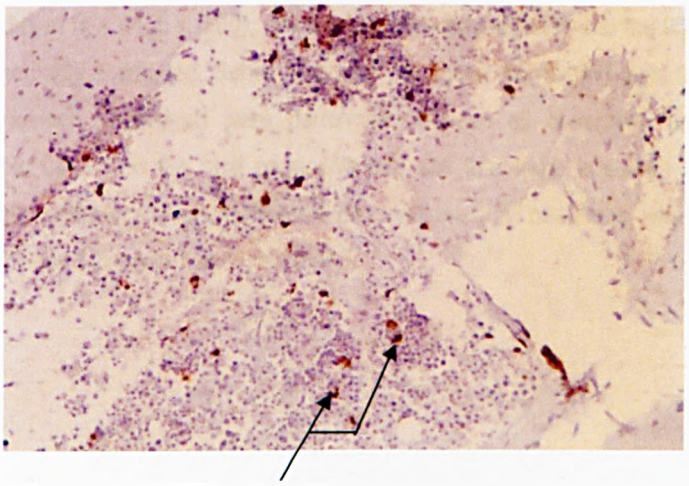

The Kappa test is not an inferential statistical test, so it does not assess whether a null hypothesis should be accepted or rejected. Kappa values occur in the range 0 to 1, where the larger values indicate a higher level of agreement between the observations of each observer. The following table (Table 04: 17)

summarises the SPSS output data for observations of the percentage cover of CD68 positive cells on each slide.

Table 04: 17 Table showing the kappa values for each inter-observer comparison.
(n = 64 cases and controls, none missing).

Observers	Observer 1	Observer 2	Observer 3	Observer 4
Observer 1	1.000	0.634	0.769	0.554
Observer 2	0.634	1.000	0.496	0.339
Observer 3	0.769	0.496	1.000	0.609≈0.61
Observer 4	0.554	0.339	0.609≈0.61	1.000

Kappa values where $0.61 \leq k \geq 0.80$ (highlighted in red) are generally accepted as 'substantial' and those where $0.41 \leq k \geq 0.60$ (highlighted in pink) are regarded as 'moderate'. For Kappa values to be regarded as 'good', they have to be ≥ 0.80 (Petrie and Sabin, 2000). Observer 1 and Observer 3 show the greatest level of agreement, and Observer 2 and Observer 4 the least.

A One-sample Kolmogorov-Smirnov test was done to determine whether the values taken by Observer 1 were normally distributed ($n = 64$, $p = 0.00$), which was statistically significant to the 95% confidence level, and therefore not normally distributed. Subsequent non-parametric correlation tests (Kendall's tau-b and Spearman's r_s correlation coefficient) were performed between all observers, and the results are summarised in Table 04: 18 on the next page. We can see that there is a high level of correlation, significant to the 99% confidence level between the observations of all observers, with the highest level of agreement again between Observer 1 and Observer 3.

Table 04: 18 Results of a Kendall's tau-b and a Spearman's r_s correlation coefficient test to determine if any correlation exists between the observations of percentage cover of CD68 positive cells on all slides made by four independent observers.

Correlations

			CD68_OB1	CD68_OB2	CD68_OB3	CD68_OB4
Kendall's tau_b	CD68_OB1	Correlation Coefficient	1.000	.769**	.816**	.502**
		Sig. (2-tailed)	.	.000	.000	.000
		N	64	64	64	64
	CD68_OB2	Correlation Coefficient	.769**	1.000	.714**	.500**
		Sig. (2-tailed)	.000	.	.000	.000
		N	64	64	64	64
	CD68_OB3	Correlation Coefficient	.816**	.714**	1.000	.549**
		Sig. (2-tailed)	.000	.000	.	.000
		N	64	64	64	64
	CD68_OB4	Correlation Coefficient	.502**	.500**	.549**	1.000
		Sig. (2-tailed)	.000	.000	.000	.
		N	64	64	64	64
Spearman's rho	CD68_OB1	Correlation Coefficient	1.000	.805**	.833**	.519**
		Sig. (2-tailed)	.	.000	.000	.000
		N	64	64	64	64
	CD68_OB2	Correlation Coefficient	.805**	1.000	.749**	.539**
		Sig. (2-tailed)	.000	.	.000	.000
		N	64	64	64	64
	CD68_OB3	Correlation Coefficient	.833**	.749**	1.000	.563**
		Sig. (2-tailed)	.000	.000	.	.000
		N	64	64	64	64
	CD68_OB4	Correlation Coefficient	.519**	.539**	.563**	1.000
		Sig. (2-tailed)	.000	.000	.000	.
		N	64	64	64	64

**. Correlation is significant at the .01 level (2-tailed).

Similar inter-observer error analyses were performed to assess the level of agreement between observers when evaluating the percentage cover of inflammatory cells on each fracture slide. A summary of the SPSS output data is presented below (see Table 04: 19).

Table 04: 19 Table showing the kappa values for each inter-observer comparison.
(n = 64 cases and controls, none missing).

Observers	Observer 1	Observer 2	Observer 3	Observer 4
Observer 1	1.000	0.647	0.241	0.174
Observer 2	0.647	1.000	0.178	0.119
Observer 3	0.241	0.178	1.000	0.176
Observer 4	0.174	0.119	0.176	1.000

Here, there is the greatest level of agreement between Observer 1 and Observer 2, which is corroborated by the non-parametric correlation tests (see Table 04: 20).

Table 04: 20 Results of a Kendall's tau-b and a Spearman's r_s correlation coefficient test to determine if any correlation exists between the observations of percentage cover of inflammatory cells with blue-stained nuclei on all slides made by four independent observers.

Correlations

			SMLL_OB1	SMLL_OB2	SMLL_OB3	SMLL_OB4
Kendall's tau_b	SMLL_OB1	Correlation Coefficient	1.000	.822**	.639**	.502**
		Sig. (2-tailed)	.	.000	.000	.000
		N	64	64	64	64
	SMLL_OB2	Correlation Coefficient	.822**	1.000	.547**	.465**
		Sig. (2-tailed)	.000	.	.000	.000
		N	64	64	64	64
	SMLL_OB3	Correlation Coefficient	.639**	.547**	1.000	.510**
		Sig. (2-tailed)	.000	.000	.	.000
		N	64	64	64	64
	SMLL_OB4	Correlation Coefficient	.502**	.465**	.510**	1.000
		Sig. (2-tailed)	.000	.000	.000	.
		N	64	64	64	64
Spearman's rho	SMLL_OB1	Correlation Coefficient	1.000	.881**	.724**	.582**
		Sig. (2-tailed)	.	.000	.000	.000
		N	64	64	64	64
	SMLL_OB2	Correlation Coefficient	.881**	1.000	.631**	.539**
		Sig. (2-tailed)	.000	.	.000	.000
		N	64	64	64	64
	SMLL_OB3	Correlation Coefficient	.724**	.631**	1.000	.591**
		Sig. (2-tailed)	.000	.000	.	.000
		N	64	64	64	64
	SMLL_OB4	Correlation Coefficient	.582**	.539**	.591**	1.000
		Sig. (2-tailed)	.000	.000	.000	.
		N	64	64	64	64

**. Correlation is significant at the .01 level (2-tailed).

The same tests (Cohen's kappa test, one-sample Kolmogorov-Smirnov test, Kendall's tau-b and Spearman's correlation coefficient) were performed to analyse the independent observers' evaluations of the percentage cover of fibroblast cells on each fracture slide. Only Observers 3 and 4 were available to record their observations (see Table 04: 21).

Table 04: 21 Table showing the kappa values for each inter-observer comparison.
(n = 64 cases and controls, none missing).

Observers	Observer 3	Observer 4
Observer 3	1.000	0.333
Observer 4	0.333	1.000

Here, there is only a fair level of agreement between the two observers (Petrie and Sabin, 2000). The non-parametric tests, however, show a statistically significant level of correlation between the observations of the two observers, to the 99% confidence level (see Table 04: 22).

Table 04: 22 Results of a Kendall's tau-b and a Spearman's r_s correlation coefficient test to determine if any correlation exists between the observations of percentage cover of fibroblast cells with blue-stained nuclei on all slides made by two independent observers.

Correlations

			LONG_OB3	LONG_OB4
Kendall's tau_b	LONG_OB3	Correlation Coefficient	1.000	.447**
		Sig. (2-tailed)	.	.000
		N	64	64
	LONG_OB4	Correlation Coefficient	.447**	1.000
		Sig. (2-tailed)	.000	.
		N	64	64
Spearman's rho	LONG_OB3	Correlation Coefficient	1.000	.478**
		Sig. (2-tailed)	.	.000
		N	64	64
	LONG_OB4	Correlation Coefficient	.478**	1.000
		Sig. (2-tailed)	.000	.
		N	64	64

**. Correlation is significant at the .01 level (2-tailed).

Bone Sialoprotein

Bone sialoprotein (BSP) is a sialic, acid-rich glycol-protein, with an approximate weight of 70 – 80 kDa, and is found in the extra-cellular matrix of bone. As a marker of osteoblasts and osteocytes, the monoclonal anti-bone sialoprotein antibody was chosen to complement the action of the CD68 antibody.

Fifty fracture slides were stained with BSP using the methodology described in Chapter 02. Staining was successful in only 34 cases (68%), with four cases (8%) exhibiting unspecific staining and 12 cases (24%) showing background staining, which rendered them unusable. Two positive and two negative controls were stained at the same time. Normal bone was used as the control tissue. An example of a successfully stained slide and a positive and negative control are given in Figure 04: 28, Figure 04: 29 and Figure 04: 30.

Figure 04: 28 A photograph of a fracture slide successfully stained with BSP, and counter-stained with haematoxylin. (BSP dilution = 1:200. Objective magnification x10).

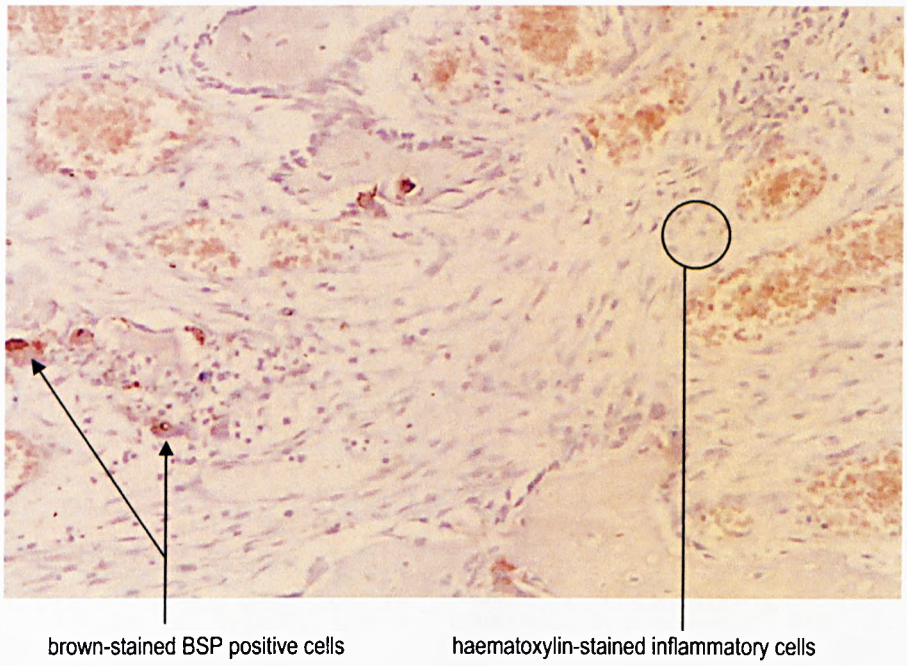

Figure 04: 29 A photograph of the BSP positive control (normal bone tissue), counter-stained with haematoxylin. (BSP dilution = 1:200. Objective magnification x10).

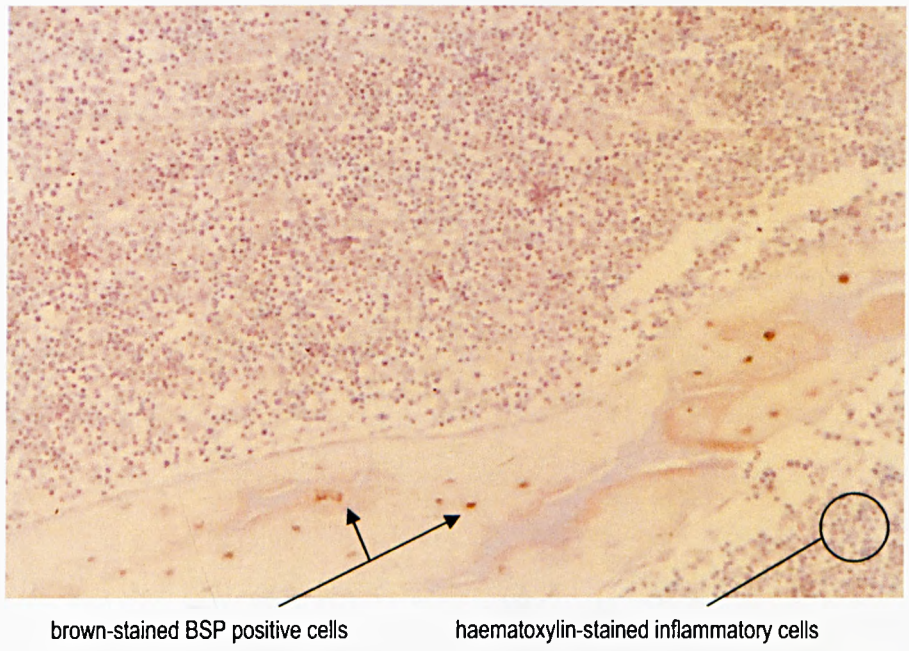

Figure 04: 30 A photograph of the BSP negative control (normal bone tissue), counter-stained with haematoxylin. (Objective magnification x10).

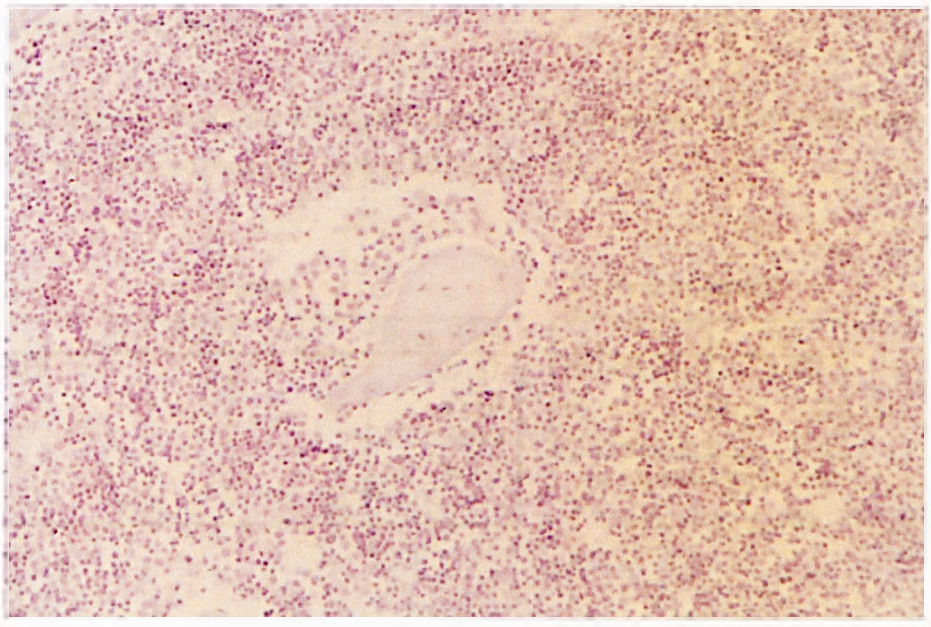

no brown-stained BSP positive cells all haematoxylin-stained inflammatory cells

It was hypothesised that variables such as the average size, the percentage cover or spatial distribution of BSP positive cells would show a correlation with the trauma-death interval values of the sample population. This can be expressed as follows:

H0: there is no statistically significant relationship between the qualitative spatial properties of the BSP positive cells and the trauma-death interval in the sample population

H1: there is a statistically significant relationship between the qualitative spatial properties of the BSP positive cells and the trauma-death interval in the sample population

In order to test this hypothesis, qualitative measurements of these variables were taken by two independent observers (see Inter-observer agreement below).

Estimated percentage cover of BSP positive cells

Percentage cover of BSP positive cells in relation to the whole photograph was measured in a semi-quantitative fashion, using the same category coding system as described above. An analysis of variance test was performed to determine whether there was a significant difference in the mean value for trauma-death interval in each of the estimated percentage cover categories. The results of the Kruskal-Wallis tests

(Table 04: 23 and Table 04: 24) show that there is no significant difference between the mean trauma-death interval values in each category, even when the out-lying trauma-death interval values are ignored. Therefore, the alternative hypothesis (H1) for the variable of the estimated percentage cover of BSP positive cells has to be rejected.

Table 04: 23 Results of a Kruskal-Wallis test to determine if any correlation exists between trauma-death interval and the estimated percentage cover of BSP positive cells.

Ranks

	BSP_COV	N	Mean Rank
TDI	0	15	27.57
	1	27	22.69
	2	3	11.33
	3	1	21.00
	Total	46	

Test Statistics[a,b]

	TDI
Chi-Square	4.045
df	3
Asymp. Sig.	.257

a. Kruskal Wallis Test

b. Grouping Variable: BSP_COV

Table 04: 24 Results of a Kruskal-Wallis test to determine if any correlation exists between trauma-death interval values under 25 days and the estimated percentage cover of BSP positive cells.

Ranks

	BSPCOV25	N	Mean Rank
TDI_25	0	12	23.58
	1	23	19.22
	2	3	11.33
	3	1	21.00
	Total	39	

Test Statistics[a,b]

	TDI_25
Chi-Square	3.121
df	3
Asymp. Sig.	.373

a. Kruskal Wallis Test

b. Grouping Variable: BSPCOV25

Estimated size of BSP positive cells

The estimated average size of the BSP positive cells was also compared to the trauma-death interval values for the sample. The average size of the cells was estimated by the author in μm^2, by comparing them to cells of known size measured during the collection of the quantitative data using *Scion Image* (see Chapter 05). A scattergraph of these values against the trauma-death interval values of the sample was plotted (see Figure 04: 31).

Figure 04: 31 Scatter-plot showing the relationship between the estimated size of the BSP positive cells and the trauma-death interval.

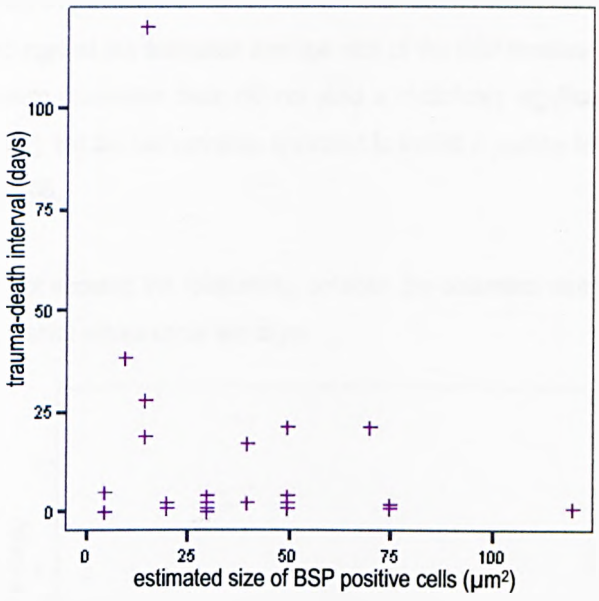

The estimated average size of the BSP positive cells was then compared to the trauma-death interval values minus the out-lying values over 25 days, and a scatter-plot generated (Figure 04: 32).

Figure 04: 32 Scatter-plot showing the relationship between the estimated size of the BSP positive cells and the trauma-death interval values under 25 days.

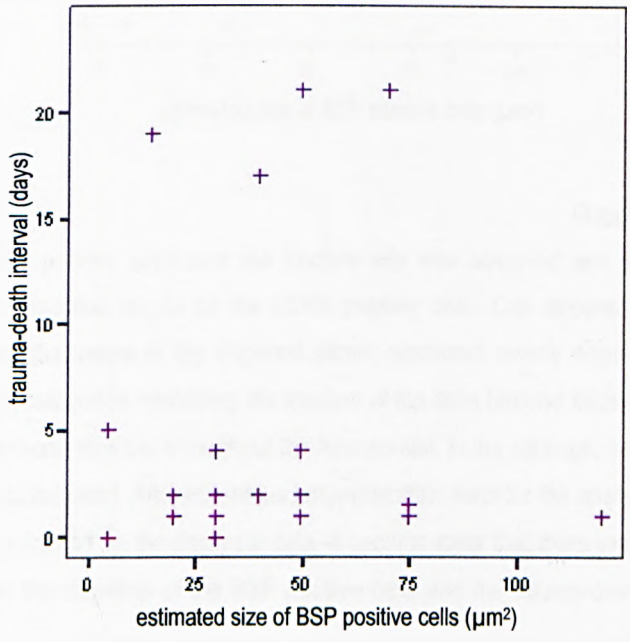

Although a Kendall's tau-b and Spearman's r_s correlation coefficient test did not produce significant results (r=0.055, n=22, p=0.649 Spearman's test), it was thought that a trend was visible, and that further narrowing of the samples might elucidate an obvious correlation. The trauma-death values smaller than 10 days were then plotted against the estimated average size of the BSP positive cells (see Figure 04: 33). Again, the non-parametric correlation tests did not yield a statistically significant result (r=0.103, n=18, p=0.828 Spearman's test), but the two variables appeared to exhibit a positive linear relationship. This will be discussed in Chapter 06.

Figure 04: 33 Scatter-plot showing the relationship between the estimated size of the BSP positive cells and the trauma-death interval values under ten days.

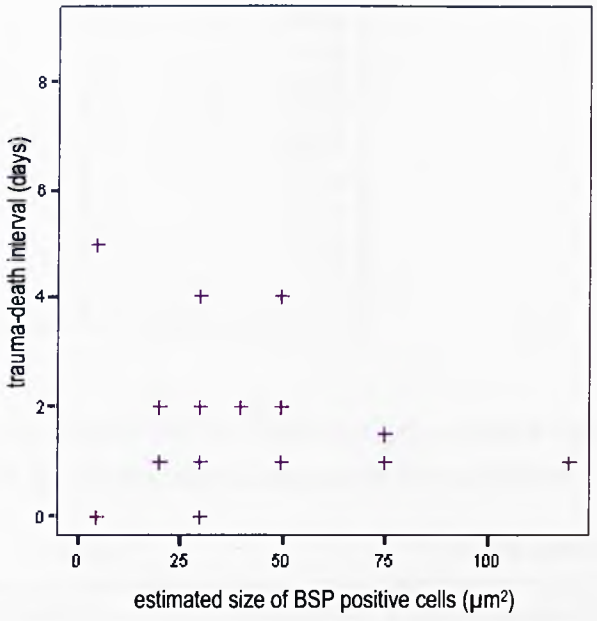

Dispersal of BSP positive cells

The dispersal of BSP positive cells over the fracture site was observed and recorded using a similar method to the one described above for the CD68 positive cells. Cell dispersal was classified into six categories describing the nature of the dispersal (none; scattered; evenly dispersed; clustered; few and dense) and into eight categories describing the location of the cells (around fractured ends; in the ECM; in the compact bone; in bone marrow; throughout the fracture site; in the cartilage; around adipose tissue and associated with red blood cells). After numerous non-parametric tests for the analysis of variance (Kruskal-Wallis tests) were performed on the dispersal data, it became clear that there were no obvious significant correlations between the dispersal of the BSP positive cells and the trauma-death interval values of the

sample, even when those trauma-death interval values over 25 days or over ten days were ignored (see Table 04: 25, Table 04: 26 and Table 04: 27).

Table 04: 25 Results of a Kruskal-Wallis test to determine if any correlation exists between trauma-death interval and the dispersal categories of BSP positive cells.

Ranks

	HOWWHERE	N	Mean Rank
TDI	0	15	25.63
	1	2	24.50
	2	7	15.86
	5	1	19.00
	11	1	19.00
	13	1	26.50
	21	1	8.00
	30	5	18.60
	31	4	30.00
	33	1	39.00
	36	2	31.25
	37	1	41.00
	40	1	2.00
	44	2	7.75
	Total	44	

Test Statistics[a,b]

	TDI
Chi-Square	16.295
df	13
Asymp. Sig.	.234

a. Kruskal Wallis Test

b. Grouping Variable: HOWWHERE

Table 04: 26 Results of a Kruskal-Wallis test to determine if any correlation exists between trauma-death interval values under 25 days and the dispersal categories of BSP positive cells.

Ranks

	HOWWH_25	N	Mean Rank
TDI_25	0	12	21.67
	1	2	24.50
	2	7	15.86
	5	1	19.00
	11	1	19.00
	13	1	26.50
	21	1	8.00
	30	4	13.50
	31	4	30.00
	36	1	19.00
	40	1	2.00
	44	2	7.75
	Total	37	

Test Statistics[a,b]

	TDI_25
Chi-Square	13.551
df	11
Asymp. Sig.	.259

a. Kruskal Wallis Test

b. Grouping Variable: HOWWH_25

Table 04: 27 Results of a Kruskal-Wallis test to determine if any correlation exists between trauma-death interval values under 10 days and the dispersal categories of BSP positive cells.

Ranks

	HOWWH_10	N	Mean Rank
TDI_10	0	9	17.61
	1	2	24.50
	2	5	9.10
	5	1	19.00
	11	1	19.00
	13	1	26.50
	21	1	8.00
	30	4	13.50
	31	1	19.00
	36	1	19.00
	40	1	2.00
	44	2	7.75
	Total	29	

Test Statistics[a,b]

	TDI_10
Chi-Square	13.868
df	11
Asymp. Sig.	.240

a. Kruskal Wallis Test

b. Grouping Variable: HOWWH_10

Cells with haematoxylin-stained nuclei

On the BSP-stained slides, haematoxylin was again used as a counter-stain, which successfully stained the nuclei of the inflammatory cells and fibroblasts associated with the fracture site. Again, the ratios of the estimated percentage cover of the BSP positive cells and each of the blue-stained cells were compared to the trauma-death interval values of the sample, in an attempt to find a significant correlation between any of these variables. Six non-parametric correlation tests (Kendall's tau-b and Spearman's r_s correlation coefficient) were performed to determine if any correlation existed between *the ratio of small cell % cover: BSP+ cell % cover* and the trauma-death interval values for the whole sample, and those under 25 days and under 10 days (see Table 04: 28, Table 04: 29, and Table 04: 30). No statistically significant correlation was seen between any of the variables.

Table 04: 28 Results of a Kendall's tau-b and a Spearman's r_s correlation coefficient test to determine if any correlation exists between the ratio of *small blue cell % cover: BSP+ cell % cover* and trauma-death interval.

Correlations

			TDI	COVRATIO
Kendall's tau_b	TDI	Correlation Coefficient	1.000	-.176
		Sig. (2-tailed)	.	.133
		N	47	46
	COVRATIO	Correlation Coefficient	-.176	1.000
		Sig. (2-tailed)	.133	.
		N	46	49
Spearman's rho	TDI	Correlation Coefficient	1.000	-.224
		Sig. (2-tailed)	.	.135
		N	47	46
	COVRATIO	Correlation Coefficient	-.224	1.000
		Sig. (2-tailed)	.135	.
		N	46	49

Table 04: 29 Results of a Kendall's tau-b and a Spearman's r_s correlation coefficient test to determine if any correlation exists between the ratio of *small blue cell % cover: BSP+ cell % cover* and trauma-death interval values under 25 days.

Correlations

			TDI_25	COVRAT25
Kendall's tau_b	TDI_25	Correlation Coefficient	1.000	-.140
		Sig. (2-tailed)	.	.275
		N	40	39
	COVRAT25	Correlation Coefficient	-.140	1.000
		Sig. (2-tailed)	.275	.
		N	39	42
Spearman's rho	TDI_25	Correlation Coefficient	1.000	-.175
		Sig. (2-tailed)	.	.286
		N	40	39
	COVRAT25	Correlation Coefficient	-.175	1.000
		Sig. (2-tailed)	.286	.
		N	39	42

Table 04: 30 Results of a Kendall's tau-b and a Spearman's r_s correlation coefficient test to determine if any correlation exists between the ratio of *small blue cell % cover: BSP+ cell % cover* and trauma-death interval values under ten days.

Correlations

			TDI_10	COVRAT10
Kendall's tau_b	TDI_10	Correlation Coefficient	1.000	-.190
		Sig. (2-tailed)	.	.196
		N	32	31
	COVRAT10	Correlation Coefficient	-.190	1.000
		Sig. (2-tailed)	.196	.
		N	31	34
Spearman's rho	TDI_10	Correlation Coefficient	1.000	-.235
		Sig. (2-tailed)	.	.203
		N	32	31
	COVRAT10	Correlation Coefficient	-.235	1.000
		Sig. (2-tailed)	.203	.
		N	31	34

The null hypothesis (H0) that states:

> there is no statistically significant relationship between the qualitative spatial properties of the BSP positive cells and the trauma-death interval in the sample population

has to be accepted.

Multiple regression analysis

Multiple regression analyses were performed to determine whether it would be possible to retrospectively predict the trauma-death interval from any combination of the variables measured from the BSP-stained slides. The errors for both the dependent and independent variables were assumed to be normally distributed. Table 04: 31 shows the results of the multiple regression analysis. In the correlation tables, we can see that there are two statistically significant correlations (significant to the 95% confidence level) between the trauma-death interval and the measured variables. These are between tdi and the estimated percentage cover of the elongated, spindle-shaped fibroblasts (correlation coeffiecient = 0.347, sig. = 0.048) and between tdi and the estimated percentage cover of living compact bone (correlation coefficient = -0.441, sig. = 0.016). The latter correlation is negative, as has been seen before. Reasons for this are discussed in Chapter 06. There is also a weak negative correlation between tdi and the size of the BSP+ cells, which is nearly statistically significant to the 95% confidence level.

The R^2 value of the regression is 0.410 (adjusted R^2 value = 0.152) and the significance level is 0.209. This suggests that only 40% of the variance in the data can be explained by these variables, and even this is an

Table 04: 31 A summary of the SPSS output showing correlations between the trauma-death interval and the BSP+ cell variables, with the R^2 value (n = 24 for all correlations).

Correlations

		TDI	BSP_COV	SIZE_NUM	HOWWHERE	SMLL_COV	LONG_COV	BONE_LIV	RBC
Pearson Correlation	TDI	1.000	-.173	-.287	.293	-.271	.347	-.441	-.089
	BSP_COV	-.173	1.000	.127	.324	.162	-.251	.110	.012
	SIZE_NUM	-.287	.127	1.000	-.402	.144	-.007	-.159	-.138
	HOWWHERE	.293	.324	-.402	1.000	-.247	-.216	-.132	.014
	SMLL_COV	-.271	.162	.144	-.247	1.000	.013	.435	-.035
	LONG_COV	.347	-.251	-.007	-.216	.013	1.000	-.283	.044
	BONE_LIV	-.441	.110	-.159	-.132	.435	-.283	1.000	.277
	RBC	-.089	.012	-.138	.014	-.035	.044	.277	1.000
Sig. (1-tailed)	TDI	.	.210	.087	.083	.100	.048	.016	.339
	BSP_COV	.210	.	.278	.061	.225	.119	.305	.477
	SIZE_NUM	.087	.278	.	.026	.251	.488	.229	.260
	HOWWHERE	.083	.061	.026	.	.122	.156	.270	.474
	SMLL_COV	.100	.225	.251	.122	.	.476	.017	.436
	LONG_COV	.048	.119	.488	.156	.476	.	.090	.419
	BONE_LIV	.016	.305	.229	.270	.017	.090	.	.095
	RBC	.339	.477	.260	.474	.436	.419	.095	.

Model Summary[b]

Model	R	R Square	Adjusted R Square	Std. Error of the Estimate
1	.640[a]	.410	.152	23.319

a. Predictors: (Constant), RBC, BSP_COV, SMLL_COV, SIZE_NUM, LONG_COV, HOWWHERE, BONE_LIV

b. Dependent Variable: TDI

ANOVA[b]

Model		Sum of Squares	df	Mean Square	F	Sig.
1	Regression	6045.002	7	863.572	1.588	.209[a]
	Residual	8700.238	16	543.765		
	Total	14745.240	23			

a. Predictors: (Constant), RBC, BSP_COV, SMLL_COV, SIZE_NUM, LONG_COV, HOWWHERE, BONE_LIV

b. Dependent Variable: TDI

Table 04: 31 continued.

Coefficients[a]

Model		Unstandardized Coefficients		Standardized Coefficients	t	Sig.	95% Confidence Interval for B	
		B	Std. Error	Beta			Lower Bound	Upper Bound
1	(Constant)	22.410	22.380		1.001	.332	-25.033	69.853
	BSP_COV	-6.105	11.814	-.116	-.517	.612	-31.150	18.940
	SIZE_NUM	-.208	.218	-.224	-.955	.354	-.669	.253
	HOWWHERE	.410	.409	.253	1.001	.332	-.458	1.277
	SMLL_COV	-.506	6.327	-.019	-.080	.937	-13.920	12.907
	LONG_COV	7.865	6.159	.280	1.277	.220	-5.191	20.921
	BONE_LIV	-.172	.133	-.331	-1.290	.215	-.455	.111
	RBC	-8.99E-02	.424	-.044	-.212	.835	-.989	.809

a. Dependent Variable: TDI

exaggerated figure (Tabachnick and Fidell, 2001). None of the regression coefficients make a statistically significant contribution to the regression and the prediction of the trauma-death interval.

Inter-observer agreement

The qualitative observations for the BSP data were made by two independent observers, between whom the inter-observer agreement can be calculated using Cohen's Kappa method. The Kappa test is not an inferential statistical test, so it does not assess whether a null hypothesis should be accepted or rejected. Kappa values occur in the range 0 to 1, where the larger values indicate a higher level of agreement between the observations of each observer. The following table (Table 04: 32) summarises the SPSS output data for observations of the percentage cover of BSP positive cells on each slide.

Table 04: 32 Table showing the kappa values for each inter-observer comparison.
(n = 53 cases and controls, none missing).

Observers	Observer 1	Observer 2
Observer 1	1.000	0.756
Observer 2	0.756	1.000

Here, there is a substantial level of agreement between the two observers (Petrie and Sabin, 2000).

A One-sample Kolmogorov-Smirnov test was done to determine whether the values taken by Observer 1 were normally distributed (n = 53, p = 0.00), which was statistically significant to the 95% confidence level, and therefore not normally distributed. Subsequent non-parametric correlation tests (Kendall's tau-b and Spearman's r_s correlation coefficient) were performed between both observers, and the results are summarised in Table 04: 33. We can see that there is a high level of correlation, significant to the 99% confidence level between the observations of both observers.

Table 04: 33 Results of a Kendall's tau-b and a Spearman's r_s correlation coefficient test to determine if any correlation exists between the observations of percentage cover of BSP+ cells on all slides made by two independent observers.

Correlations

			BSP_OB1	BSP_OB2
Kendall's tau_b	BSP_OB1	Correlation Coefficient	1.000	.871**
		Sig. (2-tailed)	.	.000
		N	53	53
	BSP_OB2	Correlation Coefficient	.871**	1.000
		Sig. (2-tailed)	.000	.
		N	53	53
Spearman's rho	BSP_OB1	Correlation Coefficient	1.000	.903**
		Sig. (2-tailed)	.	.000
		N	53	53
	BSP_OB2	Correlation Coefficient	.903**	1.000
		Sig. (2-tailed)	.000	.
		N	53	53

**. Correlation is significant at the .01 level (2-tailed).

Similar inter-observer error analyses were performed to assess the level of agreement between observers when evaluating the percentage cover of both types of blue-stained cells on each fracture slide. The Kappa values for the observations of the percentage cover of the small blue-stained cells could not be computed, as the values in each variable did not match the values of the second variable – i.e.: not all of the categories (0 to 4) were represented by both observers. A summary of the SPSS output data for the observations of the percentage cover of the elongated blue-stained cells is presented in the table below (Table 04: 34).

Table 04: 34 Table showing the kappa values for each inter-observer comparison.
(n = 53 cases and controls, none missing).

Observers	Observer 1	Observer 2
Observer 1	1.000	0.591
Observer 2	0.591	1.000

There is a moderate level of agreement between the two observers (Petrie and Sabin, 2000). The non-parametric tests performed for both types of blue-stained cell, however, show a statistically significant level

of correlation between the observations of the two observers, to the 99% confidence level (see Table 04: 35 and Table 04: 36).

Table 04: 35 Results of a Kendall's tau-b and a Spearman's r_s correlation coefficient test to determine if any correlation exists between the observations of percentage cover of small blue-stained cells on all slides made by two independent observers.

Correlations

			SMLL_OB1	SMLL_OB2
Kendall's tau_b	SMLL_OB1	Correlation Coefficient	1.000	.770**
		Sig. (2-tailed)	.	.000
		N	53	53
	SMLL_OB2	Correlation Coefficient	.770**	1.000
		Sig. (2-tailed)	.000	.
		N	53	53
Spearman's rho	SMLL_OB1	Correlation Coefficient	1.000	.817**
		Sig. (2-tailed)	.	.000
		N	53	53
	SMLL_OB2	Correlation Coefficient	.817**	1.000
		Sig. (2-tailed)	.000	.
		N	53	53

**. Correlation is significant at the .01 level (2-tailed).

Table 04: 36 Results of a Kendall's tau-b and a Spearman's r_s correlation coefficient test to determine if any correlation exists between the observations of percentage cover of elongated blue-stained cells on all slides made by two independent observers.

Correlations

			LONG_OB1	LONG_OB2
Kendall's tau_b	LONG_OB1	Correlation Coefficient	1.000	.752**
		Sig. (2-tailed)	.	.000
		N	53	53
	LONG_OB2	Correlation Coefficient	.752**	1.000
		Sig. (2-tailed)	.000	.
		N	53	53
Spearman's rho	LONG_OB1	Correlation Coefficient	1.000	.812**
		Sig. (2-tailed)	.	.000
		N	53	53
	LONG_OB2	Correlation Coefficient	.812**	1.000
		Sig. (2-tailed)	.000	.
		N	53	53

**. Correlation is significant at the .01 level (2-tailed).

Compact bone

Semi-quantitative estimations of the percentage of compact bone with intact osteocytes within lacunae (living) and the percentage of compact bone exhibiting empty lacunae were made for each fracture slide. It was hypothesised that the ratio of necrotic to living bone would be correlated to the time elapsed since fracture. However, no significant correlation could be found between these variables using Kendall's tau-b and Spearman's r_s correlation coefficient tests (see Table 04: 37).

Table 04: 37 Results of a Kendall's tau-b and a Spearman's r_s correlation coefficient test to determine if any correlation exists between the ratio of living to necrotic bone percentage cover on the CD68-stained slides and the trauma-death interval.

Correlations

			TDI	BONRATIO
Kendall's tau_b	TDI	Correlation Coefficient	1.000	-.052
		Sig. (2-tailed)	.	.666
		N	49	45
	BONRATIO	Correlation Coefficient	-.052	1.000
		Sig. (2-tailed)	.666	.
		N	45	48
Spearman's rho	TDI	Correlation Coefficient	1.000	-.066
		Sig. (2-tailed)	.	.666
		N	49	45
	BONRATIO	Correlation Coefficient	-.066	1.000
		Sig. (2-tailed)	.666	.
		N	45	48

Figure 04: 34 and Figure 04: 35 show the relationships between the percentages of compact bone on each slide composed of living and necrotic bone with the trauma-death interval for the slides stained with both immunohistochemical stains.

The multiple regression analyses of the variables visible on the immuno-stained fracture sections included the estimated percentage cover of compact bone, living and necrotic. These results have already been given, and their significance is discussed in Chapter 06.

Figure 04: 34 Scatter-plot showing the relationship between trauma-death interval and the percentage cover of the background by compact bone, the percentage of the compact bone which is living and the percentage of the compact bone which is necrotic (CD68 slides, n = 52).

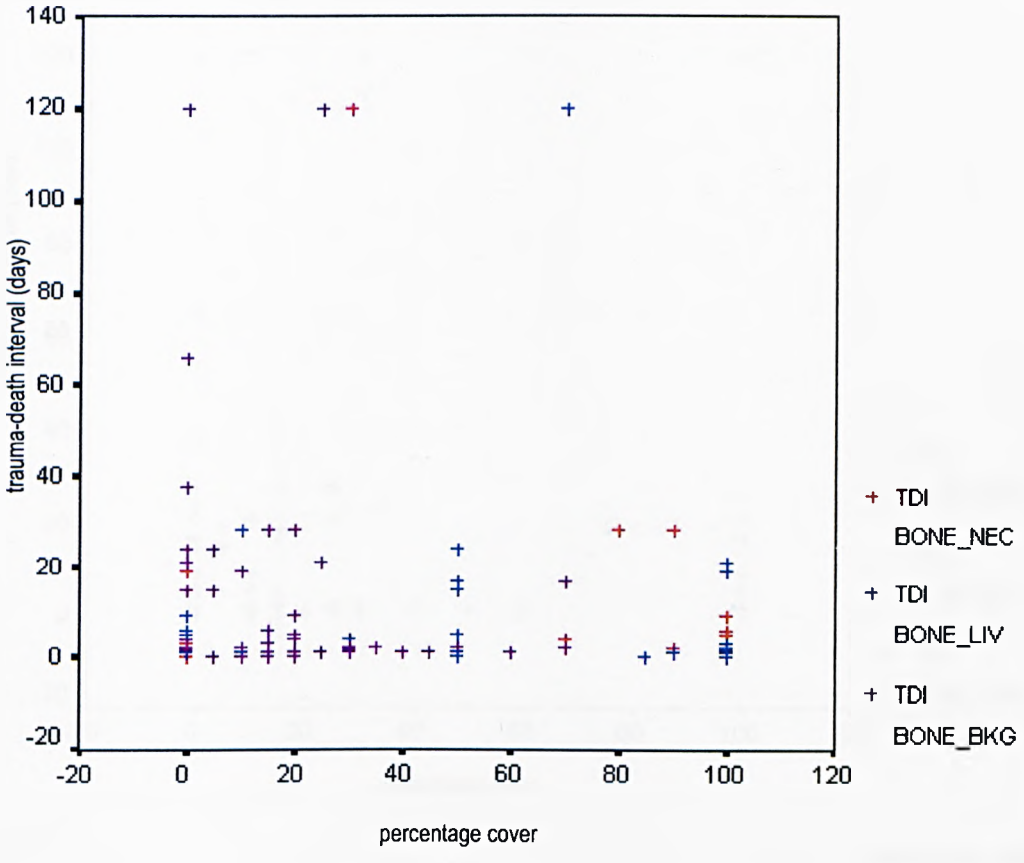

Figure 04: 35 Scatter-plot showing the relationship between trauma-death interval and the percentage cover of the background by compact bone, the percentage of the compact bone which is living and the percentage of the compact bone which is necrotic (BSP slides, n = 50).

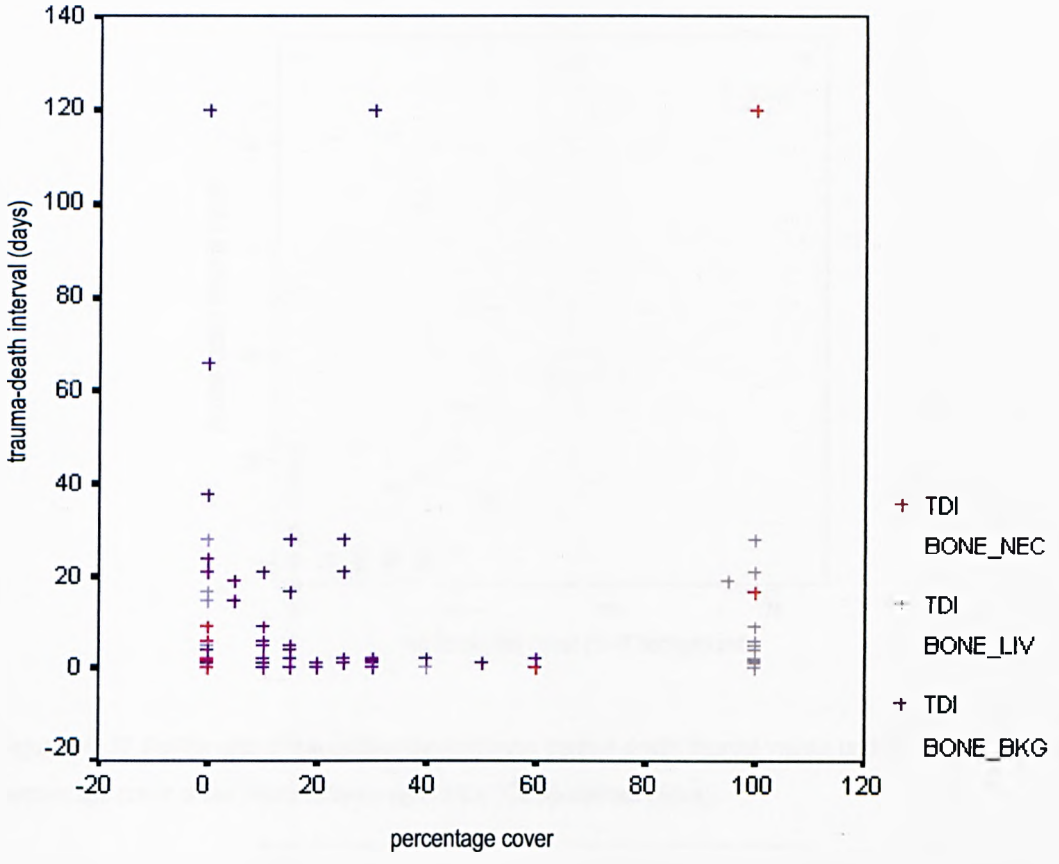

Red blood cells

It was supposed that the percentage cover of red blood cells at the fracture site might show a correlation with time since fracture, and that the data gathered would reflect the flow of blood cells towards and then away from the fracture site. Scatter-plots of the percentage cover (of the background) of red blood cells against trauma-death interval and trauma-death interval values under 25 days are given in Figure 04: 36 and Figure 04: 37. Non-parametric correlation tests were performed to quantify the relationship between red blood cell cover and trauma-death interval (see Table 04: 38 and Table 04: 39). Neither correlation is statistically significant to the 95% confidence level.

The multiple regression analyses of the variables visible on the immuno-stained fracture sections included the estimated percentage cover of red blood cells. These results have already been given, and their significance is discussed in Chapter 06.

Figure 04: 36 Scatter-plot of the relationship between trauma-death interval and the percentage cover of red blood cells on each slide (CD68-stained slides).

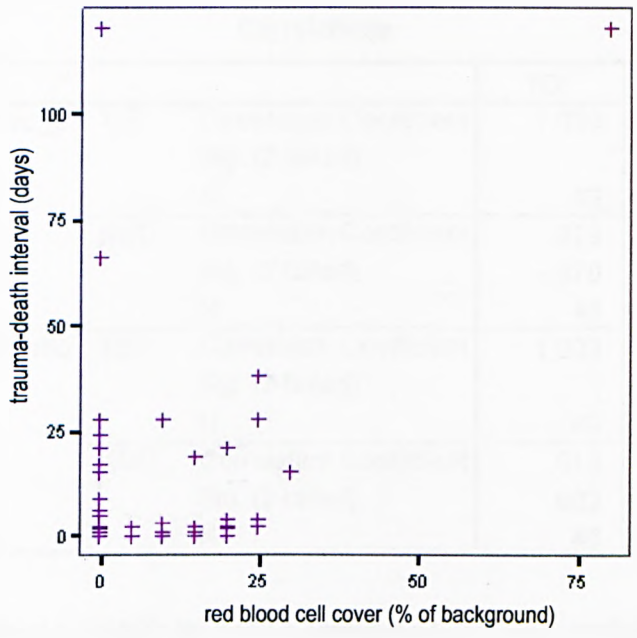

Figure 04: 37 Scatter-plot of the relationship between trauma-death interval values under 25 days and the percentage cover of red blood cells on each slide (CD68-stained slides).

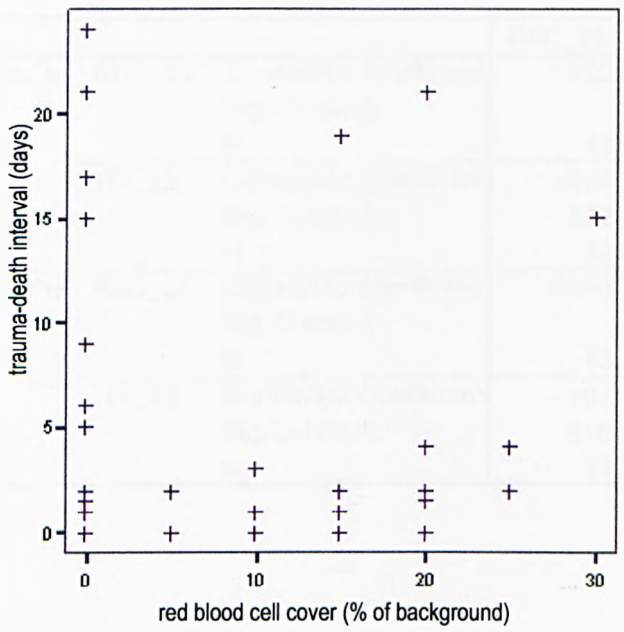

Table 04: 38 Results of a Kendall's tau-b and a Spearman's r_s correlation coefficient test to determine if any correlation exists between the percentage cover of red blood cells to the trauma-death interval (CD68-stained slides).

Correlations

			TDI	RBC
Kendall's tau_b	TDI	Correlation Coefficient	1.000	.019
		Sig. (2-tailed)	.	.870
		N	49	46
	RBC	Correlation Coefficient	.019	1.000
		Sig. (2-tailed)	.870	.
		N	46	57
Spearman's rho	TDI	Correlation Coefficient	1.000	.019
		Sig. (2-tailed)	.	.902
		N	49	46
	RBC	Correlation Coefficient	.019	1.000
		Sig. (2-tailed)	.902	.
		N	46	57

Table 04: 39 Results of a Kendall's tau-b and a Spearman's r_s correlation coefficient test to determine if any correlation exists between the percentage cover of red blood cells to the trauma-death interval values under 25 days (CD68-stained slides).

Correlations

			RBC_25	TDI_25
Kendall's tau_b	RBC_25	Correlation Coefficient	1.000	-.076
		Sig. (2-tailed)	.	.552
		N	42	39
	TDI_25	Correlation Coefficient	-.076	1.000
		Sig. (2-tailed)	.552	.
		N	39	42
Spearman's rho	RBC_25	Correlation Coefficient	1.000	-.107
		Sig. (2-tailed)	.	.518
		N	42	39
	TDI_25	Correlation Coefficient	-.107	1.000
		Sig. (2-tailed)	.518	.
		N	39	42

Summary

Summary of statistical significance of results

Table 04: 40 shows a summary of the p values and correlation coefficients obtained after performing Spearman's r_s correlation coefficient tests and Kruskal-Wallis tests for correlation on the different variables outlined above. Spearman's tests were performed on scale data, and Kruskal-Wallis tests on categorical (ie: nominal or ordinal) data. Since all three trauma-death interval ranges (whole range, ≤ 25 days, ≤ 10 days) were not normally distributed, non-parametric tests were performed on all the data. Those values marked in red are results that are statistically significant to the 95% confidence level. Those marked in pink are results that appear to be very close to being statistically significant. Values in blue ink represent the correlation value (Chi-Square value) given by the Kruskal-Wallis test. The majority of the values represent results that were statistically not significant.

Summary of time-related histological changes

Figure 04: 38 is a representation of the spread of the different variables examined against the trauma-death interval. They have been plotted using the mean trauma-death interval value for each variable, to give an idea of which variables are visible histologically at any given time period since trauma. The error bars show the standard deviation from the mean, and give an idea of the way in which the histological presence of each variable overlaps with others. It is clear that the majority of variables have long error bars due to a large standard deviation. This means that each variable was present histologically at a wide range of times since trauma. This reduces the potential value of each one individually as a predictor of trauma-death interval, but suggests that combinations of variables may be more valuable for predicting trauma-death interval in blind tests or forensic anthropology cases.

Overall summary

There are a few conclusions that have emerged from the collection and analysis of the qualitative data.

- The presence of haemosiderin granules at the fracture site is strongly positively correlated with the trauma-death interval. The difference in the mean trauma-death interval values for each classification of Perls' stain (positive or negative) is highly statistically significant (to the 95% confidence level for the whole range of tdi values, and to the 99% confidence level for the tdi values under 25 days). This suggests that the presence of haemosiderin granules is found at consistently higher average tdi values than the absence of haemosiderin, and that haemosiderin presence potentially could be used as a predictor of the trauma-death interval within broad categories.

Table 04: 40 A summary of the p values and correlation coefficients obtained after Spearman's r_s correlation coefficient statistical analyses.

Independent variable	Trauma-death interval					
	Whole range of values		Values ≤ 25 days		Values ≤ 10 days	
	p value (significance)	correlation value	p value (significance)	correlation value	p value (significance)	correlation value
Age	0.066	0.365	0.054	0.417	-	-
Perls' stain classification (+ / -)	0.049	6.045	0.021	5.313	-	-
CD68+ cells estimated % cover	0.475	3.522	0.596	1.888	-	-
CD68+ cells estimated size	0.770	-0.49	0.926	-0.017	-	-
CD68+ cell dispersal (location)	0.155	8.023	-	-	-	-
CD68+ cell dispersal (nature)	0.863	1.288	-	-	-	-
CD68+ cell dispersal (location + nature)	0.475	9.612	0.044	18.729	-	-
Ratio of lymphocyte % cover: CD68+ % cover	0.545	-0.088	0.521	-0.102	-	-
Ratio of lymphocyte size: CD68+ size	0.752	0.039	0.862	0.033	-	-
BSP+ cells estimated % cover	0.257	4.045	0.373	3.121	-	-
BSP+ cells estimated size	0.350	-0.191	0.649	0.103	0.828	0.055
BSP+ cell dispersal (location + nature)	0.234	16.295	0.259	13.551	0.240	13.868
Ratio of lymphocyte % cover: BSP+ % cover	0.135	-0.224	0.286	-0.175	0.203	-0.235
Ratio of BSP+ size: lymphocyte size	0.277	-0.164	0.649	0.069	0.828	0.024
Ratio of % cover of living: % cover of necrotic bone	0.666	-0.066	0.370	-0.148	-	-
% cover of red blood cells	0.902	0.019	0.518	-0.107	-	-

Figure 04: 38 A graph showing the mean trauma-death interval values for the categories most easily distinguishable histologically. Error bars show the standard deviation of the mean.

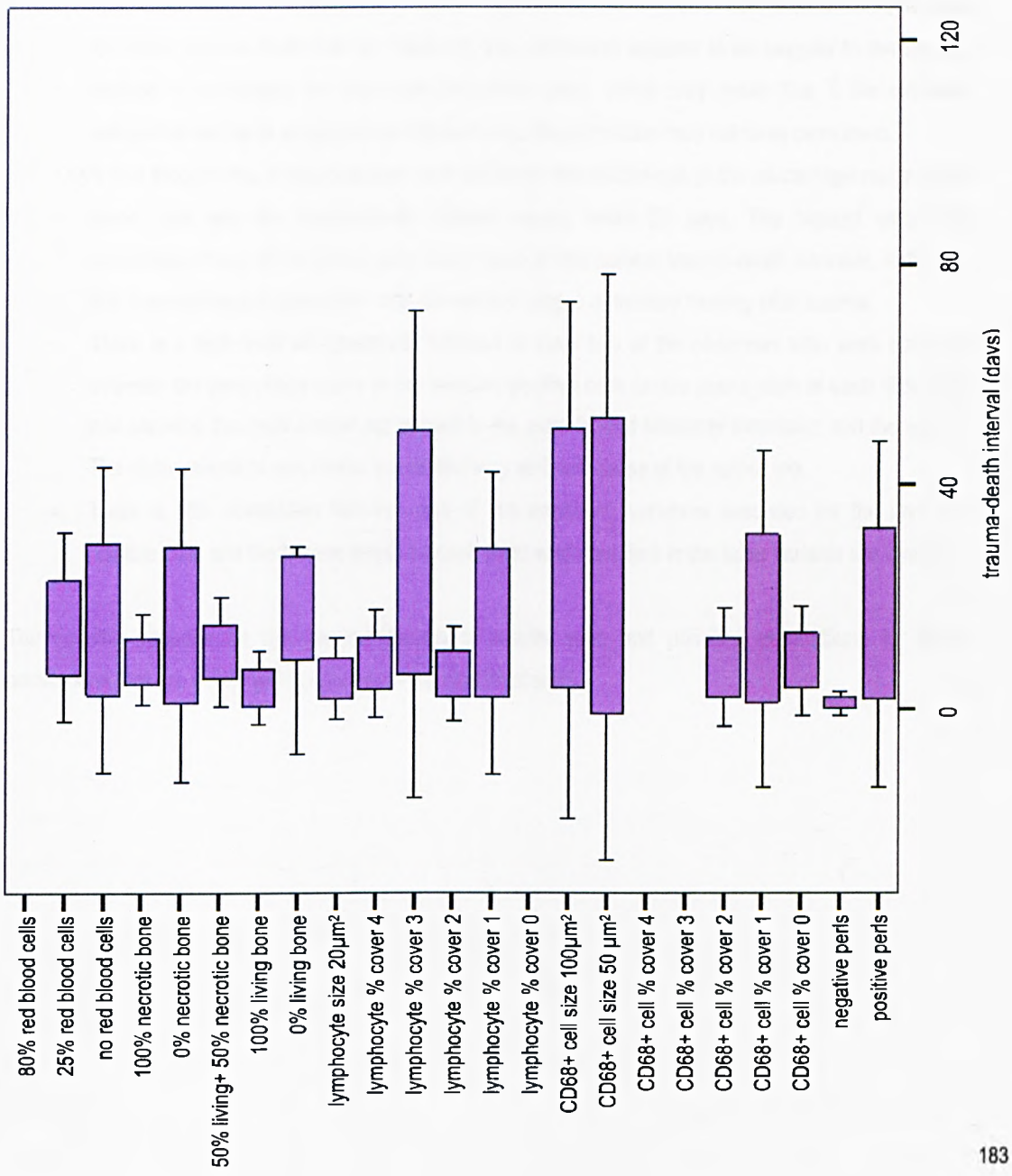

- The age of the individual is related to the trauma-death interval. There is a weak positive correlation between the two variables that is not quite statistically significant, suggesting that the older the individual, the longer the survival time.
- There appears to be a strong correlation, significant to the 95% confidence level, between the combination of the dispersal categories of the CD68+ cells and the trauma-death interval values under 25 days. This might suggest that the nature and location of the dispersal of CD68+ cells varies significantly with time since trauma, and that these variables in combination could be used to predict trauma-death interval. However, this correlation appears to be peculiar to the specific method of combining the dispersal categories used, which may mean that if the dispersal categories had been assigned in a different way, the correlation may not have been seen.
- It was thought that a vague pattern was visible on the scatter-plot of the percentage cover of red blood cells and the trauma-death interval values under 25 days. The highest values for percentage cover of red blood cells were found at the earliest trauma-death intervals, indicating that haemorrhage is associated with the earliest stages of fracture healing after trauma.
- There is a high level of agreement between at least two of the observers who were asked to estimate the percentage cover of the immuno-positive cells on the photograph of each slide. The pair showing the most overall agreement is the experienced histology technician and the author. The observations of one novice correlated very well with those of the author too.
- There is little correlation between any of the remaining variables assessed for the immuno-positive cells and the trauma-death interval, even when out-liers in the latter variable are ignored.

The possible reasons for the general pattern of results seen and possible explanations for those correlations that are visible will be discussed fully in Chapter 06.

05 : RESULTS OF QUANTITATIVE OBSERVATIONS

"Computers are useless. They can only give you answers."
Pablo Picasso (1881 - 1973)

Introduction

As described in the previous chapter, the majority of the results were gained through quantitative analysis of qualitative and semi-quantitative observations. In addition, some quantitative data about the immuno-positive cells was collected using *Scion Image* software, and subjected to statistical analysis. *Scion Image* was used as a histomorphometric analysis tool because of its status as easily available, downloadable public domain freeware with a reputation for being easy to use and accurate. It was understood that there were limitations to its capability, but these were out-weighed by its lack of cost, user-friendliness and general acceptable in scientific literature as an adequate image analysis package (Xu and Pitot, 1999; Khan, 2004).

CD68

Scion Image software was used to accurately measure the number of CD68 positive cells visible on each photograph of the fracture site, the mean size of the CD68 positive cells (in μm^2), the mean perimeter of the CD68 positive cells (in μm) and the total area covered (in μm^2) by the CD68 positive cells. As previously, these variables were compared to the trauma-death interval, to determine whether a statistically predictable relationship exists between them, which might serve as a means to estimate the trauma-death interval from the histological observations of the CD68 positive cells. Forty-nine fracture slides from 29 individuals were successfully measured using *Scion Image*.

The hypothesis behind the analyses was essentially the same as that described in Chapter 04:

> H0: there is no statistically significant relationship between the quantitative spatial properties of the CD68 positive cells and the trauma-death interval in the sample population
>
> H1: there is a statistically significant relationship between the quantitative spatial properties of the CD68 positive cells and the trauma-death interval in the sample population

CD68 positive cell number

The first variable to be examined was that of CD68 positive cell number. It was thought that the number of CD68 positive cells would be greatest at the lowest trauma-death interval values, for a number of reasons. First, the earliest stages of inflammation are characterised by a rapid influx of inflammatory cells, including

macrophages which stain positively with CD68 stain (Lydyard *et al.* 2000). These macrophages are predominantly osteoclasts, which are most abundant at a fracture site soon after the trauma, when there is the greatest amount of necrotic bone to remove. A scatter-plot investigating the relationship between macrophage number and the amount of necrotic bone is given in Figure 05: 01, but there is no clear, unmistakeable correlation.

Figure 05: 01 A scatter-plot showing the relationship between the number of CD68 positive cells and the percentage of the compact bone at the fracture site which was necrotic.

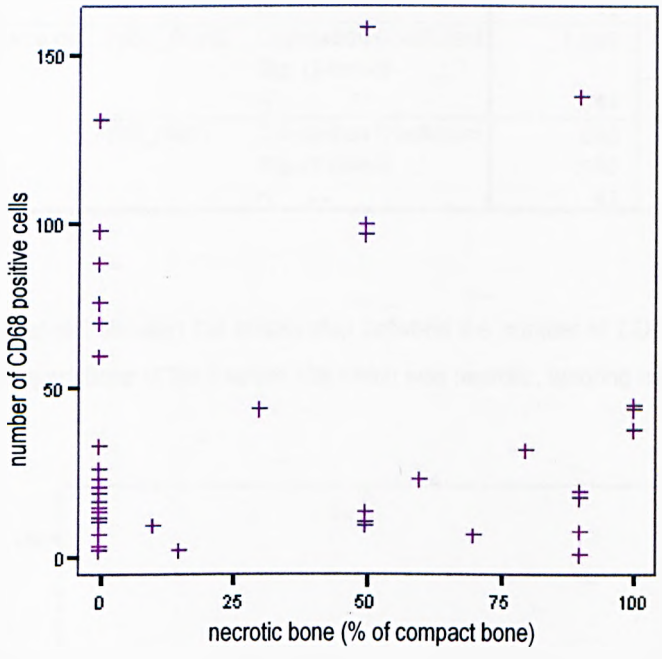

A Kendall's tau-b and Spearman's r_s correlation coefficient test (Table 05: 01) confirm that there is no statistically significant correlation between these variables. However, when we look at the same data but ignore the necrotic bone values of 0 (Figure 05: 02), we can see a clearer – although still not significant (Table 05: 02) – tendency towards a positive relationship between the number of CD68 positive cells and the necrotic bone percentages, indicating that more CD68 positive cells are found with greater amounts of necrotic bone.

Table 05: 01 Results of a Kendall's tau-b test and Spearman's r_s correlation coefficient to determine whether any correlation exists between the number of CD68 positive cells and the percentage of compact bone that was necrotic.

Correlations

			NEC_BONE	NO_PART
Kendall's tau_b	NEC_BONE	Correlation Coefficient	1.000	.070
		Sig. (2-tailed)	.	.556
		N	44	42
	NO_PART	Correlation Coefficient	.070	1.000
		Sig. (2-tailed)	.556	.
		N	42	51
Spearman's rho	NEC_BONE	Correlation Coefficient	1.000	.095
		Sig. (2-tailed)	.	.550
		N	44	42
	NO_PART	Correlation Coefficient	.095	1.000
		Sig. (2-tailed)	.550	.
		N	42	51

Figure 05: 02 A scatter-plot showing the relationship between the number of CD68 positive cells and the percentage of the compact bone at the fracture site which was necrotic, ignoring necrotic bone % values of 0.

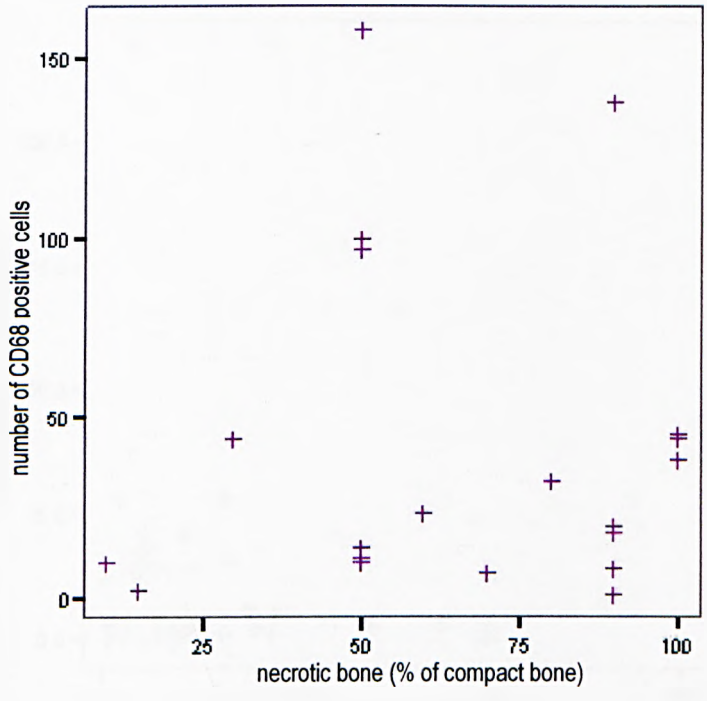

Table 05: 02 Results of a Kendall's tau-b test and Spearman's r_s correlation coefficient to determine whether any correlation exists between the number of CD68 positive cells and the percentage of compact bone that was necrotic, ignoring necrotic bone % values of 0.

Correlations

			NO_PART	NECNOT0
Kendall's tau_b	NO_PART	Correlation Coefficient	1.000	.126
		Sig. (2-tailed)	.	.463
		N	51	20
	NECNOT0	Correlation Coefficient	.126	1.000
		Sig. (2-tailed)	.463	.
		N	20	20
Spearman's rho	NO_PART	Correlation Coefficient	1.000	.150
		Sig. (2-tailed)	.	.529
		N	51	20
	NECNOT0	Correlation Coefficient	.150	1.000
		Sig. (2-tailed)	.529	.
		N	20	20

The trauma-death interval (tdi) values were plotted against the number of CD68 positive cells (see Figure 05: 03), and non-parametric correlation tests performed on the data (Table 05: 03).

Figure 05: 03 A scatter-plot showing the relationship between the trauma-death interval and the number of CD68 positive cells.

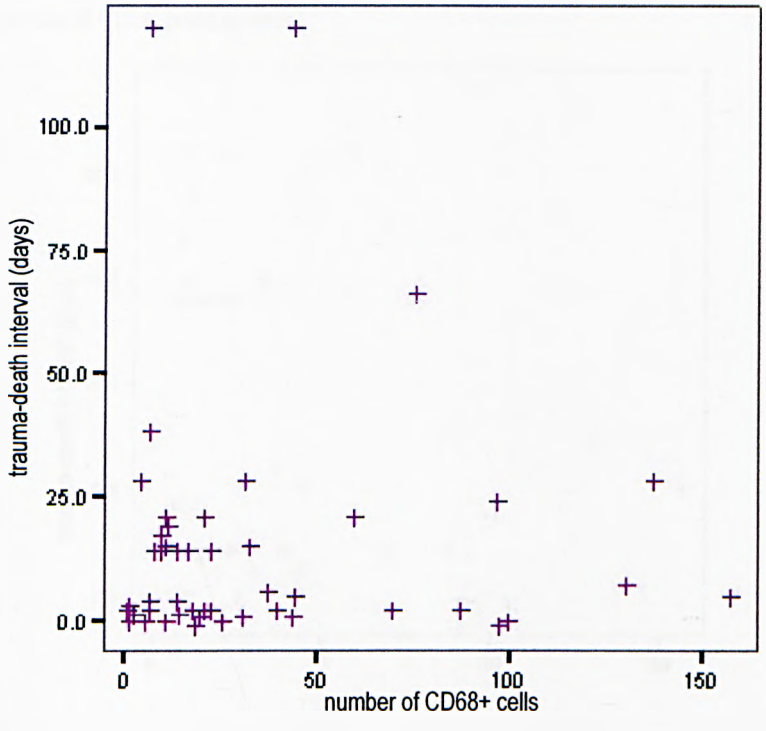

Table 05: 03 Results of a Kendall's tau-b test and Spearman's r_s correlation coefficient to determine whether any correlation exists between trauma-death interval and the number of CD68 positive cells.

Correlations

			TDI	NO_PART
Kendall's tau_b	TDI	Correlation Coefficient	1.000	.022
		Sig. (2-tailed)	.	.832
		N	49	47
	NO_PART	Correlation Coefficient	.022	1.000
		Sig. (2-tailed)	.832	.
		N	47	47
Spearman's rho	TDI	Correlation Coefficient	1.000	.038
		Sig. (2-tailed)	.	.802
		N	49	47
	NO_PART	Correlation Coefficient	.038	1.000
		Sig. (2-tailed)	.802	.
		N	47	47

Although no statistically significant correlation was seen, the clustering close to the origin of the scatter-plot suggested that it would be fruitful to look at the tdi values under 25 days (see Figure 05: 04). Again, non-parametric correlation tests were performed to quantify any correlation visible, but no statistically significant relationship was found (Table 05: 04).

Figure 05: 04 A scatter-plot showing the relationship between the trauma-death interval values under 25 days and the number of CD68 positive cells.

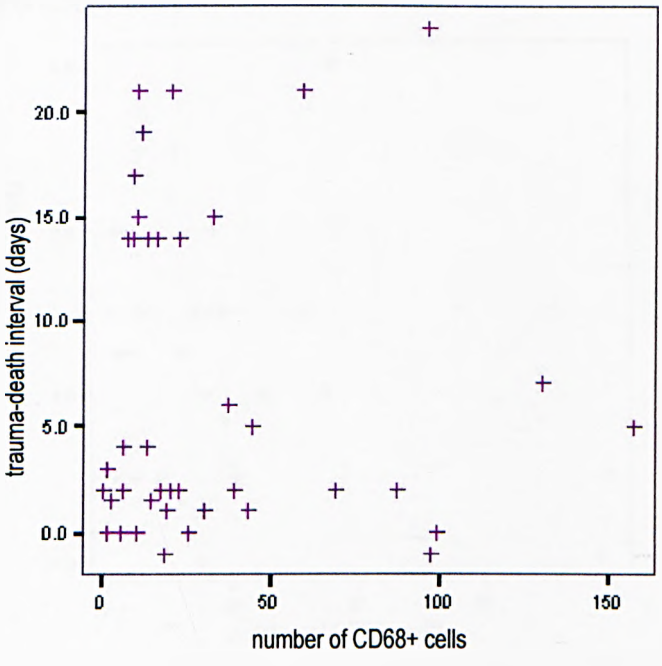

Table 05: 04 Results of a Kendall's tau-b test and Spearman's r_s correlation coefficient to determine whether any correlation exists between trauma-death interval values under 25 days and the number of CD68 positive cells.

Correlations

			TDI_25	NO_PART
Kendall's tau_b	TDI_25	Correlation Coefficient	1.000	.013
		Sig. (2-tailed)	.	.906
		N	42	40
	NO_PART	Correlation Coefficient	.013	1.000
		Sig. (2-tailed)	.906	.
		N	40	47
Spearman's rho	TDI_25	Correlation Coefficient	1.000	.011
		Sig. (2-tailed)	.	.948
		N	42	40
	NO_PART	Correlation Coefficient	.011	1.000
		Sig. (2-tailed)	.948	.
		N	40	47

Removal of the outliers of both variables was attempted, in an effort to isolate a correlation between the variables during the early trauma-death interval. A scatter-plot of trauma-death interval values under five days and number of CD68 positive cells under 100 cells was plotted (Figure 05: 05). A statistically significant correlation was still not found through the non-parametric correlation tests (Table 05: 05), but a clearer idea of the variation in CD68 positive cell number in the early trauma-death interval was gained.

Figure 05: 05 A scatter-plot showing the relationship between the trauma-death interval values under five days and the number of CD68 positive cells (1 to 100 cells only).

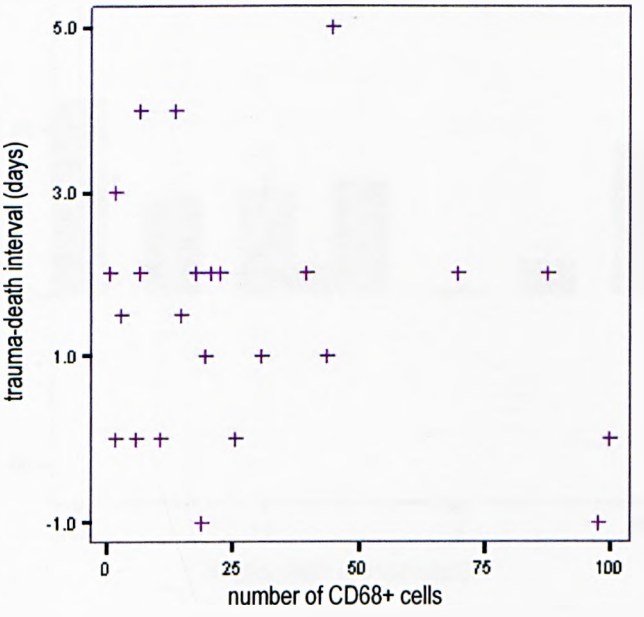

Table 05: 05 Results of a Kendall's tau-b test and Spearman's r_s correlation coefficient to determine whether any correlation exists between trauma-death interval values under 25 days and the number of CD68 positive cells (1 to 100 cells only).

Correlations

			TDI_5	NO_100
Kendall's tau_b	TDI_5	Correlation Coefficient	1.000	-.087
		Sig. (2-tailed)	.	.574
		N	26	24
	NO_100	Correlation Coefficient	-.087	1.000
		Sig. (2-tailed)	.574	.
		N	24	48
Spearman's rho	TDI_5	Correlation Coefficient	1.000	-.131
		Sig. (2-tailed)	.	.543
		N	26	24
	NO_100	Correlation Coefficient	-.131	1.000
		Sig. (2-tailed)	.543	.
		N	24	48

A graph of the mean CD68 positive cell number (under 100 cells) for each trauma-death interval value under five days is given in Figure 05: 06.

Figure 05: 06 Bar chart to show the differences in mean CD68 positive cell number (1 to 100 only) for each trauma-death interval value under five days. (Error bars represent standard deviation +/- 1.0).

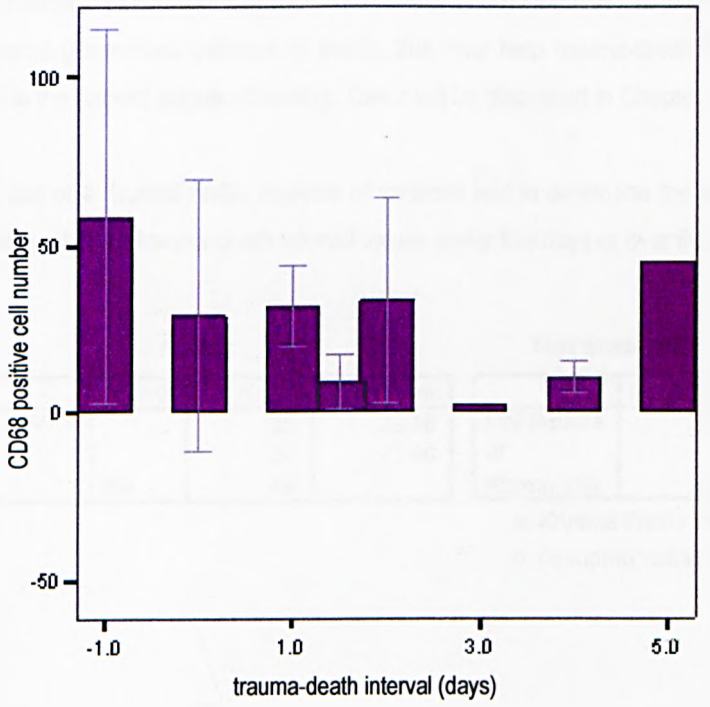

A non-parametric analysis of variance test (Kruskal-Wallis) was performed to determine whether there was a statistically significant difference between these means for each tdi category. The results are given in Table 05: 06. No statistical significance was found.

Table 05: 06 Results of a Kruskal-Wallis analysis of variance test to determine the difference in the mean CD68 positive cell number (1 to 100 only) for each trauma-death interval value under five days.

Ranks

	TDI_5	N	Mean Rank
NO_100	.0	5	10.50
	1.0	5	12.00
	2.0	8	12.94
	3.0	1	2.50
	4.0	2	7.75
	5.0	1	19.00
	Total	22	

Test Statistics[a,b]

	NO_100
Chi-Square	4.467
df	5
Asymp. Sig.	.484

a. Kruskal Wallis Test

b. Grouping Variable: TDI_5

In order to confirm that there was no statistical significance between the mean CD68 positive cell numbers and the early and later trauma-death interval values, a second analysis of variance test was performed on those tdi values under five days and those over five days. This would flag any generalised increase or decrease in CD68 positive cell numbers between the earliest and later stages of healing. The results of the Kruskal-Wallis test are given in Table 05: 07. These tests suggest that the hypothesis that the CD68 positive cell number would show a predictable correlation with trauma-death interval has to be rejected. However, it is thought that some generalised patterns or trends that may help trauma-death interval prediction are visible, especially in the earliest stages of healing. These will be discussed in Chapter 06.

Table 05: 07 Results of a Kruskal-Wallis analysis of variance test to determine the difference in the mean CD68 positive cell number for trauma-death interval values under five days or over five days.

Ranks

	TDI5BIG	N	Mean Rank
NO_PART	1	25	22.36
	2	20	23.80
	Total	45	

Test Statistics[a,b]

	NO_PART
Chi-Square	.134
df	1
Asymp. Sig.	.715

a. Kruskal Wallis Test

b. Grouping Variable: TDI5BIG

CD68 positive cell size

The next variable to be examined was that of CD68 positive cell size. Macrophages are known to increase in size as they become 'active' in areas of inflammation (Underwood, 2000). It was therefore thought that an increase in size of the CD68 positive cells should be visible at the fracture sites, especially in those cases with low trauma-death intervals. The sizes of the CD68 positive cells were measured using *Scion Image*, as described in Chapter 03. Data was generated in μm^2.

The scatter-plot of CD68 positive cell size against the whole range of trauma-death interval values is shown in Figure 05: 07. There is a considerable cluster of data points around the origin and a few outliers, and there is clearly no statistically significant correlation between the two variables (see Table 05: 08).

Figure 05: 07 A scatter-plot showing the relationship between the trauma-death interval and the mean size of the CD68 positive cells.

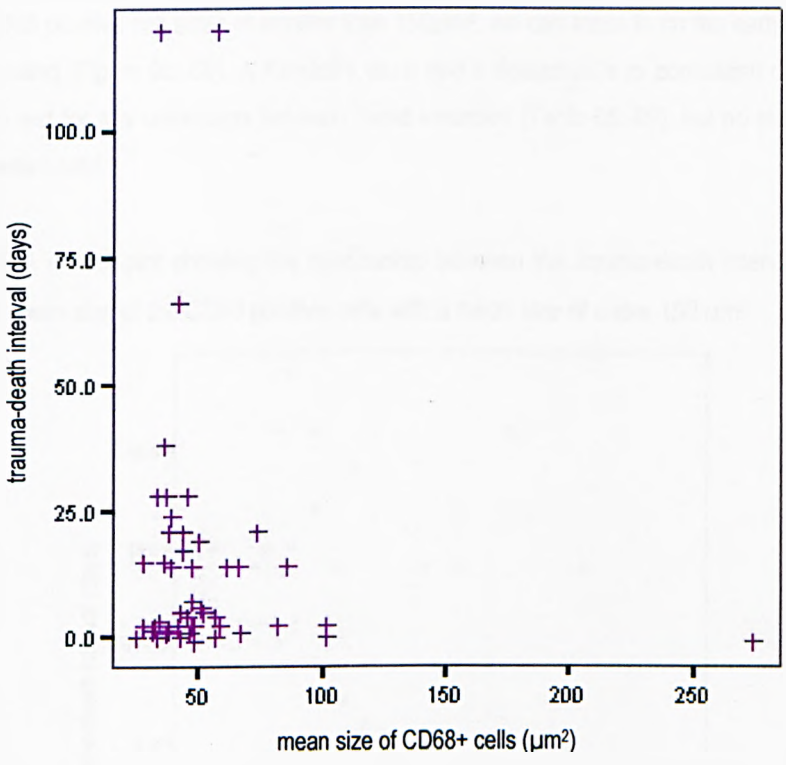

Table 05: 08 Results of a Kendall's tau-b test and Spearman's r_s correlation coefficient to determine whether any correlation exists between trauma-death interval and the mean size of the CD68 positive cells.

Correlations

			TDI	AVE_AREA
Kendall's tau_b	TDI	Correlation Coefficient	1.000	-.114
		Sig. (2-tailed)	.	.269
		N	49	47
	AVE_AREA	Correlation Coefficient	-.114	1.000
		Sig. (2-tailed)	.269	.
		N	47	47
Spearman's rho	TDI	Correlation Coefficient	1.000	-.146
		Sig. (2-tailed)	.	.328
		N	49	47
	AVE_AREA	Correlation Coefficient	-.146	1.000
		Sig. (2-tailed)	.328	.
		N	47	47

By removing the outliers of both variables, by concentrating only on trauma-death interval values under 25 days, and CD68 positive cell sizes of smaller than 150µm^2, we can focus in on the early and middle stages of fracture healing (Figure 05: 08). A Kendall's tau-b and a Spearman's rs correlation coefficient test were carried out to test for any correlation between these variables (Table 05: 09), but no statistically significant relationship was found.

Figure 05: 08 A scatter-plot showing the relationship between the trauma-death interval values under 25 days and the mean size of the CD68 positive cells with a mean size of under 150 µm^2.

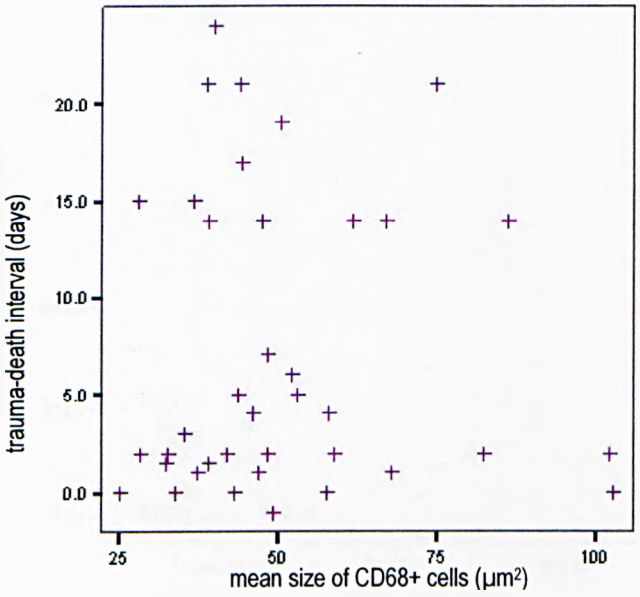

Table 05: 09 Results of a Kendall's tau-b test and Spearman's r_s correlation coefficient to determine whether any correlation exists between trauma-death interval values under 25 days and the mean size of the CD68 positive cells with a mean size of under 150 μm².

Correlations

			TDI_25	AREA_150
Kendall's tau_b	TDI_25	Correlation Coefficient	1.000	.024
		Sig. (2-tailed)	.	.836
		N	42	39
	AREA_150	Correlation Coefficient	.024	1.000
		Sig. (2-tailed)	.836	.
		N	39	46
Spearman's rho	TDI_25	Correlation Coefficient	1.000	.039
		Sig. (2-tailed)	.	.813
		N	42	39
	AREA_150	Correlation Coefficient	.039	1.000
		Sig. (2-tailed)	.813	.
		N	39	46

The length of the perimeter of the CD68 positive cells was measured as an additional size value. The trauma-death interval and the mean perimeter of the CD68 positive cells were plotted on a scatter-plot (Figure 05: 09) and the correlation value obtained (see Table 05: 10).

Figure 05: 09 A scatter-plot showing the relationship between the trauma-death interval and the mean perimeter of the CD68 positive cells.

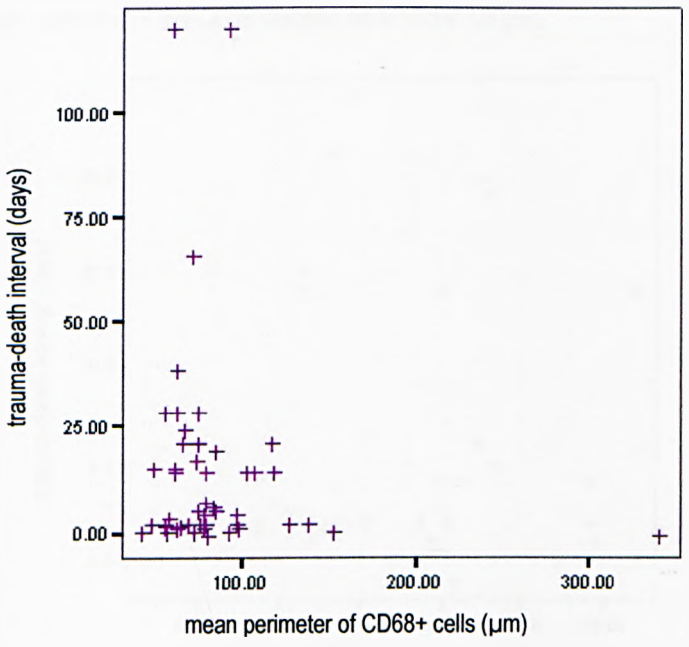

Table 05: 10 Results of a Kendall's tau-b test and Spearman's r_s correlation coefficient to determine whether any correlation exists between trauma-death interval and the mean perimeter of the CD68 positive cells.

Correlations

			TDI	AVE_PERI
Kendall's tau_b	TDI	Correlation Coefficient	1.000	-.107
		Sig. (2-tailed)	.	.302
		N	49	47
	AVE_PERI	Correlation Coefficient	-.107	1.000
		Sig. (2-tailed)	.302	.
		N	47	47
Spearman's rho	TDI	Correlation Coefficient	1.000	-.149
		Sig. (2-tailed)	.	.319
		N	49	47
	AVE_PERI	Correlation Coefficient	-.149	1.000
		Sig. (2-tailed)	.319	.
		N	47	47

Again, there was a considerable clustering of data points around the origin, and so a second scatter-plot which concentrated on the trauma-death interval values under 25 days and the CD68 positive cell perimeter values under 100µm was plotted (see Figure 05: 10), and non-parametric correlation tests for these variables performed (see Table 05: 11). Again, despite the removal of the outlying values, there was no statistically significant correlation between the two variables.

Figure 05: 10 A scatter-plot showing the relationship between the trauma-death interval values under 25 days and the mean perimeter of the CD68 positive cells under 100µm.

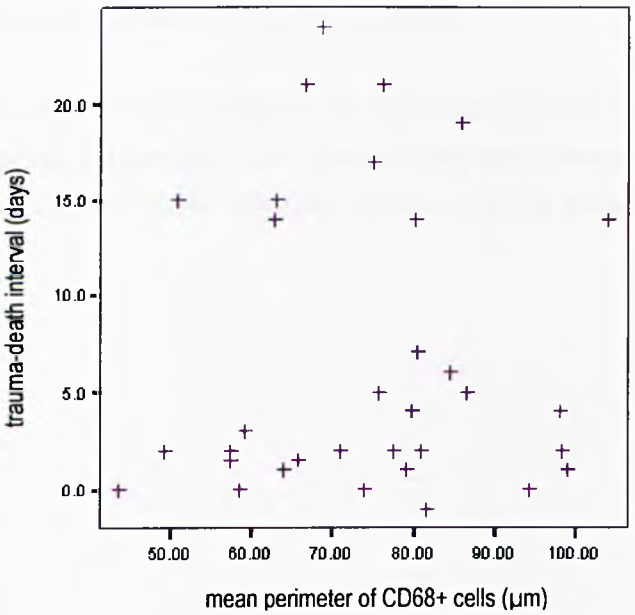

Table 05: 11 Results of a Kendall's tau-b test and Spearman's r_s correlation coefficient to determine whether any correlation exists between trauma-death interval values under 25 days and the mean perimeter of the CD68 positive cells under 100µm.

Correlations

			TDI_25	PERI_100
Kendall's tau_b	TDI_25	Correlation Coefficient	1.000	.039
		Sig. (2-tailed)	.	.755
		N	42	33
	PERI_100	Correlation Coefficient	.039	1.000
		Sig. (2-tailed)	.755	.
		N	33	40
Spearman's rho	TDI_25	Correlation Coefficient	1.000	.055
		Sig. (2-tailed)	.	.760
		N	42	33
	PERI_100	Correlation Coefficient	.055	1.000
		Sig. (2-tailed)	.760	.
		N	33	40

CD68 positive cell cover

CD68 positive cell cover was calculated using measurements of cell area generated by *Scion Image*, by dividing the total area of all the CD68 positive cells by the total area of the photograph of the fracture site. It was expected that the number and size, and therefore the general abundance of the CD68 positive cells would increase during the first week after trauma, as macrophages migrated to the area of inflammation. It was expected that there would be a steep increase in CD68 positive cell cover during the first week, followed by a plateauing of the data, as osteoclasts were still active at the fracture site resorbing necrotic bone, but no longer swamping the site in response to the trauma.

The CD68 positive cell cover was compared to the trauma-death interval values of the whole sample population, as can be seen in Figure 05: 11. Non-parametric tests were performed to establish the existence of any correlation (see Table 05: 12). No statistically significant correlation was found.

Figure 05: 11 A scatter-plot showing the relationship between the trauma-death interval and the total cover of the background by CD68 positive cells.

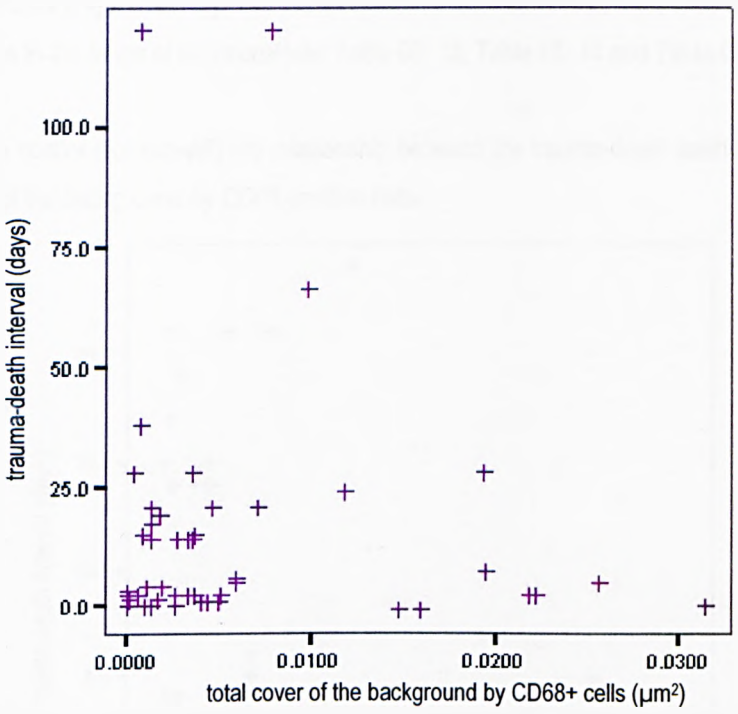

Table 05: 12 Results of a Kendall's tau-b test and Spearman's r_s correlation coefficient to determine whether any correlation exists between trauma-death interval and the total cover of the background by CD68 positive cells.

Correlations

			TDI	COVER
Kendall's tau_b	TDI	Correlation Coefficient	1.000	-.014
		Sig. (2-tailed)	.	.890
		N	49	47
	COVER	Correlation Coefficient	-.014	1.000
		Sig. (2-tailed)	.890	.
		N	47	47
Spearman's rho	TDI	Correlation Coefficient	1.000	-.028
		Sig. (2-tailed)	.	.851
		N	49	47
	COVER	Correlation Coefficient	-.028	1.000
		Sig. (2-tailed)	.851	.
		N	47	47

As the data points were clustered close to the origin, it seemed appropriate to gradually focus the attention on those data points for tdi values smaller than 25 days (see Figure 05: 12), then 15 days (Figure 05: 13) and finally five days (Figure 05: 14). The non-parametric correlation tests were also performed for each of these reductions in the range of tdi values (see Table 05: 13, Table 05: 14 and Table 05: 15).

Figure 05: 12 A scatter-plot showing the relationship between the trauma-death interval under 25 days and the total cover of the background by CD68 positive cells.

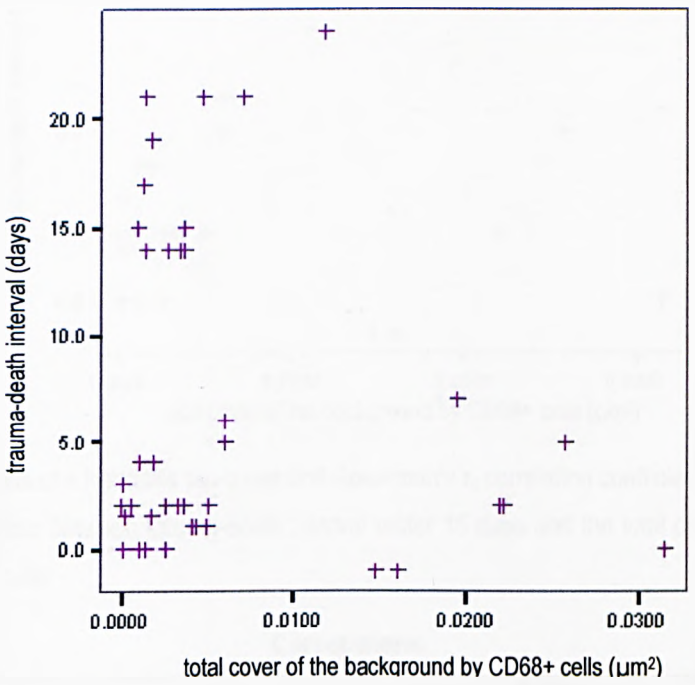

Table 05: 13 Results of a Kendall's tau-b test and Spearman's r_s correlation coefficient to determine whether any correlation exists between trauma-death interval under 25 days and the total cover of the background by CD68 positive cells.

Correlations

			TDI_25	COVER
Kendall's tau_b	TDI_25	Correlation Coefficient	1.000	-.005
		Sig. (2-tailed)	.	.963
		N	42	40
	COVER	Correlation Coefficient	-.005	1.000
		Sig. (2-tailed)	.963	.
		N	40	47
Spearman's rho	TDI_25	Correlation Coefficient	1.000	-.023
		Sig. (2-tailed)	.	.888
		N	42	40
	COVER	Correlation Coefficient	-.023	1.000
		Sig. (2-tailed)	.888	.
		N	40	47

Figure 05: 13 A scatter-plot showing the relationship between the trauma-death interval under 15 days and the total cover of the background by CD68 positive cells.

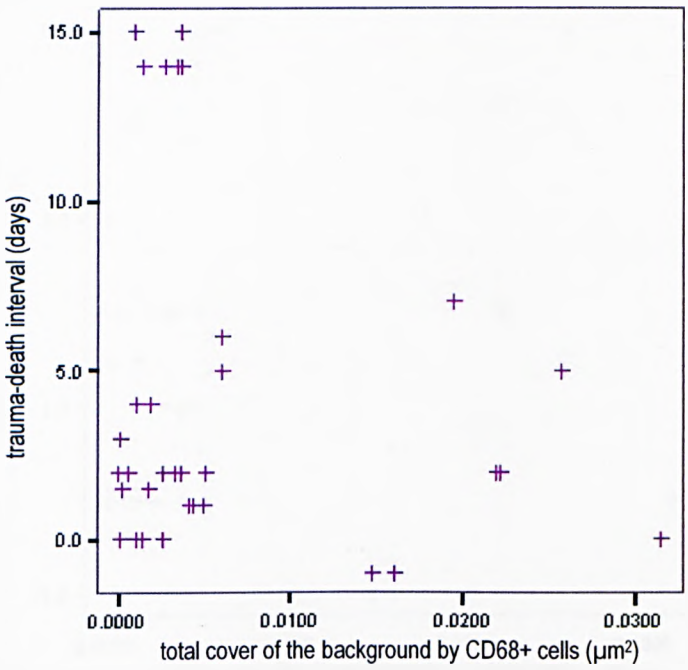

Table 05: 14 Results of a Kendall's tau-b test and Spearman's r_s correlation coefficient to determine whether any correlation exists between trauma-death interval under 15 days and the total cover of the background by CD68 positive cells.

Correlations

			TDI_15	COVER
Kendall's tau_b	TDI_15	Correlation Coefficient	1.000	-.043
		Sig. (2-tailed)	.	.730
		N	36	34
	COVER	Correlation Coefficient	-.043	1.000
		Sig. (2-tailed)	.730	.
		N	34	47
Spearman's rho	TDI_15	Correlation Coefficient	1.000	-.066
		Sig. (2-tailed)	.	.711
		N	36	34
	COVER	Correlation Coefficient	-.066	1.000
		Sig. (2-tailed)	.711	.
		N	34	47

Figure 05: 14 A scatter-plot showing the relationship between the trauma-death interval under five days and the total cover of the background by CD68 positive cells.

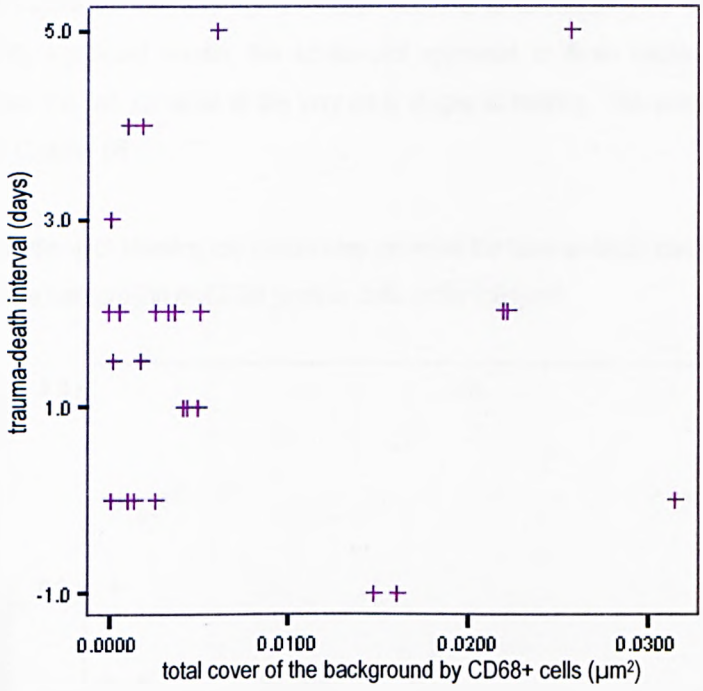

Table 05: 15 Results of a Kendall's tau-b test and Spearman's r_s correlation coefficient to determine whether any correlation exists between trauma-death interval under five days and the total cover of the background by CD68 positive cells.

Correlations

			TDI_5	COVER
Kendall's tau_b	TDI_5	Correlation Coefficient	1.000	-.025
		Sig. (2-tailed)	.	.867
		N	26	25
	COVER	Correlation Coefficient	-.025	1.000
		Sig. (2-tailed)	.867	.
		N	25	47
Spearman's rho	TDI_5	Correlation Coefficient	1.000	-.043
		Sig. (2-tailed)	.	.838
		N	26	25
	COVER	Correlation Coefficient	-.043	1.000
		Sig. (2-tailed)	.838	.
		N	25	47

The independent variable was also adjusted to remove outliers that might be skewing the results, so another scatter-plot of trauma-death interval values under five days against CD68 positive cell cover under 0.01μm² was plotted (see Figure 05: 15), and the correlation coefficients calculated (see Table 05: 16). Despite a lack of statistically significant results, the scatter-plot appeared to show evidence of a weak positive correlation between the two variables at the very early stages of healing. This possible relationship will be discussed fully in Chapter 06.

Figure 05: 15 A scatter-plot showing the relationship between the trauma-death interval under five days and the total cover of the background by CD68 positive cells under 0.01μm².

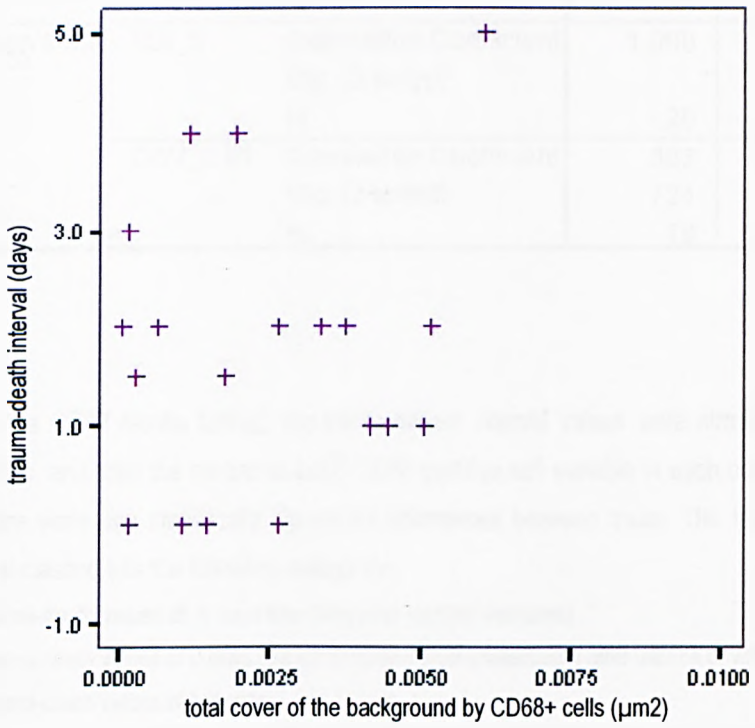

Table 05: 16 Results of a Kendall's tau-b test and Spearman's r_s correlation coefficient to determine whether any correlation exists between trauma-death interval under five days and the total cover of the background by CD68 positive cells under 0.01μm².

Correlations

			TDI_5	COV_0.01
Kendall's tau_b	TDI_5	Correlation Coefficient	1.000	.070
		Sig. (2-tailed)	.	.692
		N	26	19
	COV_0.01	Correlation Coefficient	.070	1.000
		Sig. (2-tailed)	.692	.
		N	19	38
Spearman's rho	TDI_5	Correlation Coefficient	1.000	.087
		Sig. (2-tailed)	.	.724
		N	26	19
	COV_0.01	Correlation Coefficient	.087	1.000
		Sig. (2-tailed)	.724	.
		N	19	38

Summary

To interrogate the CD68 results further, the trauma-death interval values were stratified into a range of ranked categories, and then the means of each CD68 positive cell variable in each category compared to establish if there were any statistically significant differences between them. The trauma-death interval values were first classed into the following categories:

-1: trauma-death values of -1 days (denoting post-mortem fractures)

0: trauma-death values of 0 days (denoting death either immediately after trauma or within 24 hours)

1: trauma-death values of between 1 and 7 days

2: trauma-death values of between 8 and 14 days

3: trauma-death values of between 15 and 25 days

4: trauma-death values of between 25 and 70 days

5: trauma-death values of 71 days and over

A non-parametric analysis of variance test was performed to compare these trauma-death interval categories with the mean values of CD68 positive cell number, mean size, mean perimeter length and cover. The results of this are tabulated in Table 05: 17. Despite the stratifying of the categories in the hope of amplifying any differences in the variable means, no statistically significant results were obtained.

Table 05: 17 Results of a Kruskal-Wallis analysis of variance test to determine the difference in the mean CD68 positive cell number, mean size, mean perimeter length and cover for each trauma-death interval category (-1 to 5).

Ranks

	TDI_CAT	N	Mean Rank
NO_PART	-1	2	33.00
	0	5	19.30
	1	20	25.17
	2	5	18.10
	3	8	24.63
	4	5	26.10
	5	2	22.00
	Total	47	
AVE_AREA	-1	2	39.00
	0	5	21.80
	1	20	24.75
	2	5	33.20
	3	8	20.38
	4	5	14.40
	5	2	22.50
	Total	47	
AVE_PERI	-1	2	39.00
	0	5	22.00
	1	20	24.80
	2	5	32.40
	3	8	20.88
	4	5	14.20
	5	2	22.00
	Total	47	
COVER	-1	2	40.50
	0	5	18.90
	1	20	25.13
	2	5	20.10
	3	8	23.38
	4	5	23.60
	5	2	22.25
	Total	47	

Test Statistics[a,b]

	NO_PART	AVE_AREA	AVE_PERI	COVER
Chi-Square	2.701	7.867	7.457	4.185
df	6	6	6	6
Asymp. Sig.	.845	.248	.281	.652

a. Kruskal Wallis Test

b. Grouping Variable: TDI_CAT

The categories into which the trauma-death interval values had been placed were further adjusted to make larger data sets, as below:

-1: trauma-death values of -1 days (denoting post-mortem fractures)

0: trauma-death values of 0 days (denoting death either immediately after trauma or within 24 hours)

1: trauma-death values of between 1 and 7 days

2: trauma-death values of between 8 and 14 days

3: trauma-death values of 15 days and over

Again, the means of each CD68 positive cell variable in each trauma-death interval category were compared, and an analysis of variance Kruskal-Wallis test performed (see Table 05: 18). Even with these

less discriminatory categories, no statistical significant difference was found between the CD68 cell parameters.

Table 05: 18 Results of a Kruskal-Wallis analysis of variance test to determine the difference in the mean CD68 positive cell number, mean size, mean perimeter length and cover for each trauma-death interval category (-1 to 3).

Ranks

	TDI_CAT2	N	Mean Rank
NO_PART	-1	2	33.00
	0	5	19.30
	1	20	25.17
	2	5	18.10
	3	15	24.77
	Total	47	
AVE_AREA	-1	2	39.00
	0	5	21.80
	1	20	24.75
	2	5	33.20
	3	15	18.67
	Total	47	
AVE_PERI	-1	2	39.00
	0	5	22.00
	1	20	24.80
	2	5	32.40
	3	15	18.00
	Total	47	
COVER	-1	2	40.50
	0	5	18.90
	1	20	25.13
	2	5	20.10
	3	15	23.30
	Total	47	

Test Statistics[a,b]

	NO_PART	AVE_AREA	AVE_PERI	COVER
Chi-Square	2.572	7.103	6.602	4.170
df	4	4	4	4
Asymp. Sig.	.632	.131	.158	.383

a. Kruskal Wallis Test

b. Grouping Variable: TDI_CAT2

A summary table of all the significance (p) values is included (see Table 05: 19). It is possible to see that the null hypothesis, stated earlier as

> H0: there is no statistically significant relationship between the quantitative spatial properties of the CD68 positive cells and the trauma-death interval in the sample population

has to be accepted. However, there appear to be some trends and patterns within the data that although they are not statistically significant, are interesting and informative none-the-less.

Table 05: 19 A summary of the p values obtained after Spearman's r_s correlation coefficient statistical analyses.

(Kruskal-Wallis tests performed).

Independent variable	Trauma-death interval (p values for significance)			
	Whole range of values	Values ≤ 25 days	Values ≤ 15 days	Values ≤ 5 days
Number of CD68+ cells	0.802 0.845	0.948	0.898	0.997
Number of CD68+ cells (1-100 cells only)	0.875 0.866	0.848	0.497	0.543 0.484
CD68+ cell mean size (μm²)	0.328 0.248	0.825	0.869	0.829
CD68+ cell mean size (under 150μm²)	0.554 0.432	0.813	0.739	0.755
CD68+ cell mean perimeter (μm)	0.319 0.281	0.891	0.916	0.829
CD68+ cell mean perimeter (under 100μm)	0.723 0.610	0.760	0.702	0.533
CD68+ cell cover	0.851 0.652	0.888	0.711	0.838
CD68+ cell cover (under 0.01)	0.373 0.812	0.342	0.533	0.724

Multiple regression analysis

Multiple regression analysis of the variables measured using *Scion Image* was attempted in order to discover if any of them could aid the retrospective prediction of the trauma-death interval, and supplement the findings of the simple correlations already attempted. Table 05: 20 shows a summary of the SPSS output for the multiple regression analysis. The errors for both the dependent and independent variables were assumed to be normally distributed. The correlation tables show that there are no statistically significant correlations between any of the CD68+ cell variables measured using *Scion Image* and the trauma-death interval. There appear to be weak negative correlations between the trauma-death interval and the average area, average perimeter of the CD68+ cells, as well as with the total area of the background covered by the CD68+ cells. There are obviously strong, statistically significant correlations between the size variables themselves. There is also a weak positive correlation between the trauma-death interval and the age of the individual, which has been noted before.

The multiple regression analysis obtained an R^2 value of 0.064 (adjusted R^2 value of 0.05), and a significance level of 0.726. None of the regression coefficients contributed significantly to the prediction of the trauma-death interval through regression. The highest *t* value was associated with the age variable, but its contribution was not significant to the 95% confidence level, as these values include zero.

Bone Sialoprotein

As the majority of information that could be gained from the BSP-stained slides has been described in the preceding chapter, the quantitative analysis of the data was confined to quantifying the difference between the fracture cases and the normal bone controls. Quantification was only possible of variables that the fracture cases and the normal controls shared, for example, estimated cover of BSP positive cells, and estimated cover of lymphocyte cells. Because the normal control sections were taken from un-fractured bone specimens, the controls could not be given a meaningful trauma-death interval value. This meant that the relationship between the spatial variables and the trauma-death interval could not be assessed for the controls, nor could they be compared between the fractured sample and the normal sample.

The means of each of the numerical variables such as BSP cover (given as a number on a scale of 0 to 4), lymphocyte cover (also given as a number on the 0 to 4 scale), the ratio of lymphocyte size: BSP positive cell size, and the estimated percentage cover of red blood cells were compared to the means for those variables in the normal BSP controls, using a non-parametric analysis of variance test (Kruskal-Wallis). The

Table 05: 20 A summary of the SPSS output showing correlations between the trauma-death interval and the CD68+ cell variables, with the R^2 value (n = 47 for all correlations).

Correlations

		TDI	AGE	NO_PART	AVE_AREA	AVE_PERI	COVER
Pearsor Correlation	TDI	1.000	.207	.007	-.131	-.128	-.076
	AGE	.207	1.000	.202	-.009	-.020	.047
	NO_PART	.007	.202	1.000	.077	.099	.877
	AVE_AREA	-.131	-.009	.077	.000	.995	.433
	AVE_PERI	-.128	-.020	.099	.995	1.000	.457
	COVER	-.076	.047	.877	.433	.457	1.000
Sig. (1-tailed)	TDI	.	.082	.482	.190	.195	.307
	AGE	.082	.	.087	.475	.446	.377
	NO_PART	.482	.087	.	.304	.253	.000
	AVE_AREA	.190	.475	.304	.	.000	.001
	AVE_PERI	.195	.446	.253	.000	.	.001
	COVER	.307	.377	.000	.001	.001	.

Model Summary[b]

Model	R	R Square	Adjusted R Square	Std. Error of the Estimate
1	.254[a]	.064	-.050	26.4122

a. Predictors: (Constant), COVER, AGE, AVE_AREA, NO_PART, AVE_PERI

b. Dependent Variable: TDI

ANOVA[b]

Model		Sum of Squares	df	Mean Square	F	Sig.
1	Regression	1971.787	5	394.357	.565	.726[a]
	Residual	28601.713	41	697.603		
	Total	30573.500	46			

a. Predictors: (Constant), COVER, AGE, AVE_AREA, NO_PART, AVE_PERI

b. Dependert Variable: TDI

Table 05: 20 continued.

Coefficients[a]

Model		Unstandardized Coefficients		Standardized Coefficients	t	Sig.	95% Confidence Interval for B	
		B	Std. Error	Beta			Lower Bound	Upper Bound
1	(Constant)	4.560	23.057		.198	.844	-42.005	51.126
	AGE	.152	.126	.204	1.210	.233	-.102	.406
	NO_PART	5.022E-02	.324	.076	.155	.878	-.604	.704
	AVE_AREA	-.494	1.080	-.714	-.457	.650	-2.676	1.688
	AVE_PERI	.370	.919	.642	.403	.689	-1.486	2.227
	COVER	-457.095	1812.113	-.136	-.252	.802	-4116.731	3202.541

a. Dependent Variable: TDI

results of this test are tabulated in Table 05: 21. Two statistically significant results were obtained – there was a significant difference (to the 95% confidence level) between the mean lymphocyte cover value for the fracture cases and the normal controls, and for the mean size ratio value between the fracture cases and the normal control samples.

Table 05: 21 Results of a Kruskal-Wallis analysis of variance test to determine the difference in the means of BSP positive cell cover, lymphocyte cover, *ratio of lymphocyte size: BSP positive cell size*, and the estimated percentage cover of red blood cells and the means for the same variables in the normal BSP controls (1 = case, 2 = control).

Ranks

	TYPE	N	Mean Rank
BSP_COV	1	49	25.78
	2	2	31.50
	Total	51	
SMLL_COV	1	49	25.24
	2	2	48.50
	Total	53	
	3	2	48.50
SIZE_RAT	1	49	25.10
	2	2	48.00
	Total	51	
RBC	1	49	26.67
	2	2	28.00
	Total	53	
	3	2	34.00

Test Statistics[a,b]

	BSP_COV	SMLL_COV	SIZE_RAT	RBC
Chi-Square	.372	10.050	4.914	.484
df	1	2	1	2
Asymp. Sig.	.542	.007	.027	.785

a. Kruskal Wallis Test

b. Grouping Variable: TYPE

Summary

Two main conclusions can be drawn from the quantitative analysis attempted here.

- There is no evidence of any statistically significant relationship between any of the quantifiable spatial variables and the trauma-death interval values for the immunohistochemically-stained fracture slides. This means that the null hypothesis

  H0: there is no statistically significant relationship between the quantitative spatial properties of the immuno- positive cells and the trauma-death interval in the sample population

  has to be accepted.

- There are, however, two statistically significant differences apparent when some of the mean values for the spatial variables of the BSP-stained fracture slides are compared to the same variables in the BSP-stained normal bone control slides. The ratio of BSP+ cell size: lymphocyte cell size, and the percentage cover of red blood cells show differences significant to the 95%

confidence level between the two sample sets. The possible reasons for the apparent differences will be discussed in Chapter 06.

Although few results are statistically significant, there are a few trends and patterns within the data that may shed light on the immediate microscopic phenomena that occur as bone responds to trauma. These will be discussed in Chapter 06.

06: DISCUSSION

"In theory, there is no difference between theory and practice; in practice, there is."
Chuck Reid

Introduction

The basic aim of this investigation into the histological analysis of fracture healing was to examine the nature of the relationship between the histological features associated with fracture healing and the time elapsed since fracture, or the trauma-death interval (tdi). The hypothesis of this research was based on the common sense premise that there should be a correlation between the abundance, size and distribution of osteoclasts, osteoblasts and haemosiderin granules and the trauma-death interval. The null hypothesis was that there would be no statistically significant correlation between any of these features and the trauma-death interval. Some additional specific variables relating to the fracture were also examined, to test whether the age and sex of the individual, or fracture type or fracture aetiology had any effect on the trauma-death interval.

An interpretation of the quantitative results obtained from the qualitative and quantitative observations taken is presented, as well as a thorough analysis of the considerations and limitations of the experimental procedures, with reference to how the research methodology could have been improved.

Sample population

The sample population appears to be unusual in its composition and characteristics. It is not normally distributed, and there is an atypical spread of ages, sexes and ethnic affiliation. These irregularities are undoubtedly the result of the stringent selection criteria imposed on the Medico-Legal Centre autopsy records for inclusion in the study. The selection procedures have produced a sample population which is biased towards infants and the elderly, and there is an exaggerated number of individuals in the study with fractures caused by non-accidental injury or osteoporosis.

Age

The distribution of ages in the sample population does not fit with Gaussian Normality, as can be seen from Figure 03: 01. There is an unusually high proportion of individuals under the age of one year (n = 7, 24.13%), as well as over-representation of individuals over 70 years of age. This age distribution appears to be a function of the sample selection procedure. Only a limited number of fracture cases from the Medico-Legal Centre (MLC) archives fitted the criteria for inclusion in this study, and the main criterion was a known trauma-death interval. For the majority of forensic cases reviewed, trauma-death

interval was not conscientiously recorded, except in cases of suspected child abuse. This explains the high percentage of infants under the age of one year. The over-representation of elderly individuals is most likely due to the fact that osteoporotic fractures of the femoral neck are extremely common, and good records of the events preceding and succeeding the trauma are usually available. Also, histological samples of osteoporotic fractures are taken more often by pathologists than other fractures, which contributed to their inclusion in the sample. The absence of individuals between the ages of 10 and 29 is also quite conspicuous, as this is an age group particularly prone to traumatic incidents, whether they are traffic accidents, sporting or stunt accidents or deliberate inter-personal assaults. An explanation for this may be that, in these cases, the cause of death is made obvious by the circumstances, and the pathologists deem it unnecessary to investigate further into the nature of the injuries by collecting fracture samples. As a result, there may be a void in the archived autopsy records of such cases with accompanying histology samples.

The age of the individual appears to have an effect on the trauma-death interval. Although a statistically significant relationship was not found between the age values of the sample population and the full range of trauma-death interval values (see Table 03: 02 and Figure 03: 07), a general trend was visible. The scattergraph shows a tight cluster of data points around the origin, suggesting that the youngest individuals survived the shortest time – less than 24 hours. There is also a clear grouping of data points at the other end of the age spectrum, again concentrated around the 0 days trauma-death interval mark. This suggests that the oldest individuals also survived a very short time. This complies with common sense, that the oldest and youngest individuals are the weakest and most vulnerable to death after trauma. The data points on the scattergraph only spread out from hugging the y-axis and the 0 days trauma-death interval value in the middle of the age spectrum. According to this sample, middle-aged individuals, between about 45 and 60 years old, appear to survive the longest after trauma. The individuals with the longest trauma-death interval values of 120 and 66 days were both 57 years old.

It was thought that the inclusion of large trauma-death interval values in the data set might mask any correlations between age and trauma-death interval in the earliest stages of healing, so the tdi values over 25 days were removed from the data set to test this theory. A scattergraph of trauma-death interval values under 25 days was plotted against the age of the individual (see Figure 03: 09). It was hoped that a clearer picture of how age affects the trauma-death interval soon after trauma would become visible. Indeed, the non-parametric correlation tests (Kendall's tau-b and Spearman's r_s correlation coefficient tests, see Table 03: 03) suggested that there was a statistically significant positive correlation between the age of the individual and the trauma-death interval under 25 days. This means that, in the first 25 days after trauma, the older the individual, the longer the survival time expected after trauma. Again, this complies with common knowledge, and reiterates the vulnerability

of the youngest infants in the first few hours after trauma. The first hours after trauma or admission to hospital are known to be the most critical in determining a positive outcome, and much research has been focussed on determining the factors affecting survivorship during these hours (Quigley *et al.* 1997). Age is thought to be a very significant factor, and while there is much literature on the inverse relationship between advancing age and positive outcome, this is confined to older adults. In infants and children, the reverse appears to be true.

Sex

The distribution of the sexes in the sample population was roughly equal. This is likely to be due to the inclusion of a high number of elderly post-menopausal women with osteoporotic fractures in the sample, and a high number of female victims of child abuse. Half of the female individuals in the sample were over 70 years old, and just under half (n = 6, 42.9%) were under one year of age. The age distribution of male individuals was very different, with only one male infant the victim of child abuse, but 8 individuals (53.33%) in the middle age range, between 40 and 70 years old. The low number of male infants believed to be the victims of child abuse is surprising, given the national tendency for boys to be over-represented on registers of infant victims of physical abuse (Creighton, 1992). This abnormal phenomenon may just be due to the fact that the sample size is small and is not a true representation of a cross section of the population of Sheffield and its surrounding in the last 12 years.

An analysis of the effect of sex on the trauma-death interval revealed that the mean trauma-death interval for female individuals was 13.96 days (n = 13, s.d. = 18.54), and for male individuals was 17.85 days (n = 13, s.d. = 32.59). This result was not statistically significant (ANOVA p value = 0.712), but suggests that male victims of fracture have a tendency towards slightly longer survival times. This may however, simply reflect the low number of male infant victims and a higher number in the less vulnerable middle-aged group. Both of the individuals with very high trauma-death interval values (66 and 120 days) were male.

Ethnic affiliation

The representation of different ethnic groups in the sample is an unrealistic portrayal of the true ethnic composition of the Sheffield population. A higher proportion of Asian and Afro-Caribbean individuals would have been expected. This apparent under-representation of non-White individuals is perhaps due to a failure on behalf of the pathologists to accurately record the ethnic appearance of the deceased (see Figure 03: 02). The ethnic affiliation of the individuals is likely to have often been guessed by the pathologist or police officer on duty, and has subsequently become 'fact' once written down. In many situations, it would not have been easy for the pathologists to accurately determine the true ancestral affiliation of the deceased, especially if relatives or friends were absent from the

proceedings, and so the archived autopsy records at the Medico-Legal Centre may not demonstrate the true ethnic composition of the sample.

There does not appear to be a clear relationship between ethnic affiliation and the trauma-death interval based on an analysis of this sample population. A Kruskal-Wallis test to compare the mean trauma-death interval values for each of the ethnicity categories revealed a result which was not statistically significant (p value = 0.891). However, the paucity of the information in the autopsy records may have contributed to this result, as the working sample size for this analysis was only 16 individuals. There may be scope for more research into the effect, if any, of ethnicity on survival rates after trauma.

Fracture number

Figure 03: 03 shows us that just over half of the individuals included in the study exhibited multiple fractures. Each individual had a least one fracture, and ten individuals exhibited an additional fracture, 4 had two fractures and a single individual (a three month old female child abuse victim) exhibited six fractures in total. Multiple rib fractures are very common in victims of non-accidental injury, and 38.46% of those with multiple fractures were infants. Multiple fractures are also commonly associated with osteoporosis, which has obviously contributed to the high proportion of polytrauma in the sample. The occurrence of multiple fractures exhibited by the same individual raised the working fracture sample size from 29 to 52 fractures in total.

A Kruskal-Wallis test comparing the mean trauma-death interval values of the cases with different number of fractures exhibited by the individuals showed a statistically insignificant result (p value = 0.358), suggesting that the number of fractures does not affect the overall survival time, or that other factors are more important in determining the trauma-death interval. This is a surprising result, as common sense suggests that victims of polytrauma would survive for shorter lengths of time due to the massive onslaught of multiple fractures for their bodies to heal.

Fracture location

Figure 03: 05 shows the relative frequencies of fractures of different bones, and the secondary fractures associated with them. It shows that fractures were most commonly found on multiple ribs, and found in conjunction with sternal, hyoid, humerus and pelvic fractures. Skull fractures were most frequently found with other skull and hyoid fractures, and femoral fractures were associated with rib fractures. Clavicle and vertebral fractures appeared to be found alone. The disproportionate frequency of rib fractures represents the contribution made to the sample by child abuse victims.

It was hypothesised that fracture location would have an effect on the trauma-death interval, as fractures in some locations are indicative of more serious injury than others. For example, it would be expected that skull fractures would be associated with shorter survival times, as they often found in cases where the individual has suffered severe brain injury as well. Also, debilitating fractures such as femoral or pelvic fractures were thought to be potentially linked with shorter survival times, as they can be associated with conditions such as broncho-pneumonia, often brought on by the immobility caused by the fracture. It was also expected that multiple fractures would be harder to recover from, and would be correlated with lower trauma-death interval values. Two statistical tests, ANOVA and Kruskal-Wallis tests for differences in the mean trauma-death interval values (under 25 days) for each fracture location category were performed (see Tables 03: 04 and 03: 05), but neither test produced statistically significant results. Despite this, it is possible to infer from Figure 03: 10 that these expectations were met by the sample population data. The lowest trauma-death interval values were indeed associated with the occurrence of skull fractures, multiple fractures of the ribs and single rib fractures. The longest trauma-death interval values were associated with less debilitating fractures such as those of the clavicle. The low trauma-death interval values found in conjunction with skull and multiple rib fractures represent those individuals in the sample who are either infant victims of non-accidental injury or adult victims of high impact trauma, such as road traffic accidents or falls from a height.

Fracture aetiology

The fractures exhibited by individuals in the sample population originated from a wide range of aetiologies (see Figure 03: 04). The relative frequencies of these aetiological factors appear to coincide with the causes of fracture known to be most prevalent world-wide, such as falls, and in infants, non-accidental injury. However, road traffic accidents would have been expected to contribute more substantially to the cause of fractures than is seen. Inter-personal assault plays a surprisingly important role as an aetiological factor, but this mirrors what was found during the pilot study looking at the aetiology of skull fractures (see Chapter 02).

Again, it was expected that a correlation would exist between fracture aetiology and the trauma-death interval, as fracture aetiology is often an indicator of the severity of the fracture. For example, high impact causal factors such as road traffic accidents, falls from a height, collision with a tram and non-accidental injury would be expected to cause serious injuries that would be correlated negatively with the trauma-death interval. Table 03: 06 shows the results of a Kruskal-Wallis test to determine the existence of any statistically significant difference between the mean trauma-death interval values (under 25 days) for each aetiological category. Despite a lack of statistical significance, there are general patterns visible. The lowest trauma-death interval values are obviously associated with resuscitation and undertaker's fractures (as the survival time was negative in these cases), but also with fractures caused by falls and assaults. These results are likely to have been compounded by the

fact that there were only one or two individuals in most of the aetiology categories, and so their tdi values are weighted too heavily by the statistics tests.

The trauma-death interval

The distribution of the trauma-death interval values of the sample can be seen tabulated in Figure 03: 06. This graph confirms the lack of Gaussian Normal distribution to the values which was tested using the Kolmogorov-Smirnov test (see Table 03: 01). It also shows us that there is an apparent exponential decline in the number of individuals surviving as trauma-death interval increases. This means that the greatest number of individuals survived the shortest time – less than 24 hours – and the smallest number survived the longest time – 120 days after trauma. This is to be expected, as the vast majority of the sample population are either very young or very old, which reduces their potential survival time considerably.

Perls' Prussian Blue Stain

The mean trauma-death interval value for the fracture sections which stained positively for haemosiderin was 17.097 days (n = 31, s.d. = 30.74 days), and the mean trauma-death interval value for those fracture sections which stained negatively for haemosiderin was 1.2 days (n = 5, s.d. = 2.168 days). The difference between these means was found to be statistically significant (p = 0.021) to the 95% confidence level. This implies that haemosiderin production at the fracture site is associated with increased trauma-death interval, and that in the early stages of healing haemosiderin production is limited or non-existent. This tallies with current knowledge of haemosiderin as a break-down product of blood associated with old haemorrhage, as commonly found in tissues such as skin, subcutaneous tissue and brain between four and eight days post-trauma (Vanezis, 2001). In the fracture samples of this study, all the sections which stained correctly but exhibited a negative result were those of cases with low trauma-death interval values. Sixty percent of negative sections (n = 5) had a trauma-death interval value of 0 days, 20% had a trauma-death interval value of one day, and 20% a value of five days. The positively stained sections had a range of trauma-death interval values that spanned the whole spectrum of values. This points towards the conclusion that the presence of haemosiderin granules is rarely expected in the earliest stages of healing, especially within the first 24 hours after trauma. It may be that increasing trauma-death interval is associated with increasing amounts of haemosiderin granules at the fracture site, but the dichotomous nature of the observations precludes an assessment of increasing absolute quantities of haemosiderin granules.

The Perls' Prussian Blue reaction is regarded as the most useful stain for the detection of ferric iron, and the detection of haemosiderin granules in tissues is one of the classic methods of estimating the age of haemorrhages (Vanezis, 2001). The extent of haemosiderin formation is dependent on the amount of the initial haemorrhage, and its subsequent reduction is a function of increasing wound age

(Vanezis, 2001). However, in most tissue samples where haemosiderin detection is employed, such as brain, skin, subcutaneous tissue and lung, haemosiderin deposits of less than 20% of the microscopic field are regarded as uninformative for aging of the injury (Vanezis, 2001). It may be that the same maxim applies to the presence of haemosiderin in bone, and so these results should be viewed with caution. However, it is clear that there a correlation between the positive presence of haemosiderin and increasing trauma-death interval. This preliminary result indicates that there is potential for the use of haemosiderin as a predictor of trauma-death interval in bone fractures in addition to its already recognised role in the histological dating of bruises and soft tissue injuries.

CD68

CD68 positive cells

The number, size and overall cover of macrophages at the fracture sites was measured through immunohistochemical staining of the CD68 protein, which is expressed in the cell membrane of a wide variety of macrophages, including osteoclasts. All of these variables were compared to the trauma-death interval values of the fractures, to determine if there were any predictable changes in the abundance or size of macrophages as a function of time elapsed since trauma. An analysis of the results reveals a consistently clear pattern of temporal distribution, which although not statistically significant, may contribute to the retrospective histological prediction of trauma-death interval from CD68+ cell characteristics.

CD68 positive cell number

The scattergraph of the relationship between the trauma-death interval and the number of CD68+ cells as counted using the *Scion Image* analysis software (see Figure 05: 03) shows that in the first week after trauma, the number of CD68+ cells can vary greatly. However, the highest numbers of CD68+ cells are seen during this period too. This reflects the massive proliferation of inflammatory cells during the first few hours and days after trauma. Macrophages, such as osteoclasts, rapidly migrate to the damaged area, attracted to the site by chemotaxis and the low ambient pH of the fracture site caused by hypoxia of the tissues (Sevitt, 1981). The high numbers of CD68+ cells in the first few days after fracture are also a sign of the activity of osteoclasts in removing necrotic bone and debris from the fracture site. The maximum number of CD68+ cells appears to decline steadily with increasing trauma-death interval, suggesting a relaxation in osteoclast activity as chondroblasts and osteoblasts take over with their function of callus and bone formation during the soft and hard callus stages. Macrophages remain active throughout the healing process, and the maintenance of small numbers of CD68+ cells reflects this continuous, low-level activity.

CD68 positive cell size

The scattergraphs (see Figures 04: 12 and 04: 13) showing the estimated size of the CD68 positive cells (in μm^2) plotted against the trauma-death interval reveal an interesting pattern. Although there was no statistically significant correlation between these variables (see Table 04: 05), we can see that there is an early peak in the size of the CD68+ cells in the very early stages of healing, at tdi values of two and three days. Cells of approximately $420\mu m^2$ were found at the site of a two day old fracture. The average estimated size of the CD68+ cells appears to decline slowly with increasing trauma-death interval. However, if we take a closer look at the distribution of cell size in the tdi period from 0 to 25 days (Figure 04: 13), we can see that in the first five days after fracture, CD68+ cells are present at the fracture site, ranging in average size from $5\mu m^2$ to nearly $450\mu m^2$, with the majority hovering around the 50 – $100\mu m^2$ mark. After 14 days, CD68+ cells appear with an average size of about 150-$200\mu m^2$. After 25 days post fracture, the average size of the CD68+ cells appears to remain constant at approximately $50\mu m^2$. This pattern of CD68+ cell size fluctuation is not unexpected. Increased macrophage size is associated with high cell activity, and this is at its highest during the earliest stages of healing, when the necrotic bone and debris is being removed from the fracture site. The continuous process of remodelling for years after fracture is reflected in the plateauing of the macrophage size at larger trauma-death intervals. The clear break in the presence of CD68+ cells between five and 14 days is purely a reflection of a gap in the data, as there were simply no samples from cases with a trauma-death interval of between seven and 14 days. This time period is characterised by the formation of soft callus, which may have influenced the pathologists' decision to take samples for histology from these cases. It may be that healing was easy to distinguish with the naked eye at this stage, and so histological sampling was deemed unnecessary.

As would be expected, the Scion-generated measurements of the CD68+ cell sizes mirror the observer-estimated sizes. Figure 05:07 shows the relationship between the mean size of the CD68+ cells (μm^2) and the trauma-death interval. Despite a lack of statistically significant correlation according to the Kendal's tau-b and Spearman's r_s correlation tests (see Table 05:08), the same sort of pattern as before is visible. There appears to be a peak in macrophage size in the first few days after fracture, then a slow decline in the maximum CD68+ cell size until about 25 days after fracture, and an eventual plateau in macrophage size for the remaining trauma-death interval values. Again, this coincides with what is known about macrophage activity during the different stages of fracture healing. The scattergraph showing the first few weeks after trauma in greater detail (see Figure 05: 08) shows that there appears to be a higher average macrophage size in the first week than in the cluster of points after the two week mark.

The macrophage sizes found in cases with trauma-death interval values of 0 days show nothing unexpected. For cases where trauma and death occurred less than 24 hours apart, the mean CD68+

cell size was 45.14μm² (n = 3, s.d. = 11.947). These values are not particularly different from the mean CD68+ cell sizes measured at fracture sites a few days older. This could be interpreted two ways. Either:

1) the inflammation process in the cases with a tdi value of 0 is already underway and the size of the macrophages represents the beginning of their activity that will remain unchanged for the following few days, or
2) the average size of the macrophages seen in the 0 day old fractures is much the same as the average size of macrophages in normal, un-fractured bone, and that the inflammation process has not advanced sufficiently for a change in macrophage size to be noticeable.

It is thought that the first interpretation of the observed lack of fluctuation in macrophage size is the most appropriate, as macrophage response to trauma is known to occur within the first few hours after fracture (Lydyard *et al.* 2000); and even if the inflammatory response was retarded, a visible change or noticeable increase in macrophage size would be expected in the space of a day or two. As no significant difference is seen between days 0 and three, it can be assumed that the changes in macrophage size as a response to trauma have already occurred, in the first few hours after fracture. It is unfortunately the case that, as it is extremely difficult to know precisely the time of death or the time of fracture in forensic cases such as these, it was impossible to examine and monitor histological changes occurring in a timeframe of hours rather than days.

The average size of the CD68+ cells was also examined by measuring the mean perimeter of the cells (μm). This obviously correlates extremely well with the average area of the CD68+ cells. When this measurement was compared to the trauma-death interval values of the sample, a very similar scattergraph was plotted (*Figure 05: 09*) to that of CD68+ cell area against the trauma-death interval. Again, this shows a generally greater macrophage size during the initial stages of fracture healing, followed by a gradual decline in macrophage size with increasing trauma-death interval. The average macrophage size then stays at a relatively constant level as the trauma-death interval increases past 50 days. This plateau stage reflects the continuous process of remodelling that occurs after about three months post-fracture and which may continue for several years, until the functional strength of the bone has returned to its pre-fracture levels.

Estimated percentage cover of CD68 positive cells

There was no immediately obvious difference in the mean trauma-death interval values for each of the qualitatively observed categories of estimated percentage cover of CD68 positive cells, for the entire sample population, or for those cases with trauma-death interval values under 25 days. However, despite a lack of statistically significant results, it is still possible to draw some general conclusions about the relationship between trauma-death interval and the percentage cover of CD68+ cells. The

scattergraph of the trauma-death interval values plotted against each percentage cover category (0 = 0% CD68+ cells visible, 1 = <25%, 2 = 26-50%, 3 = 51-75% and 4 = >75%, see Figure 04.20), shows that an absolute lack of CD68+ cells is associated with a relatively low trauma-death interval value, as all the sections showing an absence of immuno-positive cells were from cases with trauma-death interval values of less than 28 days. The forensic implication of this is that if a fracture section was stained correctly for CD68 and showed no immuno-positive cells, there is evidence to suggest that the trauma-death interval could be estimated at below 28 days.

The greatest number of fracture sections were classified into the category (1) denoting <25% cover of CD68+ cells. Fracture sections from the widest range of trauma-death interval values were placed in this category, suggesting that, at any stage of healing, it is most likely that the visible CD68+ cells would cover less than 25% of the microscopic field. This may suggest that the category of <25% was the easiest for the observers to classify visually. It also must be noted that this category includes those sections where only one CD68+ cell was visible, and so its status as the modal category may be misleading. However, if we assume that the decisions of the observers were based on accurate estimates of the percentage cover of CD68+ cells, and if we assume that CD68+ cells are present, a pattern emerges. The majority of the sections in category 1 had low trauma-death interval values. The lower trauma-death interval values are characterised by the presence of CD68+ cells, to varying degrees. Both the categories 2 and 3, representing 26-50% cover and 51-75% cover of CD68+ cells respectively, only had fracture sections with low tdi values in them. There was only one instance of a section exhibiting over 75% cover of CD68+ cells, which had a tdi value of 28 days. Any increase in CD68 expression, and hence macrophage activity, appears to be primarily confined to the low (< 25 days) trauma-death interval values, suggesting that if CD68+ cells are detected in the later stages of healing, they are scarce and in low concentrations. Another way of describing this is that there may be a constant low level of macrophage activity, and therefore CD68 positivity, at all stages of the healing process, with a small but noticeable rise in macrophage numbers within the first week after trauma. This complies with what is known about macrophage activity during healing. The presence of increased numbers of CD68+ cells is expected in the earliest stages of healing, within the first seven days after fracture, as osteoclasts are actively involved in the phagocytosis of the necrotic bone and debris which litters the fracture site at this time. Once the debris has been reabsorbed, a slow, continuous remodelling process begins, and the osteoclast level is kept relatively constant.

Again, the *Scion Image*-generated measurements tally very well with the semi-qualitatively made observations (see Figures 05: 11 and 05: 12). The same general trend as has been seen in the previous analyses of the CD68+ cell variables is also visible here. When the cluster of data points around the origin is scrutinised more closely, by removing the some outliers in the data (see Figures 05: 12, 05: 13, 05: 14 and 05: 15), it is possible to see the emergence of a possible weak correlation

between the total cover of the background by CD68+ cells and the trauma-death interval in the first 5 days of fracture healing. Indeed, the correlation coefficients given by the Kendall's tau-b tests and the Spearman's r_s tests appear to increase slightly as the data set examined is gradually decreased to remove outliers and to select only the data near the origin (see Tables 05: 13, 05: 14, 05: 15 and 05: 16). In Figure 05: 14 and 05: 15, we can see a weak positive correlation between the total cover of CD68+ cell cover and the trauma-death interval in the first five days post-trauma. Again, this is indicative of the proliferation of macrophages as a response to trauma, and their increased size due to their fervent resorption activity.

Dispersal of CD68 positive cells

The changing dispersal of cells throughout the fracture site is indicative of the processes of healing, as cells migrate towards different sections, or line the edges of the compact bone, or organise themselves into 'cutting zones' for resorption purposes. It was clearly a variable that might be correlated with trauma-death interval. The problem of monitoring the changing dispersal of the CD68+ cells was tackled by attempting to describe the nature of the cell dispersal over the fracture site in combination with the location of the cells. As described in Chapter 03, this was done by assigning the immuno-positive cells on each fracture slide to distinct 'where?' and 'how?' descriptive categories, and then comparing the mean trauma-death interval values for the section assigned to each category. When the whole sample was analysed, the Kruskal-Wallis tests showed that there were no statistically significant differences between the mean trauma-death interval values in each category (see Tables 04: 07 and 04: 08). Even when the descriptive categories were amalgamated to produce more sensitive, illustrative 'wherehow?' categories, no statistically significant differences were found (see Table 04: 09). However, statistically significant differences between the mean trauma-death interval values for the combined 'wherehow?' categories were found when only the trauma-death interval values under 25 days were examined (see Table 04: 10). The p value obtained was 0.044, and the difference is significant to the 95% confidence level. Figure 04: 15 portrays the difference in the mean trauma-death interval values graphically, showing that, at the lowest trauma-death interval values, the macrophages (CD68+ cells) were found to be clustered at the fracture ends, clustered throughout the fracture site, clustered in the bone marrow, clustered in the extracellular matrix (ECM) and lining the compact bone. At the higher trauma-death interval values, the macrophages were found evenly dispersed throughout the fracture site, evenly dispersed in the ECM, around the adipose tissue and within Howship's lacunae. These findings confirm that perceptible histological changes to the dispersal of macrophages take place during fracture healing, and that it may be possible to extrapolate backwards from the view down the microscope to a possible trauma-death interval value. The results from this analysis show us that, in the first few hours and days after trauma, the macrophages migrate toward the fracture site and arrange themselves in clusters. They particularly cluster around the fractured ends of the bone, and we can assume that this is to perform their function of removing necrotic bone and debris through

phagocytosis. The process of phagocytosis is triggered by movement of the phagocytic cells migrating towards and attaching to the piece of debris (Lydyard *et al.* 2000). This is clearly what we can see happening at the fracture site in the early stages of healing. Later on in the healing process, on the fracture slides with higher trauma-death interval values, the macrophages have dispersed evenly throughout the fracture site, and are no longer clustered around the fractured ends of the bone. Of particular interest is the appearance of macrophages in Howship's lacunae, as this shows us that the CD68 positive osteoclasts are actively involved in bone resorption during these later stages. This sits well with the assumption that there is a surge of activity in the earliest phases of healing, which is followed by a low-level constant maintenance of resorption activity in the remodelling stages.

Cells with haematoxylin-stained nuclei

In addition to the CD68 positive cells, the abundance and distribution of two other types of cells visible at the fracture site were assessed in relation to the trauma-death interval. Small round lymphocytes and elongated, spindle-shaped fibroblasts were visible histologically as their nuclei were stained blue by the haematoxylin counter-stain used on the immuno-stained slides. The percentage cover of these two types of easily-distinguishable cells was estimated from photographs of the CD68-stained fracture slides by the author and three independent observers in the manner described previously. Figure 04: 16 shows a three-dimensional graph of the relative frequencies of the percentage cover of the blue-stained cells (lymphocytes and fibroblasts together) and the CD68+ cells against the trauma-death interval. This graph shows us that the highest number of slides where a percentage cover score of 4 (over 76% cover) of blue-stained cells was recorded during the first week after trauma. There are also relatively high numbers of slides exhibiting 25-50% and 51-75% cover of blue-stained cells. The majority of these cells were small, round lymphocytes, which are inflammatory cells, particularly abundant during the early inflammation stages of healing. There are no fracture slides exhibiting over 76% cover of blue-stained cells after 25 days post-trauma, and the abundance of blue-stained cells appears to dramatically decline with increasing trauma-death interval. As was seen with the estimation of percentage cover of the CD68+ cells, the most number of slides were classified as category 1 (less than 25% cover) for blue-stained cells. This again suggests that this is the easiest category to identify, and that there may have been a lot of slides with a very small number of blue-stained cells present. The overall suggestion of the blue-stained cell data is that, despite a lack of a statistically significant correlation between the ratios of *blue-stained cell % cover: CD68+ cell % cover* (see Tables 04: 11 and 04: 12), there is a general pattern of a high abundance of blue-stained inflammatory cells present at the fracture site during the first weeks after trauma, followed by a decline in numbers with increasing trauma-death interval.

The sizes of the blue-stained cells were estimated, and ratios of *blue-stained cell size: CD68+ cell size* were analysed to determine if there was any statistical correlation between these ratios and the trauma-death interval (see Tables 04: 13 and 04: 14).

The scattergraph (Figure 04: 17) shows that for the majority of trauma-death interval values, the ratio of *blue-stained cell size: CD68+ cell size* was under 1.00. Where the ratio value is less than one, the cells with blue-stained nuclei are smaller than the CD68+ cells. This is true for a large cluster of data points near the origin of the scattergraph, at trauma-death intervals of under five days. Again, this coincides with the period when the CD68+ macrophages are at their most abundant and active, as they are proliferating and differentiating, and are intensely involved in resorption of necrotic bone. This relationship between the sizes of the blue-stained cells and the CD68+ cells appears to be maintained throughout the healing process, which indicates either that the cells remain approximately the same size, or that they increase or decrease in size but keep their relative proportions. It may be the case that, in the later stages of healing, both the blue-stained cells and the macrophages reduce in size due to lessened activity, as the macrophages settle into the long-term process of remodelling, and the lymphocytes are no longer reacting to the inflammation as strongly as they did initially.

Multiple regression analysis

Multiple regression analysis was performed in an attempt to quantify the contribution of each of the variables measured on the CD68-stained slides to the accurate prediction of the trauma-death interval. Table 04: 15 shows a summary of the SPSS output resulting from the standard multiple regression analysis. The errors for both the dependent and independent variables were assumed to be normally distributed. The correlation tables show that none of the CD68+ cell-related variables have a statistically significant relationship with the trauma-death interval. There is, however a statistically significant correlation between the estimated percentage cover of red blood cells and tdi, and an almost significant result for the percentage cover of living compact bone, which are discussed later. Interestingly, there is a statistically significant positive correlation between the estimated percentage cover of the CD68+ cells and the estimated percentage cover of necrotic bone. This suggests that it may be possible to retrospectively predict the trauma-death interval from the amount of necrotic bone visible on a histological slide of a fracture site. That the abundance of CD68+ cells and the amount of necrotic bone at the fracture site correlate is not a surprise – it suggests that the CD68 positive macrophages are reacting to increased levels of bone debris, and their increased area implies heightened activity. The R^2 value for the multiple regression analysis is 0.414 (adjusted R^2 value is 0.210), and the significance level of R is 0.088, which is just short of being statistically significant to the 95% confidence level. This tells us that only 40% of the variance in the data is explained by these variables, and the rest is due to other, unrecognised variables or chance. The results of the standard multiple regression analysis for the variables measured on the CD68-stained slides against the

trauma-death interval values under 25 days (see Table 04: 16) were very similar to those of the whole range of trauma-death interval values. The R^2 value was found to be 0.489 (the adjusted R^2 value = 0.262), with a significance of R value of 0.084, which again makes the significance level of the regression just shy of the 95% confidence level.

Multiple regression analysis was also performed on the measurements made from the CD68-stained slides using *Scion Image*. A summary of the results can be seen in Table 05: 20. There were no statistically significant correlations between any of the CD68+ cell variables and the trauma-death interval. However, a few weak negative correlations were visible. These were between the trauma-death interval and the average CD68+ cell size, perimeter and the total cover of the background. The multiple regression analysis obtained an R^2 value of 0.064 (adjusted R^2 value of 0.05), and a significance level of 0.726. None of the regression coefficients contributed significantly to the prediction of the trauma-death interval through regression. This suggests that although the *Scion Image*-generated measurements of the CD68+ cells cannot be reliably used to estimate the trauma-death interval, it may be possible to see a trend of decreasing macrophage abundance, size and activity with increasing trauma-death interval. This trend would probably be at its most obvious between about seven and 28 days post-trauma, as this is a time when the initial massive proliferation and differentiation of cells in response to the trauma has subsided, but the steady, constant process of bone remodelling has not yet begun.

Inter-observer agreement

The level of inter-observer agreement was calculated using Cohen's Kappa method as an index of inter-rater reliability and reproducibility (Carletta, 1996; Petrie and Sabin, 2000). The results of the Kappa analysis show that Observer 1, 3 and 2 showed the greatest level of agreement (see Table 04: 17). Observer 4 showed 'substantial' levels of agreement with Observer 3 and a 'moderate' level of agreement with Observer 1. The least level of agreement was shown between Observer 4 and Observer 2. As Cohen's Kappa analysis also accounts for the agreement that would happen between observers by chance, these results are quite interesting. Observer 1 was the author, Observer 2 an experienced histology technician in the Department of Forensic Pathology, and Observers 3 and 4 were novices. Fortunately, there was a 'substantial' level of agreement between Observers 1 and 2, and an average of these scores became the basis of the CD68+ cell and blue-stained cell percentage cover data. Observer 3, although a novice, managed to gain considerable levels of agreement with the very experienced Observer 2. Non-parametric correlation tests were performed to check the correlation between observations, and a high level of correlation, significant to the 99% confidence level, was found between the observations of all the observers (see Table 04: 18).

In order to test the hypothesis that there is a statistically significant relationship between the qualitative spatial properties of the bone sialoprotein positive (BSP+) cells and the trauma-death interval in the sample population, semi-qualitative and quantitative measurements of the immuno-positive cells on the fracture slides were taken, and compared to the trauma-death interval values.

Estimated percentage cover of BSP positive cells

The percentage cover of BSP+ cells was estimated by two independent observers using the same system of categories as described before. It was hypothesised that there would be a statistically significant difference in the mean trauma-death interval values of the sections placed in these percentage cover categories, which would suggest that the percentage cover of BSP+ cells changed predictably with the trauma-death interval. A Kruskal-Wallis test was performed to test this theory, but the results (see Tables 04: 23 and 04: 24) show that there was no significant difference between the mean trauma-death interval values in each category. This was also the case when the out-lying trauma-death interval values are ignored. However, it is possible to draw a few inferences about the changes in BSP+ cell cover in relation to the trauma-death interval. The highest percentage cover categories were mostly associated with low trauma-death interval values (see Table 06: 01). The mean tdi value for category 3 (51-75% BSP+ cell cover) was 2 days (n = 1), and for category 2 (26-50% BSP+ cell cover) was 1 (n = 3, s.d. = 1 day). There were no slides that were classified into category 4 (>76% BSP+ cell cover). The highest trauma-death interval values were associated with slides where there were no BSP+ cells visible. The mean tdi value in category 0 (0% BSP+ cell cover) was 20.13 days (n = 15, s.d. = 32.58 days).

Table 06: 01Table showing the mean trauma-death interval value for the BSP percentage cover categories, with sample size and standard deviation values.

Report

TDI

BSP_COV	Mean	N	Std. Deviation
0	20.133	15	32.577
1	12.704	27	24.108
2	1.000	3	1.000
3	2.000	1	.
Total	14.130	46	26.344

This suggests a steep decline in the abundance of the BSP positive osteoblasts, from a relatively high percentage cover in the first few days post-trauma, to a virtual absence of them by 20 days post-trauma. This pattern appears to tally with the generally accepted idea of the function of bone sialoprotein. Bone sialoprotein is expressed between days one to seven post-trauma, as it is involved in facilitating the attachment of osteoclasts to the matrix for the initial resorption process (Acebes *et al.*

1999; Roach, 1994). Between days seven and 14, bone sialoprotein is found in the burgeoning callus matrix, as it marks the transition of chondrocytes into osteoblasts (Oni, 1995). As this data also suggests, there is then a period, around the three-week post-trauma point, where no BSP is expressed. Its presence is then noticed again after about 28 days, as its expression is thought to increase in line with the onset and continuation of mineralisation (Roach, 1994), and to steady during the elongated remodelling phase (Pinero *et al.* 1995). The sample data portrays the resurgence of BSP expression during the later stages of healing to a certain extent as, of the fracture slides with trauma-death interval value of over 28 days (n = 7), 57.14% show BSP+ cell percentage cover in category 1 (<25%). The remainder show no BSP+ cells, and are classified in category 0.

BSP positive cell size

At first glance, there does not appear to be a clear relationship between the estimated size of the BSP+ cells and the trauma-death interval (see Figure 04: 31). There appears to be a wide range of osteoblast sizes in the first 24 hours after trauma, and then perhaps a slight decrease in the average size of the cells in the next few weeks. However, once the focus was concentrated on the data points around the origin, in order to elucidate more about the size of the BSP+ cells in the earliest stages of healing, a more obvious trend emerged (see Figure 04: 32 and 04: 33). At the trauma-death interval values under 25 days, but especially at those under 10 days, there appears to be a positive linear correlation between the average size of the BSP+ cells and the trauma-death interval. This suggests that, in the first five days to a week, the size of the BSP+ cells is increasing as the trauma-death interval increases, which may indicate increased cell activity during the first week when bone sialoprotein is known to be expressed. However, the correlation coefficients found using the Kendall's tau-b and Spearman's r_s tests (0.024 and 0.055 respectively) are so low, it may be that this apparent relationship is extremely weak. It would be expected that the size of the BSP+ cells would be greatest at the very earliest days post-trauma, and that a gradual decrease in activity and therefore cell size would be seen after about 14 days post-trauma, as bone sialoprotein expression is suppressed during the hard callus formation stage.

Dispersal of BSP positive cells

The nature of the dispersal of the BSP+ cells across the fracture site was described in the same manner as previously, with a combination of descriptive categories relating to the location of cells and their distribution throughout the section. It was thought that an amalgamation of the categories denoting the nature of the cell dispersal with the location of the cells would yield the most interesting results when compared to the trauma-death interval, as was the case with the CD68+ cells. However, no statistically significant differences were found between the mean trauma-death interval values in each of the amalgamated categories, despite the exclusion of more and more outliers (see Tables 04: 25 to 04: 27). It is presumed that this apparent lack of statistical significance is related to the choice of

descriptive categories, which were designed to best illustrate the perceptible differences in the distribution characteristics of the cells over the range of fracture sections. It is clear that the cells examined here, osteoclasts, osteoblasts, fibroblasts and lymphocytes, do change in abundance and distribution in relation to their changing roles in the process of fracture healing. We have seen that osteoclasts huddle around the sites of debris and necrotic bone as they prepare for phagocytosis. Bone sialoprotein is known to be expressed by osteoblasts, but is also abundant at cement lines and adjacent to the ruffled borders of the osteoclasts at the onset of mineralisation (Pinero *et al.* 1995). The design of an accurate method of monitoring these fluctuations in distribution could be a potentially rewarding avenue of investigation in the future.

Cells with haematoxylin-stained nuclei

When the estimated percentage cover values for the cells with blue-stained nuclei (lymphocytes and fibroblasts) were compared to the estimated percentage cover values of the BSP+ cells, an interesting trend emerged. Despite the lack of a statistically significant relationship between the ratio of *small blue cell % cover: BSP+ cell % cover* and the trauma-death interval, there was a weak negative correlation between these variables that was maintained even as the data set was reduced to eliminate the effect of outliers (see Tables 04: 28 to 04: 30). This suggests that lower percentage cover ratios were found to be loosely associated with higher trauma-death interval values. Small ratios below 1.00 indicate that the abundance of the BSP+ cells is greater than that of the blue-stained cells. So, the inference that can be drawn from this data is that high percentage cover of BSP+ cells in comparison with blue-stained cells is seen as the trauma-death interval increases. This can be thought to represent a decrease in inflammatory cells once the initial inflammatory phase has passed, which could be happening in conjunction with constant BSP+ cell cover, or even with a slight decrease in BSP+ cell, as long as the decline in blue-stained cell cover is steeper.

It was possible to compare the basic variables associated with cell size and abundance between the BSP-stained slides and the normal bone control samples. Table 05: 21 shows us that there is a statistically significant difference between the BSP-stained slides and the control samples for two of these variables – the estimated percentage cover of blue-stained cells (lymphocytes), and for the ratio of *lymphocyte size: BSP+ cell size*. Both of these differences are significant to the 95% confidence level. This suggests that there was a significantly different average number of lymphocytes on the fracture sections to the number visible on the normal section. The higher number of lymphocytes was associated with the fracture slides, which is expected, as lymphocytes are inflammatory cells that specifically migrate to sites of trauma. The second statistically significant result relates to the relationship in size between the BSP+ cells and the inflammatory lymphocytes. In the majority of the fracture sections, this ratio (lymphocyte: BSP+ cell) was under 1.00, indicating that the lymphocytes were generally smaller than the BSP+ osteoblasts. In the normal controls, by contrast, the ratio was

consistently above 1.00, suggesting that the lymphocytes were larger. This is likely to be due to the relative inactivity of osteoblasts in normal bone sections, as although active, they are not involved in the formation of bone as intensely as at a fracture site, and so probably maintain a smaller overall size.

Multiple regression analysis

Multiple regression analyses were performed in order to test the influence of the different variables seen in the BSP-stained slides on the prediction of the trauma-death interval, in the same manner as was done for the variables from the CD68-stained slides. A summary of the SPSS output can be seen in Table 04: 31. Again, it was assumed that the errors for both the dependent and independent variables were normally distributed. The R^2 value of the regression is 0.410 (adjusted R^2 value = 0.152) and the significance level is 0.209. The correlation tables show us that statistically significant correlations were found between the trauma-death interval and the estimated percentage cover of living compact bone (see below), and the estimated percentage cover of elongated fibroblasts. The correlation coefficient of the latter correlation was 0.347, with a p value of 0.048, which makes the correlation significant to the 95% confidence level. There is also evidence of a weak negative correlation between the size of the BSP+ cells and the trauma-death interval, which is not quite statistically significant. The positive correlation seen between the abundance of fibroblasts and the trauma-death interval suggests that the quantity of fibroblasts increases as a function of time since fracture. This makes sense, as fibroblasts are chiefly involved in the production of collagen, which is low immediately after fracture, but increases as the collagen is used to form cartilage and callus, after between one and two weeks post-fracture (Ohishi *et al.* 1998). A peak in fibroblast activity would be expected at about 14 days post-trauma. The weak negative correlation between the size of the BSP+ cells and the trauma-death interval reinforces the suggestion that the activity of the BSP+ cells decreases with increasing trauma-death interval, as we saw with the estimated percentage cover of the BSP+ cells earlier. It appears to contradict the results based on correlations between estimated BSP+ cell size and tdi, but this correlation was thought to be a very fragile one.

Inter-observer error

In order to reduce the inter-observer error, but to maintain the standards of accuracy and reliability for the data collection, two independent observers were employed to record their observations of the spatial characteristics of the BSP+ cells and the cells with haematoxylin-stained nuclei. The two observers chosen were the author and the more experienced Observer 2, the histology technician in the Department of Forensic Pathology at the University of Sheffield.

To assess the reliability and synchronisation of the estimated values, Cohen's Kappa tests were performed, which evaluated the level of agreement between the observations made by the two observers, as well as accounting for the agreement that would occur by chance. Table 04: 32 shows

that there was a 'substantial' level of agreement achieved between the observations made by Observer 1 and 2 for the estimation of the percentage cover of the BSP+ cells. This agreement was statistically significant to the 99% confidence level (see Table 04: 33). It was not possible to compute the Kappa values for the estimations of the percentage cover of the lymphocytes at the fracture sites, as all of the categories (0 to 4) were represented by both observers. However, a Kendall's tau-b and Spearman's rs test (see Table 04: 35) showed a level of correlation between the observations statistically significant to the 99% confidence level. For the estimations of percentage cover of the fibroblasts visible on the BSP-stained slides, the Kappa test indicated that a 'moderate' level of agreement was achieved (see Table 04: 34), but the non-parametric correlation tests revealed a high level of correlation between the observations, statistically significant to the 99% confidence level (see Table 04: 36). These tests prove that the inter-observer error was kept to a minimum, and that the observations and estimations of each observer can be believed to be reliable, and true representations of the histologically-visible phenomena.

Compact bone

It seems logical that the amount of living and necrotic compact bone visible at a fracture site would vary in a predictable way with the trauma-death interval. In order to test this, semi-quantitative estimations of the percentage of compact bone with intact osteocytes within lacunae (living) and the percentage of compact bone exhibiting empty lacunae (necrotic) were made for each fracture slide, and these were tested for any correlations with trauma-death interval. Non-parametric correlation tests (Kendall's tau-b and Spearman's r_s) did not find statistically significant correlations (see Table 04: 37). A very weak negative correlation was seen between trauma-death interval and the variable BONRATIO, which is the ratio of *estimated percentage cover of living compact bone: estimated percentage cover of necrotic compact bone*, but this is believed to be a spurious result given the alternative evidence of a strong statistically significant correlation between the percentage cover of living bone and the trauma-death interval, which was found as a result of multiple regression analyses.

Figures 04:34 and 04: 35 show scattergraphs of the relationship between the estimated percentage cover of living, necrotic and total compact bone with the trauma-death interval, from the CD68-stained slides and the BSP-stained slides respectively. Both show that the amount of compact bone at the fracture site varies substantially at the onset of trauma, but then that the amount of necrotic bone gradually decreases, as would be expected as resorption by osteoclasts occurs, and that the amount of living compact bone visible at the fracture site either remains constant or declines gradually. Again, this complies with the pattern of bone resorption and formation that would be expected during the fracture healing process.

For ease, the variables related to compact bone observed on the CD68-stained slides were included in the multiple regression analysis for the CD68+ cell-related variables. This did not significantly make a difference to results obtained. The results can be seen in Table 04: 15. This shows that the variable BONE_LIV (% cover of the background by living bone) made a statistically significant contribution to the regression, with a *t* value of -2.771. This is significant to the 95% confidence level. This also suggests that there is a negative relationship between the percentage cover of living compact bone visible on the slide and the trauma-death interval. This implies that with increased trauma-death interval, a lower percentage cover of living bone is expected. This initially appears contradictory to the concept of fracture healing. However, this variable was defined as the percentage cover of compact bone containing osteocytes within the lacunae, which is the appearance of established, mature compact bone. Therefore, it may be surmised that, at the fracture site, the amount of compact bone containing osteocytes *does* become reduced during fracture healing as a function of resorption and remodelling, and that is only replaced with younger callus and woven bone, and may take many years to regain the appearance of the mature bone that was present at the outset.

When the multiple regression analysis was performed using only the trauma-death interval values under 25 days, a similar result was obtained (see Table 04: 16). The variables BONE_LIV and BONE_NEC (the estimated % cover of compact bone with empty lacunae) were found to contribute significantly to the regression, as their *t* values were -3.352 and -2.633 respectively. These values are both significant to the 95% confidence level. Again, there is the suggestion of a negative relationship between BONE_LIV and the trauma-death interval, especially before 25 days post-trauma, and this is mirrored in the correlation with BONE_NEC, which is very simply negatively correlated with BONE_LIV, as the values for these variables invariably add up to 100%.

A very similar result was obtained from the multiple regression analysis of the variables measured from the BSP-stained slides. Table 04: 31 shows a summary of the SPSS output of the results. Again, a statistically significant negative relationship was found between the estimated percentage cover of living bone and the trauma-death interval. The correlation coefficient between the variable BONE_LIV and the trauma-death interval was -0.441, with a significance value of 0.014, which means that the relationship was significant to the 95% confidence level, and almost to the 99% confidence level.

Red blood cells

When the estimated percentage cover of red blood cells was compared to the trauma-death interval, it was expected that there would be a high percentage cover of blood cells in the first few days after trauma, followed by a gradual decline in their numbers as the haemorrhage was dissipated and resorbed. Figure 04: 36 and 04: 37 show scattergraphs of this variable compared to the whole range of

trauma-death interval values and those trauma-death interval values under 25 days. Tables 04: 38 and 04: 39 show the corresponding results of non-parametric correlation tests (Kendall's tau-b and Spearman's r_s). Both the scatter-graphs show that, at 0 days post-trauma, there are varying percentage cover amounts of red blood cells, ranging from 0% to about 30% cover. Both appear to show, in the first 4-5 days after trauma, a very gradual increase in the amount of red blood cells visible at the fracture site. The correlation tests did not echo this apparent relationship, as in Table 04: 39, the correlation coefficient is given as negative. However, this is not statistically significant, and the value is so low that it might be erroneous. The observable positive correlation between the estimated percentage cover of red blood cells and the trauma-death interval was confirmed by multiple regression analyses.

Multiple regression analysis

For ease, the variable of estimated percentage cover of red blood cells observed on the CD68-stained slides was included in the multiple regression analysis for the CD68+ cell-related variables. The results of this standard multiple regression analysis is presented in Table 04: 15. It appears that RBC (% cover of red blood cells) contributed significantly to the regression with a *t* value of 2.532. This value is significant to the 95% confidence level as the 95% confidence interval does not include zero as a possible value (Tabachnick and Fidell, 2001). This association is positive, and means that the higher the trauma-death interval, the higher the number of red blood cells seen at the fracture site. Although this variable was included in the study as an indicator of haemorrhage, and therefore would have been expected to be highest during the earliest inflammatory stages of healing, with an eventually tailing-off of values, it may be that it serves not only as an indicator of haemorrhage at the onset of trauma, but perhaps also of increased vascularity during healing. Certainly, in some fracture sections, the red blood cells were clearly contained within capillaries and vessels, rather than swamping the fracture site as would be expected in haemorrhage.

Prediction of the trauma-death interval

In order to consolidate and organise the inferences made as a result of the statistical analyses presented, and to facilitate the prediction of the trauma-death interval from these inferences, a summary graph was produced (see Figure 06: 01). It is only supposed to be representative of the basic fluctuations in the histologically visible features, but it may be useful for predicting the trauma-death interval by providing a reference point. For example, if the fracture slide in question exhibits haemosiderin granules, a high CD68+ cell number, with CD68+ cells a medium size, and a low percentage cover of BSP+ cells, the trauma-death interval could be roughly estimated to be about 14 days. It must be emphasised that this would only be an approximate estimate.

Figure 06: 01 A schematic diagram of the relationships between some of the histologically visible features and the trauma-death interval.

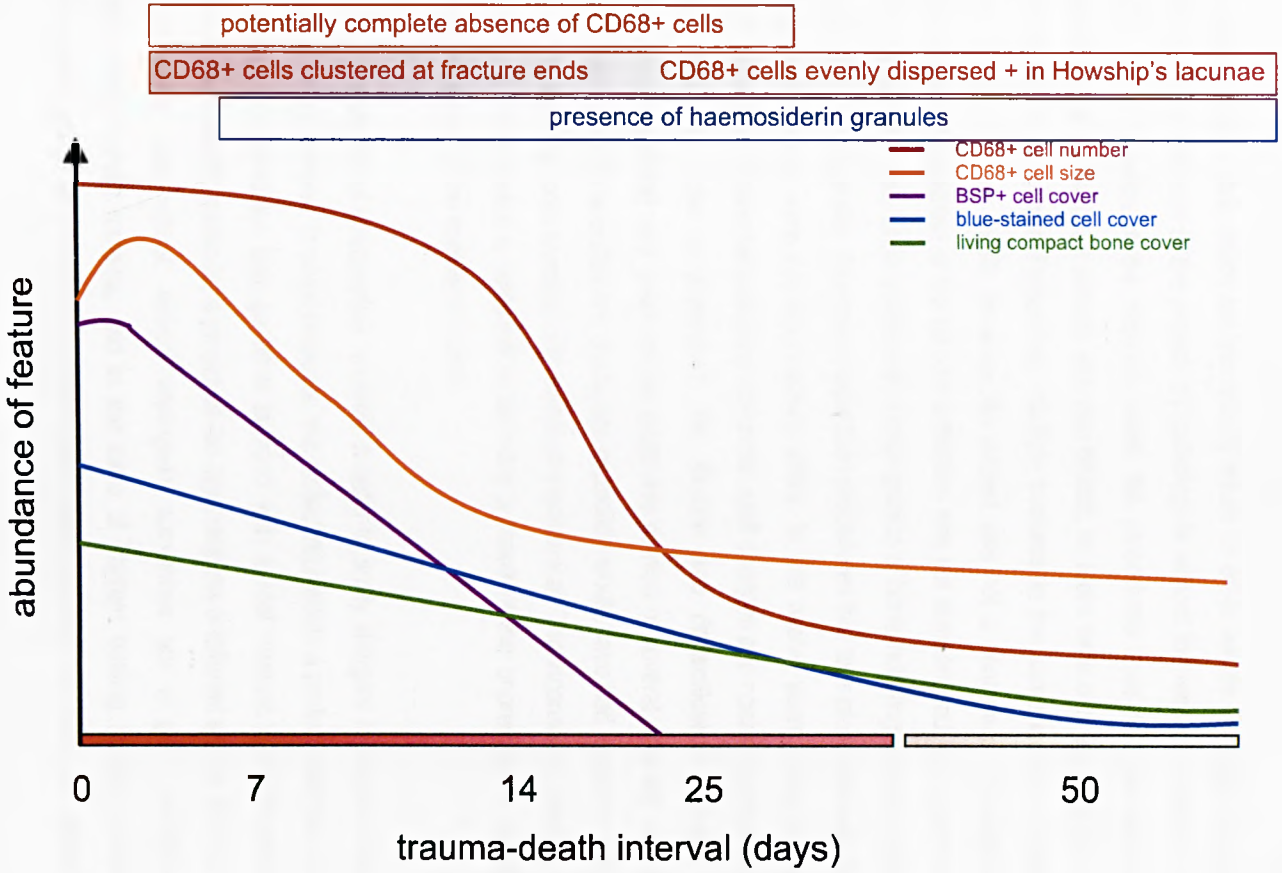

Limitations and considerations

There were considerable limitations to the experimental design and the potential findings of the research from the outset. These were mainly related to the sample selection procedure and the availability of suitable samples. In this respect, the project is a victim of it own forensic relevance. In order to ensure the applicability of this research to the forensic context, human fracture samples were secured from real-life forensic cases submitted to the Medico-Legal Centre between 1992 and 2002. This project is one of only a few studies that have applied histological fracture healing assessment to the immediate forensic context (Klotzbach *et al.* 2003), but its forensic relevance has ultimately contributed to its shortcomings, as it has proved impossible to compensate for the biased sample population, the small sample size and the lack of standardisation and compatibility between sections.

Sample

Any retrospective studies of this nature are necessarily reliant on other people. Because the samples were collected years in advance of the project, by pathologists without the research project in mind, there was little standardisation of the samples taken, the procedures used and the recording of relevant information. As a result, the sample size was limited, as there were only 29 instances where all the research criteria were met. Fortunately, multiple fractures in the same individual raised the population of fracture samples to 52. Because the project was not a concern of the pathologists collecting the samples, the location of the sample extraction was not standardised. Some pathologists extracted only the fracture itself; while others took a large section of bone including areas of unaffected bone either side of the fracture site. The bone preparation procedures that took place between autopsy and the histology laboratory were not standardised either. In the twelve years since the sample collection began, there have been technological advances, staff changes and operating guidelines that have changed the way bone is processed. The fixation and decalcification methods were unstandardised, and depended very much on the subjective opinion of several different technicians. The range of variation in the decalcification procedure especially would have had knock-on effects on the reliability of the staining, both tinctorial and immunohistochemical. The inconsistent staining found in the results of all three stains is believed to be more a result of the unpredictable variation in decalcification than a fault of the staining process.

There is obviously a degree of compromise required in order to apply stringent research methods to unpredictable forensic situations. In some respects, this project represents a perfect example of all the erratic and changeable variables that go hand in hand with a real forensic case! However, for objective, repeatable scientific methods, a project of this type requires a different sort of data set, over which the researcher has control. Animal analogues sometimes are a good substitute for experimentation using human remains, and in the case of fracture healing studies, present an opportunity to control almost all aspects of the trauma and healing process. For example, studies such

as those by Oni (1995), Ohishi *et al.* (1998) and Yaoita *et al.* (2000) have measured fluctuations in proteins and genes after fracture by creating the fracture themselves and subsequently sacrificing the animals at strict time intervals to examine the fractures histologically. Obviously, in fracture research in humans, the sample and methods are limited either to what is available post-mortem, or to what can be viewed at distinct time intervals after fracture *in vivo*. Animal experiments clearly have the advantage of minimising variables, which is something this study has been largely unable to do.

Another significant source of variation and uncertainty is that of protein degradation. This is a particularly important issue for the analysis of post-mortem forensic remains. The proteins examined here, CD68 and bone sialoprotein, are subject to the natural process of degradation after death. Fortunately, in this project, the individuals examined were all autopsied and the bone samples were all fixed shortly after death, leaving no time for the proteins to degrade. However, in the forensic context, and especially in the field of forensic anthropology, it is likely that an individual may not be discovered until some time after death. This means that the partial or complete degradation of the proteins may have occurred and would affect the histological and immunohistochemical protein profiles of any fracture samples investigated. This would hinder the prediction of the trauma-death interval from an extrapolation of the immunohistochemical character of the fracture site.

Images

The use of digital photography in the experimental procedure introduced a range of uncertainties. Firstly, a photograph of a histology slide is only a second-hand representation of the slide, and as such, image artefacts were potentially introduced, which may have disrupted the collection of data from the slides. For example, adjustments made to the brightness, contrast or focus of the image while taking the photograph may have altered the colour or visibility of certain histological features. These adjustments could as easily have improved the clarity of the slide, and so it is thought that this variability had little effect on the eventual outcome. Secondly, it was difficult to standardise the position of the fracture site in relation to the camera, which made it virtually impossible to ensure that exactly the same part of the fracture site of every slide was captured in every photograph. This, combined with the variation introduced by the orientation of the sections on the slides reduces comparability between slides. The fact that very low magnification was impossible with available equipment meant that it was not always possible to view the whole of the fracture site, and so a specific area of the fracture site often had to be chosen in an effort to standardise the slides (see Chapter 03). It would be ideal to use a microscope or image analysis programme where the whole section could be viewed at a high magnification, where it would be possible to select a standardised portion of the fracture site. The fracture slide could also be divided into a grid of squares, each viewable at high magnification, which would then allow the systematic analysis of all areas of the section.

Experimental definitions

There are some important aspects of the experimental design that need consideration. One of the assumptions of the project has been the definition of the 'fracture site'. In practice, the area closest to the fractured ends of the bone fragments was designated the fracture site, but in theory this is an area with particularly ambiguous boundaries. For example, a lot of the samples were only of one of the bone fragments, and the section ended at the break in the bone. When this was the case, how should the fracture site have been defined? The setting of the confines of the fracture site depends on the extent of the influence of the fracture on the surrounding bone and other tissues, but this is itself very problematic to measure. Is it necessary to include the whole of the affected bone in the analysis, or just everything up to a point an arbitrary distance away from the actual break? In transverse or oblique fractures, it may be fairly easy to delineate the fracture line, but what about greenstick or compression fractures? This problem with the definition of a fracture site is not simply a spatial one, as with the analysis of a variable like the trauma-death interval, there is a temporal aspect to consider. Again, there is the question of the boundaries of a fracture. When is a fracture not a fracture any more? Does a fracture site act like a fracture site forever? From a forensic anthropologist's point of view, it is known that bones fractured in adulthood can bear evidence of the fracture until (and beyond) the death of the individual, but it is unlikely that the fracture site would still show histological evidence of remodelling in a 20 or 30 year old fracture. Children's bones are renowned for being expert healers, and all evidence of the existence of a fracture can sometimes be eliminated. Does this represent the only circumstance where the end of a fracture can be pinpointed?

Inter-observer agreement

Despite the fact that three out of the four independent observers were novices (including the author!) the level of inter-observer agreement was remarkably good, especially between Observers 1 and 2. However, there are a variety of ways in which the inter-observer performance could have been improved, and the precision and accuracy of the estimation process enhanced. For example, the operational definitions of the percentage cover categories could have been improved by providing observers with examples of slides that fitted into each category, and standard classificatory definitions could have been used. Prior training in histology would have been extremely valuable for the majority of the observers, and it is certain that a lack of experience of looking at histology slides contributed to the lack of correlation between some of the estimates. The use of experienced observers would have improved the reliability and accuracy of the estimates, but they are in such demand in busy university departments that it is often difficult to secure them for projects such as this.

With hindsight, we can see that it would have been valuable to increase the stratification of the percentage cover categories, in order to obtain a more sensitive measure of the changes in cell abundance as a function of the trauma-death interval. The addition of percentage cover categories

such as <2%, 2-10% and 11-25% would have reduced the number of slides classified in the <25% category, and have spread the data out a bit more, increasing its interpretability.

Conclusions

The accurate and reliable prediction of the trauma-death interval from the histological appearance of a fracture site remains elusive. However, some interesting relationships and correlations between histologically visible features and the trauma-death interval have been found, a summary of which can be found in the next chapter. It is believed that the lack of correlation and statistically significant results seen may be due to inadequacies in the sample rather than a true reflection of the relationship between such variables; and it is expected that, if the sample size could be increased and variation between fractures reduced through the use of animal analogues or standardised post-mortem experiments; it may well be possible to elucidate the means of accurately and reliably determining the trauma-death interval from histological fracture samples. It is an issue that has been attempted in the field of forensic pathology, but as yet has been restricted to the sphere of the diagnosis of non-accidental injury in children. There is clearly much scope for extended research in this area, especially in forensic anthropology. It is also suggested that, despite a general shortage of statistically significant results that could be instantly applied to the forensic cases, this body of data represents a unique collection of information regarding the histological and immunohistochemical nature of fracture healing that has not been undertaken before.

07 : CONCLUSIONS

"This is the short and the long of it."
The Merry Wives of Windsor
William Shakespeare (1564 - 1616)

Introduction

The main conclusion that can be drawn from this work is that, although it is not yet possible to categorically predict the trauma-death interval from a histological slide of a fracture, it is possible to pinpoint certain patterns and predictable changes that could facilitate the estimation of the trauma-death interval by extrapolating backwards from the histological appearance of the fracture site. These inferences and conclusions are presented below, in succinct bullet point notation.

Sample population

- There is a general trend that the youngest and oldest individuals have the shortest trauma-death interval values. Individuals in middle age (between about 45 and 60 years) tend to survive the longest.
- There is a statistically significant positive correlation between the trauma-death interval (under 25 days) and the age of the individual. This correlation is significant to the 95% confidence level.
- There is no statistically significant result to suggest that the sex of the individual has an effect on the trauma-death interval, but male individuals were found to have slightly longer survival times than female individuals in the sample population.
- There is no evidence to suggest that the ethnic affiliation of the individual has an effect on the trauma-death interval.
- The number of fractures sustained by an individual does not statistically significantly affect the trauma-death interval.
- There is no statistically significant correlation between the location of the fracture(s) sustained and the trauma-death interval, but it is possible to infer that fractures of the skull and ribs are associated with the lowest trauma-death interval values, and those of the clavicle and femur are associated with higher trauma-death interval values.
- There appears to be no statistically significant correlation between the aetiology of the fracture(s) and the trauma-death interval.

Perl's Prussian Blue

- Evidence of positively-stained haemosiderin granules is not seen in the first 24 hours after trauma.
- The presence of positively-stained haemosiderin granules is statistically associated with trauma-death interval values later than 3 days. This association is significant to the 95% confidence level.

CD68

- Although there is no statistically significant relationship between the estimated size of the CD68+ cells and the trauma-death interval, there appears to be a pattern of an early peak in size during the first few days post-fracture, followed by a decline in CD68+ cell size, and then the maintenance of a constant CD68+ cell size after about 25 days post-fracture.
- There is a weak positive correlation between CD68 positive cell cover and the trauma-death interval in the first five days after trauma. This correlation was not found to be statistically significant.
- There is a statistically significant (to the 95% confidence level) relationship between the nature of the dispersal and the location of CD68+ cells and the trauma-death interval under 25 days. The CD68+ cells tend to be clustered around the fractured ends of bone and clustered within the extracellular matrix and the bone marrow in fractures with low trauma-death interval values, and are more evenly dispersed throughout the fracture site at higher trauma-death interval values.
- There appears to be a pattern of high abundance of blue-stained inflammatory cells present at the fracture site during the first few stages of healing, followed by a decline in estimated percentage cover of blue-stained cells with increasing trauma-death interval.

Bone sialoprotein

- There appears to be a weak negative correlation between the estimated percentage cover of BSP positive cells and the trauma-death interval in the first 20 days post-trauma. BSP+ cell cover is highest at the low trauma-death interval values, and sharply decreases to zero at 20 days. There is a low-level reappearance of BSP+ cells during the later stages of the healing process. This correlation was not found to be statistically significant.
- There is evidence of a weakly positive linear correlation between the size of the BSP+ cells and the trauma-death interval in the range of trauma-death interval values under 10 days. This correlation is not statistically significant.
- No correlation between the nature of the dispersal or the location of the BSP+ cells at the fracture site and the trauma-death interval was found.

- The estimated percentage cover of fibroblasts appears to make a statistically significant contribution to the prediction of the trauma-death interval. There is a positive correlation, which suggests that the abundance of fibroblasts increases with increased trauma-death interval.

Compact bone

- The estimated percentage of living compact bone at the fracture site appears to make a statistically significant negative contribution to the prediction of trauma-death interval through standard multiple regression. This means that, as the trauma-death interval rises, the percentage cover of living compact bone at the fracture site decreases. This correlation was confirmed in multiple regression analyses of the both the CD68-stained and the BSP-stained slides. This correlation was found to be statistically significant to the 95% confidence level.

Red blood cells

- The estimated percentage of red blood cells at the fracture site appears to make a statistically significant positive contribution to the prediction of trauma-death interval through standard multiple regression. This means that the higher the trauma-death interval, the higher the number of red blood cells seen at the fracture site. This correlation was confirmed in multiple regression analyses of the both the CD68-stained and the BSP-stained slides. This correlation was found to be statistically significant to the 95% confidence level.

Inter-observer agreement

- There were high levels of agreement between Observers 1, 2 and 3 in the estimations and observations made from the CD68-stained slides. The correlations for all observations were found to be statistically significant to the 99% confidence level.
- There was an extremely high level of agreement between Observer 1 and Observer 2 in the estimations and observations made from the BSP-stained slides. For the estimation of all types of cells, the correlation between the observations was found to be statistically significant to the 99% confidence level. The observations and estimations of each observer are believed to be reliable, true representations of the histologically-visible phenomena.

Looking ahead

It must be emphasised that this research represents only a preliminary investigation into the potential of histology and immunohistochemistry in the field of fracture dating. As such, it is one of the pioneers of this type of endeavor, and sits at the foot of the research hill with others such as Oni (1995) and Klotzbach and

colleagues (2003). It marks the beginnings of the recognition of mainstream pathological techniques by the discipline of forensic anthropology, and potentially a new strain of trauma analysis. As described in the introductory chapter, there are important applications for the accurate prediction of the trauma-death interval within forensic anthropology, beyond the sphere of the diagnosis of child abuse. In fact, the reliable and precise estimation of the trauma-death interval by any means, whether histologically based or not, would revolutionise the reconstruction of traumatic events for forensic purposes. The problem, however, is reaching the holy grail of precision and accuracy. It is hoped that this research could be built upon, and future researchers could account and compensate for the limitations that exist here. It may be most sensible and profitable to return to basics and consider animal analogues as a viable means of standardising the fracture data and controlling variables before attempting to describe human fractures.

Undoubtedly, improvements can easily be made in terms of the equipment and analysis software used. There are a wide variety of impressive and sophisticated commercial software packages available, that can significantly increase the complexity, detail and variety of collectable variables to compare to the trauma-death interval. These could include such variables as the intensity of immuno-positive staining for each type of cell, or the density of colour expressed in different areas of the fracture site. If time had been no object for this project, it would have been fruitful to examine factors such as the thickness of the periosteum, the size of compact bone lacunae, or the density of vascularity against the dependent variable of the time since trauma. The repertoire of proteins examined could also be expanded. There is certainly potential in the analysis of bone morphogenetic proteins at fracture sites, and the charting of their fluctuations with time since fracture. There is even scope for using similar immunohistochemical analyses to monitor the stages of tooth development, or bone development in infants and children. The multi-disciplinary nature of this research means that there are many different avenues open to further the investigation of temporal changes of histological phenomena.

The intention behind this research was to - if nothing else - open the eyes of the forensic anthropology community to the possibilities of incorporating proven histological and immunohistochemical methods into the standard repertoire of analytical techniques. It was hoped that this form of analysis could be successfully applied to a variety of hitherto unanswered forensic anthropology questions, and provide another weapon in the trauma analysis armoury. It is hoped now that this work will be recognised as a spring-board for continuing research into an exciting and potentially very rewarding topic that could have far-reaching consequences for the way that forensic anthropologists investigate trauma.

REFERENCES

Acebes, C.; de la Piedra, C.; Traba, M.; Seibel, M.; Martin, C.; Armas, J. and Herrero-Beaumont, G. (1999) Biochemical markers of bone remodeling and bone sialoprotein in ankylosing spondylitis. *Clinica Chimica Acta*. **289**: 99-110.

Akang, E.; Kuti, M.; Osunkoya, A.; Komolafe, E.; Malomo, A.; Shokunbi, M. and Amutta, S. (2002) Pattern of Fatal Head Injuries in Ibadan – A 10 Year Review. *Medicine, Science and the Law*, **42**(2): 160-166.

Arnold, J. and Jee, W. (1957) Bone Growth and Osteoclastic Activity as Indicated by Radioautographic Distribution of Pu239. *American Journal of Anatomy*. **101**: 367-417.

Baethmann, A.; Lehr, D. and Wirth, A. (1998) Prospective Analysis of Patient Management in Severe Head Injury. *Acta Neurochirurgica*, **71S**: 107-110.

Bandstra, R. and Carbone, L. (2001) Unusual Basal Skull Fracture in a Vehicle Equipped with an Air Bag. *The American Journal of Forensic Medicine and Pathology*. **22**(3): 253-255.

Bannister, L. (1995) Haemolymphoid System. In: Bannister, L.; Berry, M.; Collins, P.; Dyson, M.; Dussek, J. and Ferguson, M. (eds.) *Gray's Anatomy*. (*38th edition*) Churchill Livingstone, New York, USA. pp: 1399–1450.

Barou, O.; Mekraldi, S.; Vico, L.; Boivin, G.; Alexandre, C. and Lafage-Proust, M. (2002) Relationships between trabecular bone remodelling and bone vascularization: a quantitative study. *Bone*. **30**(4): 604-612.

Biswas, S. V. and Iqbal, R. (1998) *Mosby's Crash Course: Musculo-Skeletal System*. Mosby International Ltd, London, UK.

Blokhuis, T.; de Bruine, J.; Bramer, J.; den Boer, F.; Bakker, F.; Patka, P.; Haarman, H. and Manoliu, R. (2001) The reliability of plain radiography in experimental fracture healing. *Skeletal Radiology*. **30**(3): 151-156.

Bord, S.; Horner, A.; Hembry, R.; Reynolds, J. and Compston, J. (1996) Production of Collagenase by Human Osteoblasts and Osteoclasts in Vivo. *Bone*. **19**(1): 35-40.

Bostrom, M.; Yang, X. and Koutras, I. (2000) Biologics in Bone Healing. *Current Opinion in Orthopaedics.* **11**: 403-412.

Bruce, D. and Zimmerman, R. (1989) Shaken Impact Syndrome. *Pediatrics Annals* **18**: 482-494.

Burd, T.; Hughes, M. and Anglen, J. (2003) Heterotopic ossification prophylaxis with indomethacin increases the risk of long-bone nonunion. *Journal of Bone and Joint Surgery (British).* **85**(5): 700-5.

CALBIOCHEM (2003) *Anti-Bone Sialoprotein, Product Specification Sheet.* EMD Biosciences, Inc. USA.

Carletta, J. (1996) Assessing agreement on classification tasks: the kappa statistic. *Association for Computational Linguistics.* **22**(2): 1-6.

Caruso, G.; Lagalla, R.; Derchi, L.; Iovane, A. and Sanfilippo, A. (2000) Monitoring of Fracture Calluses with Color Doppler Sonography. *Journal of Clinical Ultrasound*, **28**(1): 20 – 27.

Cashman, J. and Bell, M. (2002) The multiply injured child. *Current Orthopaedics.* **16**: 442-450.

Catto, M. (1980) Healing (Repair) and Hypertrophy. In: Anderson, J. (ed.) *Muir's Textbook of Pathology. (11th edition)* Edward Arnold, UK.

Cho, H.; Stout, S. D.; Madsen, R. W. and Streeter, M. A. (2002) Population-specific Histological Age-Estimiating Method: A Model For Known African-American and European-American Skeletal Remains. *Journal of Forensic Sciences.* **47**(1): 12–18.

Claes, L.; Heigele, C.; Neidlinger-Wilke, C.; Kaspar, D.; Seidl, W.; Margevicius, K. and Augat, P. (1998) Effects of mechanical factors on the fracture healing process. *Clinical Orthopaedics.* **355**(S): 132-147.

Creighton, S. (1992) *Child abuse trends in England and Wales 1988-1990: and an overview from 1973-1990.* NSPCC, London, UK.

Cross, S. (2001) Observer accuracy in estimating proportions in images: implications for the semi-quantitative assessment of staining reactions and a proposal for a new system. *Journal of Clinical Pathology.* **54**: 385-390.

Cruess, R. and Dumont, J. (1975) Healing of bone, tendon and ligament. In: Rockwood, C. and Green, D. (eds.) *Fractures*. JB Lippincott, Philadelphia, USA.

Cuisinier, F. (1996) Bone Mineralization. *Current Opinion in Solid State and Materials Science*. **1**: 436-439.

Cummins, B. (1997) Chapter 3: Skull Fracture and Cranial Defects. In Macfarlane, R. and Hardy, D. (eds.) *Outcome After Head, Neck and Spinal Trauma*. Butterworth-Heinemann, Oxford, UK.

DAKO (1999) *Specification Sheet: Monoclonal Mouse Anti-Human Macrophage, CD68*. DAKOCytomation Laboratories, Denmark.

DeGoede, K.; Ashton-Miller, J. and Schultz, A. (2003) Fall-related upper body injuries in the older adult: a review of the biomechanical issues. *Journal of Biomechanics*. **36**: 1043-1053.

DeLacey, G.; Guilding, A.; Wignall, B.; Reidy, J. and Bradbrook, S. (1980) Mild Head Injuries: A Source of Excessive Radiography? (Analysis of a Series and Review of the Literature). *Clinical Radiology*, **31**: 457-462.

Derkx, P.; Nigg, A.; Bosman, F.; Birkenhager-Frenkel, D.; Houtsmuller, A.; Pols, H. and Van Leeuwen, J. (1998) Immunolocalization and Quantification of Noncollagenous Bone Matrix Proteins In Methylmethacrylate-Embedded Adult Human Bone In Combination with Histomorphometry. *Bone* **22**(4): 367-373.

Desai, B.; Meyer, M.; Porter, S.; Kellam, J. and Meyer, R. Jr. (2003) The effect of age on gene expression in adult and juvenile rats following femoral fracture. *Journal of Orthopedic Trauma*. **17**(10): 689-698.

Devlin, J. (2003) Personal communication. Mechanical Engineering Department, University of Sheffield.

Diamond, P.; Gale, S. and Denkhaus, H. (2001) Head injuries in skiers: an analysis of injury severity and outcome. *Brain Injury*. **15**(5): 429-434.

Doblare, M.; Garcia, J. M. and Gomez, M. J. (2003) Modelling Bone Tissue Fracture and Healing: A Review. *Engineering Fracture Mechanics*. **71**(13-14): 1809-1840.

Dudar, J. C.; Pfieffer, S. and Saunders, S. R. (1993) Evaluation of Morphological and Histological Adult Skeletal Age-At-Death Estimation Techniques Using Ribs. *Journal of Forensic Sciences*. **38**(3): 677 – 685.

Dyer, S.; Buckendahl, P. and Sampson H. (1998) Alcohol consumption inhibits osteoblastic cell proliferation and activity in vivo. *Alcohol*. **16**(4): 337-41.

Ehrlich, R.; McCloskey, E. and Daly, J. (1999) *Patient Care in Radiography, with an Introduction to Medical Imaging*. Mosby Incorporated, Missouri, USA.

Elliot, J.; Gilchrist, N. and Wells, J. (1996) The Effect of Socioeconomic Status on Bone Density in a Male Caucasian Population. *Bone*. **18**(4): 371-373.

Ellis, T.; Vezina, G. and Donahue, D. (2000) Acute Identification of Cranial Burst Fracture: Comparison between CT and MR Imaging Findings. *American Journal of Neuroradiology*, **21**: 795-801.

Erskine, L. (1959) The Mechanisms Involved in Skiing Injuries. *The American Journal of Surgery*. **97**(5): 667-671.

Escoffery, C. and Shirley, S. (2001) Fatal Head Trauma from Tree Related Injuries. *Medicine, Science and the Law*. **41**(4): 298-300.

Fisher, L.; McBride, O.; Termine, J. and Young, M. (1990) Human Bone Sialoprotein. *The Journal of Biological Chemistry*. **265**(4): 2347-2351.

Flatmark, A. (1964) Fracture Union in the Presence of Delayed Blood Coagulation. *Acta Chirurgica Scandinavica Supplementum*. **344**: 1-95.

Ford, J.; Robinson, D. and Scammell, B. (2002) The fate of soft callus chondrocytes during long bone fracture repair. *Journal of Orthopaedic Research*. **21**: 54-61.

Funk, J.; Hale, J.; Carmines, D.; Gooch, H. and Hurwitz, S. (2000) Biomechanical Evaluation of Early Fracture Healing in Normal and Diabetic Rats. *Journal of Orthopaedic Research*. **18**: 126-132.

Gean, A. (1994) *Imaging of Head Trauma*. Raven Press, New York, USA.

Giannoudis, P.; MacDonald, D.; Matthews, S. *et al.* (2000) Nonunion of the femoral diaphysis. The influence of reaming and non-steroidal anti-inflammatory drugs. *Journal of Bone and Joint Surgery.* **82B**: 655-658.

Giordano, V.; Giordano, M.; Knackfuss, I.; Apfel, M. and Gomes, R. (2003) Effect of Tenoxicam on Fracture Healing in Rat Tibiae. *Injury.* **34**(2): 85-94

Goh, K.; Ahuja, A.; Walkden, S. and Poon, W. (1997) Is Routine Computed Tomography (CT) Scanning Necessary in Suspected Basal Skull Fractures? *Injury.* **28**(5-6): 353–357.

Gruber, H. E. and Ingram, J. A. (2003) Basic Staining and Histochemical and Immunohistochemical Localizations Using Bone Sections. In: An, Y. H. and Martin, K. L. (2003) (eds.) *Handbook of Histology Methods for Bone and Cartilage.* Humana Press Inc. New Jersey, USA.

Gurley, A. and Roth, S. (1992) Bone. In: Sternberg, S. (ed.) *Histology for Pathologists.* Raven Press Ltd., New York, USA. pp: 61-79.

Hadjiargyrou, M.; Ahrens, W. and Rubin, C. (2000) Temporal expression of the chondrogenic and angiogenic growth factor CYR61 during fracture repair. *Journal of Bone and Mineral Research.* **15**(6): 1014-1023.

Hancox, N. (1972) The Osteoclast. In: Bourne, G. (ed.) *The Biochemistry and Physiology of Bone. Volume I. (2nd edition)* Academic Press, Inc. New York, USA. pp: 45-68.

Hannan, M.; Felson, D. and Hughes, B. (2000) Risk factors for longitudinal bone loss in elderly men and women: The Framingham osteoporosis study. *Journal of Bone and Mineral Research.* **15**: 710-720.

Härtl, R. and Ko, K. (1996) In Utero Skull Fracture: Case Report. *The Journal of Trauma: Injury, Infection and Critical Care.* **41**(3): 549-552.

Helling, T.; Watkins, M.; Evans, L.; Nelson, P.; Shook, J. and Van Way, C. (1999) Low Falls: An Underappreciated Mechanism of Injury. *Journal of Trauma: Injury, Infection and Critical Care.* **46**(3):453-456.

Hendler, A. and Hershkop, M. (1998) When To Use Bone Scintigraphy. It Can Reveal Things Other Studies Cannot. *Postgraduate Medicine.* **104**(5).

Hendrich, C.; Finkewitz, U. and Berner, W. (1995) Diagnostic Value of Ultrasonography and Conventional Radiography for the Assessment of Sternal Fractures. *Injury.* **26**(9): 601-604.

Hofman, P.; Nelemans, P.; Kemerink, G. J.; and Wilmink, J. (2000) Value of Radiological Diagnosis of Skull Fracture in the Management of Mild Head Injury: Meta-Analysis. *Journal of Neurosurgery and Psychiatry.* **68**: 416-422.

Hollands, C.; Winston, F.; Stafford, P. and Shochat, S. (1996) Severe Head Injury Caused by Airbag Depolyment. *The Journal of Trauma: Injury, Infection and Critical Care.* **41**(5): 920-922.

Hollinger, J.; Schmitt, J.; Hwang, K. and Buck, D. (1999) Impact of nicotine on bone healing. *Journal of Biomedical Materials Research.* **45**: 294–301.

Hughes, S.(1984) Fractures and Bone Grafts. In Galasko, C. and Weber, D. (eds.) *Current Problems in Orthopaedics: Radionuclide Scintigraphy in Orthopaedics.* Longman Group Limited. pp: 186-199.

Iancu, T. (1992) Ferritin and Hemosiderin in Pathological Tissues. *Electron Microscopy Review.* **5**: 209-229.

Irie, K.; Takeishi, H.; Tsuruga, E.; Sakakura, Y.; Nomura, S.; Ozawa, H.; Ejiri, S. and Yajima, T. (2002) Changes in Osteopontin Distribution and Matrix Mineralisation During Remodelling in Experimental Bone Formation. *Acta Histochem. Cytochem.* **35**(2): 113-118.

Ishigaki, R.; Takagi, M.; Igarashi, M. and Ito, K. (2002) Gene expression and immunohistochemical localization of osteonectin in association with early bone formation in the developing mandible. *The Histochemical Journal.* **34**: 57-66.

Islam, O.; Soboleski, D.; Symons, S.; Davidson, L.; Ashworth, M. and Babyn, P. (2000) Development and duration of radiographic signs of bone healing in children. *American Journal of Roentgenology.* **175**(1): 75-78.

Ito, Y.; Fitzsimmons, J.; Sanyal, A.; Mello, M.; Mukherjee, N. and O'Driscoll, S. (2001) Localization of chondrocyte precursors in periosteum. *Osteoarthritis and Cartilage*. **9**: 215-223.

Janssen, W. (1984) *Forensic Histopathology*. Springer-Verlag Berlin Heidelberg.

Jaworski, Z. F. G.; Duck, B. and Sekaly, G. (1981) *Kinetics of Osteoclasts and their Nuclei in Evolving Secondary Haversian Systems*. Journal of Anatomy. **133**(3): 397-405.

Jee, A.; Ragheb, J. and Morrison, G. (2003) Television Tipovers as a Significant Source of Pediatric Head Injury. *Pediatric Neurosurgery*. **38**(4): 191-194.

Jennet, B. (1980) Skull X-rays After Recent Head Injury. *Clinical Radiology*. **31**: 463-469.

Jones, J. and Trippet, R. (1992) The relationship between cigarette smoking to impaired intraoral wound healing: a review of evidence and implications for patient care. *Journal of Oral Maxillofacial Surgery*. **50**: 237-239.

Jones, N. (ed.) (1997) *Craniofacial Trauma: An Inter-disciplinary Approach*. Oxford University Press, Oxford, UK.

Junqueira, L.; Carneiro, J. and Kelley, R. (1995) *Basic Histology. (8th edition)* Prentice-Hall International, Inc. USA.

Kairys, S.; Alexander, R.; Block, R.; Everett, V.; Hymel, K. and Jenny, C. (2001) Shaken Baby Syndrome: Rotational Cranial Injuries – Technical Report (T0039). *Paediatrics*. **108**(1): 206-210.

Kakar, S. and Einhorn , T. (2004) Importance of Nutrition in Fracture Healing. In: Holick, M. and Dawson-Hughes, B. (2004) *Nutrition and Bone Health*. Humana Press, USA. pp: 85-104.

Kelly, A.; Zimmerman, R.; Snow, R.; Gandy, S.; Heier, L.; and Deck, M. (1988) Head Trauma: Comparison of MR and CT – Experience in 100 Patients. *American Journal of Neuroradiology*. **9**: 699-708.

Kenwright, J.; Richardson, J.; Goodship, A. *et al.* (1986) Effect of controlled axial micromovement on healing of tibial fractures. *Lancet.* **2**(8517): 1185-7.

Khan, H. (2004) Computer-assisted visualization and quantitation of experimental gastric lesions in rats. *Journal of Pharmacological and Toxicological Methods.* **49**: 89-95.

Khan, K.; McKay, H.; Kannus, P.; Bailey, D.; Wark, J. and Bennell, K. (2001) *Physical Activity and Bone Health.* Human Kinetics, Illanois, USA.

Kleinman, P. (1998) *Diagnostic Imaging of Child Abuse. (2nd edition)* Mosby, Missouri, USA.

Kleinman, P.; Marks, S.; Richmond, J. and Blackbourne, B. (1995) Inflicted Skeletal Injury: A Postmortem Radiologic-Histologic study in 31 infants. *American Journal of Roentgenology.* **165**: 647-650.

Klotzbach, H.; Delling, G.; Richter, E.; Sperhake, J. and Püschel, K. (2003) Post-mortem diagnosis and age estimation of infants' fractures. *International Journal of Legal Medicine.* **117**: 82-89.

Konrad, C.; Fieber, T.; Scheupfer, G. and Gerber, H. (1996) Are Fractures of the Base of the Skull Influenced by the Mass of the Protective Helmet? A Retrospective Study in Fatally Injured Motorcyclists. *The Journal of Trauma: Injury, Infection and Critical Care.* **41**(5): 854-858.

Kreel, L. and Meive, H. B. (1979) Chapter 35: Computed Tomography and Ultrasound: A Comparison. In Kreel, L. (ed.) *Medical Imaging: A Basic Course.* HM&M Publishers, Aylesbury, UK. pp: 236-240.

Leitgeb, N.; Bodenteich, F.; Schweighofer, F. and Fellinger, M. (1990) Sonographic Fracture Diagnosis. *Ultraschall in der Medizin.* **11**: 206-209.

Lewallen, D.; Chao, E.; Kasman, R. and Kelly, P. (1984) Comparison of the effects of compression plates and external fixators on early bone healing. *Journal of Bone and Joint Surgery (American).* **66**(7): 1084-1091.

Li, G.; White, G.; Connolly, C. and Marsh, D. (2002) Cell Proliferation and Apoptosis During Fracture Healing. *Journal of Bone and Mineral Research.* **17**(5): 791-799.

Lloyd, D.; Carty, H.; Roe, D. and Patterson, M. (1996) The Value of Skull X-rays in Head-Injured Children. *Injury: International Journal of the Care of the Injured.* **27**(3): 370-371.

Loder, R. (1988) The influence of diabetes mellitus on the healing of closed fractures. *Clinical Orthopaedics.* **232**: 210-216.

Lu, H.; Kraut, D.; Gerstenfeld, L. and Graves, D. (2003) Diabetes interferes with the bone formation by affecting the expression of transcription factors that regulate osteoblast differentiation. *Endocrinology.* **144**(1): 346-352.

Lumb, P. (2001) Personal communication. Lecturer in Forensic Pathology, Department of Forensic Pathology, University of Sheffield.

Lydyard, P.; Whelan, A. and Fanger, M. (2000) *Instant Notes in Immunology.* BIOS Scientific Publishers, Limited, Oxford, UK.

Maffulli, N. and Thornton, A. (1995) Ultrasonographic Appearance of External Callus in Long-Bone Fractures. *Injury.* **26**(1): 5-12.

Majeska, R.; Ryaby, J. and Einhorn, T. (1994) Direct modulation of osteoblastic activity with estrogen. *Journal of Bone and Joint Surgery (American).* **76**(5): 713-21.

Maples, W. and Browning, M. (1994) *Dead Men Do Tell Tales.* Souvenir Press. New York, USA.

Mark, H.; Nilsson, A.; Nannmark, U. and Rydevik B. (2004) Effects of fracture fixation stability on ossification in healing fractures. *Clinical Orthopaedics.* **419**: 245-50.

Marks, P. (2003) SUVs double pedestrians' risk of death. *New Scientist.* 10/12/03.

Marieb, E. N. (2001) *Human Anatomy and Physiology.* (*5th edition*) Benjamin Cummings, USA.

Martin, R. B.; Burr, D. B. and Sharkey, N. A. (1998) *Skeletal Tissue Mechanics.* Springer-Verlag New York, Inc.

Martiniakova, M.; Vondrakova, M. and Fabis, M. (2003) Investigation of the Microscopic Structure of Rabbit Compact Bone Tissue. *Scripta Medica (BRNO).* **76**(4): 215-220.

Mason, J. (2004) Personal communication. Technician, Department of Forensic Pathology, University of Sheffield.

Mather-Saul, J. (1997) *Notes from The 2nd European Forensic Anthropology Course: Trauma Analysis.* Department of Archaeological Sciences, University of Bradford. (unpublished).

Mays, S. (1998) *The Archaeology of Human Bones.* Routledge Publishers, UK.

McCarthy, M. and Gilbert, K. (1996) Cyclist Road Deaths in London 1985-1992: Drivers, Vehicles, Manouvres and Injuries. *Accident Analysis and Prevention.* **28**(2): 275-279.

McKibbin, B. (1978) The Biology of Fracture Healing in Long Bones. *Journal of Bone and Joint Surgery.* **60B**: 150-161.

McKinley, D.; Chambliss, M.; and Greensboro, N. (2000) Follow-up Radiographs to Detect Callus Formation After Fractures. *Archives of Family Medicine.* **9**: 373-374.

McRae, R. (1994) *Practical Fracture Treatment.* (*3rd edition*). Churchill Livingstone, New York, USA.

Mogbo, K.; Slovis, T.; Canady, A.; Allasio, D. and Arfken, C. (1998) Appropriate Imaging in Children with Skull Fractures and Suspicion of Abuse. *Radiology*, **208**: 521-524.

Moseley, I. (1979) Chapter 16: Computed Tomography in Craniocerebral Trauma. In Kreel, L. (ed.) *Medical Imaging: A Basic Course.* HM&M Publishers, Aylesbury, UK. pp: 107-111.

Nagy, K.; Joseph, K.; Krosner, S.; Roberts, R.; Leslie, C.; Dufty, K.; Smith, R. and Barrett, J. (1999) The Utility of Head Computed Tomography after Minimal Head Injury. *The Journal of Trauma: Injury, Infection and Critical Care*, **46**(2): 268-270.

Nakase, T.; Nomura, S.; Yoshikawa, H.; Hashimoto, J.; Hirota, S.; Kitamura, Y.; Oikawa, S.; Ono, K. and Takaoka, K. (1994) Transient and localized expression of bone morphogenetic protein 4 messenger RNA during fracture healing. *Journal of Bone and Mineral Research.* **9**(5): 651-659.

Newsome, I. (2004) Personal communication. Chief Technician, Department of Forensic Pathology, University of Sheffield.

Nicoll, S.; Denker, A. and Tuan, R. (1998) Mesenchymal Cell-Based Repair of Connective Tissue Defects: Application of Transforming Growth Factor-β Superfamily Members and Biodegradable Polymers Scaffolds. *Cells and Materials.* **8**: 99-122.

O'Connor, J. and Cohen, J. (1998) Dating Fractures. In Kleinman, P. (ed.) *Diagnostic Imaging of Child Abuse (2nd edition).* Mosby, USA.

O'Driscoll, S.; Saris, D.; Ito, Y. and Fitzimmons, J. (2001) The chondrogenic potential of periosteum decreases with age. *Journal of Orthopaedic Research.* **19**(1): 95-103.

Ohishi, T.; Takahashi, M.; Kushida, K.; Hoshino, H.; Tsuchikawa, T.; Naitoh, K. and Inoue, T. (1998) Changes of biochemical markers during fracture healing. *Archives of Orthopaedic Trauma Surgery.* **118**: 126-130.

Oni, O. (1997a) The early stages of the repair of adult human diaphyseal fractures. *Injury: International Journal of the Care of the Injured.* **28**(8): 521-525.

Oni, O. (1997b) The bony callus. *Injury: International Journal of the Care of the Injured.* **28**(9-10): 629-631.

Oni, O. (1995) Protein immunohistochemistry as a means of unravelling the mysteries of fracture repair. *Injury.* **26**(8): 523-525.

Ortner, D. and Putschar, W. (1985) *Identification of Pathological Conditions in Human Skeletal Remains.* Smithsonian Institution Press, Washington, USA.

Page, K. (1982) Bone and the Preparation of Bone Sections. In: Bancroft, J. and Stevens, A. (eds.) *Theory and Practice of Histological Techniques.* (*2nd edition*) Churchill Livingstone, Great Britain. pp: 297-331.

Petrie, A. and Sabin, C. (2000) *Medical Statistics at a Glance*. Blackwell Science, London, UK.

Pipas, L.; Schaeffer, N. and Brown, L. (2002) Falls From Rooftops After Heavy Snowfalls: The Risks of Snow Clearing Activities. *American Journal of Emergency Medicine*. **20**(7): 635-637.

Pinero, G.; Farach-Carson, M.; Devoll, R.; Aubin, J.; Brunn, J. and Butler, W. (1995) Bone Matrix Proteins in Osteogenesis and Remodelling in the Neonatal Rat Mandible as studied by Immunolocalization of Osteopontin, Bone Sialoprotein, alpha$_2$HS-Glycoprotein and Alkaline Phosphatase. *Archives of Oral Biology*. **40**(2): 145-155.

Plunkett, J. (2001) Fatal Pediatric Head Injuries Caused by Short-Distance Falls. *The American Journal of Forensic Medicine and Pathology*. **22**(1): 1-12.

Pollanen, M. (1997) The Diagnostic Value of The Diatom Test For Drowning. II. Validity: Analysis of Diatoms in Bone Marrow and Drowning Medium. *Journal of Forensic Sciences*. **42**(2): 286-290.

Prat, R. and Calatayud-Maldonado, V. (1998) Prognostic Factors in Post-Traumatic Severe Diffuse Brain Injury. *Acta Neurochirurgica*. **140**: 1257-1261.

Pritchard, J. (1964) Histology of Fracture Repair. In: Clark, J. (ed.) *Modern Trends in Orthopaedics, 4*. Butterworths, London, UK.

Pritchard, J. (1972a) General Histology of Bone. In: Bourne, G. H. (ed.) *The Biochemistry and Physiology of Bone. Volume I.* (*2nd edition*) Academic Press, Inc. New York, USA. pp: 1-21.

Pritchard, J. (1972b) The Osteoblast. In: Bourne, G. H. (ed.) *The Biochemistry and Physiology of Bone.* (*2nd edition*) Academic Press, Inc. New York, USA. pp: 21-44.

Pullan, B. (1979) Chapter 2: Computed Tomography Limits and Resolution. In Kreel, L. (ed.) *Medical Imaging: A Basic Course*. HM&M Publishers, Aylesbury, UK. pp: 10-14.

Quigley, M.; Vidovich, D.; Cantella, D.; Wilberger, J.; Maroon, J. and Diamond, D. (1997) Defining the Limits of Survivorship after Very Severe Head Injury. *The Journal of Trauma: Injury, Infection and Critical Care*. **42**(1): 7-10.

Raekallio, J. (1980) Histological Estimation of the Age of Injuries. In: Perper, J. and Wecht, C. (eds.) *Microscopic Diagnosis in Forensic Pathology*. Charles C Thomas, Illinois, USA.

Raekallio, J. and Mäkinen, P.-L. (1967) Aminopeptidases in serum and skin of rats during early wound healing. *Annales Medicinae Experimentalis et Biologiae Fenniae*. **45**: 224-229.

Reath, D.; Kirby, J.; Lynch, M. and Maull, K. (1989) Patterns of Maxillofacial Injurues in Restrained and Unrestrained Motor Vehicle Crash Victims. *The Journal of Trauma*. **29**(6): 806-810.

Reed, A.; McCarty, H.; Evans, G.; Turner, R. and Westerlind, K. (2002) The effects of chronic alcohol consumption and exercise on the skeleton of adult male rats. *Alcoholism: Clinical and Experimental Research*. **26**(8): 1269-74.

Reed, W. and Mueller, R. (1998) Spiral fracture of the humerus in a ball thrower. *The American Journal of Emergency Medicine*. **16**(3): 306-308.

Reinholt, F.; Hultenby, K.; Oldberg, A. and Heinegard, D. (1990) Osteopontin – a possible anchor of osteoclasts to bone. *Proceedings of the National Academy of Science*. **87**: 4473-4475.

Resnik C.; Stackhouse D.; Shanmuganathan K. and Young J. (1992) Diagnosis of pelvic fractures in patients with acute pelvic trauma: efficacy of plain radiographs. *American Journal of Roentgenology*. **158**(1): 109-12.

Revell, P. A. (1986) *Pathology of Bone*. Springer-Verlag Berlin Heidelberg.

Roach, H. (1994) Why does bone matrix contain non-collagenous proteins? The possible roles of osteocalcin, osteonectin, osteopontin and bone sialoprotein in bone mineralisation and resorption. *Cell Biology International*. **18**(6): 617-628.

Roberts, G.; Hughes, J. and Hourihan, M. (1998) How Images Are Produced. In Roberts, G.; Hughes, J. and Hourihan, M. (eds.) *Clinical Radiology for Medical Students*. (*3rd edition*). Butterworth-Heinemann, Oxford, UK. pp: 9-14.

Samson, H. (1998) Effect of alcohol consumption on adult and aged bone: a histomorphometric study of the rat animal model. *Alcoholism: Clinical and Experimental Research.* **22**(9): 2029-34.

Scheidler, M.; Shultz, B.; Schall, L.; Vyas, A. and Barksdale, E. (2002) Falling Televisions: The Hidden Danger for Children. *Journal of Pediatric Surgery.* **37**(4): 572-575.

Schiwy-Bochat, K. H. and Lemke, R. (1999) Iliac Cancellous Bone in Drug Addicts: A Histomorphometric Study. *Journal of Forensic Sciences.* **44**(2): 249-252.

Schmitz, M.; Finnegan, M.; Natarajan, R. and Champine, J. (1999) Effect of smoking on tibial shaft fracture healing. *Clinical Orthopaedics.* **365**: 184-200.

Schwartz, J. (1995) *Skeleton Keys: An Introduction to Human Skeletal Morphology, Development and Analysis.* Oxford University Press, New York, USA.

Sevitt, S. (1981) *Bone Repair and Fracture Healing In Man.* Current Problems in Orthopaedics series. Churchill Livingstone, New York, USA.

Shorter, N.; Jensen, P.; Harmon, B. and Mooney, D. (1996) Skiing injuries in children and adolescents. *The Journal of Trauma: Injury, Infection and Critical Care.* **40**: 997-1001.

Soames, R. W. (1995) Skeletal System. In: Bannister, L.; Berry, M.; Collins, P.; Dyson, M.; Dussek, J. and Ferguson, M. (eds.) *Gray's Anatomy.* (*38th edition*) Churchill Livingstone, New York, USA. pp: 425-737.

Solanki, P.; Mulgaonkar, K. and Rao, S. (2000) Effect of early mobilisation on grip strength, pinch strength and work of hand muscles in cases of closed diaphyseal fracture radius-ulna treated with dynamic compression plating. *Journal of Postgraduate Medicine.* **46**: 84-87.

Sommer, B.; Bickel, M.; Hofstetter, W. and Wetterwald, A. (1996) Expression of Matrix Proteins During the Development of Mineralized Tissues. *Bone* **19**(4): 371-380.

Soubrier, M.; Dubost, J-J.; Boisgard, S.; Sauvezie, B.; Gaillard, P.; Michel, J. and Ristori, J-M. (2003) Insufficiency fracture. A survey of 60 cases and review of the literature. *Joint Bone Spine.* **70**: 209-218.

Starling, S.; Heller, R. and Jenny, C. (2002) Pelvic fractures in infants as a sign of physical abuse. *Child Abuse and Neglect*. **26**: 475-480.

Steiner, G. and Sprigg, A. (1992) The Value of Ultrasound in the Assessment of Bone. *The British Journal of Radiology*, **65**: 589-593.

Stewart, R. (2004) Personal communication. Imaging Technician, Department of Pathology, University of Sheffield.

Stout, S. D. (1986) The Use of Bone Histomorphometry in Skeletal Identification: The Case of Fransisco Pizarro. *Journal of Forensic Sciences*. **31**(1): 296-300.

Stout, S. D. (1988) The Use of Histomorphometry to Estimate Age. *Journal of Forensic Sciences*. **33**(1): 121-125.

Sykaras, N. and Opperman, L. (2003) Bone morphogenetic proteins (BMPs): how do they function and what can they offer the clinician? *Journal of Oral Science*. **45**(2): 57-73.

Szachowicz, E. (1995) Facial Bone Wound Healing. *Otolaryngologic Clinics of North America*. **28**(5): 865-880.

Tabachnick, B. and Fidell, L. (2001) *Using Multivariate Statistics*. (*4th edition*) Allyn and Bacon, Needham Heights, USA.

Taitz, J.; Moran, K. and O'Meara, M. (2004) Long bone fractures in children under 3 years of age: Is abuse being missed in Emergency Department presentations? *Journal of Paediatric Child Health*. **40**: 170-174.

Tami, A.; Nasser, P.; Schaffler, M. and Knothe Tate, M. (2003) Noninvasive fatigue fracture model of the rat ulna. *Journal of Orthopaedic Research*. **21**(6): 1018-1024.

Tanrikulu, R. and Erol, B. (2001) Comparison of Computed Tomography with Conventional Radiography for Midfacial Fractures. *Dentomaxillofacial Radiology*, **30**: 141-146.

Teh, J.; Firth, M.; Sharma, A.; Wilson, A.; Reznek, R. and Chan, O. (2003) Jumpers and Fallers: a Comparison of the Distribution of Skeletal Injury. *Clinical Radiology*. **58**(6): 482-486.

Temes, R.; White, J.; Ketai, L.; Deis, J.; Pett, S.; Osler, T. and Wernly, J. (1997) Head, Face and Neck Trauma from Large Animal Injury in New Mexico. *The Journal of Trauma: Injury, Infection and Critical Care*. **43**(3): 492-495.

Thompson, D. (1981) Microscopic Determination of Age at Death in an Autopsy Series. *Journal of Forensic Sciences*. **26**(3): 470-475.

Thomsen, T.; Elle, B. and Thomsen, J. (1997) Post-mortem radiological examination in infants: Evidence of child abuse? *Forensic Science International*. **90**: 223-230.

Tomsick, T.; Chambers, A. and Lukin, R. (1978) Skull Fractures. *Seminars in Roentgenology*. **13**(1): 27-36.

Turner, R.; Kidder, L.; Kennedy, A.; Evans, G. and Sibonga, J. (2001) Moderate alcohol consumption suppresses bone turnover in adult female rats. *Journal of Bone and Mineral Research*. **16**(3): 589-94.

Underwood, J (ed.) (2000) *General and Systematic Pathology*. (*3rd edition*) Harcourt Publishers, UK.

Väänänen, H.; Liu, Y-K.; Lehenkari, P. and Uemara, T. (1998) How Do Osteoclasts Resorb Bone? *Materials Science and Engineering*. **C6**: 205-209.

van der Lei, B.; Damen , A.; Robinson, P. and Klasen, H. (1992) Spiral fracture of the proximal phalanx of the index finger by finger wrestling. *Injury*. **23**(8): 560-561.

Vanezis, P. (2001) Interpreting bruises at necropsy. *Journal of Clinical Pathology*. **54**: 348-355.

Walker, P.; Cook, D. and Lambert, P. (1997) Skeletal Evidence for Child Abuse: A Physical Anthropological Perspective. *Journal of Forensic Science*. **42**(2): 196-207.

Webb, J. and Tricker, J. (2000) A Review of Fracture Healing. *Current Orthopaedics*. **14**: 457-463.

Webber, R. and Folio, J. (1976) Radiographic Detectability of Occipital and Temporo-Parietal Fractures Induced in Cadaver Heads. *Journal of Trauma.* **16**: 115-123.

Weir, J. and Murray, A. (1998) Chapter 11: Appendix. In Weir, J. and Murray, A. D. (eds.) *Mosby's Atlas and Text of Clinical Imaging.* Mosby – Wolfe, London, UK.

Wells, P. (1979) Chapter 5: Ultrasound Limits, Resolution and Equipment. In Kreel, L. (ed.) *Medical Imaging: A Basic Course.* HM&M Publishers, Aylesbury, UK. pp: 27-32.

Wichmann, M.; Arnoczky, S.; DeMaso, C.; Ayala, A. and Chaudry, I. (1996) Depressed Osteoblast Activity and Increased Osteocyte Necrosis after Closed Bone Fracture and Hemorrhagic Shock. *The Journal of Trauma: Injury, Infection and Critical Care.* **41**(4): 628-633.

Wollheim, F. (1999) Bone sialoprotein – a new marker for subchondral bone. *Osteoarthritis and Cartilage.* **7**: 331-332.

Xu, Y-H. and Pitot, H. (1999) Building quantitative stereology data files with Scion Image, a public domain image processing and analysis software. *Computer Methods and Programs in Biomedicine.* **59**: 131-142.

Yaoita, H.; Orimo, H.; Shirai, Y. and Shimada, T. (2000) Expression of bone morphogenetic proteins and rat distal-less homol genes following rat femoral fracture. *Journal of Bone Mineral Metabolism.* **18**: 63-70.

Yeo, L. and Reed, M. (1994) Staging of healing of femoral fractures in children. *Canadian Association of Radiology Journal.* **45**(1):16-19.

Yoshioka, H.; Sakoda, K.; Kohno, H.; Hada, H. and Kurisu, K. (1997) Usefulness of Color Doppler Sonography in a Growing Skull Fracture: Case Report. *The Journal of Trauma: Injury, Infection and Critical Care.* **42**(1): 144-146.

Young, J.; Kostrubiak, I.; Resnik, C. and Paley, D. (1990) Sonographic Evaluation of Bone Production at the Distraction Site in Ilizarov Limb-Lengthening Procedures. *American Journal of Radiology.* **154**: 125-128.

Young, M. (2003) Bone matrix proteins: their function, regulation, and relationship to osteoporosis. *Osteoporosis International.* **14**(S3): S35-S42.

Zimmerman, R.; Bilaniuk, L.; Hackney, D.; Goldberg, H. and Grossman, R. (1987) Magnetic Resonance Imaging in Temporal Bone Fracture. *Neuroradiology.* **29**: 246-251.

e – REFERENCES

Auode, S. (2002) *The Pan Am 103 Crash Website.* [Internet].
Available from: http://www.geocities.com/CapitolHill/5260/victim.html. [Accessed 24/06/04].

Borrill, J.; Deakin, S. and Funk, L. (2001) *Orthoteers Orthopaedic Education Resource.* [Internet].
Available from: http://www.orthoteers.co.uk. [Accessed 09/06/04].

Bowley, D. and Boffard, K. (2002) *Pattern of injury in motor vehicle accidents.* [Internet].
Available from:http:// www.worldwidewounds.com. [Accessed 27/08/04].

Breuckmann, F. (ed.) (2000) *General Orthopaedics: Fractures.* [Internet].
Available from: http://www.dynomed.com. [Accessed 08/08/04].

Cruess, R. and Dumont, J. (1975) *Healing of bone, tendon and ligament.* [Internet].
Available from: http://www.ivis.org. [Accessed 13/08/04].

DePuy Ace Orthopaedics (2001) *Fracture Healing.* [Internet].
Available from: http://www.depuyace.com/fracture_healing. [Accessed 10/06/04].

Forensic Psychology Practice Ltd. (1999) *Non-accidental Injury.* [Internet].
Available from: http://www.forensicpsychology.co.uk/Downloads/WebNAI.pdf. [Accessed 06/08/04].

Futrell, M. (2003) *Understanding the Healing Process: The Phases of Tissue Healing and The Healing Process of Various Body Tissues.* [Internet].
Available from: http://www.cofc.edu/~futrell/healing.html. [Accessed 08/08//04].

Gardland, K. (1999) *Inferential.* [Internet].
Available from: http://www.garland.f9.co.uk/RM/inferential.htm#4. [Accessed 22/11/04].

Goyert, S. (1999) *CD68.* [Internet].
Available from: http://www.ncbi.nlm.nih.gov/prow/guide/2088387162_g.htm. [Accessed 29/06/08].

King, D. (2004) *Connective Tissue Study Guide.* [Internet].
Available from: http://www.siumed.edu/~dking2/intro/ct.htm. [Accessed 01/07/04].

Lujan, B. F. and White, R. J. (2002) *Human Physiology in Space.* National Space Biomedical Research Institute. [Internet].
Available from: http:// www.nsbri.org/HumanPhysSpace/indexb.html. [Accessed 06/08/04].

Lumb, P. (2000) *Poisoning by Sodium Nitroprusside.* [Internet].
Available from: http://forensic.shef.ac.uk.museum.html. [Accessed 29/06/04].

Marc, J. (2004) *Bone Remodelling in Diabetes Mellitus.* [Internet].
Available from: http://www.ifcc.org/ejifcc/vol13no5/1305200215n.htm. [Accessed 09/08/04].

Marcus, R.; Feldman, D. and Kelsey, J. (eds.) (2001) *Osteoporosis. Volume I. (2nd edition)* Academic Press, London, UK. [Internet].
Available from: http://www.academicpress.com. [Accessed 12/06/04].

McCardell, E. (ed.) (2002) *Smoking Inhibits Fracture Healing and Bone Formation.* [Internet].
Available from: http:// www.pharmacytimes.com/article.cfm?ID=173. [Accessed 05/08/04].

Moore, A.; McQuay, H.; Edwards, J.; Barden, J. and Derry, S. (1994) *NSAIDs, coxibs, smoking and bone.* [Internet].
Available from: http://www.jr2.ox.ac.uk/bandolier/booth/painpag/wisdom/NSAIbone.html

National Institute of Health: Osteoporosis and Related Bone Diseases – National Resource Center (2001) *Fact Sheet: Nutrition and the Skeleton.* [Internet].
Available from: http://www.osteo.org. [Accessed 07/08/04].

Nuzzo, R. (2002) *Trauma, Fractures, Bones.* [Internet].
Available from: http://www.pediatric-orthopaedics.com. [Accessed 05/08/04].

Parker, S. (2004) *Delayed and non-union.* [Internet].
Available from: http:// www.surgical-tutor.org.uk/default-home.htm?core/trauma/union.htm~right. [Accessed 08/08/04].

SAS Institute Inc. (1999) *Statistical Computations.* [Internet].
Available from: http://jeff-lab.queensu.ca/stat/sas/sasman/sashtml/proc/zompmeth.htm. [Accessed 22/11/04].

Schmidt, A. and Templeman, D. (2002) *Fracture Healing.* Proceedings of the 18th Annual Meeting of the Orthopaedic Trauma Association. [Internet].
Available from: http:// www.medscape.com/viewarticle/444926_2. [Accessed 07/08/04].

Scott, C. (1998) *The Harvard Citation Guide.* [Internet].
Available from: http://www.lmu.ac.uk/lss/ls/docs/harv4.htm. [Accessed 15/11/04].

Simpson, W. (2003) *Alcohol and Other Factors Affecting Osteoporosis Risk in Women.* National Institute on Alcohol Abuse and Alcoholism [Internet].
Available from: http:// www.niaaa.nih.gov/publications/arh26-4/292-298.htm. [Accessed 07/08/04].

StatSoft (2003a) *Kolmogorov-Smirnov.* [Internet].
Available from: http://www.statsoft.com/textbook/glosi.html. [Accessed 22/11/04].

StatSoft (2003b) *ANOVA/MANOVA.* [Internet].
Available from: http://www.statsoft.com/textbook/stanman.html. [Accessed 22/11/04].

Whitfield, J.; Morley, P. and Willick, G. (2000) *The Parathyroid Hormones: Bone-Forming Agents for Treatment of Osteoporosis.* [Internet].
Available from: http://www.medscape.com. [Accessed 08/08/04].

APPENDIX 01

Letter to South Sheffield Research Ethics Committee

THE UNIVERSITY OF SHEFFIELD

Academic Unit of Forensic Pathology

Dr M P Evison, Senior Lecturer in Forensic and Biological Anthropology

The Medico - Legal Centre
Watery Street

Tel: -
Fax: -
Mobile: -
email: -
WWW: -

Professor Christopher Taylor
South Sheffield Research Ethics Committee

12th May 2004

Dear Professor Taylor,

PhD research project involving archived material

We are writing to ask for your advice concerning a PhD research project being conducted by Miss Anna Williams, of which we are cosupervisors.

Anna is investigating the trauma–death interval in rib fractures by using a histopathological and immunohistochemical analysis of formalin-fixed wax-embedded rib fracture specimens from the forensic pathology archive.

When Anna's project was planned in 2001 it was common practice to use archived residual fixed material of this kind for research. The tissue was obtained lawfully under the Coroners rules. Anna's samples were anonymised and taken from the archived residue of the tissue. There was no assumption at that time that ethical approval should be sought.

In 2004, Professor James Underwood became a co-supervisor and raised concerns about the absence of ethical committee approval for the project. Following a number of well-publicised incidents concerning the use of post-mortem tissue it is clear that the assumptions made at the start of Anna's project need to be reconsidered, albeit retrospectively.

We emphasise that the tissue from which Anna's specimens were derived was not extra tissue taken from the deceased for research purposes. The forensic pathologist did not envisage use for research when the tissue samples were collected and the issue of consent would not have arisen. It would probably be impossible to obtain consent now, given the time that has elapsed since the tissue was originally taken and the practical difficulty of identifying and arranging to approach relatives.

Anna has recently completed her laboratory work and is analysing her results. We have discussed the situation with her advisor, Professor Chris Milroy, who asks us to point out that Anna has behaved conscientiously in every aspect of her project, but finds herself in an uncertain situation that is an understandable source of anxiety.

We are facing a problem that we believe is the consequence of changing assumptions regarding the research use of post-mortem tissues and we would be very grateful if you could advise us if and how we might proceed with Anna's project.

Yours sincerely,

Martin Evison (Academic Unit of Forensic Pathology)

James Underwood (Academic Unit of Pathology)

CC: Professor Chris Milroy (Academic Unit of Forensic Pathology)

APPENDIX 02

Sample population data (see Chapter 03)

PM number	Sex	Age (years)	Ethnicity	Cause of death	Trauma aetiology	Trauma-death interval (days)
14017	f	92	white	broncho-pneumonia due to fracture	assault	24
12866x	m	0.2	white	head injury	abuse	0
13405	m	39	unrecorded	lacerated spleen due to blunt chest trauma	unknown	2
13548	m	34	white	chest + abdominal injury	rta	15
12021	f	86	white	broncho-pneumonia	undertaker's fracture'	neg
12163	m	44	white	head injury	assault	1
10540h	f	57	white	broncho-pneumonia due to fracture	fall	66
11172x	m	75	white	mi due to coronary atherscIerosis	undertaker's fracture'	neg
9417	m	90	white	ischaemic heart disease due to coronary + chest injury	hit by tram	21
9440	f	0.7	asian	head injury	abuse	1-2
9888x	m	57	afro-cari	pulmonary embolism due to fracture	fall down stairs	17
7920x	m	62	asian	broncho-pneumonia due to fracture	assault	38
8262	m	83	unrecorded	pulmonary thrombosis due to leg deep vein thrombosis	fall	1-3
7512x	f	0.3	white	hydrocephalus	resuscitation	1
6682x	f	0.4	white	head injury	abuse	0
7522x	m	58	white	contusion of lungs + rib fracture	fall	3
5477x	f	0.1	white	head injury	abuse	19
5591	f	83	unrecorded	ruptured spleen	fall	7
5776	f	0.2	white	head injury	abuse	2
5817h	m	57	white	respiratory distress due to head injury + paraplegia	rta	120
5919	f	96	unrecorded	fat embolism due to fracture	fall	1
6258	m	77	white	general debility + Parkinson's disease	fall out of bed	4

PM number	Sex	Age (years)	Ethnicity	Cause of death	Trauma aetiology	Trauma-death interval (days)
4995x	f	0.3	unrecorded	head injury	abuse	2
5304	m	77	white	coronary occlusion	undertaker's fracture'	neg
5430	m	71	unrecorded	broncho-pneumonia due to fracture	fall	5
4165	m	60	unrecorded	broncho-pneumonia due to fracture	fall	4
4327	f	75	unrecorded	scepticaemic shock due to fracture	fall	28
3061	f	75	unrecorded	broncho-pneumonia due to fracture	fall	21
5405	f	98	unrecorded	broncho-pneumonia due to fracture	assault	9

APPENDIX 03

Materials used (see Chapter 03)

Some items may have been used during multiple stages of the procedures described in Chapter 03: Materials and Methodology. They have only been referenced once in this list.

Dissection at autopsy

10% buffered formalin solution

white plastic tubs of varying sizes to hold tissue samples

Decalcification

4M formic acid

'Cut up' procedure

Cell Path System II standard white plastic tissue cassettes

Tissue processing

paraffin wax granules

Shandon Hypercentre XP Processor

70% formalin solution

xylene

alcohol

Tissue embedding

Raymond A Lamb Blockmaster II Embedding Centre

metal moulds in a range of 4 standard sizes

heatable tweezers

cool plate

scalpel

56°C incubator

'sledge-based' microtome

Cutting sections

Raymond A Lamb cold plate

Slee Mainz Cut 4060 Rotary Microtome

Feather S35 microtome blades

fine paintbrush

pre-warmed water bath

distilled water

pencil

BDH Laboratory Supplies Premium glass microscope slides

BDH Laboratory Supplies Polysine-coated glass microscope slides

37°C incubator

Tinctorial staining

Mayer's haematoxylin stain

eosin stain

Shandon Linistain GLX machine

mobile rack clips for slides

2% acetic acid

sodium hydrogen carbonate

Perl's Prussian Blue stain

2% potassium ferrocyanide

2% hydrochloric acid

stopwatch

circular filter paper

glass funnel

1% Neutral Red counter-stain

xylene-based DPX mountant

coverslips

mounting tweezers

metal slide racks

Immunohistochemical staining

plastic slide racks

condensation chamber and lid

plastic vials

30% hydrogen peroxide solution

refrigerator

DAB tablets

DABout filtration system

tris buffered saline (pH 7.6)

calculator

laboratory coat

latex gloves

DAKOCytomation monoclonal anti-CD68 antibody, human (mouse-derived)

DAKOCytomation PAP-pen

Kim-wipes tissues

hand-dropper

calibrated pipettes of a range of sizes

plastic pipette nibs

DAKOCytomation Protein Block

DAKOCytomation Link Antibody

DAKOCytomation Streptavidin solution

steek racks

glass rack containers

CALBIOCHEM monoclonal anti-bone sialoprotein antibody, human (mouse-derived)

microwave

citrate buffer solution

2 litre margarine or ice-cream tub

Digital Photography

Fuji S1 Pro digital camera

BH-2 Olympus microscope

daylight blue filter

Image Analysis

haemocytometer

Scion Image Beta 4.02 for Windows 95 to XP

APPENDIX 04

Photographs of histology and immunohistochemistry sections (see Chapter 03)

All photographs were taken using a Fuji S1 Pro digital camera, using a x10 objective. These are photographs of histology slides made from formalin-fixed, paraffin-embedded, decalcified blocks of human bone excised from around the fracture site. The sections were stained with Perls' Prussian Blue stain for haemosiderin granules, a monoclonal (mouse-derived) anti-human, anti-CD68 antibody (1 in 100 dilution) and a monoclonal (mouse derived) anti-human, anti-bone sialoprotein antibody (1 in 200 dilution).

Slide reference numbers	
5304	1
11172	2
12866A	3
12866B#a	4
12866B#b	5
12866D	6
5919	7
6682B	8
7512A	9
7512B	10
7512C	11
7512D	12
7512E	13
7512F	14
12163A	15
12163B	16
12163C	17
9440A	18
9440B	19
13405A#l	20
13405A#r	21
4995A	22
4995C	23

4995D	24
5776C	25
5776D	26
8262A	27
8262B	28
7522B	29
4165B	30
6258	31
5430A	32
5430B	33
5591	34
5405	35
13548A	36
13548B	37
9888B	38
5477B	39
3061A	40
3061B	41
14017A	42
4327A	43
4327B	44
4327C	45
7920	46
10540	47
5817A	48
5817B	49

Trauma-death interval(days)	Perls' Prussian Blue	CD68	BSP
-1	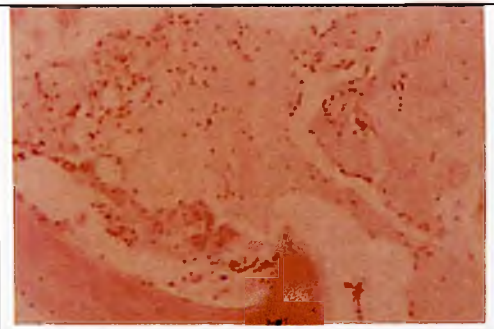	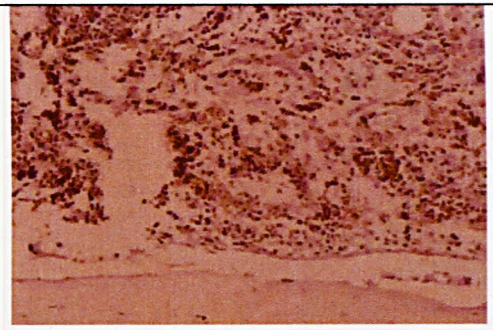	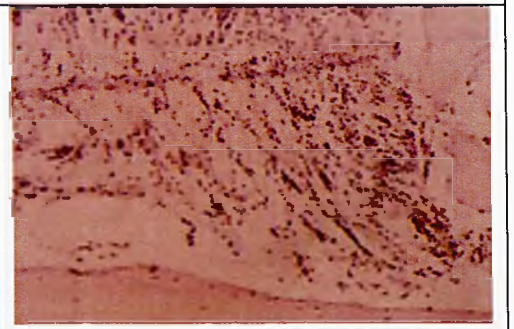
-1		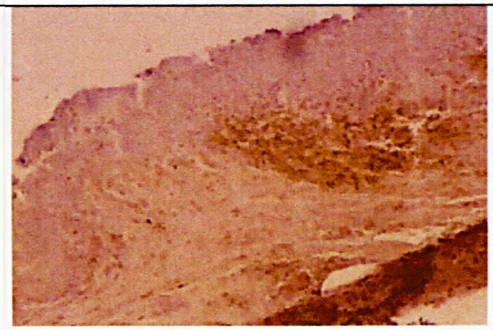	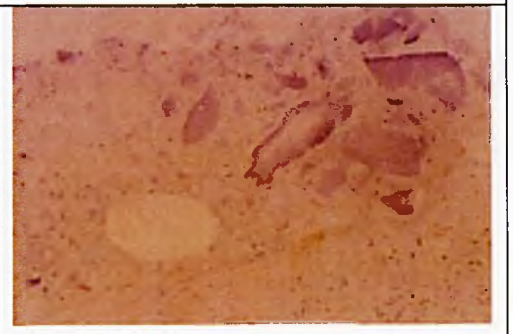

Trauma-death interval(days)	Perls' Prussian Blue	CD68	BSP
0 (epiphyseal growth plate,	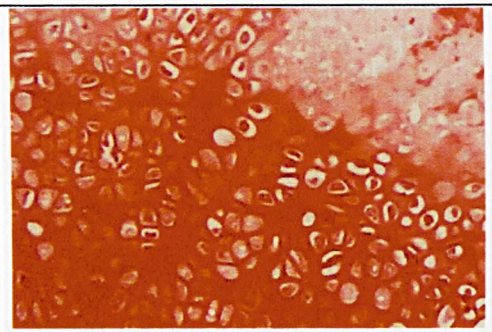	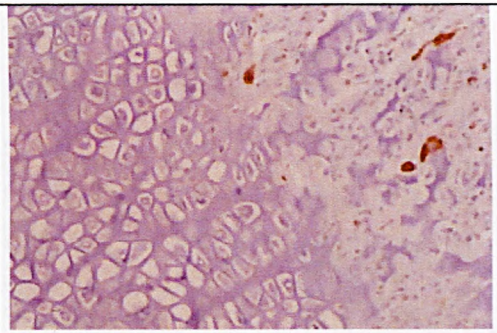	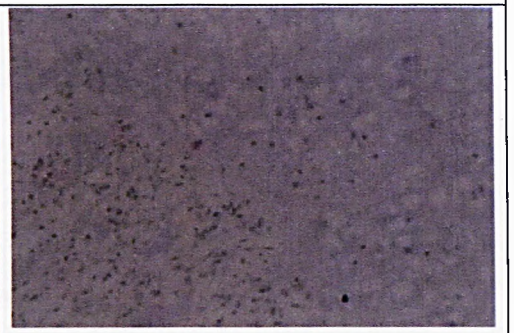
0	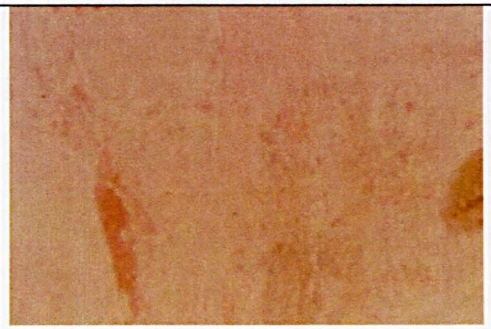	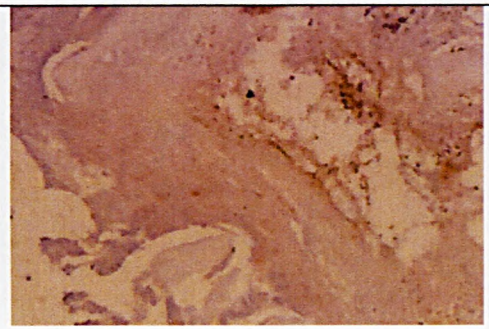	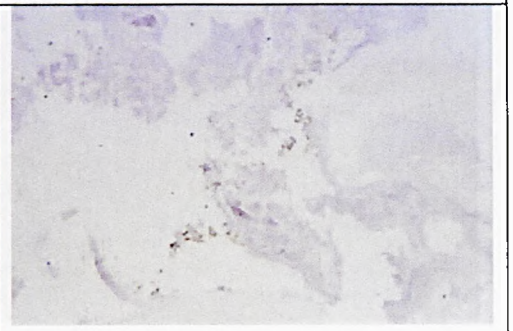

Trauma-death interval(days)	Perls' Prussian Blue	CD68	BSP
0	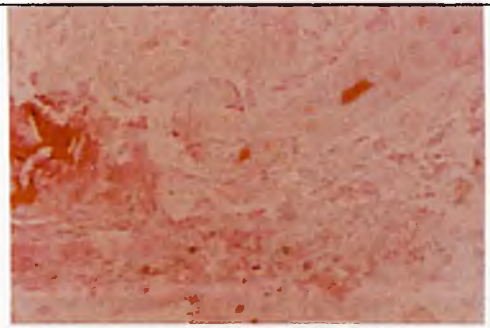	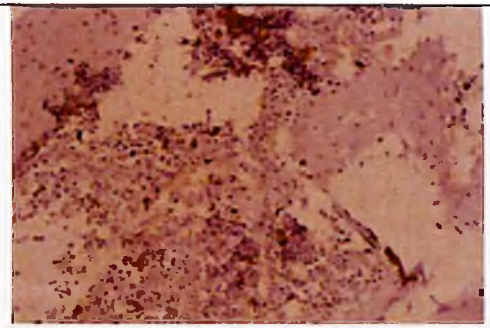	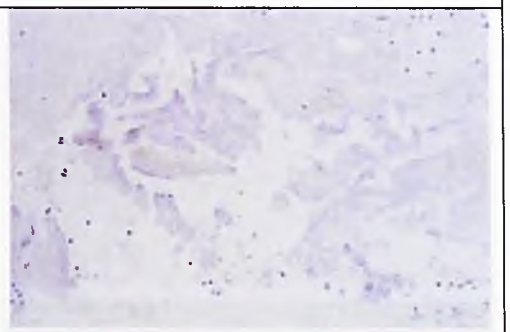
0		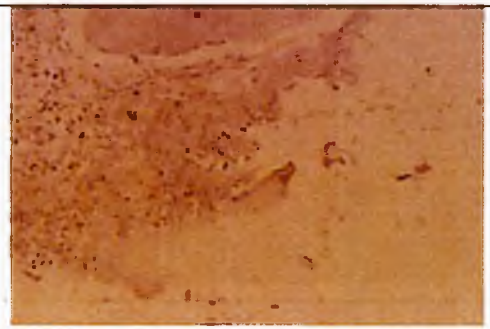	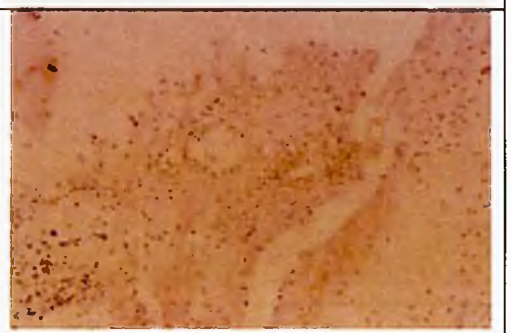

Trauma-death interval(days)	Perls' Prussian Blue	CD68	BSP
0	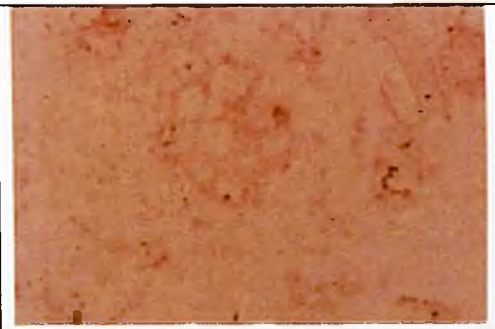	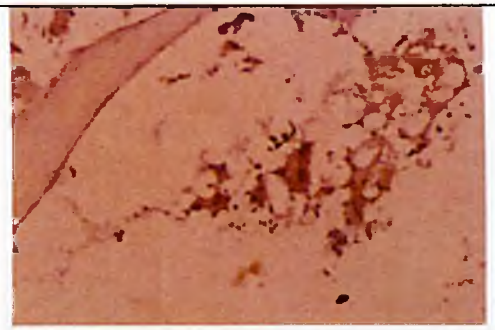	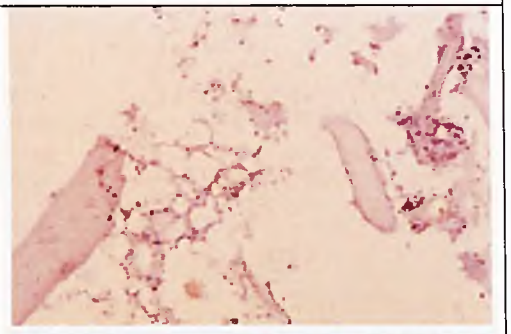
0	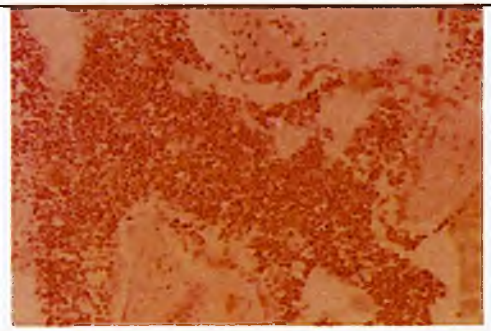	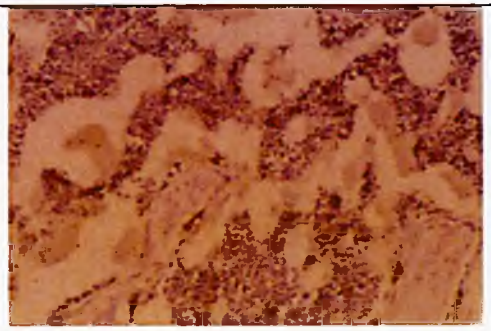	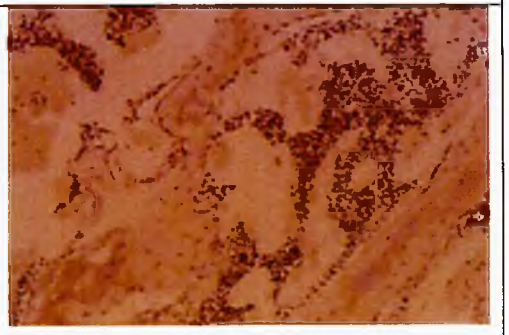

Trauma-death interval(days)	Perls' Prussian Blue	CD68	BSP
1	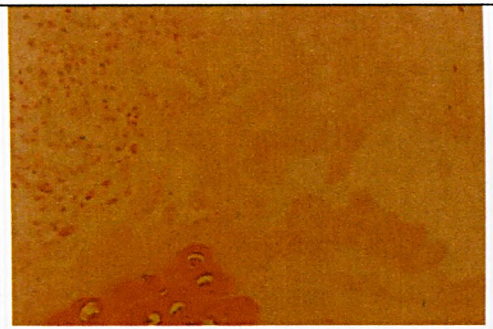	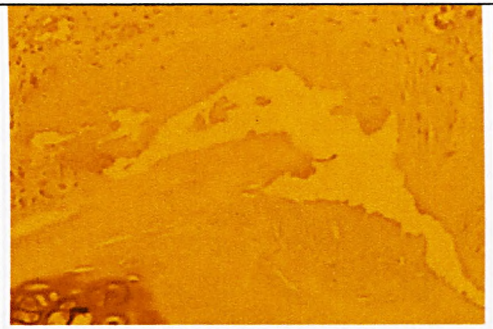	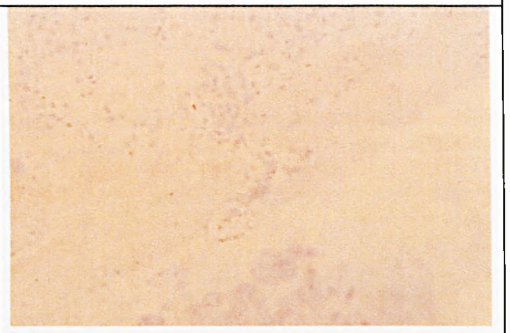
1	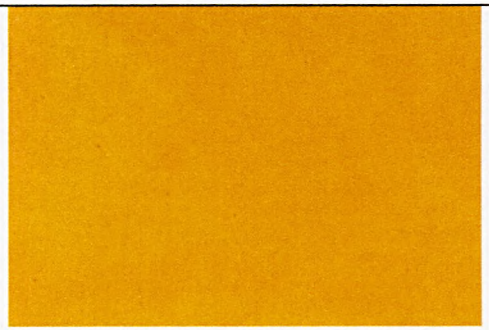	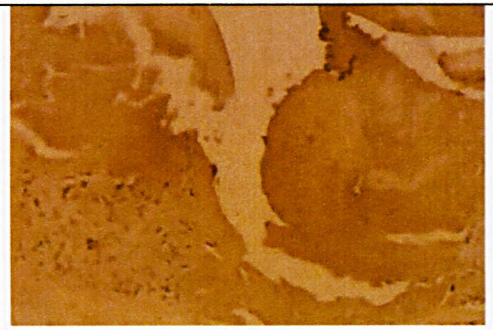	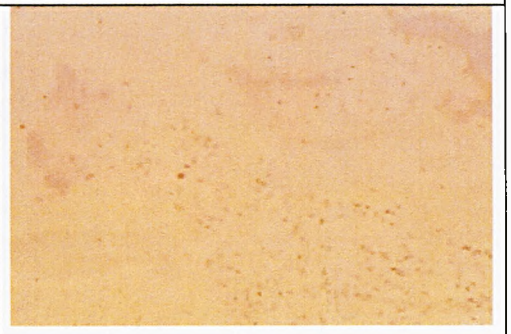

Trauma-death interval(days)	Perls' Prussian Blue	CD68	BSP
1			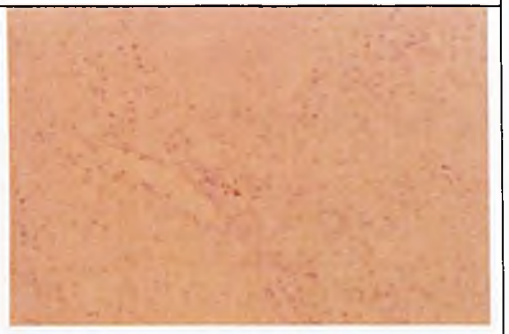
1	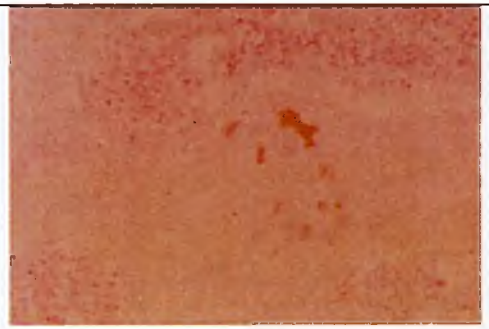	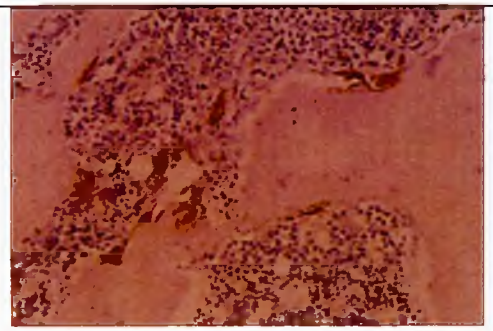	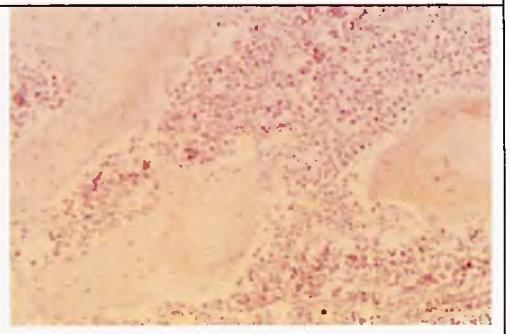

Trauma-death interval(days)	Perls' Prussian Blue	CD68	BSP
1		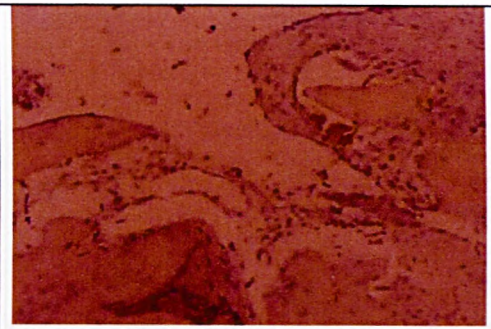	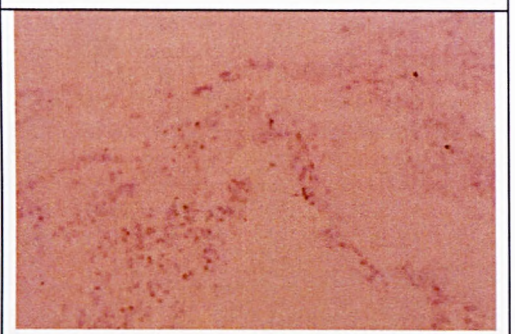
1		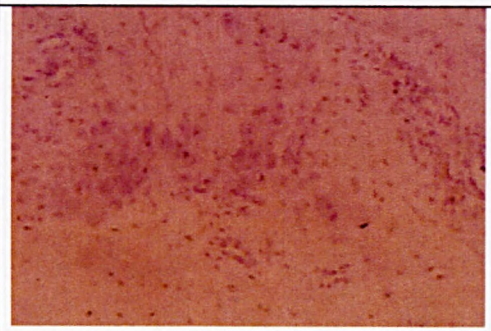	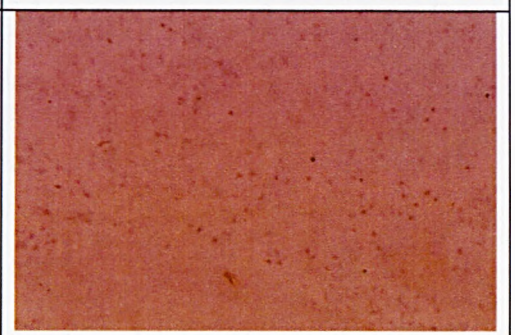

Trauma-death interval(days)	Perls' Prussian Blue	CD68	BSP
1	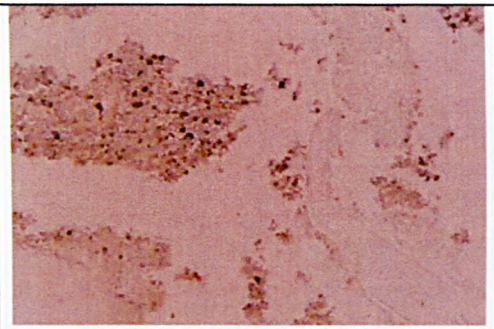	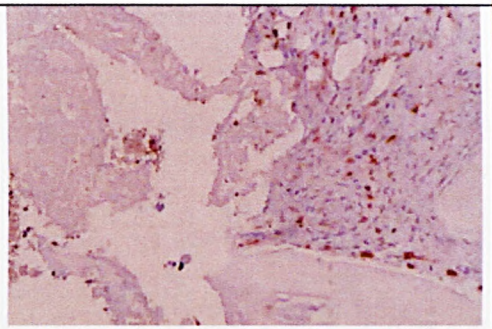	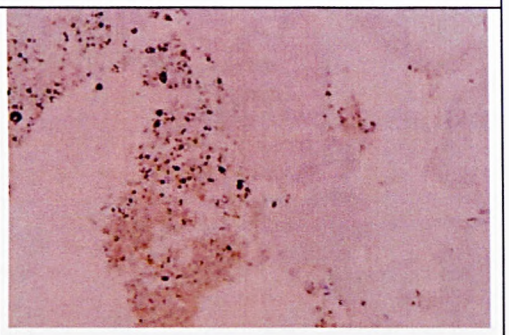
1	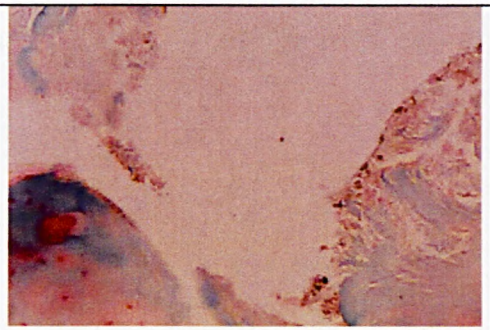	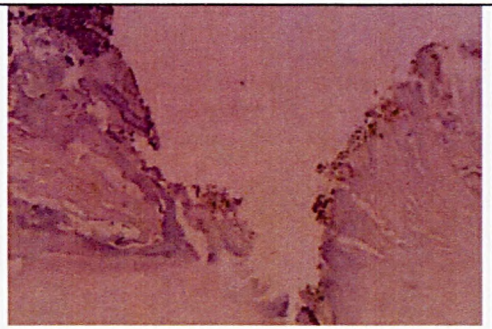	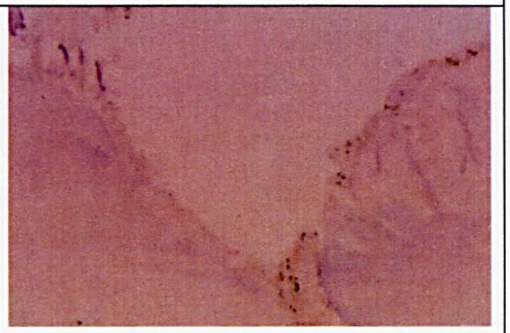

Trauma-death interval(days)	Perls' Prussian Blue	CD68	BSP
1	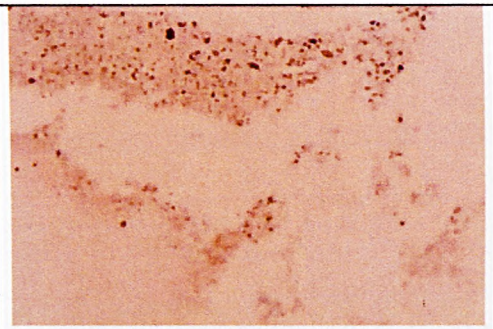	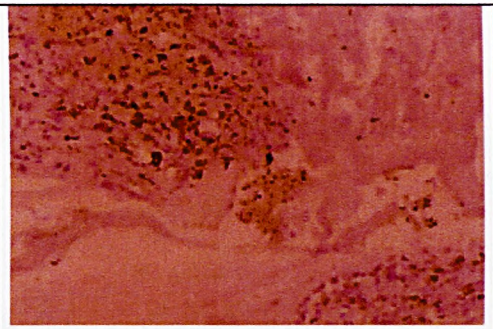	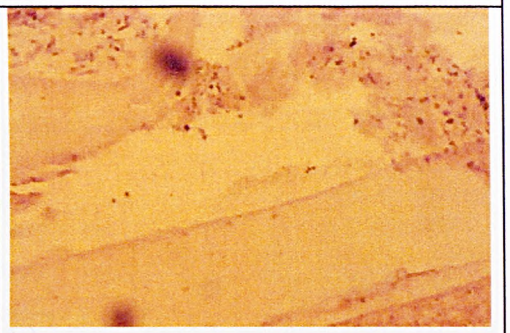
1.5		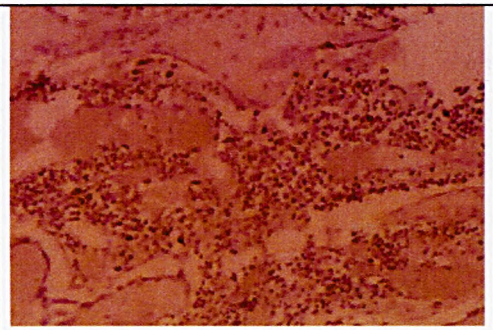	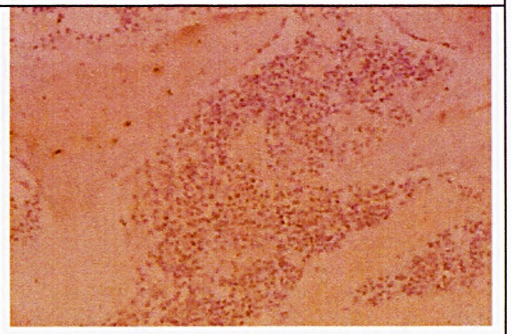

Trauma-death interval(days)	Perls' Prussian Blue	CD68	BSP
1.5		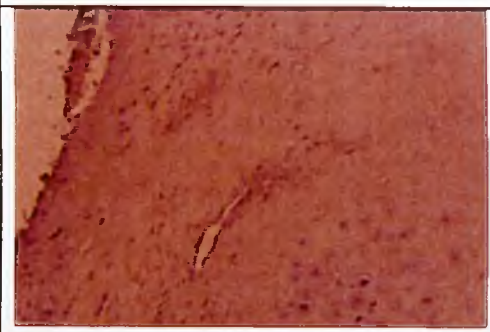	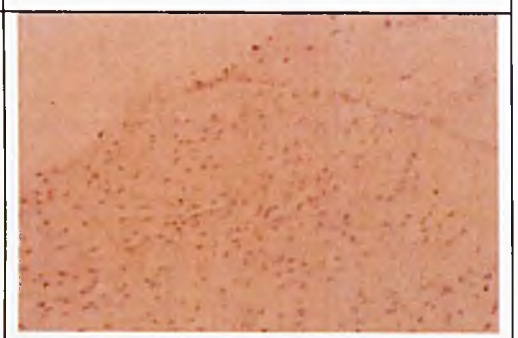
2	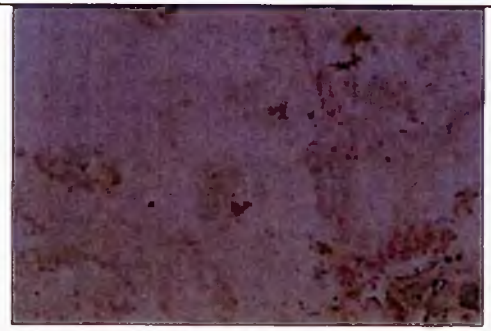	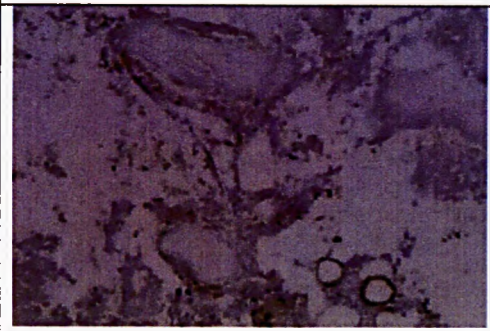	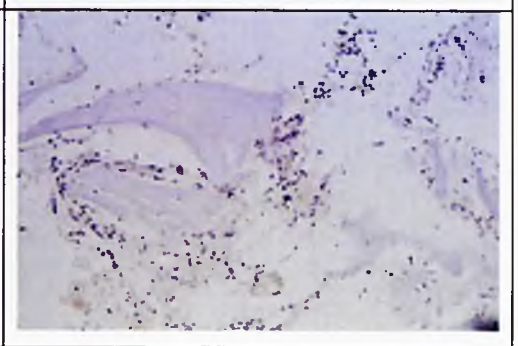

Trauma-death interval(days)	Perls' Prussian Blue	CD68	BSP
2	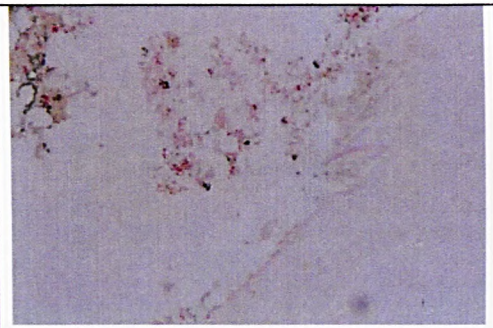	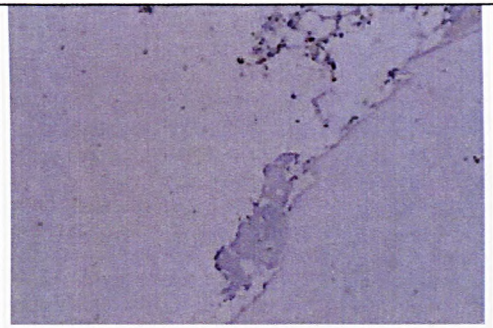	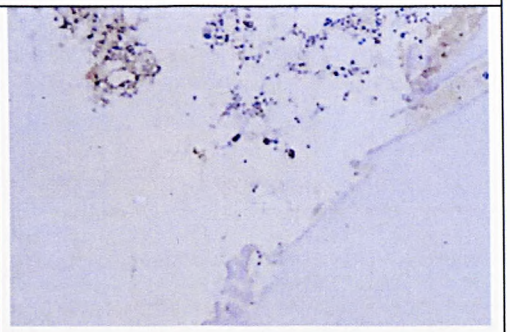
2	no Perls' stained slide	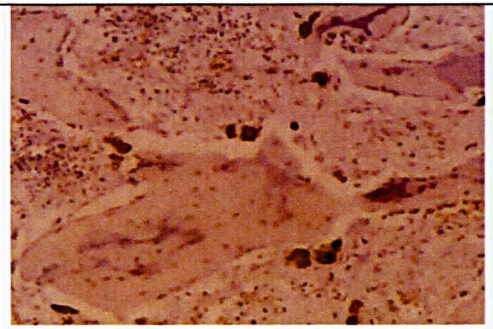	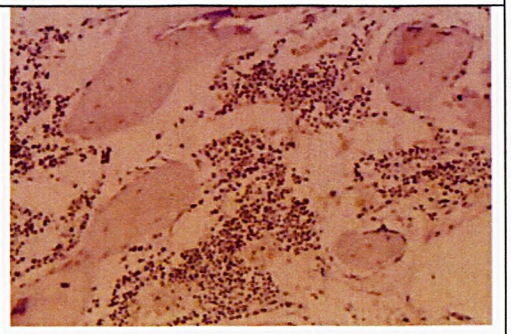

Trauma-death interval(days)	Perls' Prussian Blue	CD68	BSP
2	no Perls' stained slide	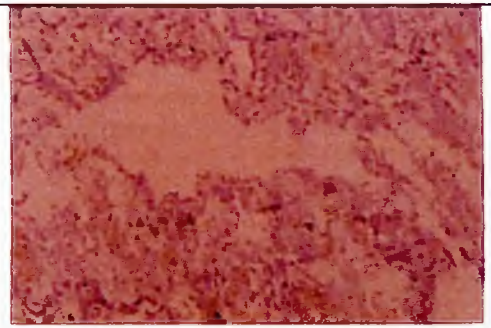	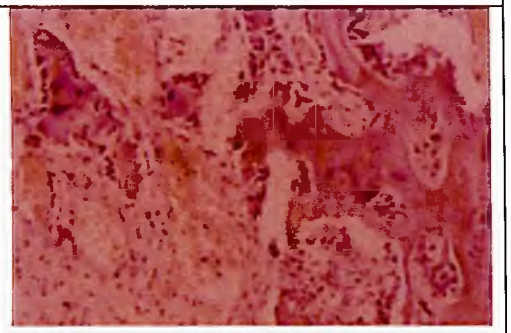
2		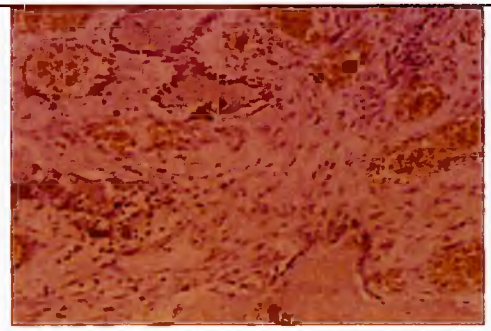	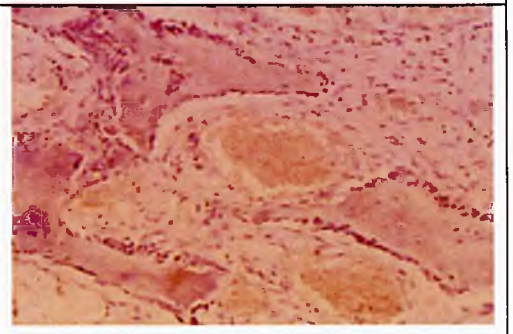

Trauma-death interval(days)	Perls' Prussian Blue	CD68	BSP
2	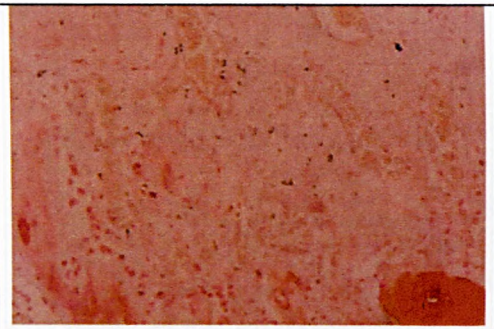	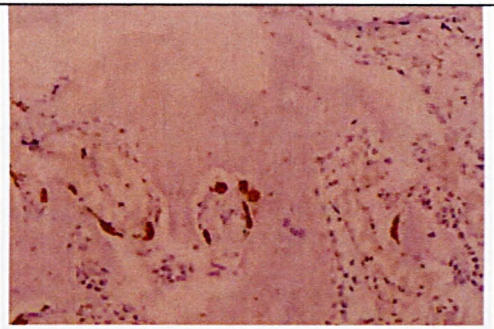	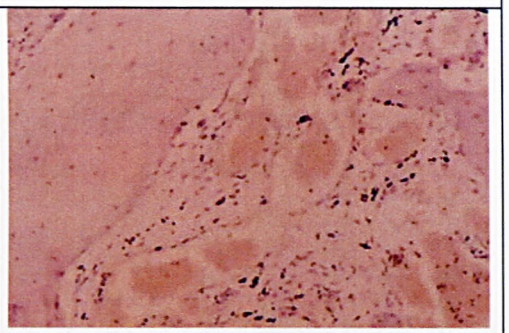
2	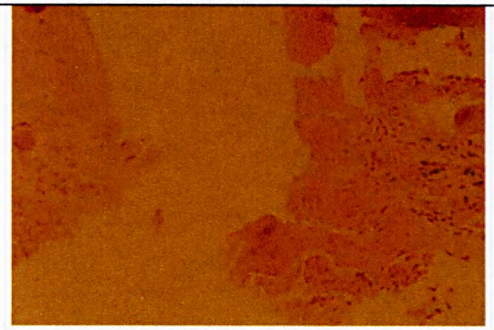	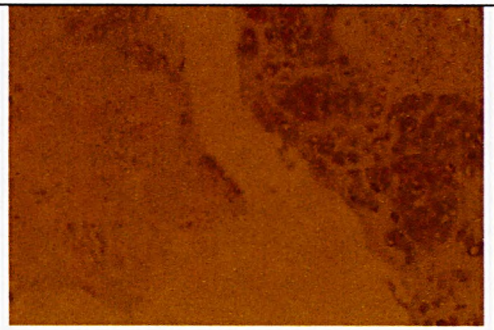	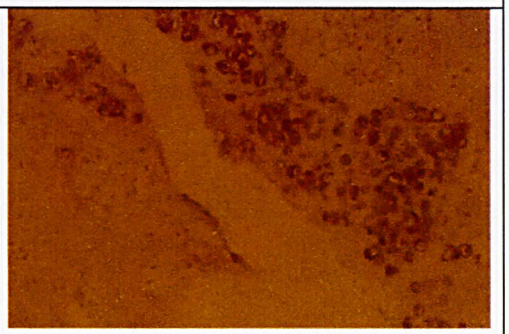

Trauma-death interval(days)	Perls' Prussian Blue	CD68	BSP
2	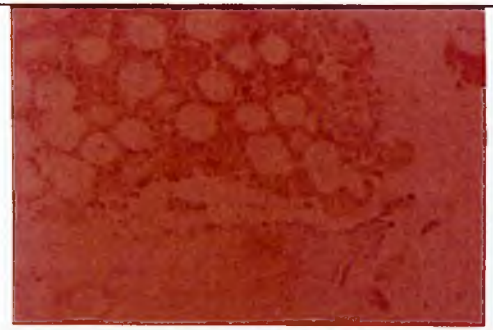	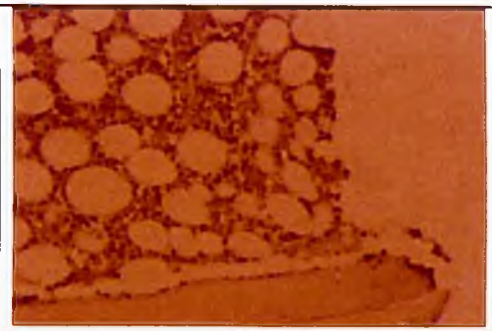	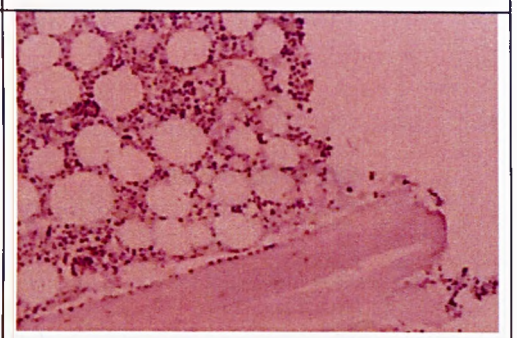
2	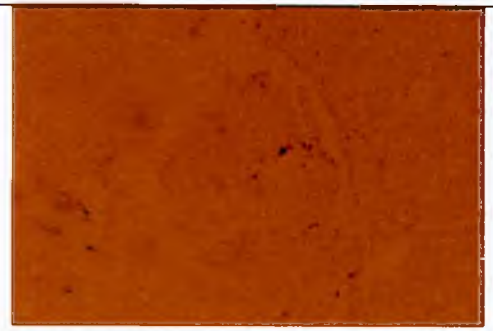	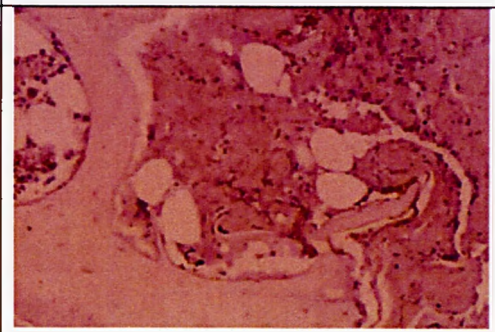	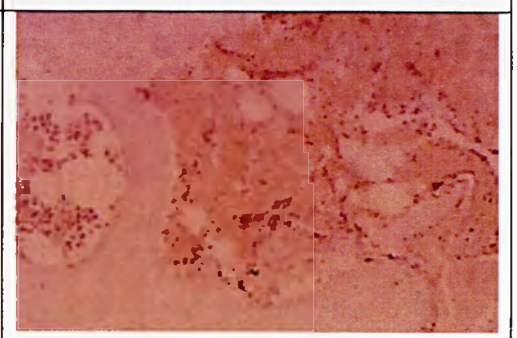

Trauma-death interval(days)	Perls' Prussian Blue	CD68	BSP
3		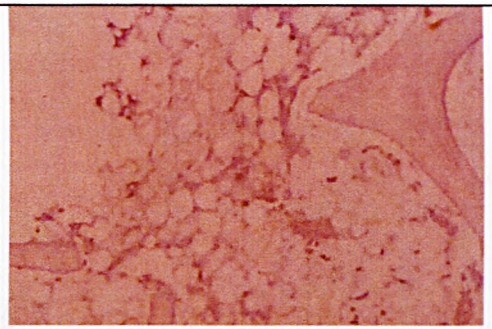	no BSP-stained slide
4		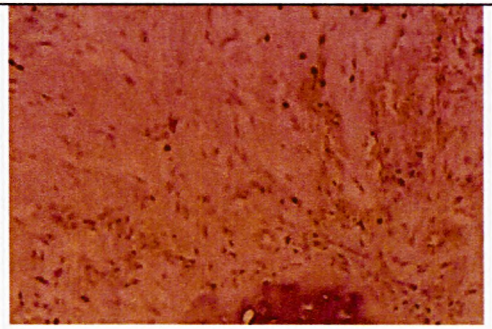	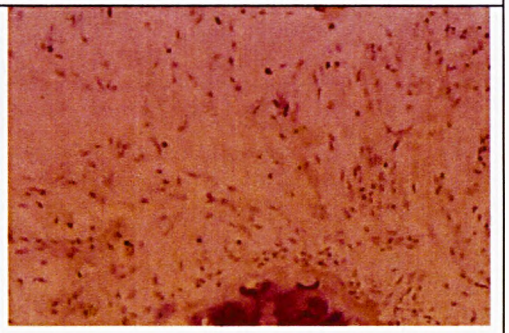

Trauma-death interval(days)	Perls' Prussian Blue	CD68	BSP
4	no Perls' stained slide	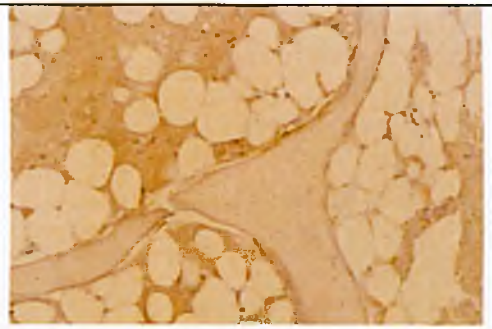	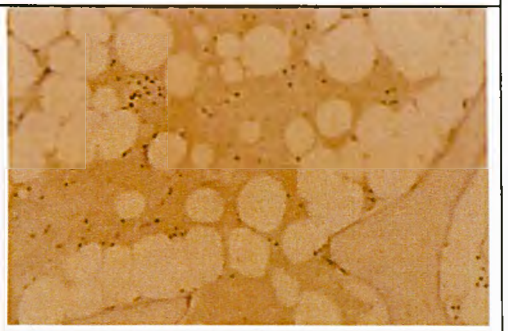
5		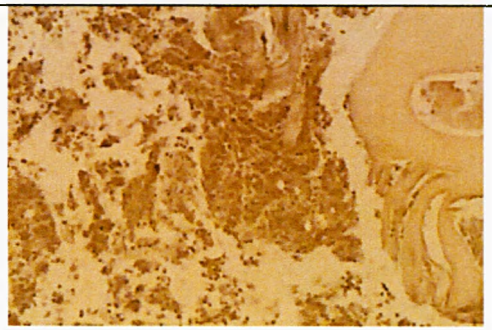	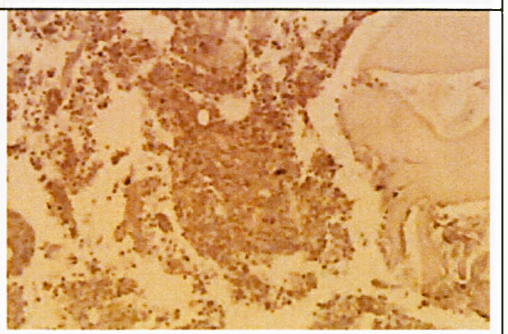

Trauma-death interval(days)	Perls' Prussian Blue	CD68	BSP
5	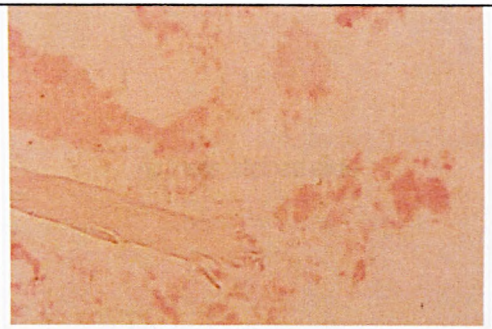	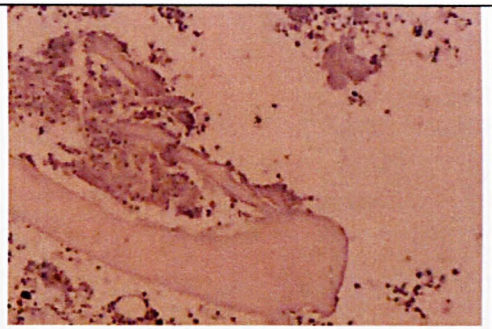	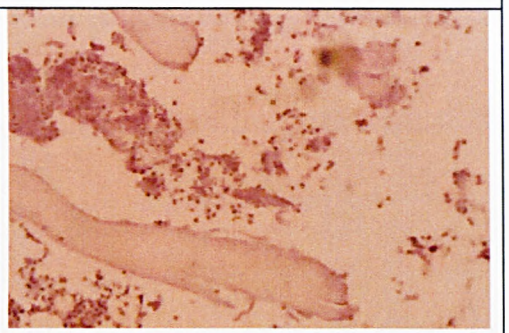
6		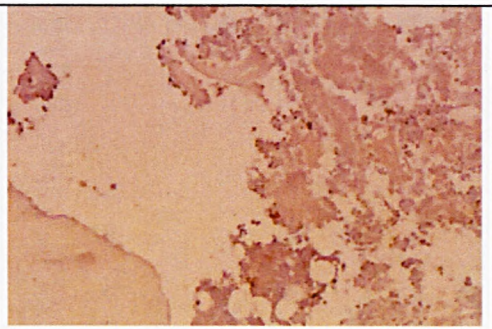	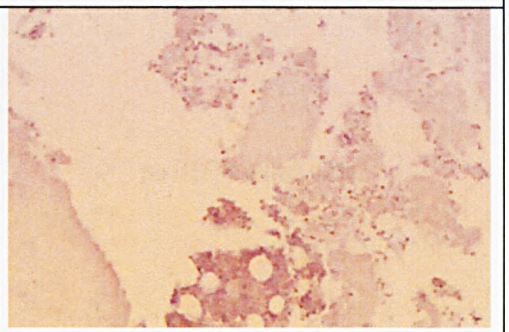

Trauma-death interval(days)	Perls' Prussian Blue	CD68	BSP
9	no Perls' stained slide	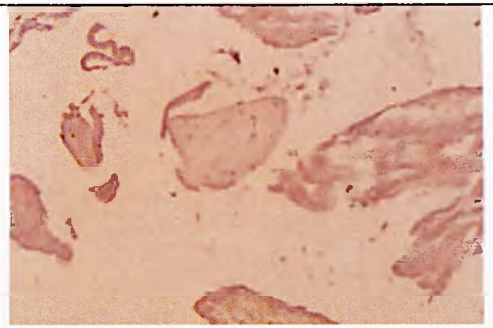	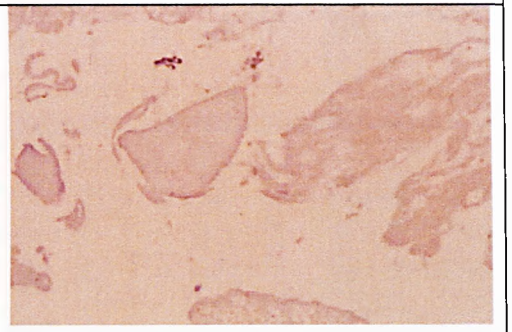
15		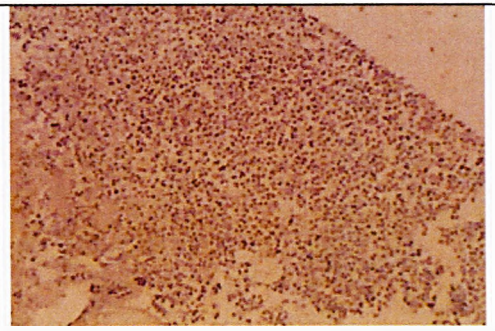	no BSP-stained slide

Trauma-death interval(days)	Perls' Prussian Blue	CD68	BSP
15		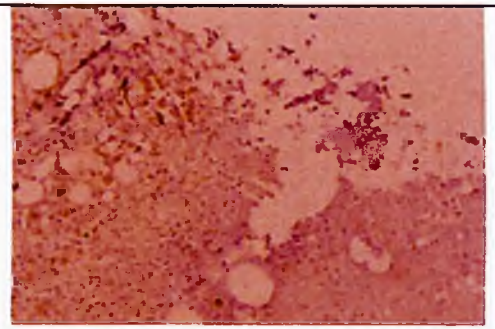	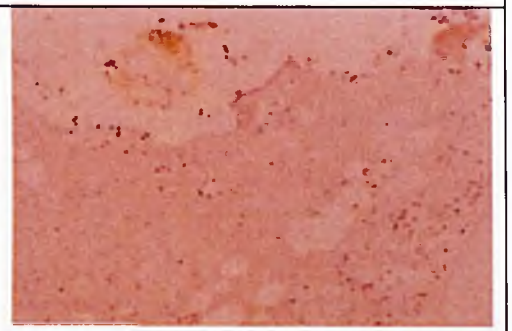
17			

Trauma-death interval(days)	Perls' Prussian Blue	CD68	BSP
19	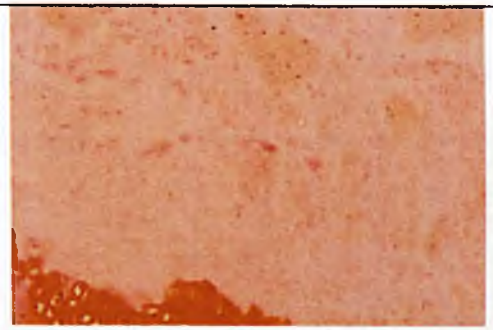	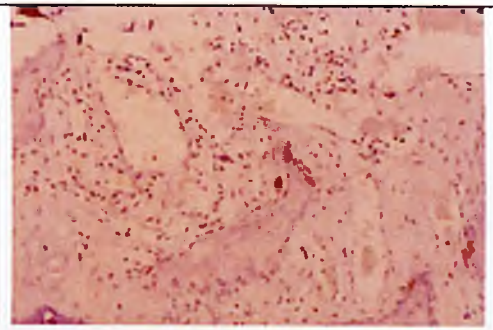	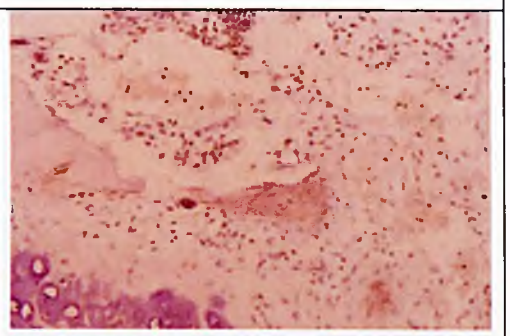
21	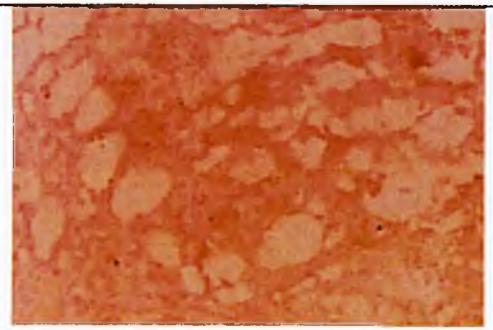	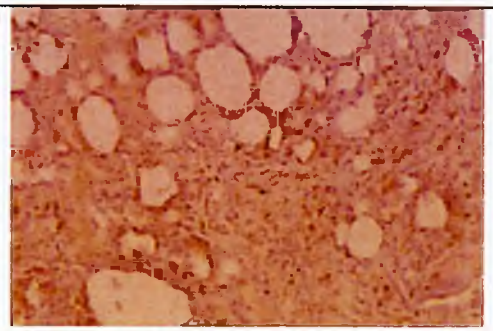	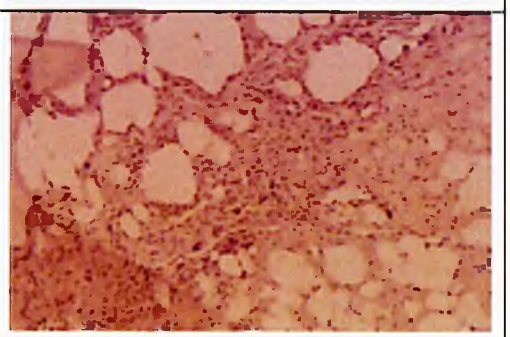

Trauma-death interval(days)	Perls' Prussian Blue	CD68	BSP
21	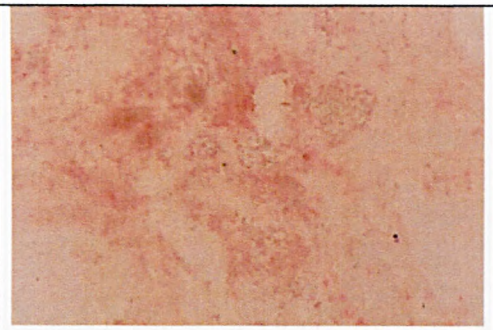	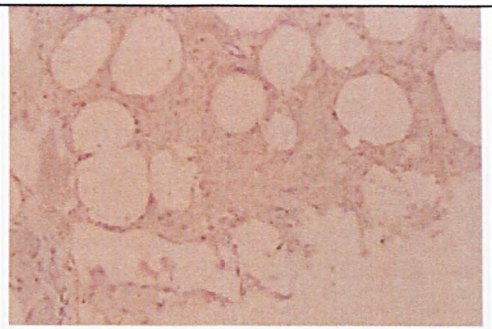	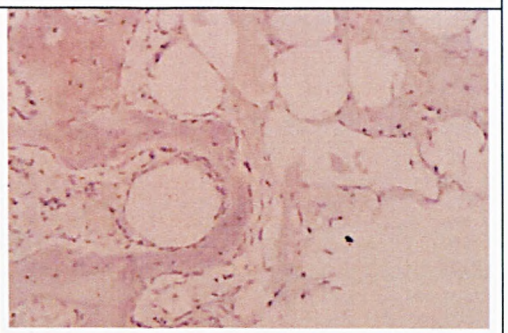
24		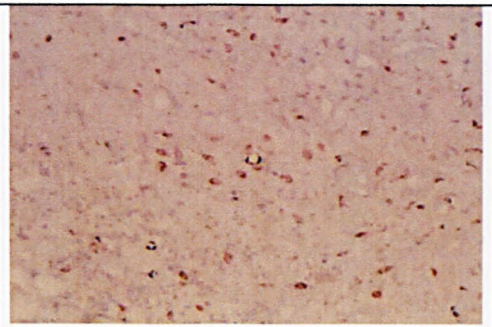	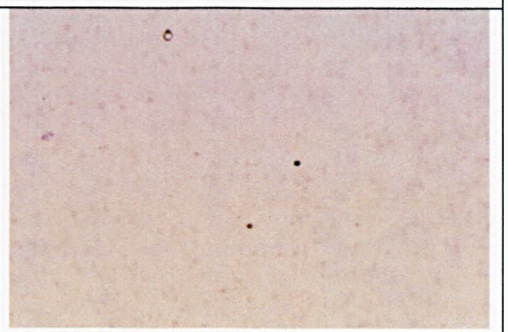

Trauma-death interval(days)	Perls' Prussian Blue	CD68	BSP
28		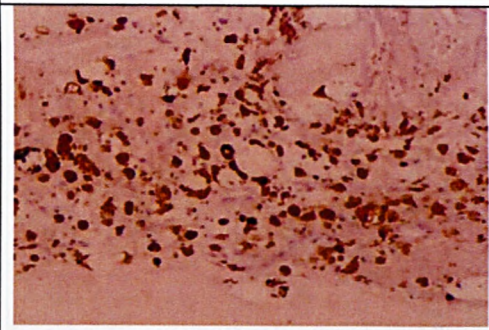	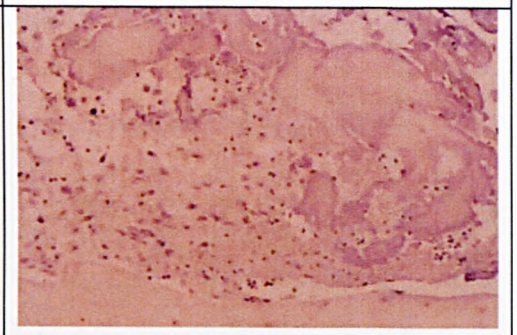
28	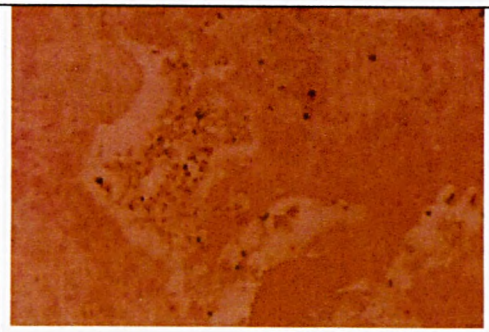	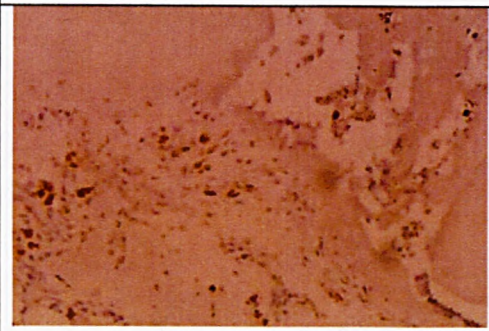	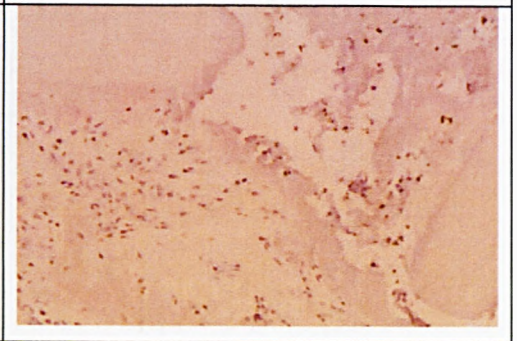

Trauma-death interval(days)	Perls' Prussian Blue	CD68	BSP
28	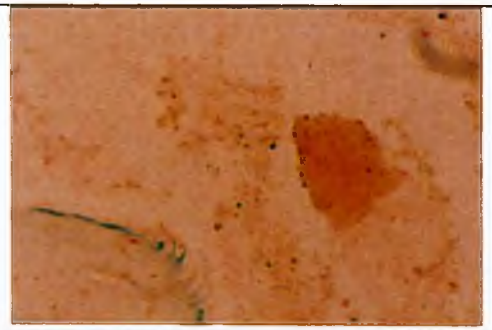	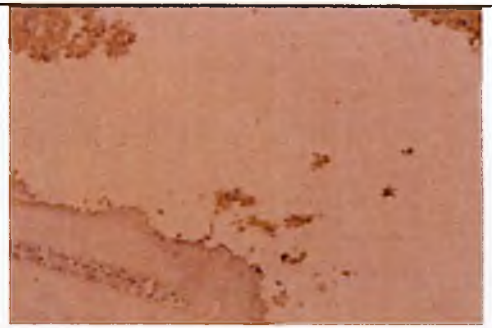	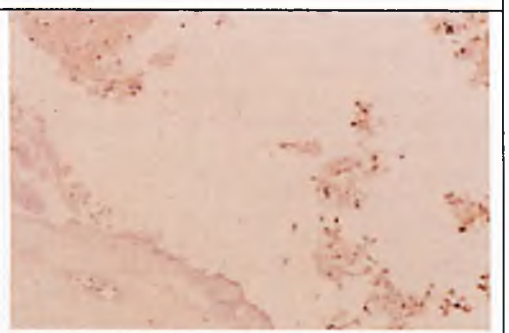
38	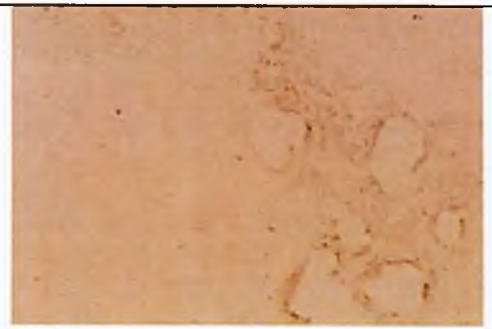	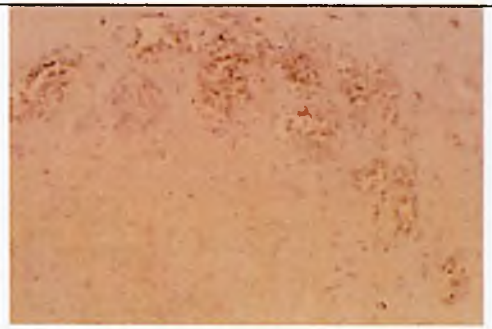	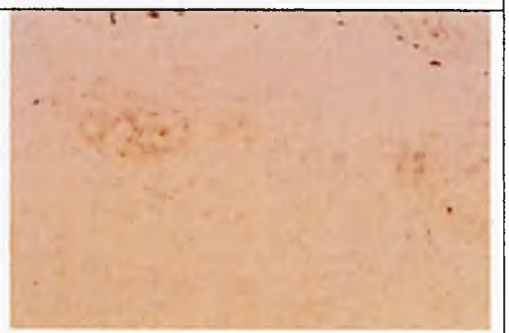

Trauma-death interval(days)	Perls' Prussian Blue	CD68	BSP
66	no Perls' stained slide	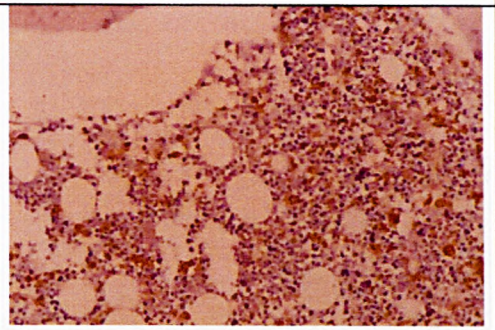	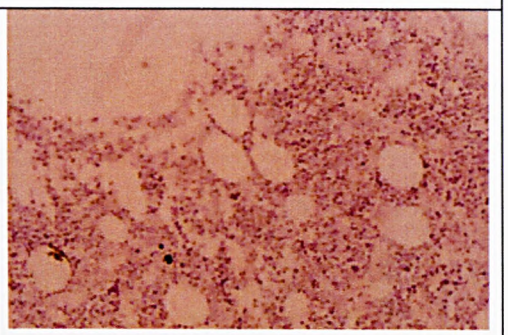
120	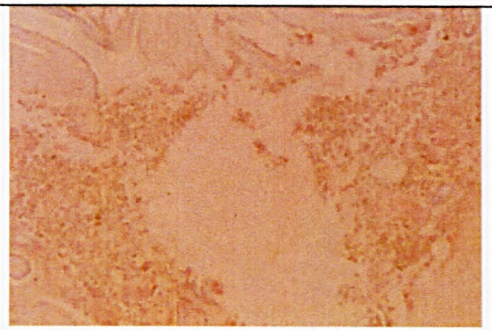	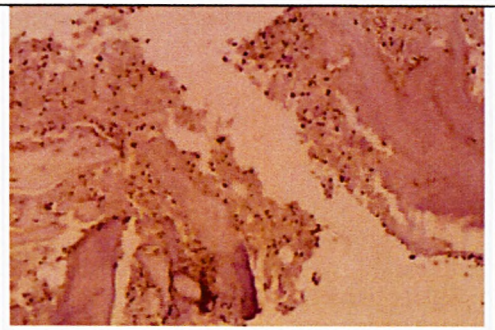	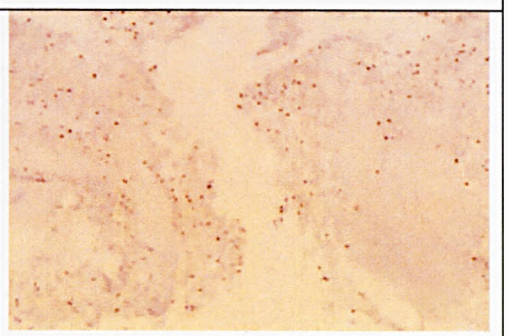

Trauma-death interval(days)	Perls' Prussian Blue	CD68	BSP
120	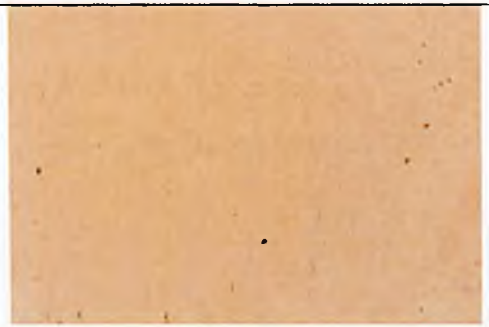	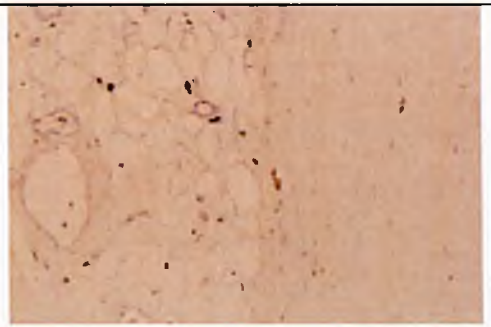	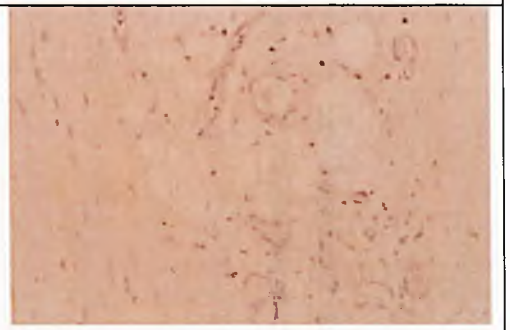

APPENDIX 05

Multiple observer recording form

Blank recording form for each independent observer to use to record observations taken from the photographs of the immunohistochemically stained slides.

Recording form for Observer 2 *Immuno stain: _____ qualitative results*

PM no.	Immuno+ cells (CD68 / BSP)			Cells with blue-stained nuclei (round and elongated)			Other observations
	cover	ave size (μm^2)	observations	cover	ave size (μm^2)	observations	(r.b.c, fat globules, compact bone % necrosis)
10540							
11172							
12021							
12163A							
12163B							
12163C							
12866B #a							
12866B nr#a							
12866D							
13405A #l							
13405A #r							
13548A							
13548B							
14017A nr#							
14017A							
3061A							
3061B							
4165B							
4327A							
4327B							
4327C							
4995A							
4995C							
4995D							
5304							
5405							
5430A							
5430B							
5477B							
5591							
5776C							
5776D							

Recording form for Observer 2 *Immuno stain: _____ qualitative results*

5817A							
5817B							
5919							
6258							
6682B							
7512A							
7512B							
7512C							
7512D							
7512E							
7512F							
7522B							
7920							
8262A							
8262B							
9417B							
9417C							
9440A							
9440B							
9888B							
neg controls							
1							
2							
3							
4							
5							
6							
pos controls							
1							
2							
3							
4							
5							
6							